Resonant generation and refraction of dispersive shock waves in one-dimensional nonlinear Schrödinger flows

Antin M. Leszczyszyn

Supervisor: Dr Gennady A. El

Department of Mathematical Sciences

Loughborough University

Loughborough, Leicestershire LE11 3TU

United Kingdom

December 14, 2011

Certificate of originality

This is to certify that I am responsible for the work submitted in this thesis, that the original work is my own except as specified in acknowledgments or in footnotes, and that neither the thesis nor the original work contained therein has been submitted to this or any other institution for a degree.

..... (Signed)

..... (Date)

Abstract

In the Thesis, two important theoretical problems arising in the theory of one-dimensional defocusing nonlinear Schrödinger (NLS) flows are investigated analytically and numerically: (i) the resonant generation of dispersive shock waves (DSWs) in one-dimensional NLS flow past a broad repulsive penetrable barrier; and (ii) the interaction of counter-propagating DSW and a simple rarefaction wave (RW), which is referred to as the DSW refraction problem. The first problem is motivated by the recent experimental observations of dark soliton radiation in a cigar-shaped BEC by sweeping through it a localised repulsive potential; the second problem represents a dispersive-hydrodynamic counterpart of the classical gas-dynamics problem of the shock wave refraction on a RW, and, apart from its theoretical significance could also find applications in superfluid dynamics. Both problems also naturally arise in nonlinear optics, where the NLS equation is a standard mathematical model and the 'superfluid dynamics of light' can be used for an all-optical modelling of BEC flows.

The main results of the Thesis are as follows:

(i) In the problem of the transcritical flow of a BEC through a wide repulsive penetrable barrier an asymptotic analytical description of the arising wave pattern is developed using the combination of the localised "hydraulic" solution of the 1D Gross-Pitaevskii (GP) equation with repulsion (the defocusing NLS equation with an added external potential) and the appropriate exact solutions of the Whitham-NLS modulation equations describing the resolution of the upstream and downstream discontinuities through DSWs. We show that the downstream DSW effectively represents the train of dark solitons, which can be associated with the excitations observed experimentally by Engels and Atherton (2008).

(ii) The refraction of a DSW due to its head-on collision with the centred RW is considered in the frameworks of two one-dimensional defocusing NLS models: the standard cubic NLS equation and the NLS equation with saturable nonlinearity, the latter being a standard model for the light propagation through photorefractive optical crystals. For the

cubic nonlinearity case we present a full asymptotic description of the DSW refraction by constructing appropriate exact solutions of the Whitham modulation equations in Riemann invariants. For the NLS equation with saturable nonlinearity, whose modulation system does not possess Riemann invariants, we take advantage of the recently developed method for the DSW description in non-integrable dispersive systems to obtain key parameters of the DSW refraction.

In both problems, we undertake a detailed analysis of the flow structure for different parametric regimes and calculate physical quantities characterising the output flows in terms of relevant input parameters. Our modulation theory analytical results are supported by direct numerical simulations of the corresponding full dispersive initial value problems (IVP).

Dedication

To my friends and family, with love and respect.

Thought

When all you have is a hammer, the whole world looks like a nail.

Acknowledgements

My supervisor Dr Gennady El. Your enthusiasm has inspired me at every meeting. You have supplied me with powerful tools and ideas. For this, I thank you.

Thank you to my collaborators and colleagues in the field, our discussions on problems that have arisen have been very helpful.

I would like to thank M.A. Hoefer and P. Engels for granting me permission to reprint figures from their paper.

Thank you to all my proof readers, especially my big sister Oksana, I cannot thank you enough.

Thank you to all of my friends and office mates in the mathematics department. Your distractions have saved my mind.

To all my running and training partners over the years. We have pounded the earth and our bodies together. This has given me the release from work that I needed. I hope I did not bore you with my moaning.

And thank you to my closest friends, you have listened to me and without your support I could not have completed this thesis.

Abbreviations

BEC- Bose-Einstein condensate

BVP- Boundary value problem

DFT- Discrete Fourier transform

DSW- Dispersive shock wave

EPD- Euler-Poisson-Darboux

FFT- Fast-Fourier transform

fKdV- Forced Korteweg – de Vries

GP- Gross-Pitaevskii

IFFT- Inverse fast-Fourier transform

IST- Inverse scattering transform

IVP- Initial value problem

KdV- Korteweg – de Vries

KdV-B- Korteweg – de Vries – Burgers'

NLS- Nonlinear Schrödinger

ODE- Ordinary differential equation

PDE- Partial differential equation

RW- Rarefraction wave

sNLS- Saturable nonlinear Schrödinger

SWE- Shallow water equations

Key words

Wave breaking, dispersive hydrodynamics, dispersive shock wave, rarefaction wave, soliton, nonlinear modulations, Whitham equations, Riemann invariants, Gurevich-Pitaevskii problem, Bose-Einstein condensate, photorefractive optical media, nonlinear wave interactions.

Contents

Chapter 1

Introduction and outline of research

The formation of shock waves is the salient feature of hydrodynamic flows. In classical, viscous fluids, shock dynamics can be well understood mathematically in the context of a dissipative regularisation of conservation laws. There are, however, a number of fluids with negligible dissipation whose dominant regularising mechanism is dispersion. Most notably, superfluidic Bose-Einstein condensates (BECs) and optical waves in defocusing nonlinear media fall within this class of dispersive fluids. The superfluid counterparts of viscous shock waves, the so-called dispersive shock waves (DSWs), are nonlinear expanding wavetrains exhibiting solitons near one of the edges and degenerating into a linear wavepacket near the opposite edge. These DSWs have yielded novel multi-scale nonlinear wave dynamics and interesting interaction behaviour and have recently become an object of intensive theoretical and experimental investigations, notably due to a number of ground breaking BEC experiments, [1, 2], where these waves represent a striking manifestation of quantum statistics on a macroscopic scale. Another actively developing area of the experimental and theoretical DSW research is laser optics where the DSWs represent nonlinear interference or diffraction patterns forming in the propagation of powerful laser beams through an optical crystal with refractive index defects [3–5]. In a completely different physical context, DSWs (also called undular bores, especially in classical fluid dynamics applications) have been found to play

an important role in the mesoscale atmosphere and ocean processes.

One of the fundamental mathematical models of dispersive hydrodynamics is the nonlinear Schrödinger (NLS) equation which often arises as the equation for an envelope of a weakly nonlinear wave packet propagating in a medium with quadratic nonlinear response. However, in a number of applications the NLS equation and its modifications can describe the propagation of a wave field (not necessarily an envelope) of an arbitrary amplitude. For example, the wave function of a rarefied BEC is known to be very well described by the Gross-Pitaevskii (GP) equation, which represents the cubic NLS equation with an added external potential (a trap or an obstacle potential). Depending on the character of interatomic interactions in a BEC, one deals with focusing (attractive interactions) or defocusing (repulsive interactions) case. Another area of the application of the NLS equation is the propagation of a powerful laser beam through optical crystals. In the thesis, we restrict ourselves to the one-dimensional defocusing case, when the medium (a BEC or an optical medium) supports stable dark (or gray) solitons propagating on a non-zero background. Our main concern will be with the analytical and numerical description of DSW generation and interaction in two configurations:

- **The resonant (transcritical) generation of DSW in one-dimensional NLS flows past broad repulsive penetrable barriers**.

  This problem is motivated by the recent experimental findings by Engels and Atherton [6] who observed the radiation of dark soliton in quasi-1D BECs subjected to a moving localised repulsive potential. One of the unusual features observed in the experiment was a *finite interval of the BEC flow velocities* (in the potential barrier reference frame) for which the soliton radiation takes place. In other words, the superfluidity breakdown via the radiation of dark solitons (or, more generally, DSWs) occurs when the BEC velocity $v \in [v^-, v^+]$, where the values $v^\pm$ depend on the strength (amplitude) of the potential barrier. The most effective generation of solitons occurs in the resonant case when the flow velocity is equal to the speed of sound in the BEC. This effect

is specific to 1D flows and is in sharp contrast with the classical notion of the *single critical velocity* v_c in multi-dimensional superfluid flows past obstacles, so that the superfluidity breakdown either via the radiation of linear waves (Landau [7]) or via the emission of quantised vortices (Feynman [8]) occurs for all $v > v_c$.

The general theoretical framework for the study of 1D superfluid flows past broad repulsive penetrable potentials was developed by Hakim [9] who proposed a very suggestive mathematical analogy with transcritical shallow water flows past localised topographies. This latter problem was studied analytically and numerically by Grimshaw and Smyth [10] and Smyth [11] in the framework of the forced Korteweg – de Vries (fKdV) equation. The corresponding NLS problem was studied in [9] numerically. In the Thesis, this problem is solved analytically.

- **The interaction of counter-propagating superfluid DSW and a simple rarefaction wave (RW)**, which is referred to as the **DSW refraction problem**.

  This problem represents a dispersive-hydrodynamic counterpart of the classical gas-dynamics problem of the shock wave refraction on a RW (see e.g. the monograph by Courant and Friedrischs [12]), and, apart from its pure theoretical significance, is important for the understanding of superfluid dynamics in some physically relevant configurations. Various interactions of RWs and DSWs in BECs were recently studied experimentally and numerically in [13, 14]. For *uni-directional* KdV flows, the problem of the overtaking DSW-RW interaction was considered by Ablowitz, Baldwin and Hoefer [15]. The bi-directional DSW-RW interactions studied in the Thesis, to the best of our knowledge, have not been considered analytically before. The model problem of the head-on DSW-RW interaction solved in the Thesis, provides a general analytical framework for the study of the more specific interaction problems of interests for BEC dynamics and nonlinear optics.

The main mathematical tool in the description of DSWs/undular bores is the Whitham

method of slow modulations [16], which is based on fully nonlinear multiple-scale expansions (or, alternatively, on an appropriate equivalent averaging technique) applied to nonlinear dispersive PDEs. The Whitham equations were for the first time applied to the description of DSWs by Gurevich and Pitaevskii [17] who considered the problem of the decay of an initial discontinuity for the KdV equation. A similar problem for the defocusing NLS equation was first considered by Gurevich and Krylov [18] and later, more comprehensively, by El et. al. [19]. Since then, there has been a large number of research works investigating the dynamics of DSWs for the NLS equation. The majority of these works considered the generation and dynamics of isolated DSWs freely propagating in homogeneous media. The interactions of DSWs with external potentials and/or with hydrodynamic waves (like RWs or other DSWs) are far less explored and the results of the Thesis make a contribution to this area of dispersive hydrodynamics and its applications.

The main results of the Thesis have been published in two research papers [20] and [21].

The structure of the Thesis is as follows.

Chapter 2 introduces main concepts, notions and methods of the Thesis. These include the method of characteristics, Riemann invariants and hodograph solutions (including the generalised hodograph method for multi-component hydrodynamic type systems). The description of the fundamental wave breaking phenomenon is followed by the classification of different types of the resolution of the breaking hydrodynamic singularities. The central notion of the dispersive shock wave (DSW) is introduced and some of the recent experimental and theoretical works on the DSW dynamics in BECs and nonlinear optics are reviewed. The Chapter is concluded with the general description of the Whitham method of slow modulations which is one of the main mathematical methods used in the Thesis.

Chapter 3 outlines the basic properties of the defocusing cubic NLS equation (dispersion relation, dispersionless limit, conservation laws, travelling wave solutions) necessary for the subsequent application of the Whitham method of slow modulations, which is presented in

Section 3.2. The Riemann invariant form of the modulation equations is introduced. The structure of the characteristic velocities is analysed and the their behaviour in the linear and soliton limits is considered. This Chapter is based on the results of papers [2, 22–24].

Chapter 4 details the DSW theory for the NLS equation using the Gurevich-Pitaevskii type matching conditions for the modulation equations in Riemann invariants. Although majority of the results of this Chapter were obtained earlier, we give some new, more direct proofs and derivaions. We will begin by discussing simple centred DSW and RW solutions in the NLS dispersive hydrodynamics using the appropriate similarity solutions of the NLS-Whitham modulation equations. We will then present a full classification for the decay of an arbitrary discontinuity problem where the solution will generally be a combination of two simple waves, either DSWs or/and RWs. We then continue with a more general class of modulation solutions obtained by the hodograph transform and show how the hodograph NLS modulation equations are reduced to the classical Euler-Poisson-Darboux equation, whose general solution is known very well. Finally, we present a recent extension of the Gurevich-Pitaevskii theory to the modulation systems which generally do not possess the Riemann invariant structure and typically arise when averaging non-integrable dispersive systems. This 'dispersive shock fitting' method was developed by El (2005) and here we illustrate this method by recovering all key results of the 'integrable' NLS modulation theory for simple DSWs presented earlier in this Chapter.

In the rest of the Thesis, the results and methodologies detailed in Chapters 3, 4 are used to address two specific new problems. In Chapter 5 we consider the problem of the transcritical BEC flows past broad penetrable repulsive barriers in BECs. The phenomenon of the generation of dark soliton trains for a certain interval of the BEC flow velocities observed in recent experiment [6] is explained. Using a suggestive analogy with transcritical shallow water flows past variable topographies (Grimshaw and Smyth (1986)), we construct analytical modulation solutions to the defocusing NLS equation with an external potential (the GP equation). Our solutions describe the dark soliton generation via the formation of

the steady 'hydraulic' transition over the potential barrier and the resolution of the arising upstream and downstream hydraulic jumps via two simple DSWs. A detailed classification of the arising wave patterns in the parameter space of the BEC flow velocity and the potential strength is presented. The drag force exerted on the BEC is calculated. All the obtained analytical results are supported by direct numerical simulations.

Chapter 6 considers the interaction of the counter-propagating DSW and RW in the superfluid NLS flows. This problem represents a dispersive counterpart of the classical viscous shock wave refraction problem formulated by Courant and Friedrischs in 1940s. The analysis of the interaction is performed by employing the hodograph modulation solutions presented earlier in Chapter 4. The modulation solutions describing the behaviour of two interacting waves at all stages of the evolution are constructed and the key parameters of the DSW refraction are calculated. In particular, we present an explicit analytical expression for the DSW phase shift due to refraction on the RW. The analytical results are supported by numerical simulations.

In Chapter 7 we will again consider the DSW refraction problem but this time in the framework of the NLS equation with saturable nonlinearity describing the powerful light beams propagation in nonlinear photorefractive media. The saturable NLS equation (sNLS) is not integrable by the inverse scattering transform (IST) and Riemann invariants are not available for the associated modulation system. We extend the dispersive shock fitting method of El (2005) to derive the key physical parameters of the DSW refraction in sNLS flows and compare our analytical results with numerical solutions.

The Appendix is devoted to the description of numerical methods used in the Thesis.

Chapter 2

Hyperbolic waves and dispersive hydrodynamics: an overview

2.1 Shallow water equations and the Hopf equation

Our theoretical understanding of many fluid flows, including flows in oceans, lakes, canals, plasmas, superfluids and in the atmosphere, often starts by considering very simplified models. For many fluid flow considerations, the shallow water equations (SWE) are often used as a starting point. They have the form

$$\begin{aligned} h_t + (hu)_x &= 0, \\ u_t + uu_x + h_x &= 0. \end{aligned} \tag{2.1}$$

Here $h(x,t)$ is the total fluid depth and $u(x,t)$ is the depth–averaged horizontal velocity, x, t are the spatial and temporal coordinates; all variables are non-dimensional. This model describes motion of a thin layer of fluid of constant density under the effect of gravity.

Although being a highly simplified model, the SWE capture many features of fluid flows and can often give a qualitatively accurate description for large-scale, non-thin layer flows of constant density. At the same time, the SWE have their limitations, governing only

single layer, free surfaces. Being a system of nonlinear hyperbolic equations the SWE do not include any dissipative or dispersive terms, so for a broad class of initial conditions, the solution profiles steepen and become multi-valued after a finite time: the behaviour that is usually referred to as a wave-breaking [16, 25, 26].

To clarify the wave breaking behaviour, we consider a special class of solutions to the SWE, called *simple waves*, which is selected by a restriction $h = h(u)$. Substituting this into the shallow water system (2.1) we readily get

$$h'(u) = \pm\sqrt{h}. \tag{2.2}$$

Integrating we obtain

$$\tfrac{1}{2}u - \sqrt{h} = \text{constant} \quad \text{or} \quad \tfrac{1}{2}u + \sqrt{h} = \text{constant}. \tag{2.3}$$

Then for each of the relationships (2.2) both equations (2.3) collapse into a single *simple wave* equation:

$$u_t + c_+(u)u_x = 0, \qquad \text{or} \quad u_t + c_-(u)u_x = 0 \tag{2.4}$$

respectively. Here

$$c_\pm(u) = u \pm \sqrt{h(u)} \tag{2.5}$$

are the speeds of the right- $(+)$ or left- $(-)$ propagating simple waves (the labels "right-" and "left-" propagating refer to the reference frame moving with the flow speed u) .

By introducing the new variables

$$\lambda_\pm = \tfrac{1}{2}u \pm \sqrt{h}, \tag{2.6}$$

instead of h and u we cast the SWE (2.1) in the canonical Riemann invariant form

$$\frac{\partial \lambda_\pm}{\partial t} + V_\pm \frac{\partial \lambda_\pm}{\partial x} = 0, \tag{2.7}$$

$\lambda_\pm$ are the Riemann invariants and

$$V_+ = \tfrac{1}{4}(3\lambda_+ + \lambda_-), \quad V_- = \tfrac{1}{4}(3\lambda_- + \lambda_+). \tag{2.8}$$

are the characteristic velocities which are expressed in terms of the original variables h, u as

$$V_\pm = u \pm \sqrt{h}, \tag{2.9}$$

One can see that the characteristic velocities $V_\pm$ are simply $c_\pm$ in equation (2.4) with h and u being independent variables.

Setting one of these Riemann invariants (λ_- for example) to be constant, $\lambda_- = \lambda_-^0$, we obtain the simple wave equation for the right propagating wave (first equation in (2.4)). Similarly, setting $\lambda_+ = \lambda_+^0$ constant we obtain the left propagating simple wave equation.

Using the substitution $v = c(u)$ we reduce the simple wave equation $u_t + c(u)u_x = 0$ to the so-called Hopf equation

$$v_t + vv_x = 0, \tag{2.10}$$

which is the model equation for the study of uni-directional nonlinear dispersionless wave propagation. We shall be interested in the solutions, for $t > 0$ of the initial value problem (IVP) for the Hopf equation with initial data

$$v(x, 0) = v_0(x) \tag{2.11}$$

where $v_0(x)$ is some continuous function.

2.2 Simple waves: method of characteristics and wave breaking

2.2.1 Characteristic solution

We solve the IVP (2.10), (2.11) using the method of characteristics. The idea is that a linear combination in the form

$$a(v,x,t)\frac{\partial v}{\partial t} + b(v,x,t)\frac{\partial v}{\partial x}, \tag{2.12}$$

can be interpreted as the directional derivative of $v(x,t)$ in the direction $\mathbf{r} = (\mathbf{a}, \mathbf{b})$ in the (x,t) plane.

A characteristic curve or characteristic $\mathcal{C}$ is introduced in the (x,t) plane by the condition that the tangent vector is (a,b) at each point of $\mathcal{C}$. For the Hopf equation $a(v,x,t) = 1$, $b(v,x,t) = v$ so that at each point of $\mathcal{C}$ we have

$$\frac{dx}{dt} = \frac{b}{a} = v \tag{2.13}$$

Now, along $\mathcal{C}$, $v = v(x(t),t)$ and

$$\frac{\partial v}{\partial t} + v\frac{\partial v}{\partial x} = \frac{\partial v}{\partial t} + \frac{dx}{dt}\frac{\partial v}{\partial x} = \frac{dv}{dt}, \tag{2.14}$$

Now, the IVP

$$\begin{aligned} \frac{\partial v}{\partial t} + v\frac{\partial v}{\partial x} &= 0\,, \\ t = 0: \qquad v &= v_0(x)\,, \quad -\infty < x < \infty \end{aligned} \tag{2.15}$$

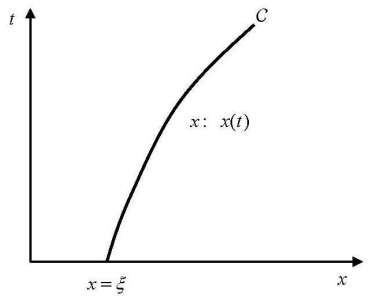

Figure 2.1: A characteristic curve in the (xt) - plane

can be re-written in the characteristic form:

$$\text{on } \mathcal{C}: \begin{cases} \dfrac{dx}{dt} = v\,, \quad x(0) = \xi, & (a) \\ \\ \dfrac{dv}{dt} = 0\,, \quad v(0) = v_0(\xi)\,, & (b) \end{cases} \tag{2.16}$$

where ξ is a parameter (the initial point on the characteristic curve).

Integrating (2.16a,b) we obtain the characteristic solution on $\mathcal{C}$

$$\begin{aligned} v &= v_0(\xi), & (a) \\ x &= \xi + t v_0(\xi). & (b) \end{aligned} \tag{2.17}$$

Note that characteristics $\mathcal{C}$ given by (2.17b) are straight lines.

By varying ξ we get the solution in the whole (x,t) region provided $1 + tv_0'(\xi) \neq 0$ (solvability of (2.17b) for $\xi(x)$ at a given t). It is not difficult to verify by direct calculation that solution $v(x,t)$ specified by (2.17a), (2.17b) does solve the IVP.

Combining (2.17a) and (2.17b) we obtain the solution $v(x,t)$ of the IVP in an implicit form

$$x = vt + x_0(v)\,, \tag{2.18}$$

where $x_0(v) = v_0^{-1}(v)$ is the function inverse to $v_0(x)$ (note that by assuming $x_0(v)$ to be an arbitrary function in (2.18) we get a general solution to the Hopf equation).

2.2.2 Rarefaction waves

Rarefaction waves (RWs) represent an important class of of solutions to the Hopf equation. Consider the IVP

$$v_t + vv_x = 0, \quad x \in \mathbb{R}, \quad t > 0, \quad v(x,0) = v_0(x), \tag{2.19}$$

where

$$v_0 = \begin{cases} v_2, & if \quad x \leq 0 \\ monotonically\ increasing, & if \quad 0 \leq x \leq L \\ v_1, & if \quad x \geq L. \end{cases} \tag{2.20}$$

where $v_1 > v_2$ (i.e. $v_0'(x) > 0$ for $0 \leq x \leq L$). The characteristic solution

$$v = v_0(\xi), \quad x(r) = v \cdot t + \xi, \tag{2.21}$$

describes an expansion fan (or a RW) (see Figure 2.2 left). Since the characteristics do not

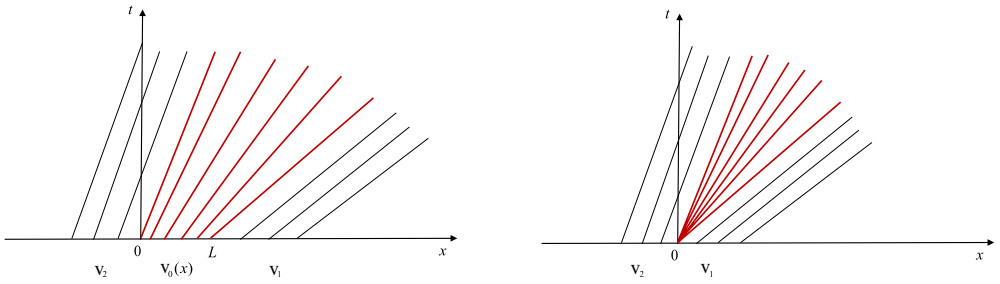

Figure 2.2: Expansion fan of characteristics in a RW. Left: general configuration. Right: centred fan

intersect at $t > 0$, we obtain the solution $v(x,t)$ as a single-valued function for all $t > 0$, i.e. the RW solution is *global*.

In the limiting case, when $L \to 0$ we obtain a centred fan where all characteristics between v_2 and v_1 pass through the origin, see Figure 2.2 right. The centred fan solution $v(x,t)$, $t > 0$

is described explicitly as

$$v = \begin{cases} v_2, & if \quad x \le v_2 t \\ \frac{x}{t}, & if \quad v_2 t \le x \le v_1 t \\ v_1, & if \quad x \ge v_1 t\,. \end{cases} \tag{2.22}$$

The corresponding profiles of $v(x,t)$, for $t = 0$ and $t > 0$ are shown in Figure 2.3.

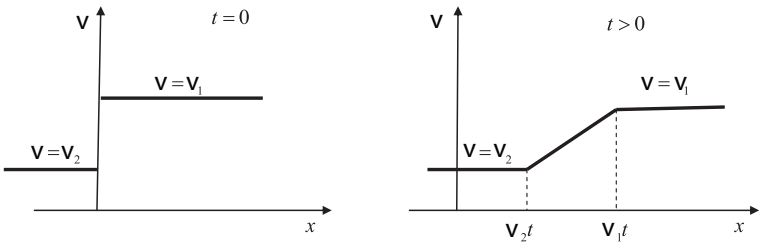

Figure 2.3: Centred RW. Left: initial conditions, $t = 0$. Right: wave profile for $t > 0$.

2.2.3 Wave breaking

Let us again look at the characteristic solution

$$v = v_0(\xi), \quad x = v \cdot t + \xi, \tag{2.23}$$

but now assume that the initial profile $v_0(\xi)$ has a section, where $v_0'(\xi) < 0$. This implies that the condition $1 + v_0'(\xi)t \neq 0$ of solvability of the characteristic equation $x = \xi + v \cdot t$ for $\xi(x,t)$ will fail for some

$$t = -\frac{1}{v_0'(\xi)} > 0. \tag{2.24}$$

This happens for the first time on the characteristic $\xi = \xi_b$, where $|v_0'(\xi)|$ assumes its maximum value; if $v_0(r)$ is smooth function, this implies $v_0''(\xi_b) = 0$. So

$$t_b = -\frac{1}{v_0'(\xi_b)} = \frac{1}{|v_0'(\xi_b)|} \tag{2.25}$$

One can see that the derivatives

$$v_t = -\frac{v_0(\xi)v_0'(\xi)}{1+v_0'(\xi)t}, \qquad v_x = \frac{v_0'(\xi)}{1+v_0'(\xi)t} \tag{2.26}$$

become infinite at $t = t_b$ and we have a gradient catastrophe. This is the wave breaking point. The described characteristic construction is illustrated in Figure 2.4.

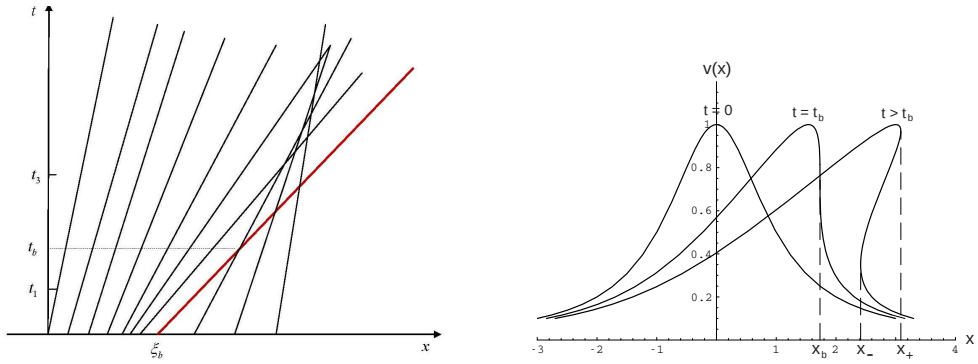

Figure 2.4: Wave breaking. Left: Intersection of characteristics at (x_b, t_b); Right: Gradient catastrophe formation at $t = t_b$ and the multi-valued wave profile for $t > t_b$

To better understand the qualitative meaning of the wave breaking phenomenon we note that from the characteristic form of the Hopf equation,

$$\frac{dv}{dt} = 0 \quad on \quad \frac{dx}{dt} = v, \tag{2.27}$$

one can conclude that each value of v propagates with its own speed v. So, if the initial profile has a decreasing part, the points with greater values of v will overtake those with smaller values of v, which will lead to the steepening of the profile $v(x)$ and at some moment $t = t_b > 0$ one can expect the occurrence of the gradient catastrophe, $|\frac{\partial v}{\partial x}| \to \infty$.

In the simplest case of a step initial conditions for the Hopf equation (2.15)

$$v_0(x) = \begin{cases} v_2, & if \quad x < 0 \\ v_1, & if \quad x > 0, \end{cases} \tag{2.28}$$

where $v_2 > v_1$, the wave breaking occurs at $t = 0$. Formal multi-valued solution for $t > 0$ is a centred compression wave with overhanging, see Figure 2.5. The corresponding behaviour of characteristics is shown in Figure 2.6

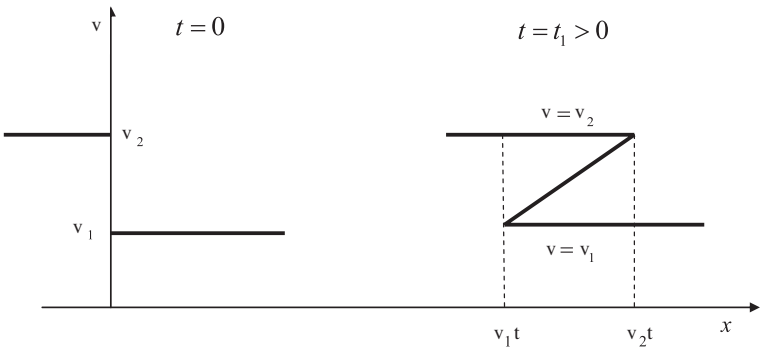

Figure 2.5: Left: initial conditions. Right: multi-value solution, $t > 0$.

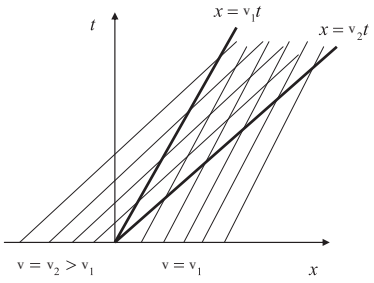

Figure 2.6: Characteristics behaviour in the solution to the step evolution problem

For arbitrary smooth initial conditions, the wave-breaking time is most conveniently calculated using an implicit solution of the Hopf equation

$$x - vt = f(v), \tag{2.29}$$

where $f(v)$ is the inverse of the initial function $v_0(x)$. Then, at the breaking point one must have

$$t = t_b : \qquad \frac{\partial x}{\partial v} = 0, \qquad \frac{\partial^2 x}{\partial v^2} = 0. \tag{2.30}$$

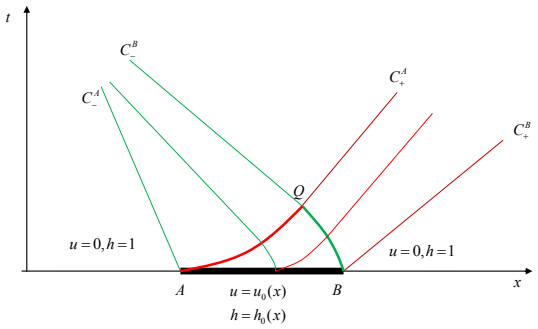

Figure 2.7: Interaction of two simple waves in the region ABQ of the (xt) plane: behaviour of charactersitics. Outside this region there are two separately propagating simple waves.

From (2.29), (2.30) we obtain for the wave-breaking time:

$$t_b = -f'(v_b)\,, \qquad f''(v_b) = 0\,, \tag{2.31}$$

where v_b is the value of v at the breaking point, which coincides with the value of v at the inflection point of the initial profile $v_0(x)$.

2.3 Interaction of simple waves: hodograph solution

A simple wave represents a disturbance propagating along a single characteristic family. For a general Cauchy problem for the SWE (2.1), i.e. when the initial conditions $u(x,0) = u_0(x)$, $h(x,0) = h_0(x)$ do not satisfy one of the simple wave relations (2.3), i.e. $\frac{1}{2}u_0(x) - \sqrt{h_0(x)} \neq const$, $\frac{1}{2}u_0(x) + \sqrt{h_0(x)} \neq const$, both families of characteristics $\frac{dx}{dt} = V_\pm(h,u)$ carry non-trivial disturbances so we need more general solutions than those described so far. A typical behaviour of characteristics in such a general solution is shown in Figure 2.7. One can see that outside the region ABQ there are two separate simple waves propagating in opposite directions. Within ABQ the simple waves interact and cannot be described individually using the solutions of the Hopf equation. To describe the interacting simple waves analytically we make use of the so-called hodograph transformation, which is achieved by interchanging the role of dependent and independent variables in the SWE (2.1).

We have $u = u(x,t)$, $h = h(x,t)$ and, assuming that the mapping $(x,t) \mapsto (u,h)$ is invertible, consider the inverse functions

$$x = x(u,h), \qquad t = t(u,h). \tag{2.32}$$

Now, using implicit differentiation or otherwise we obtain the relations between the derivatives

$$h_t = -\frac{x_u}{J}, \quad u_t = \frac{x_h}{J}, \quad h_x = \frac{t_u}{J}, \quad u_x = -\frac{t_h}{J}, \tag{2.33}$$

where $J = \frac{\partial(x,t)}{\partial(u,h)} = x_u t_h - x_h t_u$ is the Jacobian of the transformation. It is clear that the hodograph transformation requires that $J \neq 0$, $J^{-1} \neq 0$.

Substituting (2.33) into (2.1) we obtain the linear system,

$$x_u - u t_u + h t_h = 0, \quad x_h - u t_h + t_u = 0 \tag{2.34}$$

(note that the Jacobian cancels due to the absence of undifferentiated terms). Cross-differentiation yields a single second-order linear PDE for t:

$$t_{uu} - h t_{hh} = 2 t_h. \tag{2.35}$$

Introducing the characteristic variables (the Riemann invariants) $\lambda_\pm = \frac{1}{2}u \pm \sqrt{h}$ instead of h, u in (2.35) we arrive at the classical Euler-Poisson-Darboux (EPD) equation

$$\frac{\partial^2 t}{\partial \lambda_- \partial \lambda_+} = \frac{2}{\lambda_+ - \lambda_-}\left(\frac{\partial t}{\partial \lambda_+} - \frac{\partial t}{\partial \lambda_-}\right), \tag{2.36}$$

whose general solution is known very well (see e.g. [27]).

While the SWE are dramatically simplified under the hodograph transform, the hodograph equations are usually not very convenient for solving IVPs. Consider general initial

conditions

$$t = 0 : \qquad h = \mathcal{H}(x), \quad u = \mathcal{U}(x) \tag{2.37}$$

for the shallow water system (2.1). Expressions (2.37), in principle, parametrically define a curve in the hodograph (u, h)-plane, where one specifies $t = 0$ and x. These are the boundary conditions for the hodograph equations. Unfortunately, in most cases these boundary conditions turn out to be quite awkward so the hodograph solutions are not often used in gas and fluid dynamics. There are, however, some exceptional configurations when hodograph solutions are extremely valuable. A classical example: nonlinear shallow water waves on a sloping beach [28].

For simple waves (i.e. when $h = h(u)$), the hodograph transform is degenerate (the Jacobian $J = 0$) so the simple wave solutions are not captured by the hodograph method. Also, the Jacobian vanishes at the wave breaking point of the general solution, which corresponds to multi-valuedness of the solution.

Note that in the classical hodograph construction, it is essential that the number of independent variables coincides with the number of dependent variables. It turns out, however, that for a certain class of systems of hydrodynamic type, called semi-Hamiltonian systems, the hodograph transform can be generalised to the the number of components greater than two. The corresponding *generalised hodograph transformation* was introduced by Tsarev in 1985 and will be described in Section 2.5.2.

2.4 Beyond the wave breaking: discontinuous, viscous and dispersive shocks

As already was mentioned, the multi-valued behaviour beyond the breaking point is not physically acceptable so one needs to do one of the following:

(i) To retain the model equations (the Hopf equation or the SWE) but extend the class of admissible solutions to include discontinuous solutions (shocks)

or

(ii) To extend the mathematical model by including additional dissipative or dispersive terms to regularise the breaking singularities. The form of the regularising term(s) depends on the physical properties of the medium through which the wave propagates.

Below we briefly consider both outlined possibilities.

2.4.1 Discontinuous shocks

Let us consider the simple wave equation $\rho_t + c(\rho)\rho_x = 0$ in a conservative form

$$\partial_t \rho + \partial_x q = 0, \tag{2.38}$$

where $\rho = v$ and $q = Q(\rho) = \int c(\rho)d\rho$. The differential conservation equation (2.38) is usually derived from the integral form of some fundamental physical conservation law (like conservation of mass, momentum etc). Importantly, the integral conservation law admits a broader class of solutions than its differential consequence, in particular, one can derive solution in the form of a propagating discontinuity (a shock). A standard consideration of the balance of the "mass", $\int_{x_1}^{x_2} \rho dx$, through the surface of discontinuity leads to the following reformulation of the basic problem:

$$\rho_t + q_x = 0, \quad \textit{at points of continuity}, \tag{2.39}$$

$$-U[\rho] + [q] = 0, \quad \textit{at discontinuity points}. \tag{2.40}$$

where $[\cdot]$ denotes the jump across the discontinuity and $U(t) = \dot{s}(t)$ is the shock speed. Condition (2.40) is usually called "shock condition". There is a formal correspondence between the differential equation and the shock condition (2.40), namely,

$$\frac{\partial}{\partial t} \leftrightarrow -U[\cdot]\,, \quad \frac{\partial}{\partial x} \leftrightarrow [\cdot]\,. \tag{2.41}$$

Note that the shock condition can also be written as

$$U = \frac{q_2 - q_1}{\rho_2 - \rho_1} = \frac{Q(\rho_2) - Q(\rho_1)}{\rho_2 - \rho_1}, \quad where \;\; \rho_{1,2} \equiv \rho(s^{\pm}, t). \tag{2.42}$$

The direct association of a shock condition with a differential conservation law is not unique (e.g. two equivalent conservation laws $u_t + (u^2/2)_x = 0$ and $(u^2)_t + (2u^3/3)_x = 0$ would lead to different shock conditions). To derive a physically admissible shock condition one should use only the differential conservation law directly originating from an integral physical conservation law.

The simplest case when the wave breaking occurs is the decay of an initial discontinuity problem for the simple-wave equation:

$$\rho_t + c(\rho)\rho_x = 0, \qquad t > 0\,, \qquad -\infty < x < \infty, \tag{2.43}$$

$$t = 0: \quad \rho = \begin{cases} \rho_2, & if \quad x < 0 \\ \rho_1, & if \quad x > 0\,, \quad (\rho_2 > \rho_1) \end{cases} \tag{2.44}$$

with $c'(\rho) > 0$.

We have seen in Section 2.2.3 that the wave breaking of the step (2.44) will occur immediately at $t = 0$. The resulting discontinuous solution is

$$\rho(x,t) = \begin{cases} \rho_2, & if \quad x < Ut \\ \rho_1, & if \quad x > Ut\,, \end{cases} \tag{2.45}$$

where the shock velocity is

$$U = \frac{Q(\rho_2) - Q(\rho_1)}{\rho_2 - \rho_1}, \quad Q(\rho) = \int c(\rho) d\rho. \tag{2.46}$$

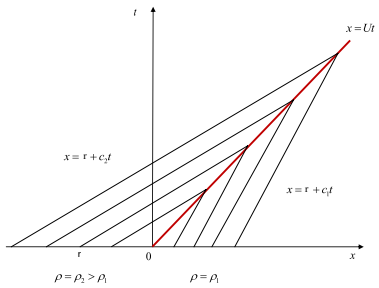

Figure 2.8: Characteristics' behaviour in the discontinuous solution to the Hopf equation.

For the particular case of the Hopf equation with $c(\rho) = \rho$, $Q(\rho) = \frac{1}{2}\rho^2$ we have

$$U = \frac{\rho_1 + \rho_2}{2}. \tag{2.47}$$

The characteristics' behaviour in the obtained discontinuous solution can be seen in Figure 2.8. Here $c_1 = c(\rho_1)$, $c_2 = c(\rho_2)$. Since $\rho_2 > \rho_1$ and $c'(\rho) > 0$ we have $c_2 > c_1$. The shock condition (2.40) should be complemented by the inequality

$$c_2 > U > c_1. \tag{2.48}$$

Condition (2.48) guarantees stability of a shock wave. In gas dynamics it is associated with the requirement that entropy of a gas must increase across the shock. Conditions of the type (2.48) are often called Lax's entropy conditions [31].

Consider now a *system* of hyperbolic differential conservation laws

$$\frac{\partial}{\partial t} f_i(x, t, \mathbf{u}) + \frac{\partial}{\partial x} g_i(x, t, \mathbf{u}) = 0\,, \quad i = 1, \ldots, n, \tag{2.49}$$

where $\mathbf{u} = (u_1, u_2, \ldots, u_n)$ are dependent variables, f_i are the conserved densities and g_i the corresponding fluxes. Assuming that system (2.49) is derived from integral equations for physical conserved quantities (mass, momentum, energy, etc.) one can introduce discontin-

uous solutions with the jump conditions across the shock

$$-U[f_i] + [g_i] = 0\,, \quad i = 1, 2, \ldots, n\,, \tag{2.50}$$

where U is the velocity of the shock. Often (especially in gas dynamics) conditions (2.50) are called the *Rankine-Hugoniot* shock conditions.

As an example, we derive the shock conditions for the hyperbolic SWE (2.1) describing dynamics of a *bore* – an analog of a shock in shallow water flows. Using physical conservation laws for "mass" $\int h dx$ and "momentum" $\int (hu) dx$ we obtain the hydrodynamic jump conditions across the bore in the form

$$\begin{aligned} -U[h] + [uh] &= 0, \\ -U[uh] + [hu^2 + \frac{1}{2}gh^2] &= 0. \end{aligned} \tag{2.51}$$

Eliminating U from the bore jump conditions one can find a restriction on admissible values of h and u at both sides of the bore

$$u_2 - u_1 = (h_2 - h_1)\sqrt{\frac{h_1 + h_2}{2h_1 h_2}}. \tag{2.52}$$

Note that this restriction does not arise for a shock wave in a single hydrodynamic conservation law. For the bore speed U we obtain

$$U = u_1 + h_2\sqrt{\frac{h_1 + h_2}{2h_1 h_2}}. \tag{2.53}$$

2.4.2 Regularised viscous shock waves

We now look at the second way of removing the multi-valued region in the breaking profile of the solution of the simple wave equation (2.10) – a *regulatisation* of the wave breaking singularity by taking into account higher order terms in the underlying physical model.

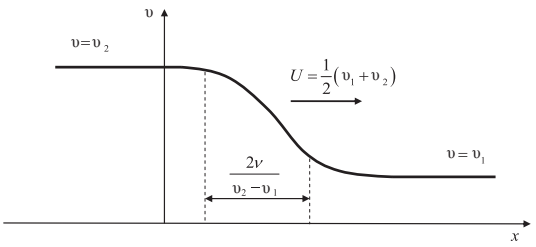

Figure 2.9: Viscous shock wave profile

Often these higher order terms describe dissipation in the medium due to viscosity. The simplest viscous correction to the Hopf equation is usually proportional to v_{xx} and the generic mathematical model describing the structure of viscous shocks is the famous Burgers' equation

$$v_t + vv_x + \nu v_{xx} = 0. \tag{2.54}$$

where $\nu > 0$ is a constant (viscosity coefficient). The solution of the Burgers' equation in the form of the travelling wave $v = v(\xi)$, where $\xi = x - Ut - x_0$, where U is the wave speed and x_0 is the initial phase, has the form of the so-called "Taylor's profile"

$$v(x,t) = v_1 + (v_2 - v_1)\frac{\exp\{-(v_2 - v_1)\xi/(2\nu)\}}{1 + \exp\{-(v_2 - v_1)\xi/(2\nu)\}}\,. \tag{2.55}$$

Solution (2.55) describes a smooth step transition connecting two constant states $v = v_2$ and $v = v_1$, $v_2 > v_1$. (see Figure 2.9) One can see that the transition profile (2.55):

- Propagates with the shock velocity $U = \frac{1}{2}(v_1 + v_2)$;
- Has the characteristic width $\Delta = \frac{2\nu}{v_2 - v_1}$, so $\Delta \to 0$ as $\nu \to 0$ for fixed $v_{1,2},\ v_1 \neq v_2$.

Hence the constructed exact particular solution of the Burgers' equation is consistent with the discontinuous shock wave theory and the viscous transition layer (2.55) just reveals the internal structure of the "discontinuity" in the classical dissipative shock wave.

We note that the general solution to the Burgers' equation is obtained using the famous Cole-Hopf transformation

$$v = -2\nu\frac{\phi_x}{\phi}, \tag{2.56}$$

which reduces the Burgers' equation (2.58) to the classical linear heat equation

$$\phi_t = \nu\phi_{xx}, \tag{2.57}$$

for which the general solution is well known.

2.4.3 Dispersive regularisation of a shock

In some media the effects of dissipation are negligibly small compared with the effect of dispersion. Resolution of the wave breaking singularities in such dispersion-dominated media is accompanied by the generation of nonlinear wavetrains called dispersive shock waves (DSWs). DSWs represent unsteady, expanding wave structures and have a distinctive spatial structure characterised by successive solitons forming at one of DSW's edges and transforming into a linear wave packet near the the opposite edge [16, 25]. Unlike the classical shock, the DSW has two different speeds associated with its propagation: the speeds of the trailing and the leading edges.

Physically, DSWs manifest themselves as undular bores on rivers (famous examples include the undular bore observed on the river Severn) and in density-stratified waters of coastal oceans, as collisionless shocks in rarefied plasmas and as nonlinear diffraction patterns in laser optics. Having been recognised for decades as a phenomenon of fundamental physical significance and playing for dispersive fluid flows the role analogous to that of viscous shocks in classical fluid dynamics, DSWs have gained special interest recently due to ground breaking experiments on Bose-Einstein condensates [2]. Furthermore, an optical analogue of superfluid DSWs realised in recent experiments [3] has made it possible to investigate nonlinear BEC phenomena in an all-optical setting providing further venue for experimental

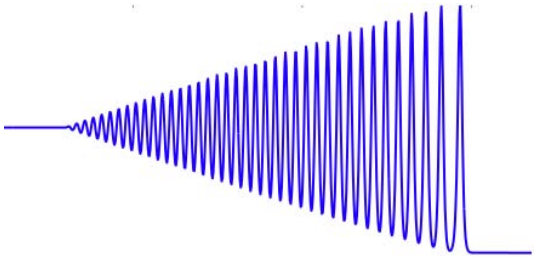

Figure 2.10: Oscillatory structure of dispersive shock wave in the KdV equation

studies of this universal physical phenomenon in its"pure" dissipationless form.

The simplest dispersive correction to the Hopf equation is proportional to v_{xxx} and the corresponding generic mathematical model describing the structure of DSWs in media with negative dispersion is the KdV equation

$$v_t + vv_x + v_{xxx} = 0. \tag{2.58}$$

A typical example of the DSW solution to the KdV equation is shown in Figure 2.10.

An analytical description of the DSW for the KdV equation (2.58) was for the first time constructed by Gurevich and Pitaevskii [17] using the Whitham method of slow modulations [16]. The main assumption in the theory of Gurevich and Pitaevskii was that the DSW can be *locally* described by the travelling wave solution of the KdV equation (i.e. is the cnoidal wave):

$$v(x,t) = \alpha - (\alpha - \beta)\mathrm{sn}^2\big(\sqrt{(\alpha-\gamma)/2}(x - ct), m\big), \tag{2.59}$$

where

$$c = \frac{1}{3}(\alpha + \beta + \gamma), \qquad m = \frac{\alpha - \beta}{\alpha - \gamma}. \tag{2.60}$$

Here α, β and γ are constant parameters (integrals of motion) and $0 \leq m \leq 1$ is the modulus. When $m = 0$, the cnoidal solution (2.59) becomes a vanishing amplitude linear wave; when $m = 1$ it transforms into the KdV soliton. If the parameters α, β and γ are allowed to

vary slowly, their x, t-evolution is governed by the Whitham modulation equations, obtained by averaging of three KdV conservation laws [16, 29]. In particular, the modulus m varies across the DSW from $m = 0$ at the trailing edge to $m = 1$ at the leading edge. Using the numerically established structure of a DSW, Gurevich and Pitaevskii formulated a special system of matching conditions for the KdV-Whitham system and found its similarity solution describing the variations of α, β and γ in the DSW forming as a result of the decay of an initial discontinuity $v(x, 0) = AH(-x)$, where A is a constant and $H(x)$ is the Heaviside step function. In particular, it follows from the Gurevich-Pitaevskii solution, that the DSW is confined to a uniformly expanding region $-At < x < \frac{2}{3}At$, and the soliton amplitude at the DSW leading edge is $a_s = 2A$. A detailed description of the Gurevich-Pitaevskii approach applied to the defocusing NLS equation will be presented later in the next Section but we mention here that the key to the the construction of the modulation solutions for both KdV and defocusing NLS equations is the existence of the Riemann invariants for the associated Whitham systems.

Since the pioneering Gurevich-Pitaevskii paper, there have been a significant number of research works studying formation and evolution of DSWs for the KdV equation (see e.g. [30] and references therein). One should separately mention the series of works by Lax, Levermore and Venakides [31, 32] on the zero dispersion limit of the KdV equation where they rigorously proved that the DSWs are indeed asymptotically described by the solutions of the KdV-Whitham equations.

2.4.3.1 Dispersive shock waves in Bose-Einstein condensates

One of the main examples of DSWs considered in the Thesis are relevant to the superfluid dynamics of Bose-Einstein condensates (BECs). Below we shall briefly outline some properties of BECs and present a list of some important recent experimental and theoretical works on the DSW dynamics in BECs

A BEC is a quantum fluid created by cooling weakly interacting boson gas to less than

one millionth of a degree above absolute zero. This state of matter was predicted by Einstein (1925) by generalising Bose's work on the statistical mechanics of photons to atoms. The work introduced the idea of BECs, the condensates modelled by Bose-Einstein statistics, which describes the statistical distribution of bosons (particles with integer spin) over the energy states in thermal equilibrium.

The first experimental realisation of the BEC was accomplished by Eric A. Cornell and Carl E. Wieman [33] and Wolfgang Ketterle [34] in 1995; for which they were awarded the Nobel Prize in Physics in 2001. The BEC was created by cooling rubidium atoms (Cornell and Wieman) and sodium atoms (Ketterle) to 20 nanoKelvin, i.e. $20\text{x}10^{-9}$ degrees above absolute zero - a temperature achieved using a combination of laser and evaporative cooling methods. At this temperature, very close to absolute zero, the constituent parts of the atom extend over a large area and are then free to flow between one another; thus each atom may occupy the same dimensional space and share the same energy state, thus becoming indistinguishable. In other words, the atoms coalesce into a single 'fluid' or 'cloud' known as the BEC, which some refer to as a superatom. The induced BEC dynamics provide an opportunity to conduct very subtle experiments where a number of macroscopic effects may be observed such as formation of bright and dark solitons, vortices and DSWs.

During the creation of the BEC, the atoms are held in place by a magnetic trap whose potential prevents the fluid from expanding. Once the BEC has been created, waves may be induced in several ways. The BEC can be made to move through different guides [35]. Laser beams can be used to create disturbances in the BEC. For instance, in the experiment by Cornell's JILA group [1] a 2D 'pancake' sample of a BEC was 'pierced' with a powerful laser beam leading to the formation of the so-called 'blast waves' [2] (see Figure 2.12). These blast waves were identified in [2] with circular DSWs using earlier analytical results of [19] on the 1D DSW dynamics in the defocusing NLS equation. A typical profile of the DSW solution to the 1D defocusing NLS equation is shown in Figure 2.11. One can see that, compared to the KdV dynamics (see Fig. 2.10), the DSW in the defocusing NLS dispersive hydrodynamics

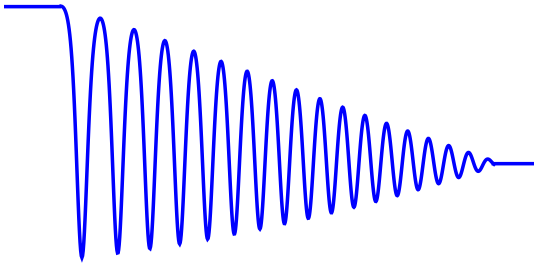

Figure 2.11: Oscillatory structure of right-propagating DSW in the defocusing NLS equation

has a 'reversed' structure with the *trailing dark soliton* and the leading linear wavepacket.

In a different series of experiments by Cornell's group [1], laser beams served as localised obstacles for BEC flows creating oblique DSWs confined to a Mach cone [24, 36] and linear waves located outside this cone [37], which can be interpreted as BEC 'ship-waves' [38]. The BEC can also be confined to an elongated trap such that the dynamics become effectively one-dimensional; then sweeping of a broad laser beam through the BEC has been found to be accompanied by the generation of a train of dark solitons [6] (see Figure 2.13). As was shown in [20], this soliton train effectively represents a DSW slowly propagating downstream the laser beam.

BEC represents a unique model 'laboratory' for the study of nonlinear waves in a theoretical sense since it is a superfluid (i.e. a purely conservative medium), where the dynamics are described very well by one of the canonical nonlinear wave equations, namely, an extended version of the NLS equation, called the Gross-Pitaevskii (GP) equation [39]. The GP equation is essentially a multi-dimensional NLS equation with an added external potential term. It reads

$$i\hbar\frac{\partial\psi}{\partial t} = -\frac{\hbar^2}{2m}\triangle\psi + V(\mathbf{r})\psi + g|\psi|^2\psi. \tag{2.61}$$

Here ψ is a complex field variable (the so-called order parameter, or condensate wave function), $\hbar$ is Planck's constant, g is an effective coupling constant ($g > 0$ corresponds to BEC with repulsive interactions between atoms and allows for the formation of dark solitons [25]; $g < 0$ corresponds to the attractive interactions and the formation of bright solitons [25, 39]),

and $V(\mathbf{r})$ is the potential of the external forces acting on the condensate, e.g. the confining trap potential or the potential acting on the BEC in the form of a submerged obstacle in the BEC.

An important feature of the GP equation is that its one-dimensional reduction coincides with the *integrable* nonlinear Schrödinger (NLS) equation with an added potential term

$$2i\psi_t + \psi_{xx} - 2g|\psi|^2\psi - 2V_0(x,t)\psi = 0. \tag{2.62}$$

As we already mentioned, there are experimental configurations where the one-dimensional BEC dynamics arise naturally; these configurations are also of significant theoretical interest for two mutually complementary reasons: (i) 1D dynamics often admits full analytical description and could provide important insights to the dynamics in the more complicated configurations; (ii) some non-trivial features of 1D BEC dynamics are absent in higher dimensions. The 1D setting will be the focus of the Thesis.

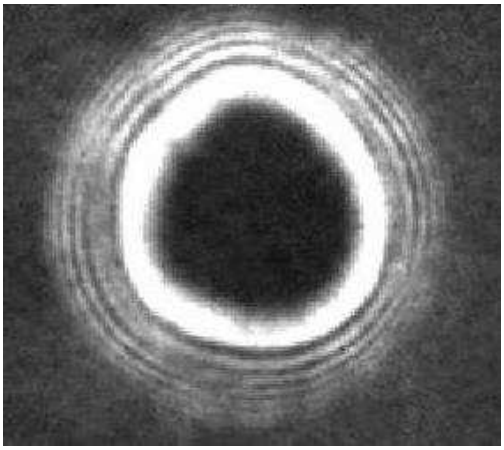

Figure 2.12: Experimental figure of a blast wave (circular DSW) in a defocusing BEC [2]. Reprinted figure with permission from M.A. Hoefer, M.J. Ablowitz, I. Coddington, E.A. Cornell, P. Engels and V. Schweikhard, Physical Review Letters, *Dispersive and classical shock waves in Bose-Einstein condensates and gas dynamics*, **74**, 023623, 2006. Copyright (2006) by the American Physical Society.

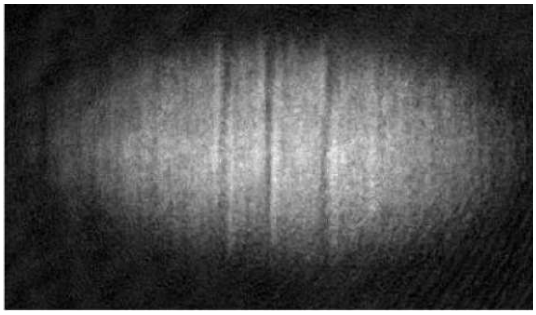

Figure 2.13: Experimental figure of the density distribution in a one-dimensional defocusing BEC after the laser beam has been swept through it [6]. Dark fringes are the signatures of dark solitons. Reprinted figure with permission from P. Engels and C. Atherton, Physical Review Letters, *Stationary and non-stationary fluid flow of a Bose-Einstein condensate through a penetrable barrier*, **99**, 160405, 2007. Copyright (2007) by the American Physical Society.†

Observations of DSWs in BEC have spurred a number of experiments in other media, where DSWs are a key feature and reveal important information about physical properties of the medium through which they propagate. From the mathematical point of view, the DSWs in BECs are of great interest as they provide a unique field of application of some rather refined mathematical theories connected, in particular, with integrable dynamics. In most other fluids DSWs come under the effect of dissipation, which leads to significant alterations

of the DSW properties (and the corresponding mathematical analysis) – to be discussed in the Subsection 2.4.4 below. As such, experimental studies of DSWs in the context of BECs have been met with considerable interest. Theoretical study of DSWs in BECs have also been of great interest for other areas of applied mathematics where the Whitham method [16] has been utilised. A sample of recent important experimental, analytical and numerical publications on DSW dynamics in BECs is summarised in Table (2.1).

Table 2.1: Summary of recent work on DSWs in BECs

Work carried out	Author(s)	Experimental (E)/ Analytical (A)/ Numerical (N)	Date	Reference
First experimental observations of blast waves in BECs reported.	Cornell	E	2004	[1]
First analytical description of 1D DSW in the BEC context.	Kamchatnov, Gammal, Kraenkel	A/N	2004	[40]
A method to generate DSWs in BEC using Feshbach resonances proposed.	Perez-Garcia, Konotop, Brazhnyi	A	2004	[41]
Blast waves experimentally observed in BECs identified with DSWs.	Hoefer, Ablowiz et.al	E/A	2006	[2]
Global regularisation to describe two-phase interactions of NLS DSWs.	Hoefer, Ablowitz	A	2007	[13]
DSW generation in BECs via one-dimensional interactions of degenerate RWs.	Hoefer, Engels, Chang	A/N	2008	[14]
Two-dimensional DSWs as oblique soliton trains in BEC flows past obstacles.	El, Kamchatnov	A	2006	[36]
Dark soliton generation in the quasi-1D BEC flow past penetrable barrier.	Engels, Atherton	E	2007	[6]
Generation of piston DSWs in BECs.	Hoefer, Ablowitz, Engels	A/N	2008	[42]
DSW generation in the transcritical BEC flow through a penetrable barrier.	Leszczyszyn et al.	A/N	2009	[20]
Stationary 2D DSW generation in hypersonic BEC flows past slender obstacles.	El et al	A/N	2009	[24]
Non-stationary 2D DSW generation in supersonic BEC flows past corners.	Hoefer and Ilan	A/N	2009	[43]

2.4.3.2 Dispersive shock waves in nonlinear optics

Nonlinear crystal optics is a branch of optics that describes the behaviour of light in nonlinear media, i.e. in media whose dielectric permittivity depends on the light intensity. This nonlinearity is typically only observed at very high light intensities. Nonlinear optics has

been a rapidly growing field in recent decades, as it has many uses: in lasers, telescopes and in fiber optics communication systems. A particular interest has been drawn to the properties of optical solitons due to their potential technological applications in the telecommunication technologies (see, e.g., [45, 46]). Different kinds of solitons have been observed in various nonlinear optical media and their behavior has been explained in the frameworks of such mathematical models as NLS and generalised nonlinear NLS equations for different dimensions and geometries, so that one can consider the properties of single solitons as well enough understood. The properties of optical DSWs have been far less explored. One of the first theoretical papers on optical DSWs [44] was devoted to a systematic study of 1D DSWs in optical fibers with application to transoceanic communication systems. This was done in the framework of the defocusing cubic NLS equation. The recent renewed interest to optical DSWs has been greatly stimulated by the possibility to reproduce, in all-optical settings, the results of very expensive BEC experiments. Indeed, an analogy between the propagation of light beams in nonlinear media and superfluid flow is well known and quite suggestive. Formally, it is based on a mathematical similarity of the equations for electromagnetic field evolution of light beams in paraxial approximation and GP equations for superfluid motion of BECs of dilute gases.

In the series of experiments [3] by J. Fleischer's Princeton group the BEC DSW dynamics have been quite accurately reproduced using the laser beam propagation through self-defocusing photorefractive crystals. Some experimental figures from this work can be seen in Figure 2.14. Photorefractive materials can be also used to store temporary, erasable holograms and are useful for holographic data storage [47]. The paraxial light beam propagation along z-axis through the photorefractive crystal is described by the NLS equation with saturable nonlinearity (the sNLS equation) [45, 48, 50]

$$2i\psi_t + \psi_{xx} - \frac{2|\psi|^2}{1+\gamma|\psi|^2}\psi = 0, \tag{2.63}$$

where $\psi(x,z)$ is the complex optical field envelope and γ is the saturation parameter. Pho-

torefractive optical solitons were first observed in the experiment [51] and the formation of photorefractive DSWs was first observed in [52] where the beam non-uniformities gave rise to the singularities which were resolved by DSWs. Another very interesting photorefractive DSW experiment was recently reported in [5], where the transcritical (resonant) generation of DSWs was observed, similar to the Engels-Atherton BEC experiment [6] discussed in the previous subsection. The results of this experiment were interpreted in [5] as nonlinear wave tunneling accompanied by the generation of transmitted and reflected DSWs.

To study the BEC effects using such an optical modelling it is important to quantify the effects of the optical saturation on the DSW formation and evolution since such a saturation is not present in BECs. For that purpose, the theory of DSWs in the sNLS equation is necessary. Unlike the cubic NLS equation (which can be obtained from equation (2.63) by setting $\gamma = 0$ in it), the sNLS equation (2.63) with $\gamma \neq 0$ is not integrable by the IST method and the associated Whitham modulation system does not possess Riemann invariants so that the analytical modulation solutions are very difficult (or even impossible) to obtain. Nevertheless, it was shown in [53–55] that in this case the main characteristics of the DSW can be found by using some general properties of the Whitham equations which remain present even when one deals with non-integrable dispersive-hydrodynamic equations. Some refer to this method as El's method [56] and it was used in [57] to construct an analytical description of DSWs in the framework of the sNLS equation (2.63). We shall refer to it as the dispersive shock fitting method. This method will be discussed in subsequent section (4.7) and used in Section 6 to describe the head-on interactions of the photorefractive DSWs and RWs.

A sample of recent important experimental, analytical and numerical publications on DSWs in nonlinear optical media is summarised in Table (2.2).

Table 2.2: Summary of previous work on optical DSWs

Work carried out	Author(s)	Date	Reference
Optical wave breaking was observed in the propagation of light through a nonlinear fibre.	Rothenberg, Grischkowsky	1989	[58]
Modulation theory of 1D optical DSWs in NRZ optical communication systems.	Kodama	1999	[44]
DSWs observed in photorefractive nonlinear optical crystals.	Wan, Jia, Fleischer	2007	[3]
Experimental observation of DSW in optical media with thermal nonlinearity.	Ghofraniha, Conti, Ruocco, Trillo	2007	[59]
Observation of DSWs in optical media with nonlocal nonlinearity.	Barsi, Wan, Sun, Fleischer	2007	[4]
Modulation theory of 1D DSWs in photorefractive materials.	El et. al	2007	[57]
Nonlinear optical wave tunnelling accompanied by the DSW generation (experiment).	Wan, Muenzel, Fleischer	2010	[5].

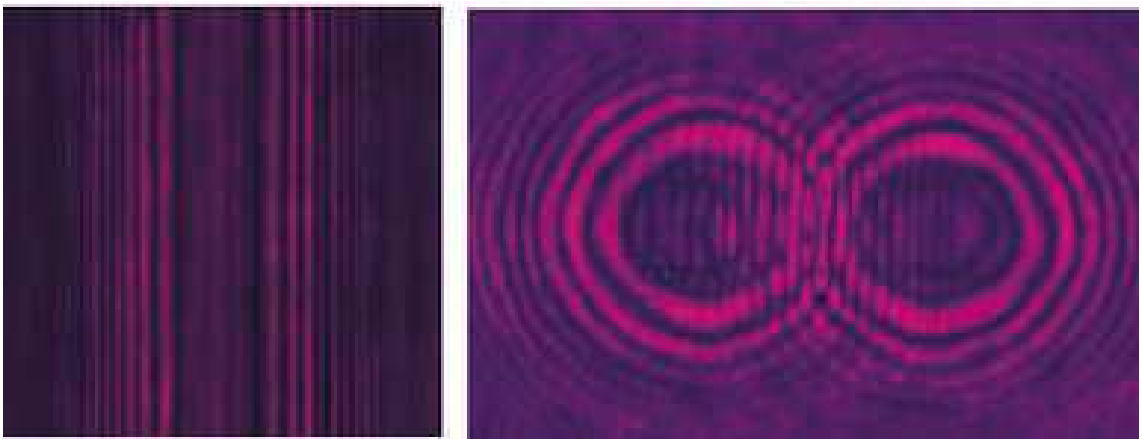

Figure 2.14: Optical experimental figures of two one-dimensional DSWs and two interacting two dimensional DSWs performed at Princeton University [3]. Permission obtained for reprint of figure.

2.4.4 Effects of weak dissipation on a dispersive shock wave

While our main concern in the Thesis will be with purely conservative, superfluid DSWs, for the completeness of the exposition we also briefly describe the combined effect of weak

dissipation and dispersion on the structure of a shock wave. Such dispersive-dissipative resolution of the wave breaking singularity is often modelled by the KdV-Burgers' (KdV-B) equation

$$u_t + uu_x + u_{xxx} = \nu u_{xx}, \tag{2.64}$$

where $0 < \nu \ll 1$.

We consider solutions of the KdV-B equation (2.15) with the boundary conditions at infinities

$$u \to \begin{cases} u_2 & x \to -\infty, \\ u_1 & x \to +\infty\,, \end{cases} \tag{2.65}$$

where $u_2 > u_1$. We shall look for a steady profile moving with constant velocity U, i.e. a travelling wave $u = u(\xi)$, where $\xi = x - Ut$. Then the KdV-B equation becomes an ODE,

$$-Uu_\xi + uu_\xi + u_{\xi\xi\xi} = \nu u_{\xi\xi}. \tag{2.66}$$

Integrating once we obtain an ODE for a nonlinear oscillator with damping

$$u_{\xi\xi} + u^2/2 - Uu + C = \nu u_\xi, \tag{2.67}$$

where U, C are found from boundary conditions (2.65) (assuming $u_\xi, u_{\xi\xi} \to 0$ as $|\xi| \to \infty$):

$$U = \frac{1}{2}(u_1 + u_2)\,, \quad C = \frac{1}{2}u_1 u_2\,, \tag{2.68}$$

i.e. the oscillatory solution moves as a whole with the classical shock speed.

The detailed phase plane analysis of the ODE (2.68) has been performed by Johnson in [60]. The main result of this analysis is the existence of the critical value ν_{cr} for the viscosity coefficient ν so that for $\nu < \nu_{cr}$ the solution has an oscillatory profile and exhibits a solitary wave at the leading edge while for $\nu > \nu_{cr}$ the solution is smooth, and for $\nu \gg 1$ it asymptotically transforms into the viscous shock Taylor's profile (2.55).

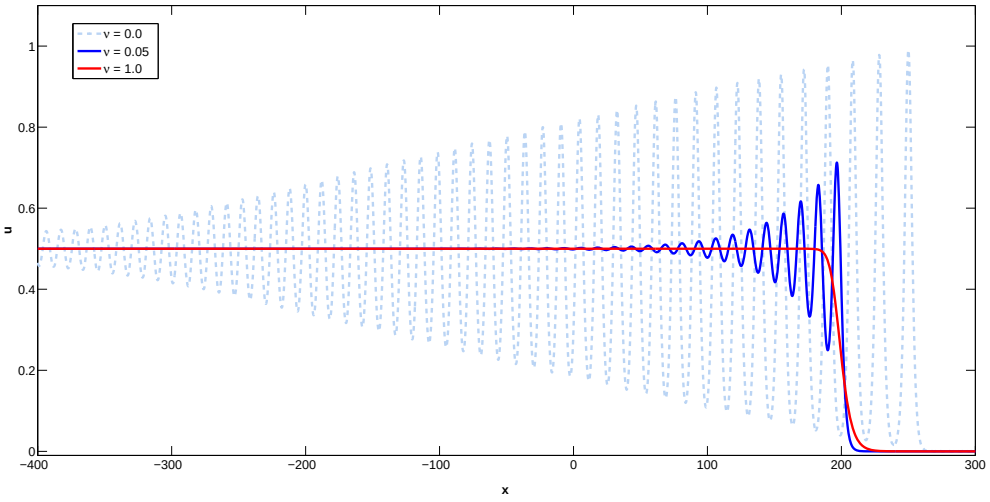

Figure 2.15: The comparison of the shock profiles for KdV-B equation for different values of the viscosity coefficient ν. Dashed line: $\nu = 0$, the conservative unsteady DSW of the KdV equation; Solid blue line: the oscillatory shock profile for $0 < \nu < \nu_{cr}$; Solid red line: smooth viscous shock profile for $\nu > \nu_{cr}$.

The comparison of KdV-B shock wave profiles for different values of the viscosity coefficient ν is shown in Figure 2.15. It should be stressed that, despite the fact that, similar to the 'pure' DSW in the KdV equation, the KdV-B shock for $\nu < \nu_{cr}$ has an oscillatory profile and exhibits a solitary wave at its leading edge, there are crucial differences between the two waves. Firstly, for $0 < \nu < \nu_{cr}$ the leading soliton amplitude is $a_s = 1.5A$ rather than $a_s = 2A$ for the KdV equation, where $A = u_2 - u_1$ is the jump across the shock. Most importantly, and in sharp contrast with the purely conservative DSW of the KdV equation, the KdV-B shock is a *steady* oscillatory structure propagating as a whole with a single *classical shock* speed and thus, has global properties of classical shocks rather than DSWs – see Figure 2.15.

2.5 Hyperbolic quasi-linear systems

Our previous analysis was restricted to a single Hopf (simple wave) equation and its dissipative and dispersive regularisations in the form of the Burgers', KdV, and KdV-B equations. All these equations describe uni-directional evolution of a single quantity. Generally, of

course, waves can propagate in both directions (in an appropriate reference system) and also there can be more than one physical quantity describing the system. This establishes our interest in multi-component quasi-linear systems of a general form

$$u_t^i + A_j^i(\mathbf{u}, x, t)u_x^j = 0\,, \quad i = 1, \ldots, N\,, \tag{2.69}$$

where $\mathbf{u}(x,t) = \{u^1, u^2, \cdots, u^N\} \in \mathbb{R}^N$, the eigenvalues of the $\mathbb{R}_{N\times N}$ matrix $\mathbf{A}(\mathbf{u}, x, t)$ are real and there are N linearly independent left eigenvectors.

A typical example is the classical shallow water system ($N = 2$), equation (2.1).

2.5.1 Characteristics and Riemann invariants

Riemann invariants and the corresponding characteristic velocities for the SWE were formally introduced in Section 2.1 (see (2.6 – 2.8)). In this Section we outline the connection of the Riemann invariant form of a hyperbolic system of hydrodynamic type with the theory of characteristics for the general case $N \geq 2$.

2.5.1.1 $N = 2$

We start with the systematic derivation of the Riemann invariant form (2.7) for the SWE (2.1). The SWE (2.1) contain information about the rate of change of h, u in different directions of the (x,t) plane. Let us now consider the linear combination

$$\{u_t + uu_x + h_x\} + m\{h_t + hu_x + uh_x\} = 0, \tag{2.70}$$

where m is determined by the condition that equation (2.70) assumes a uni-directional form, in which both quantities h and u are differentiated in the same direction:

$$\{u_t + vu_x\} + m\{h_t + vh_x\} = 0. \tag{2.71}$$

Now comparing equations (2.70) and (2.71) we find

$$u + mh = u + \frac{1}{m} = v, \tag{2.72}$$

which gives $m = \pm\frac{1}{\sqrt{h}}$ so that $v = v_\pm = u \pm \sqrt{h}$.

Setting these values in (2.71), we have

$$(\tfrac{1}{2}u \pm \sqrt{h})_t + (u \pm \sqrt{h})(\tfrac{1}{2}u \pm \sqrt{h})_x = 0. \tag{2.73}$$

The values $\lambda_\pm = u \pm 2h$, which remain constant along the respective characteristics $\frac{dx}{dt} = u \pm \sqrt{h}$, are called the Riemann invariants. The SWE in the Riemann form are given by diagonal system (2.7), where $V_\pm = u \pm \sqrt{h}$ are the characteristic velocities.

2.5.1.2 $N > 2$

To generalise the approach outlined in the previous subsection we consider an N-component quasi-linear system

$$u^i_t + A^i_j(\mathbf{u}, x, t)u^j_x = 0\,, \quad j = 1, \ldots, N\,, \tag{2.74}$$

(summation over repeating indices is assumed). Also, for simplicity we assume $A(\mathbf{u}, x, t) = A(\mathbf{u})$. We introduce a linear combination

$$l_i\{u^i_t + A^i_j(\mathbf{u})u^j_x\} = 0\,, \tag{2.75}$$

where $\mathbf{l} = \mathbf{l}(\mathbf{u})$ is some vector.

The PDE (2.75) assumes the characteristic form:

$$l_i\frac{du^i}{dt} = 0 \quad \text{on} \quad \frac{dx}{dt} = \lambda \tag{2.76}$$

$$\text{provided} \quad l_iA^i_j = \lambda l_j\,, \tag{2.77}$$

so that $\mathbf{l} = \mathbf{l}^{\{k\}}$ is the left eigenvector of the matrix A corresponding to the eigenvalue $\lambda = \lambda^k(\mathbf{u})$, where λ^k, $k = 1, 2, \ldots, N$ are the roots of the characteristic equation

$$|A_i^j - \lambda \delta_i^j| = 0. \tag{2.78}$$

System (2.74) is called hyperbolic if the eigenvectors $\mathbf{l}^{\{k\}}$ form a basis (i.e. if there are N linearly independent eigenvectors $\mathbf{l}^{\{k\}}$).

Each equation in the characteristic form (2.76) introduces its own linear combination of the derivatives $l_i du^i/dt$ (we omit the upper index $\{k\}$ for l_i). In some cases it is possible to find an integrating factor $\mu(\mathbf{u})$ such that

$$\mu l_i du^i = dr \tag{2.79}$$

where $r = r(\mathbf{u})$. Equation (2.79) is equivalent to the requirement that

$$\mu l_i = \tfrac{\partial r}{\partial u^i}, \quad i = 1, \ldots, N. \tag{2.80}$$

If $N = 2$ one can always find an equation for μ by cross-differentiating (2.80). If the system has two independent eigenvectors $\mathbf{l}^{\{k\}}$ (hyperbolicity), there are two integrating factors μ^k and two corresponding functions $r^1(\mathbf{u})$, $r^2(\mathbf{u})$. However, for $N > 2$ the system of equations for μ is overdetermined and, generally, inconsistent.

If it is possible to introduce r^k for each of N characteristic forms (2.76), then the system of characteristic equations becomes

$$\frac{dr^k}{dt} = 0 \quad on \quad \frac{dx}{dt} = V^k(\mathbf{r}), \tag{2.81}$$

where $V^k(\mathbf{r}) = \lambda^k(\mathbf{u}(\mathbf{r}))$ are the characteristic speeds. Equations (2.81) are equivalent to a diagonal system:

$$r_t^k + V^k(\mathbf{r}) r_x^k = 0, \quad k = 1, \ldots, N, \tag{2.82}$$

(no summation over k is assumed!). Thus r^k are the Riemann invariants. As we have seen, Riemann invariants always exist for hyperbolic hydrodynamic type systems of two equations but for $N > 2$ they can exist only in exceptional cases.

2.5.2 Generalised hodograph method

Earlier, in Section 2.3 we formulated the hodograph method for the integration of one-dimensional hydrodynamic type systems consisting of two equations. In 1985 S. Tsarev proposed the *Generalised Hodograph Method* [61], which, under certain conditions, is applicable to systems with $N > 2$. .

Theorem (Tsarev 1985): *The general local smooth non-constant, $r^i_x \neq 0$, solution of the diagonal hyperbolic hydrodynamic type system*

$$r^k_t + V^k(\mathbf{r})r^k_x = 0, \quad k = 1, \dots, N \tag{2.83}$$

has the form

$$x - V^i(\mathbf{r})t = W^i(\mathbf{r})\,, \tag{2.84}$$

where N functions $W^i(\mathbf{r})$ satisfy linear overdetermined system of PDEs

$$\frac{\partial_i W^j}{W^i - W^j} = \frac{\partial_i V^j}{V^i - V^j}\,, \quad i, j = 1, \dots, N, \quad i \neq j, \quad \partial_i \equiv \frac{\partial}{\partial r^i} \tag{2.85}$$

provided the characteristic velocities $V^i(\mathbf{r})$ satisfy the following set of semi-Hamiltonian conditions

$$\partial_j \frac{\partial_k V^i}{V^k - V^i} = \partial_k \frac{\partial_j V^i}{V^j - V^i}, \quad i \neq j \neq k\,. \tag{2.86}$$

This theorem establishes two conditions of *integrability* of a hydrodynamic type system: (i) existence of the full system of Riemann invariants; (ii) semi-Hamiltonian property (2.86).

2.6 Whitham method of slow modulations

The famous Inverse Scattering Transform (IST) method is a powerful tool to analyse behaviour of solutions to the so-called completely integrable systems such as the KdV equation, the cubic NLS equation and many other nonlinear wave equations. The IST method, however, has a number of restrictions to its applicability. Apart from the existence of the so-called Lax pair for the equation, it requires that initial conditions must decay sufficiently rapidly as $x \to \pm\infty$. Even within the boundaries of its formal applicability, the IST is not effective when one has to deal with solutions involving large number of solitons as the N-soliton solutions become increasingly difficult to analyse with growth of N. Since the DSW evolution involves the production of the increasing number of waves (including solitons) and also, the DSW solutions tend to different values as $x \to \pm\infty$, the IST (at least in its canonical form) cannot be applied to the DSW description, even in integrable systems.

In the 1960s, G. Whitham developed an asymptotic theory to treat the problems involving periodic travelling wave solutions (cnoidal waves (2.59) in the KdV equation context) rather than individual solitons. It is clear that the periodic travelling wave solution to a nonlinear dispersive wave equation as such, similar to the plane monochromatic wave in linear wave theory, does not transfer any 'information' and does not solve any reasonable class of IVPs (except for the problem with the initial data in the form of a cnoidal wave). However, one can try to construct a *modulated cnoidal wave*, a nonlinear analog of a linear wave packet, which can presumably be an asymptotic outcome in some class of the nonlinear dispersive IVPs.

The Whitham method is based on the scale separation and can be viewed as a fully nonlinear version of the multiple-scale perturbation theory, in which the 'fast' wave is a fully nonlinear periodic solution of the original dispersive equations while the 'slow' wave describes its modulation (variations of the mean, the amplitude, wavelength, frequency etc). The modulation equations can be obtained in several ways:

1. By using formal multiple scale expansions, in which the leading term is the periodic

travelling wave solution, parametrised by several 'integrals of motion' (constants of integration). Then the equations describing slow evolution of these integrals of motion arise as conditions of the absence of an unbounded growth in the first order approximation in the small parameter $\epsilon \ll 1$ defining the spatio-temporal scale separation (see [62]).

2. By applying an appropriate averaging technique (averaging of the conservation laws or an averaged variational principle) [16, 29].

Both approaches lead to the same system of modulation equations, which are usually referred to as the Whitham equations. Below we outline the original Whitham method [29] for obtaining the modulation equations by formal averaging of dispersive conservation laws over the family of periodic travelling wave solutions. This procedure is more convenient for our purposes than other techniques.

We consider a general *dispersive-hydrodynamic system* of the form

$$\mathbf{K}_{M,N}(\mathbf{U}; \partial_t \mathbf{U}, \partial_{tt}^2 \mathbf{U}, \dots; \partial_x \mathbf{U}, \partial_{xx}^2 \mathbf{U}, \dots) = 0, \tag{2.87}$$

where $\mathbf{K}$ is a vector operator and $\mathbf{U}(x,t)$ is a vector function and M, N are the orders of the system with respect to the $t-$ and $x-$ derivatives respectively. When calling the system (2.87) a dispersive hydrodynamic system we assume that

- it has real linear dispersion relation $\omega = \omega_0(k)$, and also $\omega_0''(k) \neq 0$;
- its dispersionless limit represents a hyperbolic system of hydrodynamic type (see Chapter 2) (the dispersionless limit is formally obtained by replacing $x \mapsto \epsilon x$, $t \mapsto \epsilon t$ and then letting $\epsilon \to 0$ while assuming boundedness of all derivatives of $\mathbf{U}(x,t)$ involved).

Examples of dispersive-hydrodynamic systems include the KdV equation, the defocusing NLS equation, the Boussinesq systems for shallow water waves and many others. On the other hand, say, the sine-Gordon equation $\phi_{tt} - \phi_{xx} + \sin\phi = 0$ is not a dispersive-hydrodynamic

system as it does not have a dispersionless limit in the form of a system of hydrodynamic type.

We assume that system (2.87) possesses a family of periodic travelling wave solutions of the form $\mathbf{U} = \mathbf{U}(\theta)$, where $\theta = kx - \omega t - \theta_0$, k being the wavenumber, ω the wave frequency and θ_0 is the initial phase. For such a family, the system (2.87) can be reduced to an ODE of the form

$$(kf_\theta)^2 = G(f), \tag{2.88}$$

for one of the components of the vector $\mathbf{U}$ in (2.87) so that

$$f = f(\theta), \quad \theta = kx - \omega t - \theta_0, \quad f(\theta + 2\pi) = f(\theta). \tag{2.89}$$

We assume that the function $G(f)$ has at least three real roots $f_1 < f_2 < f_3$ so that it can be represented as

$$G(f) = (f - f_1)(f - f_2)(f - f_3)H(f), \tag{2.90}$$

and $H(f)$ is a 'well-behaved' function, with any zeros lying outside the interval (f_1, f_3). This is a typical situation for dispersive-hydrodynamic systems. Let $H > 0$. Then the $2\pi-$periodic solution specified by (2.88) oscillates between the roots f_1 and f_2. From the condition of 2π -periodicity we find the wavenumber k as

$$k = \pi \left(\int_{f_1}^{f_2} \frac{df}{\sqrt{G(f)}} \right)^{-1}. \tag{2.91}$$

Then the wavelength is given by $L = 2\pi/k$. The travelling wave (2.89) is parametrised by N constants of integration $C_j, j = 1, \cdots, N$ (one can use any set of N independent integrals of motion as the parameters, i.e. the roots f_j themselves, the wavenumber, the frequency, the amplitude, the mean value, etc.)

Let $F(f)$ be some functional defined on the solutions of the equation (2.87). We introduce

the averaging over the family of the periodic travelling wave solutions, by

$$\begin{aligned}\overline{F}(C_1, C_2, \ldots, C_N) = \frac{1}{2\pi}\int_0^{2\pi} F(f(\theta); C_1, \ldots, C_N))d\theta \\ = \frac{k}{\pi}\int_{f_1}^{f_2} \frac{F(f)df}{\sqrt{G(f)}}.\end{aligned} \tag{2.92}$$

We now introduce the 'slow' variables $X = \epsilon x$ and $T = \epsilon t$, $\epsilon \ll 1$ and let $C_j = C_j(X, T)$ (i.e., in particular, $k = k(X, T)$, $\omega = \omega(X, T)$). Assume $F = F(\theta, C_1, C_2, \ldots, C_N)$ and express partial t- and x- derivatives as asymptotic expansions

$$\frac{\partial F}{\partial t} = -\omega\frac{dF}{d\theta} + \epsilon\frac{\partial F}{\partial T} + \mathcal{O}(\epsilon^2)\,, \qquad \frac{\partial F}{\partial x} = k\frac{dF}{d\theta} + \epsilon\frac{\partial F}{\partial X} + \mathcal{O}(\epsilon^2). \tag{2.93}$$

Then, in view of periodicity of F in θ, the averages of the derivatives (2.93) are calculated as

$$\overline{\frac{\partial}{\partial t}F} = \epsilon\frac{\partial}{\partial T}\overline{F} + \mathcal{O}(\epsilon^2)\,, \qquad \overline{\frac{\partial}{\partial x}F} = \epsilon\frac{\partial}{\partial X}\overline{F} + \mathcal{O}(\epsilon^2). \tag{2.94}$$

Assume that the dispersive hydrodynamics system (2.87) has at least N local independent conservation laws of the form

$$\partial_t P_j + \partial_x Q_j = 0, \qquad j = 1, \ldots, N\,, \tag{2.95}$$

where P_j and Q_j are some functions of the field variables $\mathbf{U}$ and their derivatives. Then applying the averaging (2.92) to the system of conservation laws (2.95) we obtain a closed system of evolution equations for $C_j(X, T)$ in the conservative form

$$\frac{\partial}{\partial T}\overline{P}_j(C_1, \ldots, C_N) + \frac{\partial}{\partial X}\overline{Q}_j(C_1, \ldots, C_N) = 0\,, \quad j = 1, \cdots N. \tag{2.96}$$

System (2.96) is called the Whitham modulation system. It is a system of hydrodynamic type and the order of the Whitham system is equal to the number of independent integrals of motion in the periodic solution. Generally, system (2.96) does not possess Riemann

invariants for $N > 2$ (see Section 2.5.1.2), however, in some special cases the Riemann invariants do exist due to very special properties of the original dispersive hydrodynamic system. This is the case, for instance, for the modulation systems associated with the KdV, NLS and other completely integrable equations. Moreover, the modulation systems obtained by averaging of nonlinear dispersive integrable (by IST) systems turn out to be semi-Hamiltonian (see (2.86)), i.e. integrable by the generalised hodograph transform (2.84), (2.85). Thus, integrability is inherited under the Whitham averaging.

There is a deep connection between the structure of the IST spectrum of the travelling wave solution and the Riemann invariants of the modulation system. For the KdV equation, this connection was discovered in a very general, multiphase form, by Flaschka, Forest and McLaughlin [49] and for the NLS equation by Forest and Lee [22] and Pavlov [23]. The method of finding Riemann invariants for integrable averaged systems used in the cited papers is based on the finite-gap integration theory (see e.g. [64]) and is quite technical. A simpler version of this method applicable to the single-phase averaging was developed by Kamchatnov [25].

One should emphasise that, unlike the IST method, the Whitham method of slow modulations can be applied to *non-integrable* dispersive-hydrodynamic systems. Of course, for such systems with $N > 2$ the modulation Riemann invariants do not exist.

Often, dispersion-hydrodynamic systems have more conservation laws than required for obtaining the modulation system (say, integrable systems like the KdV or NLS equations have infinite number of conservation laws). The important result is that all modulation systems obtained by the averaging of any N independent conservation laws are equivalent.

Apart from the averaged conservation laws (2.96) there is one more conservative modulation equation, which is consistent with the closed modulation system (2.96) but has no local dispersive conservation law as a counterpart before the averaging. This equation is the

conservation of waves law and has the form

$$k_T + \omega_X = 0\,. \tag{2.97}$$

Equation (2.97) naturally arises in the formal multiple-scale perturbation approach to the modulation theory (equivalent to the Whitham averaging) as the condition of the existence of slowly modulated single-phase solutions with the 'fast' phase $S(X,T)/\epsilon$ such that the local wavenumber and local frequency are defined as $k = S_X$ and $\omega = -S_T$ respectively (see e.g., [16, 62])). Then equation (2.97) follows from the equality of the mixed derivatives, $S_{XT} = S_{TX}$. We note that in the periodic solution $k = k(C_1, \ldots, C_N)$ and $\omega = \omega(C_1, \ldots, C_N)$ so the wave conservation law, being consistent with the full modulation system, can be used instead of any of the local averaged conservation laws.

The properties of the modulation system associated with the defocusing NLS equation will be discussed in Chapter 3.

Chapter 3

The defocusing NLS equation: periodic solutions and modulation system

The analysis of DSW dynamics in the superfluid flows is done in the framework of the nonlinear modulation (Whitham) system associated with the defocusing NLS equation. In this Chapter, we present the main results of the modulation theory of the defocusing NLS equation. Although majority of these results were obtained earlier, we give some new, more direct, proofs and derivations.

As outlined in Section 2.6, there are two main ingredients required for the derivation of the modulation system for a dispersive-hydrodynamic equation: (i) the family of periodic travelling wave solutions and (ii) a certain number of dispersive conservation laws. Then the Whitham modulation equations (2.96) are obtained by the averaging (2.92) of the conservation laws over the period of the travelling wave solution. The number of conservation laws required for the averaging is $N-1$, where N is the number of integrals of motion parametrising the periodic solution. The obtained modulation system is then closed by the wave conservation law (2.97).

The defocusing one-dimensional NLS equation is

$$2i\psi_t + \psi_{xx} - 2|\psi|^2\psi = 0, \tag{3.1}$$

where ψ is the complex field variable, x is the spatial coordinate and t is time. Generally, it describes evolution of an envelope (amplitude) of a small-amplitude modulated wavepacket propagating in a nonlinear medium with strong dispersion. It also describes evolution of the wave function of a rarefied BEC with repulsive inter-atomic interactions. Note, that in the BEC context there is no small-amplitude approximation in the derivation of (3.1), the small parameter being the BEC density (see [**?**]). At last, equation (3.1) describes spatial 'evolution' of the complex optical field in the propagation of a paraxial light beam through the nonlinear medium with the defocusing quadratic (Kerr) nonlinearity (see Section 2.4.3.2).

Let us begin by discussing some important basic properties of the NLS equation (3.1).

3.1 NLS equation: basic properties and travelling wave solutions

3.1.1 Basic properties

3.1.1.1 Dispersive-hydrodynamic form

By means of the so-called Madelung transformation [63]

$$\psi = \sqrt{\rho}\exp(i\int^x u(x',t)dx'), \tag{3.2}$$

we can conveniently represent the NLS equation in its dispersive-hydrodynamic form. Here $\rho > 0$ and u are real variables. By substituting (3.2) into the NLS equation (3.1) and

separating real and imaginary parts we obtain the system

$$\rho_t + (\rho u)_x = 0, \tag{3.3}$$

$$u_t + uu_x + \rho_x + (\frac{\rho_x^2}{8\rho^2} - \frac{\rho_{xx}}{4\rho})_x = 0. \tag{3.4}$$

Here the variable ρ has the meaning of the 'fluid' density and u the 'fluid' flow velocity. We note that in the BEC context ρ and u are actual condensate density and velocity. In the nonlinear optics context, ρ is the light intensity and u is the local value of the wave vector component transverse to the direction of the light beam propagation, in addition t is the spatial coordinate along the beam propagation direction. One can observe that equation (3.3) and the first three terms in equation (3.4) are the well-known SWE (2.1). The last term in equation (3.4) is the dispersive term. It describes the effects of the 'quantum pressure' in the BEC context and the spatial diffraction effects in nonlinear optics.

3.1.1.2 Dispersionless limit

To consider the dispersionless, long-wave limit of the NLS equation (3.3), (3.4) we introduce the change of variables $x' = \epsilon x$ and $t' = \epsilon t$, where $\epsilon \ll 1$. Then in new variables the hydrodynamic system (3.3) and (3.4) becomes

$$\begin{aligned} \rho_{t'} + (\rho u)_{x'} &= 0, \\ u_{t'} + uu_{x'} + \rho_{x'} + \epsilon^2(\frac{\rho_{x'}^2}{8\rho^2} - \frac{\rho_{x'x'}}{4\rho})_{x'} &= 0. \end{aligned} \tag{3.5}$$

Letting $\epsilon \to 0$ and assuming smoothness of $\rho(x,t)$ and $u(x,t)$ we obtain, on omitting primes, the NLS dispersionless limit equations

$$\rho_t + (\rho u)_x = 0, \quad u_t + uu_x + \rho_x = 0, \tag{3.6}$$

which are nothing but the SWE (2.1) with density ρ playing the role of total depth h. As shown in Section 2.1, equations (3.5) can be represented in the Riemann invariant form (2.7) with Riemann invariants

$$\lambda_{\pm} = \tfrac{1}{2}u \pm \sqrt{\rho} \tag{3.7}$$

and characteristic velocities (2.8).

For sufficiently smooth initial conditions one can generally expect that the evolution (3.6) would lead to the solution profile steepening and then to the wave breaking. In the vicinity of the breaking point, one cannot ignore the dispersive term so that the dispersive resolution of the wave breaking singularity results in the generation of a nonlinear wavetrain – a DSW – as was outlined in Chapter 2.

3.1.1.3 Linear dispersion relation

Substituting $\rho = \rho_0 + \rho_1 \exp(i(kx - \omega t))$ and $u = u_0 + u_1 \exp(i(kx - \omega t))$, where $\rho_1 \ll \rho_0$ and $u_1 \ll u_0$, into the system (3.3), (3.4) and linearising with respect to ρ_1, u_1 we obtain the relationship between frequency ω and the wavenumber k:

$$\omega = ku_0 \pm k\sqrt{\rho_0 + \tfrac{1}{4}k^2}. \tag{3.8}$$

Equation (3.8) is the dispersion relation for the defocusing NLS equation (the spectrum of the so-called Bogolyubov modes in the BEC context). The two signs in equation (3.8) correspond to the two directions in which the waves can propagate relative to the background flow u_0. One can readily see that $\omega'' > 0$ (positive dispersion) so the small-amplitude long waves will propagate faster than small-amplitude short waves.

3.1.1.4 Conservation laws

Being a completely integrable equation, the NLS equation (3.1) exhibits an infinite number of conservation laws of the form

$$\partial_t P_j + \partial_x Q_j = 0. \tag{3.9}$$

As we shall see, the single-phase periodic NLS travelling wave solution is parametrised by four independent constants. Therefore, formally, we shall need only three NLS conservation laws for the Whitham averaging (the fourth equation will be the wave conservation law (2.97)).

The first conservation law corresponds to the mass, the second to the momentum and the third to energy conservation:

$$\partial_t \rho + \partial_x(\rho u) = 0, \tag{3.10}$$

$$\partial_t(\rho u) + \partial_x(u^2\rho + \tfrac{1}{2}\rho^2 + \frac{\rho_x^2}{8\rho} - \frac{\rho_{xx}}{4} + \frac{\rho_x^2}{8\rho}) = 0, \tag{3.11}$$

$$\partial_t(\rho u^2 + \tfrac{1}{2}\rho^2 + \frac{\rho_x^2}{8\rho}) + \partial_x(\rho u^3 + 2\rho^2 u + \frac{\rho_x^2 u}{8\rho}) = 0. \tag{3.12}$$

3.1.2 Travelling wave solution

We shall seek the periodic travelling wave solution for the NLS equation (3.1) in the form:

$$\psi(\theta) = A(\theta)\exp\left(i\phi(\theta)\right), \quad \theta = x - ct, \tag{3.13}$$

where $c = \omega/k$ is the phase velocity. Applying this ansatz and separating real and imaginary parts, we obtain

$$-cA' + A'\phi' + \frac{A\phi''}{2} = 0, \tag{3.14}$$

$$Ac\phi' + \tfrac{1}{2}A'' - \tfrac{1}{2}A\phi'^2 - A^3 = 0. \tag{3.15}$$

Integrating the first equation we obtain

$$\phi' = c - \frac{2c_1}{A^2}, \tag{3.16}$$

where c_1 is a constant of integration.

Substituting (3.16) into equation (3.15), the system is reduced to

$$Ac^2 + A'' - \frac{4c_1^2}{A^3} - 2A^3 = 0. \tag{3.17}$$

Multiplying by A' and integrating, we obtain

$$-A^4 + c^2A^2 + A'^2 + \frac{4c_1^2}{A^2} + c_2 = 0, \tag{3.18}$$

where c_2 is the second integration constant.

At this point it is convenient to introduce $\rho = A^2$ and $u = \phi'$, which is consistent with the hydrodynamic transformation (3.2). Then equation (3.18) becomes

$$\rho'^2 = 4(\rho^3 - c^2\rho^2 - 4c_1^2 - c_2\rho) \equiv Q(\rho), \tag{3.19}$$

and instead of (3.16) we have

$$u = c - \frac{2c_1}{\rho} \tag{3.20}$$

Equation (3.19) describes motion of a 'particle' in the potential $-Q(\rho)$, where $\rho > 0$ is the 'coordinate' of the 'particle'. A periodic motion takes place when the function $Q(\rho)$ has three real roots $0 < e_1 < e_2 < e_3$, then the particle oscillates between e_1 and e_2. In Figure (3.1), three typical configurations of $Q(\rho)$ are shown corresponding to a general nonlinear periodic wave (solid line – three distinct roots e_1, e_2, e_3), linear wave of infinitesimally small

amplitude (dashed line – double root $e_1 = e_2$) and a (dark) soliton (dash-dotted line – double root $e_2 = e_3$). Introducing the roots $0 < e_1 < e_2 < e_3$ of the polynomial $Q(\rho)$ we represent equation (3.19) in the form

$$\rho'^2 = 4(\rho - e_1)(\rho - e_2)(\rho - e_3). \tag{3.21}$$

Thus we have the relationships between the parameters in (3.19)and the roots of the polynomial:

$$c_1^2 = \tfrac{1}{4} e_1 e_2 e_3 \,, \qquad c_2 = e_1 e_2 + e_1 e_3 + e_2 e_3. \tag{3.22}$$

Note that we do not present the relationship for the phase speed $c(e_1, e_2, e_3)$ as, due to the invariance of the NLS equation under the transformation

$$\psi(x,t) \to \exp(-i\tilde{c}(x - \tfrac{1}{2}\tilde{c}t))\psi(x - \tilde{c}t, t), \tag{3.23}$$

the phase speed c can be taken as the fourth arbitrary constant ($\tilde{c} \to c$) along with e_1, e_2, e_3. Equation (3.21) has the well-known integral in terms of the Jacobi elliptic function sn (see, e.g. [65])

$$\rho(x,t) = e_1 + (e_2 - e_1)\mathrm{sn}^2(\sqrt{e_3 - e_1}(x - ct - \theta_0), m), \tag{3.24}$$

where θ_0 is an arbitrary initial phase and the modulus

$$m = \frac{e_2 - e_1}{e_3 - e_1} \,, \qquad 0 \le m \le 1 \,. \tag{3.25}$$

The solution (3.24) is an analog of the famous cnoidal wave solution (as a matter of fact (3.25) can be re-written in terms of Jacobi elliptic *cn* function) so we shall use this term for the solution (3.24) as well.

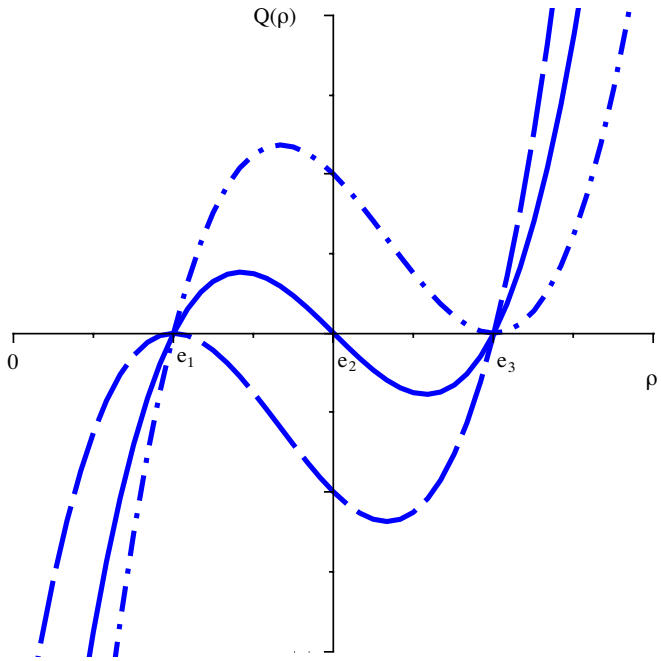

Figure 3.1: Plot of the 'potential' function $Q(\rho)$. Solid line – periodic nonlinear oscillations, has three roots e_1, e_2, e_3. Dashed curve corresponding to the linear (harmonic) limit has the double root $e_2 = e_1$. Dash-dotted curve corresponding to the soliton configuration has has the double root $e_2 = e_3$.

The formula (3.20) for the hydrodynamic velocity can be rewritten in the form

$$u(x,t) = c - \sigma \frac{\sqrt{e_1 e_2 e_3}}{\rho}, \tag{3.26}$$

where $\sigma = \pm 1$; $\sigma = 1$ corresponds to the waves propagating to the right and $\sigma = -1$ to the left propagating waves.

Thus, the travelling wave solution to the defocusing NLS equation is parametrised by four independent constants (integrals of motion) e_1, e_2, e_3 and c. The fifth arbitrary constant θ_0 represents the phase shift and will not affect the subsequent modulation analysis, which is based on the averaging over the period. However, we will show that in some modulation solutions this parameter plays an important role and can be represented as a function of the 'basic' four parameters e_1, e_2, e_3 and c (or some other equivalent set of their independent combinations).

The amplitude of the travelling wave $a = e_2 - e_1$. The wavelength L is defined as

$$L = \int_0^L d\theta = 2\int_{e_1}^{e_2} \frac{d\rho}{\sqrt{Q(\rho)}} = 2\int_{e_1}^{e_2} \frac{d\rho}{\sqrt{4(\rho-e_1)(e_2-\rho)(e_3-\rho)}} = \frac{2}{\sqrt{(e_3-e_1)}}K(m), \tag{3.27}$$

where $K(m)$ is the complete elliptic integral of the first kind.

We present expressions for the averaged density and velocity in the periodic solution (3.24), (3.26). We introduce the averaging of a functional $F(\rho(x,t))$ over the period of the NLS cnoidal wave (3.24) by (see (2.92))

$$\overline{F}(e_1,e_2,e_3,c) = \frac{1}{2\pi}\int_0^{2\pi} F(\rho(\theta);e_1,e_2,e_3,c))d\theta = \frac{k}{\pi}\int_{e_1}^{e_2} \frac{F(\rho)d\rho}{\sqrt{(\rho-e_1)(e_2-\rho)(e_3-\rho)}}, \tag{3.28}$$

where $k = \frac{2\pi}{L}$. Then

$$\bar{\rho} = e_3^2 - (e_3-e_1)^2\frac{\mathrm{E}(m)}{\mathrm{K}(m)}, \qquad \bar{u} = c + \frac{e_2e_1}{e_3}\Pi_1\big(\frac{(e_3^2-e_1^2)}{e_3^2}, m\big)/\mathrm{K}(m), \tag{3.29}$$

where $E(m)$ and $\Pi_1(\nu,m)$ are the complete elliptic integrals of the second and third kind respectively. For the averaged momentum $\overline{\rho u}$ we have

$$\overline{\rho u} = \bar{\rho}c - \sigma\sqrt{e_1e_2e_3}. \tag{3.30}$$

The quantities (3.29), (3.30) will become the important physical characteristics of the oscillatory flow in the DSW.

There are two important limiting cases of the cnoidal wave solution (3.24): the linear wave and the soliton.

Linear (harmonic) limit, $m \to 0$.

The linear limit is achieved by letting $m \to 0$ (i.e. the vanishing amplitude $a = e_2 - e_1 \to 0$) in the travelling wave solution. For $m \ll 1$ we have an asymptotic representation

$$\rho(x,t) \simeq e_1 + \frac{e_2 - e_1}{2} \cos\left(2\sqrt{e_3 - e_1}(x - ct)\right). \tag{3.31}$$

Equation (3.31) describes a linear periodic wave propagating on the background $\rho = \rho_0 = e_1 = e_2$. Passing to the linear limit in (3.27) we get for the wavenumber $k = 2\pi/L = \sqrt{e_3 - e_1} = \sqrt{e_3 - \rho_0}$. Also from (3.26) we have for the phase speed $c = u_0 + \sigma\sqrt{e_3}$, where u_0 is the background velocity ($u \to u_0$ as $a \to 0$). Then, taking into the account that $c = \omega/k$ we readily recover the defocusing NLS equation linear dispersion relation (3.8).

Soliton limit, $m \to 1$.

The soliton solution is obtained when $m \to 1$, i.e. $e_2 \to e_3$ (i.e. $k \to 0$). In this, infinite-wavelength limit, we obtain from (3.25)

$$\rho(x,t) = e_3 - \frac{e_3 - e_1}{\cosh^2\left(\sqrt{e_3 - e_1}(x - ct)\right)}. \tag{3.32}$$

This describes the 'dark' (or 'grey') soliton propagating on non-zero background $\rho \to e_3 = \rho_0$ as $|x| \to \infty$. The soliton amplitude is given by $a = e_3 - e_1$. Considering (3.26) at $|x| \to \infty$ and assuming $\rho \to \rho_0$, $u \to u_0$ as $|x| \to \infty$ we obtain the relationship

$$c = u_0 + \sigma\sqrt{(\rho_0 - a)}, \tag{3.33}$$

connecting the soliton speed c with its amplitude a and the background flow ρ_0, u_0. This relationship can be viewed as a defocusing NLS soliton 'dispersion relation'.

3.2 NLS-Whitham equations

Allowing the parameters e_1, e_2, e_3, c of the travelling wave solution (3.24) to be slowly varying functions of x and t, one can obtain, via the averaging or direct multiple-scales perturbation procedure, a modulated nonlinear periodic wave where the evolution of e_1, e_2, e_3, c is governed by the NLS-Whitham modulation equations. [22, 23]. The general description of the Whitham method was presented in Section 2.6.

3.2.1 Averaged conservation laws

According to the Whitham prescription [16], to derive the modulation system for e_1, e_2, e_3, c one should average (3.28) three NLS conservation laws (3.10) – (3.12) over the period of the travelling wave solution (3.24) and close the system by the wave number conservation law (2.97). As a result we obtain the NLS-Whitham system in the form

$$\partial_t \overline{u} + \partial_x(\overline{\rho u}) = 0. \tag{3.34}$$

$$\partial_t(\overline{\rho u}) + \partial_x(\overline{u^2\rho + \tfrac{1}{2}\rho^2 + \frac{\rho_x^2}{8\rho} - \frac{\rho_{xx}}{4} + \frac{\rho_x^2}{8\rho}}) = 0. \tag{3.35}$$

$$\partial_t(\overline{\rho u^2 + \tfrac{1}{2}\rho^2 + \frac{\rho_x^2}{8\rho}}) + \partial_x(\overline{\rho u^3 + 2\rho^2 u + \frac{\rho_x^2 u}{8\rho}}) = 0. \tag{3.36}$$

$$\partial_t k + \partial_x(kc) = 0, \tag{3.37}$$

where all dependent variables are expressed in terms of four 'natural' modulation parameters $e_1(x,t), e_2(x,t), e_3(x,t)$ and $c(x,t)$. Note, that we did not formally introduce new 'slow' independent variables $X = \epsilon x$ $T = \epsilon t$, $\epsilon \ll 1$ in the modulation system (3.34) – (3.37), instead, from now on we shall use the same notations x, t for the independent variables in the modulation system simply assuming that the dependent modulation variables vary on a much larger spatio-temporal scale than the typical period and the wavelength of the travelling wave solution.

3.2.2 Riemann invariant representation

System (3.34) – (3.37) for $e_1(x,t), e_2(x,t), e_3(x,t)$ and $c(x,t)$ is a system of hydrodynamic type with a very complicated coefficient matrix (one can see explicit expressions (3.29) and (3.30) for some of the *simplest* averages involved), and no apparent structure. This makes a direct analytical integration of this system a very difficult task. However, it was shown in [22] and [23] that, by introducing new dependent variables $\lambda_1 \le \lambda_2 \le \lambda_3 \le \lambda_4$ by relationships

$$\begin{aligned} e_1 &= \tfrac{1}{4}(\lambda_1 - \lambda_2 - \lambda_3 + \lambda_4)^2, \\ e_2 &= \tfrac{1}{4}(\lambda_1 - \lambda_2 + \lambda_3 - \lambda_4)^2, \\ e_3 &= \tfrac{1}{4}(\lambda_1 + \lambda_2 - \lambda_3 - \lambda_4)^2, \\ c &= \tfrac{1}{2}(\lambda_1 + \lambda_2 + \lambda_3 + \lambda_4), \end{aligned} \tag{3.38}$$

the modulation system (3.34) – (3.37) reduces to the diagonal Riemann form

$$\frac{\partial \lambda_i}{\partial t} + V_i(\lambda_1, \lambda_2, \lambda_3, \lambda_4)\frac{\partial \lambda_i}{\partial x} = 0, \quad i = 1, 2, 3, 4, \tag{3.39}$$

where $\lambda_1, \lambda_2, \lambda_3, \lambda_4$ are the Riemann invariants and the characteristic velocities V_i can be computed using the universal formula [66]

$$V_i = (1 - \frac{1}{L}\ln L)\partial_i c, \tag{3.40}$$

where $\partial_i \equiv \frac{\partial}{\partial \lambda_i}$ and the wavelength L defined by (3.27), is expressed in terms of the Riemann invariants λ_i (3.38) by

$$\begin{aligned} L(\boldsymbol{\lambda}) &= \int_{\lambda_3}^{\lambda_4} \frac{d\lambda}{\sqrt{(\lambda - \lambda_1)(\lambda - \lambda_2)(\lambda - \lambda_3)(\lambda_4 - \lambda)}} \\ &= \int_{\lambda_1}^{\lambda_2} \frac{d\lambda}{\sqrt{(\lambda - \lambda_1)(\lambda_2 - \lambda)(\lambda_3 - \lambda)(\lambda_4 - \lambda)}} \\ &= \frac{2\mathrm{K}(m)}{\sqrt{(\lambda_4 - \lambda_2)(\lambda_3 - \lambda_1)}} > 0, \quad i = 1, 2, 3, 4, \end{aligned} \tag{3.41}$$

where the modulus

$$m = \frac{(\lambda_2 - \lambda_1)(\lambda_4 - \lambda_3)}{(\lambda_4 - \lambda_2)(\lambda_3 - \lambda_1)}. \tag{3.42}$$

The phase velocity $c(\boldsymbol{\lambda})$ is given by (3.38).

The universal 'potential' representation (3.40) for the characteristic velocities is obtained by considering the wave conservation law (3.37) as a consequence of the closed modulation system in the Riemann form (3.39). Indeed, substituting $k = k(\boldsymbol{\lambda})$, $c = c(\boldsymbol{\lambda})$ into (3.37), and using (3.39) to express $\partial_t \lambda_i = -V_i(\boldsymbol{\lambda})\partial_x \lambda_i$ we obtain

$$\sum_{i=1}^{4} \left[-V_i \frac{\partial k}{\partial \lambda_i} + (\frac{\partial k}{\partial \lambda_i} c + k \frac{\partial c}{\partial \lambda_i}) \right] \frac{\partial \lambda_i}{\partial x} = 0. \tag{3.43}$$

Since the derivatives $\partial \lambda_i / \partial x$ are independent, each term in the square brackets in (3.43) must vanish, which yields representation (3.40) on using that $k = 2\pi/L$.

Substituting explicit expressions (3.41), (3.38) for $L(\boldsymbol{\lambda})$ and $c(\boldsymbol{\lambda})$ respectively we obtain

$$\begin{aligned}
V_1(\lambda_1, \lambda_2, \lambda_3, \lambda_4) &= \tfrac{1}{2} \sum \lambda_i - \frac{(\lambda_4 - \lambda_1)(\lambda_2 - \lambda_1)\mathrm{K}(m)}{(\lambda_4 - \lambda_1)\mathrm{K}(m) - (\lambda_4 - \lambda_2)\mathrm{E}(m)}, \\
V_2(\lambda_1, \lambda_2, \lambda_3, \lambda_4) &= \tfrac{1}{2} \sum \lambda_i + \frac{(\lambda_3 - \lambda_2)(\lambda_2 - \lambda_1)\mathrm{K}(m)}{(\lambda_3 - \lambda_2)\mathrm{K}(m) - (\lambda_3 - \lambda_1)\mathrm{E}(m)}, \\
V_3(\lambda_1, \lambda_2, \lambda_3, \lambda_4) &= \tfrac{1}{2} \sum \lambda_i - \frac{(\lambda_4 - \lambda_3)(\lambda_3 - \lambda_2)\mathrm{K}(m)}{(\lambda_3 - \lambda_2)\mathrm{K}(m) - (\lambda_4 - \lambda_2)\mathrm{E}(m)}, \\
V_4(\lambda_1, \lambda_2, \lambda_3, \lambda_4) &= \tfrac{1}{2} \sum \lambda_i + \frac{(\lambda_4 - \lambda_3)(\lambda_4 - \lambda_1)\mathrm{K}(m)}{(\lambda_4 - \lambda_1)\mathrm{K}(m) - (\lambda_3 - \lambda_1)\mathrm{E}(m)},
\end{aligned} \tag{3.44}$$

where $\mathrm{E}(m)$ is the complete elliptic integral of the second kind.

3.2.2.1 Properties of the NLS-Whitham system

Below we list some important properties of the NLS-Whitham system, which will be used in the DSW analysis of the Thesis.

- **Hyperbolicity**. The Riemann invariants λ_i defined by (3.38) are real. It then follows from (3.44) that the characteristic velocities (3.44) are always real and distinct as long as the Riemann invariants do not coincide. One can also prove the existence of four independent left eigenvectors if for the case of multiple values of the Riemann invariants. So system (3.39) is hyperbolic.

- **Genuine nonlinearity**. Differentiating (3.40)

$$\partial_i V_i = \frac{L}{2(\partial_i L)^2}\partial_{ii}^2 L, \tag{3.45}$$

and using the integral representations of L (3.27), one can deduce that $\partial_{ii}^2 L > 0$ for all i, which then immediately implies

$$\partial_i V_i > 0 \quad for\ all\ i, \tag{3.46}$$

so the NLS-Whitham system (3.39) and (3.44) is genuinely nonlinear [67].

- **Characteristic velocity ordering**. Using (3.40) and the integral representations (3.27) by direct calculation

$$i > j \quad implies \quad V_i > V_j. \tag{3.47}$$

Thus, the ordering $\lambda_1 \leq \lambda_2 \leq \lambda_3 \leq \lambda_4$ of the Riemann invariants implies a similar ordering $V_1 \leq V_2 \leq V_3 \leq V_4$ for the characteristic velocities.

- **Integrability.** Using the 'potential' representation (3.40) for the characteristic velocities it is not difficult to show (see [66]) that the relationships (2.86) are identically satisfied, that is the NLS-Whitham system is semi-Hamiltonian, i.e. integrable by the generalised hodograph transform (see Section 2.5.2).

We note that properties (3.46) and (3.47) were established in [44, 68] using finite-gap integration framework for the derivation of the Whitham equations.

Now we consider the soliton and harmonic limits for the NLS-Whitham system following the earlier consideration of these limits for the periodic wave.

Soliton limit, $m = 1$.

In this limit $\lambda_2 = \lambda_3$, so we have

$$V_2 = V_3 = \tfrac{1}{2}(\lambda_1 + 2\lambda_2 + \lambda_4). \tag{3.48}$$

This is nothing but the dark soliton velocity (see formula (3.55) below). The remaining two characteristic velocities become

$$V_1 = \tfrac{3}{2}\lambda_1 + \tfrac{1}{2}\lambda_4, \quad V_4 = \tfrac{3}{2}\lambda_4 + \tfrac{1}{2}\lambda_1. \tag{3.49}$$

One can see that V_1 and V_4 coincide with the characteristic velocities of the SWE (the dispersionless limit of the NLS equation) (2.8) where $\lambda_1 = \lambda_-$ and $\lambda_4 = \lambda_+$.

Linear (harmonic) limit, $m = 0$

The harmonic limit $m = 0$ can be achieved in two different ways: $\lambda_2 = \lambda_1$ or $\lambda_3 = \lambda_4$ (see (3.42)).

When $\lambda_3 = \lambda_4$:

$$\begin{gathered} V_3 = V_4 = \lambda_4 + \tfrac{1}{2}(\lambda_1 + \lambda_2) + \frac{2(\lambda_4 - \lambda_2)(\lambda_4 - \lambda_1)}{2\lambda_4 - \lambda_2 - \lambda_1}, \\ V_1 = \tfrac{3}{2}\lambda_1 + \tfrac{1}{2}\lambda_2, \quad V_2 = \tfrac{3}{2}\lambda_2 + \tfrac{1}{2}\lambda_1. \end{gathered} \tag{3.50}$$

When $\lambda_2 = \lambda_1$:

$$V_2 = V_1 = \lambda_1 + \tfrac{1}{2}(\lambda_3 + \lambda_4) + \frac{2(\lambda_3 - \lambda_1)(\lambda_4 - \lambda_1)}{2\lambda_1 - \lambda_3 - \lambda_4}, \qquad V_3 = \tfrac{3}{2}\lambda_3 + \tfrac{1}{2}\lambda_4, \quad V_4 = \tfrac{3}{2}\lambda_4 + \tfrac{1}{2}\lambda_3. \tag{3.51}$$

Using the NLS linear dispersion relation (3.8) and explicit expressions for $k(\boldsymbol{\lambda})$ and $\omega(\boldsymbol{\lambda}) = kc$ it is not difficult to show that in both cases $\lambda_2 = \lambda_1$ and $\lambda_3 = \lambda_4$ the multiple characteristic velocity coincides with the linear group velocity $c_g = \partial\omega/\partial k$. The case $\lambda_3 = \lambda_4$ corresponds to the right-propagating linear wave (sign '+' in the linear dispersion relation) and $\lambda_2 = \lambda_1$ – to the left-propagating wave (sign '−' in the linear dispersion relation).

Also, similar to the soliton limit, the remaining characteristic velocities coincide with the characteristic velocities of the SWE.

Thus, in both harmonic and soliton limits the fourth-order modulation system (3.39) reduces to the system of three equations, two of which agree with the dispersionless limit of the NLS equation (3.6) (the SWE). This property makes possible the matching of the modulation solution with the solution to the dispersionless limit equations at the point where $m = 0$ or $m = 1$. This matching is central to the Gurevich-Pitaevskii problem.

3.2.2.2 Periodic solution in the Riemann invariant parametrisation

It is also instructive to present the NLS periodic solution (3.24) and its limiting forms as $m \to 0$ and $m \to 1$ in the Riemann invariant parametrisation. Using relationships (3.38) one casts the periodic solution (3.24) into the form

$$\begin{gathered} \rho(x,t) = \tfrac{1}{4}(\lambda_4 - \lambda_3 - \lambda_2 + \lambda_1)^2 + (\lambda_4 - \lambda_3)(\lambda_2 - \lambda_1)sn^2(\sqrt{(\lambda_4 - \lambda_2)(\lambda_3 - \lambda_1)}\theta, m), \\ u = c - \frac{C}{\rho}, \\ C = \tfrac{1}{8}(-\lambda_1 - \lambda_2 + \lambda_3 + \lambda_4)(-\lambda_1 + \lambda_2 - \lambda_3 + \lambda_4)(\lambda_1 - \lambda_2 - \lambda_3 + \lambda_4), \\ \theta = x - ct - \theta_0, \end{gathered} \tag{3.52}$$

$$m = \frac{(\lambda_2 - \lambda_1)(\lambda_4 - \lambda_3)}{(\lambda_4 - \lambda_2)(\lambda_3 - \lambda_1)}, \tag{3.53}$$

The wave amplitude $a = (\lambda_4 - \lambda_3)(\lambda_2 - \lambda_1)$.

Linear limit, $m \to 0$

The linear periodic solution is obtained when either $\lambda_2 \to \lambda_1$ or $\lambda_3 \to \lambda_4$ and is given by (we present only the formula for $\lambda_4 - \lambda_3 \ll 1$):

$$\rho(x,t) \simeq \tfrac{1}{4}(\lambda_1 - \lambda_2 + \lambda_3 - \lambda_4)^2 + \frac{(\lambda_3 - \lambda_4)(\lambda_2 - \lambda_1)}{2} \cos\left(2\sqrt{(\lambda_2 - \lambda_3)(\lambda_1 - \lambda_4)}(x - ct)\right). \tag{3.54}$$

Here background density is given by $\rho_0 = \frac{1}{4}(\lambda_1 - \lambda_2)^2$ and the phase velocity $c = \frac{1}{2}(\lambda_1 + \lambda_2 + 2\lambda_4)$. Also note that in the linear limit the wavelength (3.41) becomes $L = \frac{2}{\sqrt{(\lambda_2 - \lambda_3)(\lambda_1 - \lambda_4)}}\pi$.

Soliton limit

In the limit as $m \to 1$ (i.e. as $\lambda_3 \to \lambda_2$) the travelling wave solution (3.52) becomes a dark soliton

$$\rho = \tfrac{1}{4}(\lambda_4 - \lambda_1)^2 - \frac{(\lambda_4 - \lambda_2)(\lambda_2 - \lambda_1)}{\cosh^2(\sqrt{(\lambda_4 - \lambda_2)(\lambda_2 - \lambda_1)}(x - ct - \theta_0))}, \tag{3.55}$$

where $\rho_s = \frac{1}{4}(\lambda_4 - \lambda_1)^2$ is the background density, $a_s = (\lambda_4 - \lambda_2)(\lambda_2 - \lambda_1)$ is the soliton amplitude and $c_s = \lambda_1 + 2\lambda_2 + \lambda_4$ is the soliton velocity. The velocity profile in the dark soliton is given by second formula in (3.52), where one sets $\lambda_2 = \lambda_3$.

Chapter 4

DSW theory for NLS equation

The generic mechanism of the formation of DSWs via dispersive regularisation of the wave breaking singularities was outlined in Section 2.4.3. In this Chapter, we present analytical solutions describing the evolution of the so-called 'simple DSWs' in the dispersive hydrodynamics governed by the defocusing NLS equation (3.1). These solutions will then be used in Chapters 5,6 and 7 as 'building blocks' for the more complicated NLS flow configurations involving the interaction of simple DSWs with external potentials and hydrodynamic RWs.

We first consider the NLS equation in the dispersive hydrodynamics form (3.3), (3.4) with initial conditions

$$\rho(x,0) = \rho_0(x), \qquad u(x,0) = u_0(x)\,, \tag{4.1}$$

where the functions $\rho_0(x)$ and $u_0(x)$ are assumed to vary on a large spatial scale, $\Delta x \gg 1$. Then, at the initial stage of the evolution one can neglect the NLS dispersive term and describe the evolution by the dispersionless limit of the NLS equation, i.e. by the SWE, until the moment of the formation of the wave-breaking singularity, when the spatial derivatives become large and one has to take dispersion into account, which results in the generation of a nonlinear wavetrain – a DSW.

There are two approaches for the analytical description of DSWs using the Whitham modulation theory. In the Gurevich-Pitaevskii approach [17, 18] one supplies the Whitham

equations with certain *boundary conditons* ensuring the continuous matching of the average flow at the (free) DSW boundaries. In the other approach proposed by Kodama (see [44, 69]) one uses the so-called 'regularised *initial value problem*' for the Whitham equations. The Gurevich-Pitaevskii formulation is more general and can be applied to any type of dispersive-hydrodynamic IVPs while the Kodama's setting is only applicable to the dispersive-hydrodynamic problems with piecewise-constant initial conditions. In the Thesis we shall use the Gurevich-Pitaevskii type problem formulation and its generalisation to non-integrable systems proposed in [53].

4.1 Gurevich-Pitaevskii problem for the NLS-Whitham system

Gurevich and Pitaevskii (1974) in their pioneering work [17] studied the DSW problem in the context of the KdV equation (they referred to the DSW as to the collisionless shock wave). The key assumption in the Gurevich-Pitaevskii theory is that the DSW can be asymptotically represented as a slowly modulated periodic (cnoidal) wave. The appropriate modulation providing matching of the DSW with external hydrodynamic flows is then found by solving the Whitham equations equipped with certain boundary (matching) conditions. The solution of the Whitham equations is then substituted into the periodic wave solution of the original equation. The resulting modulated periodic solution *asymptotically* describes the DSW transition between two smooth flows. Thus, instead of solving the original IVP for the dispersive wave equation the Gurevich-Pitaevskii problem is to solve a boundary problem for the associated system of modulation equations.

The Whitham equations are of hydrodynamic type (i.e they don't contain higher order derivatives, unlike the NLS equation itself). This implies non-existence of the global solution for a general IVP [29]. Indeed, due to genuine nonlinearity of the NLS-Whitham equations (see Section 3.2.2.1), the modulation parameters λ_i would develop infinite derivatives (gradi-

ent catastrophe) in finite time in their profiles, which would make the whole Whitham system invalid as it is based on the assumption of the slowly modulated cnodial wave. Therefore, the Whitham equations should be supplied with certain initial or boundary conditions ensuring the existence of the global solution. By the existence of global modulation solution one implies a continuous dependence of the *mean values* of the oscillating hydrodynamic in the DSW on the initial data for the original dispersive equation. The existence of the global solution for DSWs is clearly supported by the results of direct numerical simulations. One needs to stress that the accuracy of the modulation solution for DSW increases with time as the small parameter in the problem is proportional to the ratio of the dispersion length (order of unity in standard normalisation of the NLS equation) to the width of the oscillating zone, the latter increasing with time.

The asymptotic modulation construction of Gurevich and Pitaevskii was later rigorously justified by Lax, Levermore and Venakides [70] by considering the singular zero dispersion limit in the IST theory for the KdV equation. The Lax-Levermore-Venakides approach was extended to the defocusing NLS equation by Jin, Levermore and McLaughlin [68]. We, however, mention that the advantage of the direct Gurevich-Pitaevskii formulation is that it does not rely on the integrability, in the IST sense, of the nonlinear dipersive wave equation and so can be extended to a more general class of nonlinear dispersive wave equations (see [53]).

In the Gurevich-Pitaevskii formulation, one requires a continuous matching of the mean flow at the edges of the DSW. More specifically, for the NLS equation we require continuity (not necessarily smoothness) of the mean density $\overline{\rho}$ and the mean momentum $\overline{\rho u}$ at the DSW boundaries $x^{\pm}(t)$, where the mean values $\overline{\rho}$ $\overline{\rho u}$ must match with the corresponding hydrodynamic quantities ρ and ρu in the smooth flow outside the DSW region described by the dispersionless limit of the NLS equation (i.e. by the SWE). The boundaries $x^{\pm}(t)$ are unknown at the onset, and their determination is part of the problem solution. From general reasoning, supported by the results of direct numerical simulations, one can suggest that the

matching of the DSW with non-oscillating external flow can only occur at the points where either $m \to 0$ (linear oscillations of infinitesimally small amplitude, $a \to 0$) or $m \to 1$ (finite-amplitude oscillations of vanishing wavenumber, $k \to 0$ – solitary waves). The DSW edge, where $m \to 0$ is usually referred to as linear, or harmonic, and the edge, where $m \to 1$ as the soliton edge (see Figure 4.1 left). Then the DSW matching problem for the modulation equations is formulated as follows:

The upper x, t-plane is split into three domains (see Figure 4.1): 'external' smooth solution regions $x < x^-$ and $x > x^+$, where the solution is governed by the dispersionless limit of the NLS equation, and the 'internal' DSW region $[x^-, x^+]$, where the dynamics are described by the Whitham equations. Then at the boundaries $x^\pm(t)$ confining the DSW region the following matching conditions must be satisfied:

$$\begin{aligned} &\text{Trailing (soliton) edge} \quad x = x^-(t): \quad k = 0\,, \quad \overline{\rho} = \rho^-\,, \quad \overline{u} = u^-\,, \\ &\text{Leading (harmonic) edge} \quad x = x^+(t): \quad a = 0\,, \quad \overline{\rho} = \rho^+\,, \quad \overline{u} = u^+\,. \end{aligned} \tag{4.2}$$

Here we have used the notations $\rho^\pm \equiv \rho_e(x^\pm, t)$, $u^\pm \equiv u_e(x^\pm, t)$, where $(\rho_e(x^\pm, t), u_e(\rho_e(x^\pm, t)$ is the solution to the SWE (3.6) with initial conditions (4.1) for the full NLS equation (3.3), (3.4).

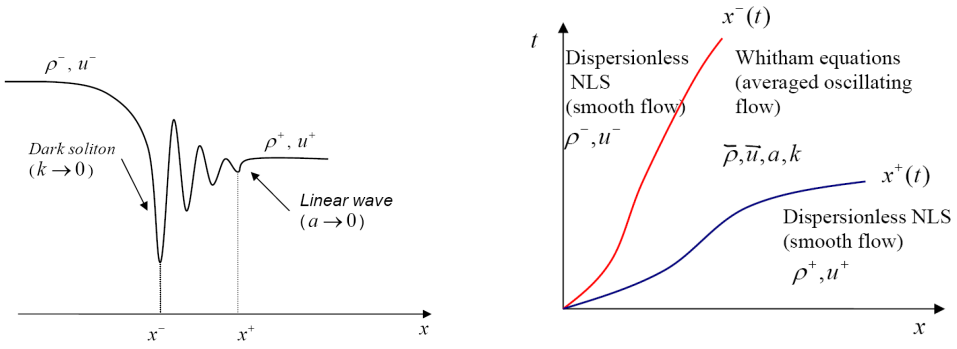

Figure 4.1: Left: oscillatory structure of the right-propagating DSW for the defocusing NLS equation; Right: splitting of the xt-plane in the associated Gurevich-Pitaevskii problem.

The Gurevich-Pitaevskii matching conditions (4.2) can be most conveniently reformulated

in terms of the dispersionless NLS Riemann invariants $\lambda_\pm = \frac{1}{2}u \pm \sqrt{\rho}$. Substituting the expressions for $\overline{\rho}$, $\overline{u}$, a and k in terms of λ_j from Chapter 3 one obtains an invariant form of the matching conditions [18, 19]:

$$\begin{aligned} x = x^-(t): &\quad \lambda_3 = \lambda_2,\ \lambda_4 = \lambda_+^e,\ \lambda_1 = \lambda_-^e, \\ x = x^+(t): &\quad \lambda_3 = \lambda_4,\ \lambda_2 = \lambda_+^e,\ \lambda_1 = \lambda_-^e \end{aligned} \tag{4.3}$$

for the right propagating DSW; and

$$\begin{aligned} x = x^-(t): &\quad \lambda_2 = \lambda_1,\ \lambda_4 = \lambda_+^e,\ \lambda_3 = \lambda_-^e, \\ x = x^+(t): &\quad \lambda_2 = \lambda_3,\ \lambda_4 = \lambda_+^e,\ \lambda_1 = \lambda_-^e, \end{aligned} \tag{4.4}$$

for the left-propagating DSW. Here $\lambda_\pm^e(x,t)$ is the solution of the SWE (3.6) with the initial conditions (4.1) expressed in terms of $\lambda_\pm$. We stress one more time that *free boundaries* $x^\pm(t)$ are unknown at the onset and their determination is an inherent part of the solution.

As we already mentioned, matching conditions (4.4) reflect the numerically observed spatial structure of the DSW in the NLS equation with the dark soliton at the trailing edge and the linear wave packet at the leading edge. One can also see that these conditions are consistent with the structure of the NLS-Whitham modulation system described in Section 3.2.2.1. For example, for the right-propagating DSW, at the trailing edge x^- one has a solitary wave, $m = 1$ (therefore, $\lambda_3 = \lambda_2$ – see (3.42)). Also, in this soliton limit, the Whitham equations for λ_4 and λ_1 transform into the SWE (see (3.49)) so one naturally requires the continuous matching of λ_4 with λ_+ and λ_1 with λ_- at $x = x^-(t)$. Hence the first matching condition (4.4). A similar reasoning applies to the opposite, leading edge – see (3.50).

It also follows from the properties of the modulation system described in Section 3.2.2.1 that the boundaries $x^\pm$ are multiple characteristics of the Whitham system and can be found

from the ordinary differential equations (right-propagating DSW):

$$\begin{aligned} \frac{dx^-}{dt} &= V_2(\lambda_1,\lambda_2,\lambda_2,\lambda_4) = V_3(\lambda_1,\lambda_2,\lambda_2,\lambda_4), \\ \frac{dx^+}{dt} &= V_3(\lambda_1,\lambda_2,\lambda_4,\lambda_4) = V_4(\lambda_1,\lambda_2,\lambda_4,\lambda_4), \end{aligned} \tag{4.5}$$

with the right-hand sides defined on the solution $\lambda_i(x,t)$ of the Gurevich-Pitaevskii matching problem. The multiple characteristic velocities $V_2 = V_3$ and $V_3 = V_4$ in (4.5) are explicitly given by equations (3.48) and (3.51) respectively.

4.2 Simple DSWs

The defocusing NLS equation (3.1) is a two-wave equation, therefore, an initial discontinuity of the flow density and/or velocity (hence four initial arbitrary parameters) generally decays into two waves (DSWs and/or RWs). These are analogs of simple waves in the shallow water dynamics (see Section 2.1). It is clear that, to generate a single simple DSW out of an initial discontinuity, one needs to impose an additional condition on the jumps of ρ and u. Below, following [18, 19], we construct the modulation solutions for the right- and left- propagating DSWs. These solutions will be utilised in the subsequent chapters of the Thesis.

4.2.1 Right-propagating DSW

Let us consider the initial data in the form of a sharp step

$$t = 0: \quad \rho = \begin{cases} \rho_0 > 1 & if \quad x < 0 \\ 1 & if \quad x > 0, \end{cases}, \quad u = \begin{cases} u_0 & if \quad x < 0 \\ 0 & if \quad x > 0. \end{cases} \tag{4.6}$$

Under certain restriction on the values of ρ_0 and u_0, this initial step will correspond to the generation of a right-propagating DSW.

We now assume the described above modulation description of the DSW and make use of the Gurevich-Pitaevskii problem formulation. First we observe that, since both the mod-

ulation equations (3.39) and the initial data (4.6) are invariant with respect to the linear transformation $x \to cx,\ t \to ct,\ c = constant$, the modulation variables must be functions of a self-similar variable $\tau = x/t$ alone, i.e. $\lambda_j(x,t) = \lambda_j(\tau)$. Thus, the Whitham system (3.39) reduces to the system of ODEs:

$$\frac{d\lambda_j}{d\tau}(V_j - \tau) = 0, \quad j = 1,2,3,4. \tag{4.7}$$

System (4.7) only has non-trivial solutions if three of the Riemann invariants λ_i are constants and the remaining, fourth invariant, say λ_j depends on τ and satisfies algebraic equation $V_j = \tau$. The choice of the varying Riemann invariant λ_j and the values of the constant invariants follow from the matching conditions (4.3), which assume the form for the new self-similar independent variable $\tau = x/t$:

$$\begin{aligned} \tau = \tau_- : \quad & \lambda_3 = \lambda_2,\ \lambda_4 = \tfrac{1}{2}u_0 + \sqrt{\rho_0},\ \lambda_1 = \tfrac{1}{2}u_0 - \sqrt{\rho_0}, \\ \tau = \tau_+ : \quad & \lambda_3 = \lambda_4,\ \lambda_1 = \lambda_- = -1,\ \lambda_2 = \lambda_+ = 1, \end{aligned} \tag{4.8}$$

where $\tau_\pm$ are the unknown constant speeds of the DSW edges, $x_\pm = \tau_\pm t$. It is now not difficult to see that the only possible choice for the right-propagating DSW is to set λ_1, λ_2 and λ_4 constants, namely,

$$\lambda_1 = \tfrac{1}{2}u_0 - \sqrt{\rho_0} = -1, \quad \lambda_2 = 1, \quad \lambda_4 = \tfrac{1}{2}u_0 + \sqrt{\rho_0}, \tag{4.9}$$

and for λ_3 we have $V_3(-1,1,\lambda_3, 2\sqrt{\rho_0} - 1) = \tau$.

From the first expression for the constant λ_1 we obtain a relationship between ρ_0 and u_0 across a simple DSW:

$$u_0 = 2(\sqrt{\rho_0} - 1)\,, \tag{4.10}$$

which defines the family of admissible jumps (4.6) producing a single, right propagating DSW. We note that (4.10) coincides with the condition (2.3) for the right-propagating simple

wave solution of the SWE. Substituting u_0 from (4.10) into expression for λ_4 (4.9) we obtain

$$\lambda_4 = 2(\sqrt{\rho_0} - 1). \tag{4.11}$$

Summarising, the BVP (4.7) (4.8) has the solution in the form of a centred simple wave in which all but one Riemann invariants are constant:

$$\lambda_4 = 2\sqrt{\rho_0} - 1, \lambda_2 = 1, \lambda_1 = -1, \quad V_3(-1, 1, \lambda_3, 2\sqrt{\rho_0} - 1) = \frac{x}{t}, \tag{4.12}$$

or, explicitly, using the expression (3.44) for the characteristic velocity V_3,

$$\tfrac{1}{2}(\lambda_3 + 2\sqrt{\rho_0} - 1) - \frac{(2\sqrt{\rho_0} - 1 - \lambda_3)(\lambda_3 - 1)}{(\lambda_3 - 1) - (2\sqrt{\rho_0} - 2)\frac{\mathrm{E}(m)}{\mathrm{K}(m)}} = \frac{x}{t}. \tag{4.13}$$

The obtained solution for the Riemann invariants is schematically shown in Figure 4.2, left. It provides the required modulation of the cnoidal wave (3.52) in the DSW transition.

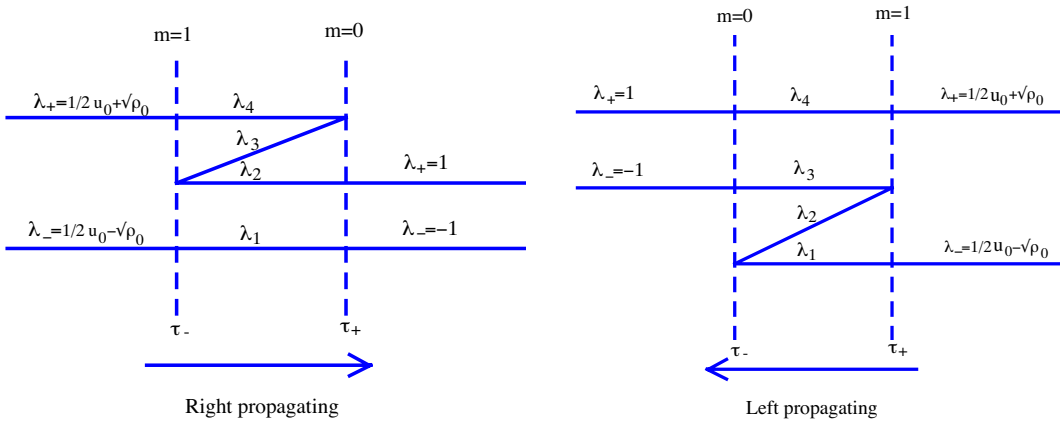

Figure 4.2: Schematic behaviour of the Riemann invariants in the right and left propagating DSWs.

Since the solution (4.13) represents a characteristic fan, it never breaks up for $t > 0$ and therefore is global. The speeds $\tau_{\mp}$ of the trailing and leading edges of the right-propagating

DSW are found by assuming $m = 0$ and $m = 1$ respectively in the solution (4.13):

$$\begin{aligned} \tau_- &= \sqrt{\rho_0}, \\ \tau_+ &= \frac{8\rho_0 - 8\sqrt{\rho_0} + 1}{2\sqrt{\rho_0} - 1}, \end{aligned} \tag{4.14}$$

Thus, the DSW is confined to an expanding zone $\tau_- t \leq x \leq \tau_+ t$.

The amplitude of the dark soliton at the trailing edge is given by

$$a_s = 4(\sqrt{\rho_0} - 1). \tag{4.15}$$

4.2.2 Left-propagating DSW

We shall also need the solution for the left-propagating simple DSW which we find by considering an initial step with a slightly different normalisation than (4.6):

$$t = 0: \quad \rho = \begin{cases} 1 & if \quad x < 0 \\ \rho_0 > 1 & if \quad x > 0, \end{cases}, \quad u = \begin{cases} 0 & if \quad x < 0 \\ u_0 & if \quad x > 0. \end{cases} \tag{4.16}$$

Again, under certain restriction on ρ_0 and u_0 this initial step will correspond to the generation of a single left-propagating DSW. The purpose of introducing two different normalisations of the initial steps for the left- and right-propagating DSWs is that in both chosen normalisations the DSW will propagate *into* the equilibrium region with $\rho = 1$ and $u = 0$.

For a left propagating self-similar DSW the Gurevich-Pitaevskii matching conditions (4.4) assume the form

$$\begin{aligned} \tau = \tau_-: \quad & \lambda_2 = \lambda_1, \ \lambda_4 = \lambda_+ = 1, \ \lambda_3 = \lambda_- = -1, \\ \tau = \tau_+: \quad & \lambda_2 = \lambda_3, \ \lambda_4 = \tfrac{1}{2}u_0 + \sqrt{\rho_0}, \ \lambda_1 = \tfrac{1}{2}u_0 - \sqrt{\rho_0}\,. \end{aligned} \tag{4.17}$$

Now, from (4.7), (4.17) the only possible choice is to set λ_1, λ_3 and λ_4 constants, and for λ_2 one has an implicit solution $V_2 = \tau$.

Explicitly, the constant Riemann invariants are

$$\lambda_1 = \tfrac{1}{2}u_0 - \sqrt{\rho_0}, \quad \lambda_3 = -1, \quad \lambda_4 = \tfrac{1}{2}u_0 + \sqrt{\rho_0} = \lambda_+ = 1. \tag{4.18}$$

The last relation provides a restriction on the admissible values of ρ_0 and u_0 (i.e. for the initial jumps (4.16)) for the family of left-propagating DSWs (cf. (4.10))

$$u_0 = 2(1 - \sqrt{\rho_0}). \tag{4.19}$$

Then

$$\lambda_1 = 1 - 2\sqrt{\rho_0}. \tag{4.20}$$

For the varying invariant λ_2 we have, on using (3.44), an implicit equation

$$V_2(1 - 2\sqrt{\rho_0}, \lambda_2, -1, 1) = \tfrac{1}{2}(1 - 2\sqrt{\rho_0} + \lambda_2) + \frac{(-1-\lambda_2)(\lambda_2 - 1 + 2\sqrt{\rho_0})}{(-1-\lambda_2) - (-2 + 2\sqrt{\rho_0})\frac{\mathrm{E}(m)}{\mathrm{K}(m)}} = \frac{x}{t}. \tag{4.21}$$

The obtained solution for the Riemann invariants is schematically shown in Figure 4.2, right. The edge speeds $\tau_\pm$ of the left-propagating DSW are found by assuming $m = 1$ and $m = 0$ respectively in the solution (4.21):

$$\begin{aligned} \tau_+ &= -\sqrt{\rho_0}, \\ \tau_- &= \frac{8\rho_0 - 8\sqrt{\rho_0} + 1}{1 - 2\sqrt{\rho_0}}. \end{aligned} \tag{4.22}$$

The amplitude of the trailing dark soliton is given by the same expression (4.15).

4.2.3 Vacuum points

It was shown in [19] that in the defocusing NLS flows, unlike the KdV type flows, it is possible to observe zero density points, termed vacuum points. Importantly, the vacuum points can occur in the solutions of the IVPs not containing vacuum states in the initial

data. This effect has no analogue in both viscous shallow water dynamics and in the DSW dynamics in media with negative dispersion supporting bright solitons.

Let us consider the soliton solution (3.55) of the defocusing NLS equation. It is clear that, if the soliton amplitude a_s is equal to the value of the background flow ρ_s, the density at the soliton minimum $\rho_m = 0$. According to (3.52), the flow velocity given by $u = c - \frac{C}{\rho}$ becomes singular at the vacuum point (which implies the rapid phase change in the wave function ψ (see (3.2)). Now, to obtain the condition of the occurrence of the vacuum point at the trailing (soliton) edge of the right-propagating DSW we set the soliton background flow $\rho_s = \rho_0$ and, using expression (4.15) for the trailing soliton amplitude a_s in the right-propagating DSW, find the critical value ρ_0 of the initial density jump, for which the vacuum point occurs exactly at the DSW trailing edge. This happens when $\rho_s = a_s$, which yields

$$\rho_0 - 4(\sqrt{\rho_0} - 1) = 0, \qquad \Rightarrow \qquad \rho_0 = 4. \tag{4.23}$$

If

$$\rho_0 \geq 4, \tag{4.24}$$

then the vacuum point is generated somewhere *inside* the DSW. Its position is found from the condition $\rho_m = 0$, where $\rho_m = \frac{1}{4}(\lambda_4 - \lambda_3 - \lambda_2 + \lambda_1)^2$ is the value of density at the troughs of the periodic solution (3.52). Substituting constant Riemann invariants λ_1, λ_2 and λ_4 (4.12) into this expression we obtain the value of $\lambda_3 = 2\sqrt{\rho_0} - 3 \equiv \lambda_3^v$ at the vacuum point. Substituting $\lambda_3 = \lambda_3^v$ into the modulation solution (4.13) we find the location of the vacuum point

$$x_v = V_3(-1, 1, \lambda_3^v, 2\sqrt{\rho_0} - 1)t \tag{4.25}$$

The greater ρ_0 is, the closer the vacuum point comes to the linear DSW edge of the DSW. Asymptotically, it appears at the linear edge as $\rho_0 \to \infty$.

In conclusion we note that, while the flow velocity u becomes singular at the vacuum point, the momentum ρu remains finite. The flow velocity itself changes its sign across the

vacuum point leading to the counterflow, i.e. if the vacuum point occurs inside the DSW the fluid flows into the DSW from both sides.

The density, velocity and momentum profiles in a right-propagating DSW with the vacuum point inside are shown in Figure 4.3.

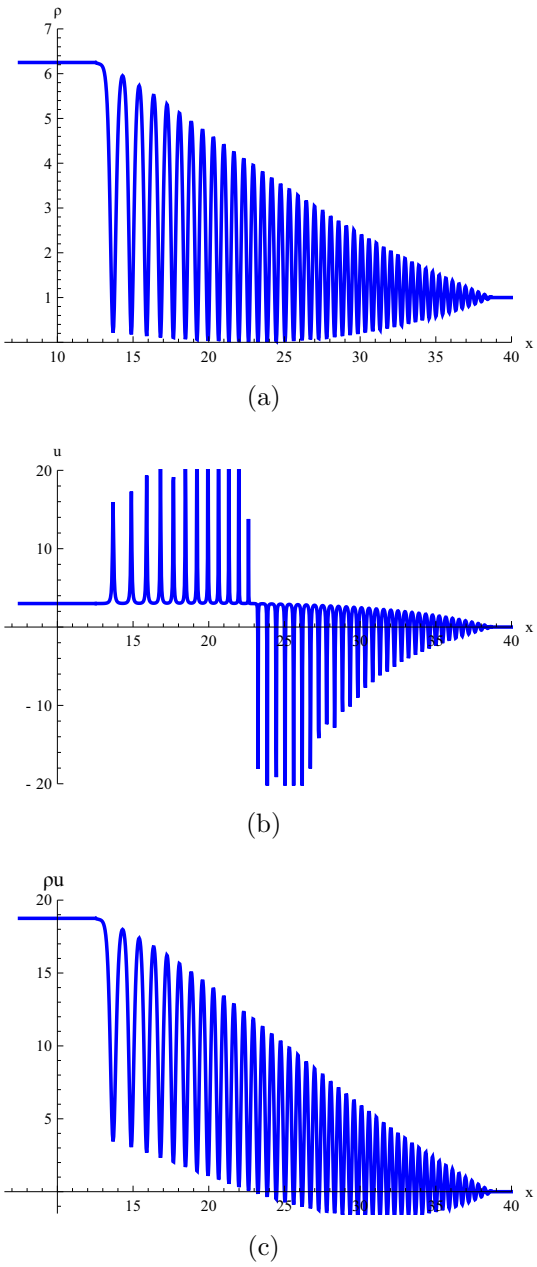

Figure 4.3: Behaviour of the (a) density ρ; (b) velocity u and (c) momentum ρu in the right-propagating NLS DSW with a vacuum point inside.

4.3 Rarefaction waves

We also briefly describe the second type of waves forming in the Riemann (decay of an initial discontinuity) problem for the defocusing NLS equation. These are the rarefaction waves (RWs) asymptotically described by the centred simple-wave solutions of the dispersionless limit equations for the defocusing NLS equation (the SWE (2.1)).

For the right propagating wave, one has

$$\lambda_- = constant,\ V_+ = \frac{x}{t}. \tag{4.26}$$

For the left propagating wave, one has

$$\lambda_+ = constant,\ V_- = \frac{x}{t}. \tag{4.27}$$

E.g, the centred right-propagating RW solution connecting two constant flows with $\rho = \rho_0 < 1$, $u = u_0 = 2(\sqrt{\rho_0} - 1)$ at $x \to -\infty$ and $\rho = 1$, $u = 0$ as $x \to \infty$ is given explicitly by the similarity solution

$$\rho = \begin{cases} \rho_0 & x < x_-, \\ \frac{1}{9}(2 + \frac{x}{t})^2 & x_- > x > x_+, \\ 1 & x > x_+. \end{cases} \tag{4.28}$$

The boundaries $x_\pm$ of the RW are

$$x_- = (3\sqrt{\rho_0} - 2)t, \quad x_+ = t, \tag{4.29}$$

The velocity profile in this right-propagating RW is found from the simple wave relationship $u = 2(\sqrt{\rho} - 1)$.

Analogously, for the centred left-propagating RW connecting the constant states with

$\rho = 1$, $u = 0$ as $x \to -\infty$ and $\rho = \rho_0$, $u_0 = 2(1 - \sqrt{\rho_0})$ an explicit similarity solution is

$$\rho = \begin{cases} 1 & x < x_-, \\ \frac{1}{9}(2 - \frac{x}{t})^2 & x_- > x > x_+, \\ \rho_0 & x > x_+, \end{cases} \tag{4.30}$$

where the RW boundaries x_-, x_+ are given by

$$x_- = -t, \quad x_+ = (2 - 3\sqrt{\rho_0})t. \tag{4.31}$$

The velocity profile in the left-propagating RW is given by the simple-wave relationship $u = 2(1 - \sqrt{\rho})$.

The Riemann invariant configurations for the right- and left propagating RW are shown in Figure 4.4. One can see that the centred RW solutions (4.28) and (4.30) of the dispersionless

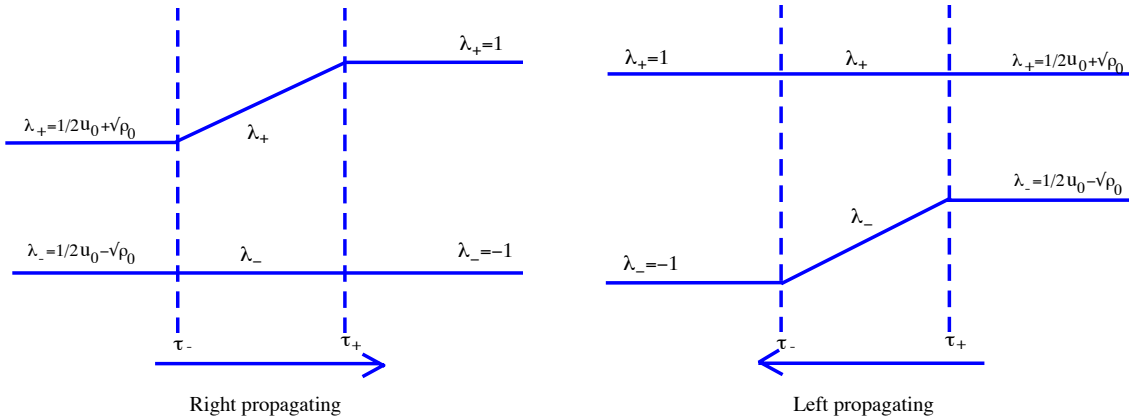

Figure 4.4: Behaviour of the Riemann invariants in the right- and left-propagating RWs.

limit equations exhibit weak discontinuities at the boundaries $x = x_\pm$. These discontinuities are resolved in full dispersive NLS hydrodynamics with the aid of linear wavetrains which smooth out with time [17].

4.4 Decay of an arbitrary discontinuity

The problem of the evolution of a general initial discontinuity depends on four arbitrary parameters and generally involves two centred simple waves, DSW and/or RW. Each discontinuity can be resolved into a combinations of such waves. In this section we will present a complete classification of all the possible cases (see [18, 19]).

Without loss of generality, let us consider the initial jump ($t = 0$) in the form

$$\begin{aligned} \rho = \rho_0, \quad u = u_0, \quad x < 0 \\ \rho = 1, \quad u = 0, \quad x > 0, \end{aligned} \tag{4.32}$$

where $\rho_0 > 0, u_0$ are constants. Reformulating (4.32) in terms of 'dispersionless' Riemann invariants $\lambda_\pm$ we have

$$\begin{aligned} \lambda_+ = 1, \qquad \lambda_- = -1, \qquad x > 0 \\ \lambda_+ = \tfrac{1}{2}u_0 + \sqrt{\rho_0}, \quad \lambda_- = \tfrac{1}{2}u_0 - \sqrt{\rho_0}, \quad x < 0, \end{aligned} \tag{4.33}$$

We can illustrate all the arising cases with the aid of a diagram in λ_-, λ_+-plane of the initial conditions, see Figure 4.5.

Plotting the Riemann invariants for each case, we have (see Figure 4.6).

As can be seen, one obtains 6 regions:

1. one RW and one DSW (left- and right- propagating respectively),
2. two DSWs,
3. one RW and one DSW (right- and left- propagating respectively),
4. two RWs,
5. two RWs (with a vacuum region between them),

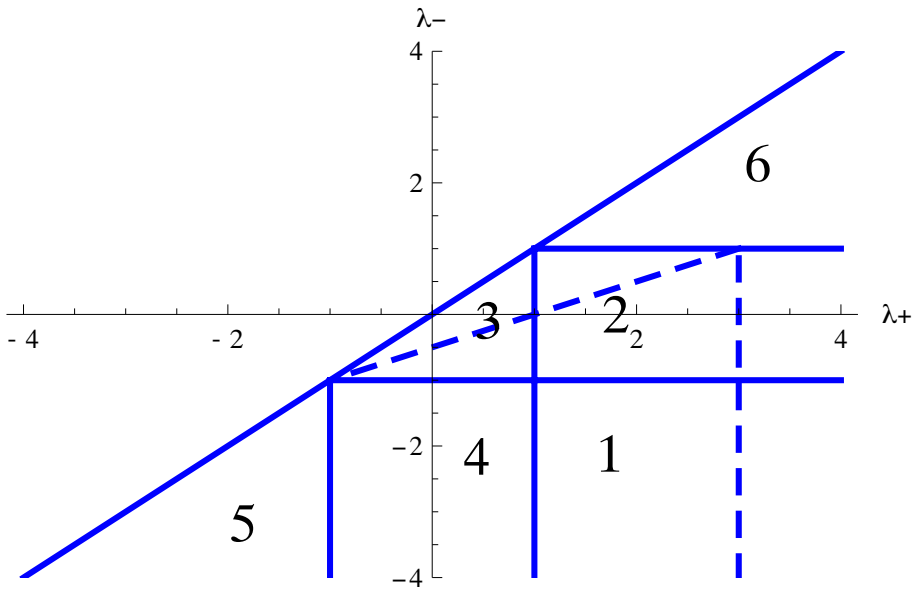

Figure 4.5: λ_+, λ_--plane diagram for the classification of the wave patterns arising in the decay of an initial discontinuity problem for the defocusing NLS equation.

6. two DSWs separated by a uniform oscillating 'plateau' (non-modulated periodic solution).

In regions 1),2),3) and 4) the density and velocity in the constant flow 'plateau' separating two counter-propagating waves are $\rho = \frac{1}{4}(\lambda_+ + 1)^2,\ u = \lambda_+ - 1$.

The dashed line across regions 2) and 3) corresponds to a vacuum point appearance in the left-propagating DSW.

The dashed line across regions 1),2) corresponds to a vacuum point appearance in the right-propagating DSW.

We note that region 6) always contains a vacuum point.

Some numerical plots illustrating different cases of the decay of a step are presented in Appendix.

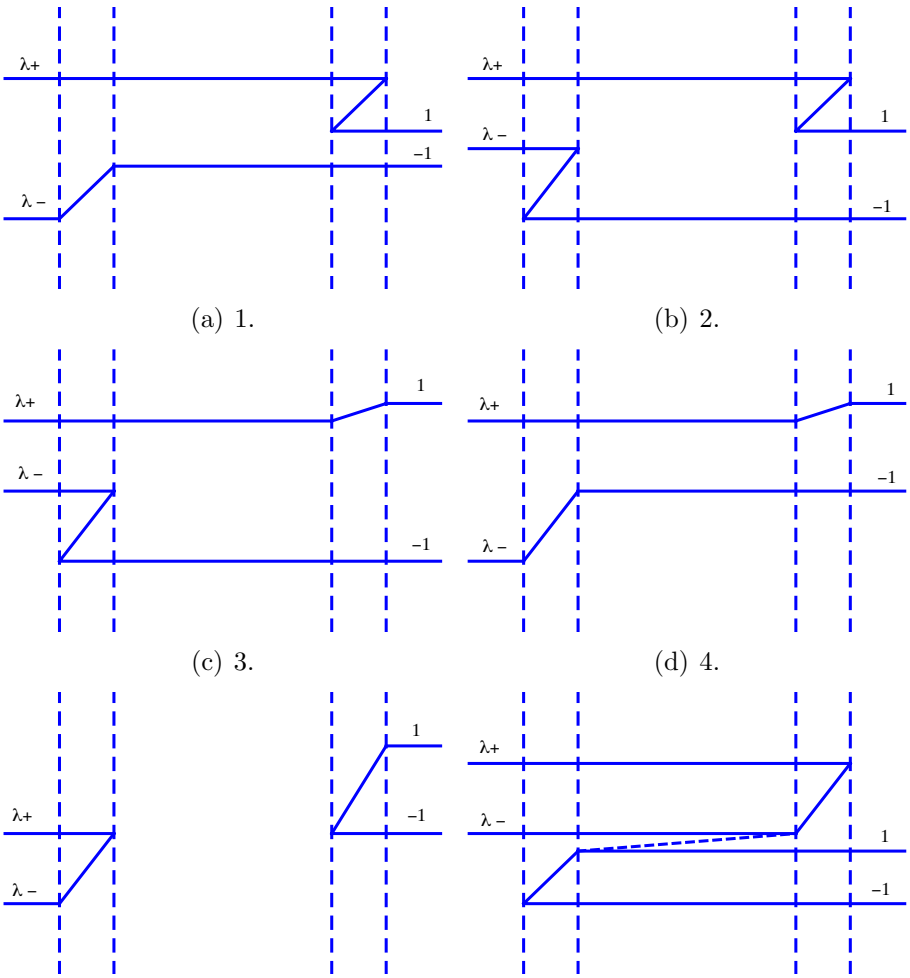

Figure 4.6: The Riemann invariant behaviour in the decay of an initial discontinuity problem. The parameter region numbers correspond to Figure 4.5.

4.5 Hodograph solution and reduction to the Euler-Poisson-Darboux equation

In the modulation solution describing a simple DSW in the NLS dispersive hydrodynamics three Riemann invariants are fixed and only one Riemann invariant varies. Now we consider a more general modulation solution by fixing only two Riemann invariants. This system will be used in Chapter 6 to describe the interaction of a simple DSW with a RW. Since we have two dependent and two independent variables, we can use the classical hodograph transform described in Section 2.3. Actually, as we shall see, the formalism of the more general, Generalised Hodograph Transform (2.84), (2.85) will prove to be very useful even in this, classical (2×2) configuration.

We fix two of the four Riemann invariants in the modulation system (3.39), (3.44),

$$\lambda_i = \lambda_{i0} = const, \quad \lambda_j = \lambda_{j0} = const, \quad i \neq j, \tag{4.34}$$

in order to reduce system (3.39) to the system

$$\frac{\partial \lambda_k}{\partial t} + V_k(\lambda_k, \lambda_l)\frac{\partial \lambda_k}{\partial x} = 0, \quad \frac{\partial \lambda_l}{\partial t} + V_l(\lambda_k, \lambda_l)\frac{\partial \lambda_l}{\partial x} = 0, \tag{4.35}$$

for the remaining two invariant $\lambda_k(x,t), \lambda_l(x,t)$. Here $l \neq k \neq i \neq j$, and $V_{k,l}(\lambda_k, \lambda_l) \equiv V_{k,l}(\lambda_{i0}, \lambda_{j0}, \lambda_k, \lambda_l)$.

In the region where both λ_l and λ_k are not constant, one can introduce the hodograph transform, i.e consider x and t as functions of λ_l and λ_k (see Section 2.3),

$$x = x(\lambda_l, \lambda_k), \quad t = t(\lambda_l, \lambda_k). \tag{4.36}$$

Transforming system (4.35) into this new coordinate system we obtain linear PDEs

$$x_{\lambda_k} - V_l(\lambda_l, \lambda_k)t_{\lambda_k} = 0, \quad x_{\lambda_l} - V_k(\lambda_l, \lambda_k)t_{\lambda_l} = 0 \tag{4.37}$$

for x and t as functions of λ_l and λ_k. Note that this method requires $\partial_x \lambda_{k,l} \neq 0$.

Now,we make the change of variables

$$W_k = x - V_k t, \quad W_l = x - V_l t, \tag{4.38}$$

which reduces system (4.37) to the symmetric system for $W_k(\lambda_l, \lambda_k), W_l(\lambda_l, \lambda_k)$:

$$\frac{\partial_k W_l}{W_k - W_l} = \frac{\partial_k V_l}{V_k - V_l}, \quad k \neq l, \quad \partial_k = \partial/\partial_k. \tag{4.39}$$

We note in passing that the above symmetric hodograph construction can be realised for any pair of Riemann invariants taken as independent variables. Moreover, it remains valid even if three or all four Riemann invariants vary. The compatibility conditions for hodograph transforms in all planes (λ_i, λ_k) lead to the Semi-Hamiltonian condition (2.86).

The symmetry between V_l and W_l in (4.39) and the 'potential' structure

$$V_i(\lambda) = (1 - \frac{L}{\partial_i L}\partial_i)c, \quad i = 1, .., 4, \quad \partial_i = \partial/\partial\lambda_i, \tag{4.40}$$

of the vector functions (λ_k, λ_l) implies the possibility of introducing a single scalar function $g(\lambda_l, \lambda_k)$ instead of the vector (W_k, W_l)

$$W_i = (1 - \frac{L}{\partial_i L}\partial_i)g, \quad i = 3, 4, \tag{4.41}$$

or, using (4.40)

$$W_i = g + 2(V_i - c)\partial_i g. \tag{4.42}$$

Substituting (4.40), (4.41) into (4.39) and taking into account the expression (3.41) for the wavelength L we arrive at the Euler-Poisson-Darboux (EPD) equation for $g(\lambda_l, \lambda_k)$ first obtained in the KdV context in [72] and in the NLS context in [66] (also see [71])

$$2(\lambda_l - \lambda_k)\partial^2_{kl} g = \partial_l g - \partial_k g. \tag{4.43}$$

Equation (4.43) was obtained for the KdV modulation system in . It is remarkable that system (4.35) describing a complicated interaction of modulated dispersive waves, reduces, in the hodograph plane, to the EPD equation (4.43), which describes interaction of two simple waves in classical, *dispersionless* shallow water theory.

The general solution of the EPD equation (4.43) can be represented in the form (see for instance [27])

$$g = \int_{a_1}^{\lambda_k} \frac{\phi_1(\lambda)d\lambda}{\sqrt{(\lambda - \lambda_k)(\lambda_l - \lambda)}} + \int_{a_2}^{\lambda_l} \frac{\phi_2(\lambda)d\lambda}{\sqrt{(\lambda - \lambda_k)(\lambda_l - \lambda)}}, \tag{4.44}$$

where $\phi_{1,2}(\lambda)$ are arbitrary (generally complex) functions and $a_{1,2}$ are arbitrary constants which could be absorbed into $\phi_{1,2}$.

As a matter of fact, the same construction can be used for any pair of Riemann invariants while the remaining two are fixed. Moreover, equations (4.37)–(4.41) are valid even when all Riemann invariants vary (see [66, 71]). This is possible for two reasons: firstly the NLS modulation system (3.24) (3.44) is integrable via the generalised hodograph transform [61] which converts it into overdetermined consistent system (4.39) where $k, l = 1, .., 4, k \neq l$. Secondly, the 'potential structure' of the characteristic speeds (4.40) makes it possible to use the same substitution (4.41) for all $k = 1, .., 4$ which results in the consistent overdetermined

system of six EPD equations (4.43) involving all pairs $\lambda_l, \lambda_k, l \neq k$.

Thus, the problem of integration of the nonlinear Whitham system (3.24) with rather complicated coefficients (3.44) is essentially reduced to solving the classical linear EPD equation (4.43) with certain boundary conditions following from the Gurevich-Pitaevskii matching conditions. As a result, one should be able to express the functions $\phi_{1,2}(\lambda)$ in the general solution (4.44) in terms of the initial or boundary conditions for the NLS equation. This will be done in Chapter 6 for a specific configuration involving bi-directional interaction of a DSW with a RW.

Note, that the classical hodograph solution does not include the special family of the simple wave solutions as the latter correspond to the vanishing of the Jacobian of the hodograph transform $(\lambda_k.\lambda_l) \to (x,t)$ [16]. However, the similarity solution can be formally included in the hodograph solution in the generalised form (4.38). Indeed, putting one of $W_k = 0$ and setting constant all the Riemann invariants λ_j with $j \neq k$ one arrives at the similarity solution, in which $\lambda_k = \lambda_k(x/t)$ is implicitly specified by the equation $V_k = x/t$.

4.6 Modulation phase shift

In the non-modulated periodic travelling wave solution (3.52) the initial phase θ_0 is an independent arbitrary parameter. In the *modulated periodic solution*, θ_0 is no-longer an independent constant parameter but rather becomes a slow function of x, t. As such, it is better described as the modulation phase shift. It was shown in [73], that the function $\theta_0(x,t)$ can be found from the requirement that the local wavenumber $k = 2\pi/L$ and the local frequency $\omega = kc$ in the modulated wave (3.52) must satisfy the generalised phase relationships

$$k = \Theta_x, \quad \omega = -\Theta_t, \tag{4.45}$$

where

$$\Theta = k\theta = kx - \omega t - k\theta_0 \tag{4.46}$$

is the angular phase. Relations (4.45) imply the 'conservation of waves' law (3.37),

$$k_t + \omega_x = 0, \tag{4.47}$$

which is consistent with the modulation system (3.52). Thus, we can obtain the representation

$$V_i = \frac{\partial_i \omega}{\partial_i k}, \tag{4.48}$$

for the characteristic speeds, equivalent to (3.40).

For the general modulation relation (4.45) to be consistent with the linear x, t dependence of the phase (4.46) entering the local single-phase NLS solution (3.52) one must assume that the phase shift is completely determined by the evolution of the Riemann invariants $\lambda_i(x,t)$, i.e.

$$\theta_0(x,t) = \vartheta_0(\lambda_1, \lambda_2, \lambda_3, \lambda_4). \tag{4.49}$$

To obtain ϑ_0 , we differentiate (4.46)

$$\Theta_x = k + \sum_{i=1}^{4} \{x\partial_i k - t\partial_i \omega - \vartheta_0 \partial_i k - k\partial_i \vartheta_0\} \partial_x \lambda_i. \tag{4.50}$$

Comparing (4.45) with (4.50) we see that for any pairs $i, j, i \neq j$ we have

$$x\partial_i k - t\partial_i \omega - \vartheta_0 \partial_i k - k\partial_i \vartheta_0 = 0, \quad x\partial_j k - t\partial_j \omega - \vartheta_0 \partial_j k - k\partial_j \vartheta_0 = 0, \tag{4.51}$$

provided $\partial_x \lambda_{i,j} \neq 0$. Using (4.48) and $k = 2\pi/L$ the system (4.51) can be transformed to

$$x - V_n t = \big(1 - \frac{L}{\partial_n L}\partial_n\big)\vartheta_0, \quad n = i, j, \quad i \neq j. \tag{4.52}$$

Comparing equation (4.52) with the modulated hodograph solution (4.39),(4.41), we can identify the phase shift $\vartheta_0(\lambda) = \theta_0(x,t)$ with the solution $g(\lambda(x,t))$ to the relevant BVP for

the EPD equation (4.44), i.e.

$$\theta_0(x,t) = g(\lambda(x,t)). \tag{4.53}$$

We should also note that from (4.52) that one should set $\theta_0 = 0$ for the simple centred DSW described by the modulation solution in which all but one Riemann invariants are constant and the varying invariant, say λ_m, is implicitly specified by the equation $x - V_m t = 0$. The condition θ_0 then implies that in the dispersive Riemann decay of a step problem the DSW trailing dark soliton is centred exactly at the trailing edge $x_-(t)$.

4.7 DSW fitting method

As we have seen on the example of the defocusing NLS equation, the Whitham equations inherit the integrability property from the original, dispersive system and can be represented in this case in a diagonal, Riemann form. This allows for the construction of explicit analytic modulation solutions describing the DSW dynamics. However, in many physically relevant cases the nonlinear dispersive wave propagation is described by non-integrable systems. Such systems often arise in the description of fully nonlinear dispersive waves, which are far less explored analytically than the weakly nonlinear waves described by the KdV, NLS and similar integrable equations. As was shown by Whitham himself [16], in a non-integrable case, one can still derive the modulation equations via averaging of the available conservation laws but the Riemann form for these equations is normally not available, which makes full analytical description of DSWs in non-integrable systems a very difficult task. On the other hand, there is a strong numerical evidence that the DSW resolution of breaking singularities in such non-integrable dispersive systems is qualitatively similar to that observed in their small-amplitude integrable counterparts in the sense that the 'non-integrable' DSWs have the slowly modulated periodic structure and are characterised by two asymptotic regimes (linear and soliton) allowing for the matching with the external, non-oscillating flow. The analytical method to study the DSW dynamics in non-integrable dispersive-hydrodynamic

systems was developed by El and collaborators [53, 55]. This method is sometimes referred to as the 'DSW fitting method' [56] as it represents a dispersive conservative counterpart of the classical shock wave fitting when the propagating discontinuity (shock) is 'fitted' in the external smooth flow using certain transition conditions (Rankine-Higoniot jump conditions and Lax's entropy conditions) – see Section 2.4.1. As a matter of fact, the transition conditions for a DSW do not coincide with classical shock transition conditions since the DSW expands in time, so the classical analysis of the conservation laws across the (fixed width) shock transition does not apply.

The DSW fitting method allows one to obtain all the key physical parameters of the simple DSW transition between two constant hydrodynamic states bypassing global integration of the Whitham modulation equations. Namely, the method yields certain hydrodynamic transition condition across the DSW, the location of the DSW boundaries and the amplitude of the leading (or trailing) soliton, i.e. all experimentally observable DSW parameters.

To this end, let us demonstrate this method using the cubic defocusing NLS equation as a test example. Our aim is to recover some of the key results of Section 4.2 without using the integrable structure of the NLS equation (namely, without using the Riemann invariants for the associated modulation system) and also without global integration of the Whitham equations. In Chapter 7 we shall apply this method to describe the interaction of DSW and RW in a genuinely non-integrable system, the saturable NLS equation (2.63) describing the light beam propagation through nonlinear photorefractive crystals.

We consider the defocusing NLS equation in the dispersive hydrodynamic form (3.3), (3.4) with discontinuous initial conditions (4.32) (without any *a priori* restrictions on the values of ρ_0 and u_0).

4.7.1 Dispersive shock fitting method requirements

To be amenable to the dispersive shock fitting method [53] the equation under consideration must satisfy several very general requirements. It must

- Have a real-valued linear dispersion relation $\omega_0(k)$.
- Admit a dispersionless limit in the form of a hyperbolic system of hydrodynamic type, which can be expressed in the Riemann invariant form.
- Support a family of periodic travelling wave solutions admitting two limits: harmonic (linear) and solitary wave limit.
- Posses a sufficient number of independent conservation laws. By 'sufficient' one implies that the number of available conservation laws is no less than the number of independent parameters in the periodic solution.

All these requirements can be relatively easily verified for a given specific dispersion-hydrodynamic system. In particular, the results presented in Chapter 3 show that the defocusing NLS satisfies all these requirements.

The main *assumption* of the DSW fitting method is that the Whitham system obtained by averaging the conservation laws is *hyperbolic* for the modulation solutions of our interest. This requirement can only be verified indirectly, say by *a posteriori* numerical check of the DSW stability. The hyperbolicity of the Whitham system allows one to use general properties of characteristics and, in particular, use the fact of the *existence* of the simple-wave solutions to the hyperbolic system of hydrodynamic type [74]. Although in the absence of Riemann invariants such solutions are usually not obtainable analytically, the DSW fitting method enables one to establish some key properties of these solutions.

4.7.2 Summary of the method: simple DSW transition conditions

Let a simple centred DSW of the defocusing NLS equation (or some its non-integrable generalisation) propagate to the right and connects two different constant hydrodynamic states (ρ^-, u^-) at the trailing edge and (ρ^+, u^+) at the leading edge, $\rho^- > \rho+$. Then the DSW edges propagate with constant velocities and Gurevich-Pitaevskii matching conditions

in a physical form (4.2) can be written as

$$\begin{aligned} x = s^- t: \quad & k = 0\,, \;\; \overline{\rho} = \rho^-\,, \;\; \overline{u} = u^-\,, \\ x = s^+ t: \quad & a = 0\,, \; \overline{\rho} = \rho^+\,, \; \overline{u} = u^+\,, \end{aligned} \tag{4.54}$$

where s^+, s^- are the speeds of the leading and trailing edges respectively. Then, it was shown in [53, 55] using the time reversibility argument that the following hydrodynamic transition condition across the right-propagating DSW must be satisfied:

$$\lambda_-(\rho^-, u^-) = \lambda_-(\rho^+, u^+), \tag{4.55}$$

i.e. the value of the hydrodynamic Riemann invariant λ_- is 'transferred' across the right-propagating DSW. Explicitly, for the NLS equation

$$\tfrac{1}{2}u^- - \sqrt{\rho^-} = \tfrac{1}{2}u^+ - \sqrt{\rho^+}\,. \tag{4.56}$$

For the left-propagating DSW an analogous condition is formulated in terms of the zero jump of λ_+ across the DSW.

The DSW fitting method is based on the fact, that the Whitham modulation systems admit *exact reductions* for the wave regimes corresponding to those realised at the DSW edges, i.e. when $a = 0$ and $k = 0$. Importantly, this property does not depend on the availability of the Riemann invariant form and is connected with the origin of the Whitham equations as certain averages over the family of periodic solutions with two limiting regimes: linear and soliton. Say, the zero-amplitude reduction for the NLS-Whitham system (3.34) – (3.37) has the form (note that in the zero-amplitude limit the oscillations do not contribute to the averaging so $\overline{u^2} = \overline{u}^2$, $\overline{\rho u} = \overline{\rho} \cdot \overline{u}$ etc.):

$$\begin{gathered} a = 0, \;\; \bar{\rho}_t + (\bar{\rho}\bar{u})_x = 0, \qquad \bar{u}_t + \bar{u}\bar{u}_x + \bar{\rho}_x = 0, \\ k_t + [\omega_0(k, \bar{\rho}, \bar{u})]_x = 0, \end{gathered} \tag{4.57}$$

where

$$\omega_0(k,\bar{\rho},\bar{u}) = k\bar{u} + k\sqrt{\bar{\rho}+\tfrac{k^2}{4}} \tag{4.58}$$

is the NLS dispersion relation (3.8) for linear waves propagating against slowly varying background with locally constant values of $\bar{\rho}, \bar{u}$. Equations (4.57) comprise a closed system, which represent an *exact* zero-amplitude reduction of the full Whitham system (3.34)-(3.37). It has been shown in [53] that the simple-wave solution $\bar{u} = \bar{u}(\bar{\rho})$, $k = k(\bar{\rho})$ to the system (4.58) subject to the first matching condition (4.54) and transition condition (4.55) yields the necessary information about the DSW leading (linear) edge, which propagates with the linear group velocity, $dx^+/dt = \partial\omega_0/\partial k$.

The zero-wavenumber, $k = 0$, reduction of the Whitham system is obtained by introducing a *conjugate wave number* $\tilde{k}$, which for the NLS equation is defined as

$$\tilde{k} = \pi\left(\int_{e_2}^{e_3} \frac{d\rho}{\sqrt{-Q(\rho)}}\right)^{-1} \tag{4.59}$$

(cf. (3.27) for the 'normal' wavenumber $k = 2\pi/L$). It can be shown (see [57]) that when $m \to 1$, the conjugate wavenumber $\tilde{k} \to \kappa$, where κ is the inverse soliton half-width (sometimes called the soliton wavenumber). We note that the conjugate wavenumber $\tilde{k}$ remains finite when $k \to 0$ and vanishes when $a \to 0$. The asymptotic analysis of the modulation system for $k \to 0$ is somewhat more involved than that for the zero-amplitude limit above but, again, as shown in [53], the simple-wave solution $\bar{u} = \bar{u}(\bar{\rho})$, $\tilde{k} = \tilde{k}(\bar{\rho})$ of the limiting system, subject to the second matching condition (4.54) and transition condition (4.55) yields the necessary information about the DSW trailing edge, which propagates with the NLS soliton velocity, $dx^-/dt = \overline{u} + \sqrt{\overline{\rho} - a}$ (see (3.33)).

We now formulate the summary of the general DSW fitting method of [53, 55] in the application to the dispersive hydrodynamic systems with positive dispersion, i.e. having the linear dispersion relation $\omega_0 = \omega_0(k)$ such that $\omega_0'' > 0$. These are the systems of the

defocusing NLS type, in which the DSW exhibits dark solitons at the trailing edge $x^-(t)$ and degenerates into a linear wave packet at the leading edge $x^+(t)$.

The results can be summarized as follows. Let the dispersionless limit of the governing equations be represented in the Riemann form with the Riemann invariants $\lambda_\pm(\rho, u)$ and the respective characteristic velocities $V_\pm(\rho, u)$ such that the $\lambda_- = constant$ corresponds to the simple wave propagating to the right. Let the linear dispersion relation for the wave propagating on the background $\bar\rho$, $\bar u$ have the form $\omega = \omega_0(k, \bar\rho, \bar u)$. Then the DSW propagating to the right and connecting two different constant states (ρ^-, u^-) and (ρ^+, u^+), $\rho^- > \rho^+$ satisfies the following transition conditions:

(i) the relationship between the admissible values of (ρ^-, u^-) and (ρ^+, u^+), which can be connected by a single DSW

$$\lambda_-(\rho^-, u^-) = \lambda_-(\rho^+, u^+) \equiv \lambda_0 \tag{4.60}$$

(ii) the equations for the DSW edges $x^\pm = s^\pm t$ where the speeds $s^\pm$ are specified by the expressions

$$s^+ = \frac{\partial \Omega_0}{\partial k}(k^+, \rho^+)\,, \qquad s^- = \frac{\Omega_s(\kappa^-, \rho^-)}{\kappa^-}\,, \tag{4.61}$$

where

$$\Omega_0(k, \bar\rho) = \omega_0(k, \bar\rho, \bar u(\bar\rho))\,, \qquad \Omega_s(\kappa, \bar\rho) = -i\Omega_0(i\kappa, \bar\rho)\,. \tag{4.62}$$

Here the dependence $\bar u = \bar u(\bar\rho)$ is given by

$$\lambda_-(\bar\rho, \bar u) = \lambda_0\,. \tag{4.63}$$

The parameters k^+, κ^- in Eqs. (4.61) are found as $k^+ = k(\rho^+)$, $\kappa^- = \kappa(\rho^-)$, where the functions $k(\bar\rho)$ and $\kappa(\bar\rho)$ are determined from the ordinary differential equations:

$$\frac{dk}{d\bar\rho} = \frac{\partial\Omega_0/\partial\bar\rho}{V(\bar\rho) - \partial\Omega_0/\partial k}\,, \qquad k(\rho^-) = 0\,, \tag{4.64}$$

$$\frac{d\kappa}{d\bar{\rho}} = \frac{\partial\widetilde{\Omega}_0/\partial\bar{\rho}}{V(\bar{\rho}) - \partial\widetilde{\Omega}_0/\partial\kappa}\,, \qquad \kappa(\rho^+) = 0\,, \tag{4.65}$$

where $V(\bar{\rho}) = V_+(\bar{\rho}, \bar{u}(\bar{\rho}))$.

(iii) the 'entropy' conditions providing consistency of (i) and (ii):

$$V_-(\rho^-, u^-) < s^- < V_+(\rho^-, u^-), \quad V_+(\rho^+, u^+) < s^+, \quad s^+ > s^-\,. \tag{4.66}$$

Conditions (4.66) represent a DSW analog of Lax's exntropy conditions for viscous shocks (see Section 2.4.1).

Thus, the DSW fitting conditions (4.60) – (4.66) require only the linear dispersion relation of the governing system and the Riemann invariants and characteristic velocities of its nonlinear dispersionless limit. We stress that the construction (4.60) – (4.66) does not require availability of the Riemann invariant form for the *full Whitham system*.

4.7.3 DSW fitting method results for the defocusing NLS equation

We now apply conditions (4.60) – (4.66) to the right-propagating DSW of the defocusing NLS equation (3.3), (3.4). In order to be able to compare our results with earlier results of Section 4.2.1 we set $\rho^+ = 1$, $u^+ = 0$, $\rho^- = \rho_0 > 1$, $u^- = u^0$. The necessary ingredients are:

$$\lambda_- = \frac{1}{2}u - \sqrt{\rho}, \quad V_+ = u + \sqrt{\rho}\,, \quad \omega_0(k, \bar{\rho}, \bar{u}) = k\bar{u} + k\sqrt{\bar{\rho} + \tfrac{k^2}{4}}\,. \tag{4.67}$$

Now substituting (4.67) into (4.60) – (4.66) we obtain:

(i) The simple DSW hydrodynamic transition condition (4.60) assumes the form:

$$u_0 = 2(\sqrt{\rho_0} - 1)\,. \tag{4.68}$$

This is consistent with relationship (4.10) derived in Section 4.2.1 from the exact solution of the NLS-Whitham system in Riemann invariants.

(ii) **The DSW edge speeds**.

(a) *Leading (linear) edge.*

We need first to calculate the functions $V(\bar{\rho})$ and $\Omega_0(k,\bar{\rho})$ entering the definitive ODE (4.64). Using (4.67), (4.68) and (4.62) we obtain

$$V_+(\bar{\rho}) = 3\sqrt{\bar{\rho}} - 2, \quad \Omega_0(k,\bar{\rho}) = \omega_0(k,\bar{\rho},\bar{u}(\bar{\rho})) = k\left(2(\sqrt{\bar{\rho}}-1) + \sqrt{\bar{\rho}+\tfrac{k^2}{4}}\right). \tag{4.69}$$

Substituting (4.69) into (4.64) one obtains, after introducing a new variable α instead of k by the relation

$$\alpha = \sqrt{1+\frac{k^2}{4\bar{\rho}}}, \tag{4.70}$$

an ODE

$$\frac{d\alpha}{d\bar{\rho}} = -\frac{\alpha+1}{2\bar{\rho}}, \tag{4.71}$$

with the initial condition

$$\alpha(\rho_0) = 1. \tag{4.72}$$

Once the solution $\alpha(\bar{\rho})$ is found, the wavenumber k^+ at the leading edge, where $\bar{\rho} = \rho^+ = 1$, is determined as

$$k^+ = k(1) = 2\sqrt{\alpha(1)^2 - 1}. \tag{4.73}$$

The velocity of the propagation of the leading edge is defined by the equations (4.61)

$$s^+ = \frac{\partial\Omega}{\partial k}(k^+,1) = 2\alpha(1) - \frac{1}{\alpha(1)}. \tag{4.74}$$

Now, equation (4.71) is readily integrated to give

$$\alpha(\bar{\rho}) = \frac{2\sqrt{\rho_0}}{\sqrt{\bar{\rho}}} - 1. \tag{4.75}$$

Thus, from equation (4.74)

$$s^+ = \frac{8\rho_0 - 8\sqrt{\rho_0} + 1}{2\sqrt{\rho_0} - 1}. \tag{4.76}$$

This is consistent with the result calculated earlier (4.14) using the solution of the NLS-Whitham system in the Riemann invariant form.

b) Trailing (soliton) edge

For the determination of the trailing edge we need the conjugate linear dispersion relation $\widetilde{\Omega}_0(\kappa, \bar{\rho}) = -i\Omega_0(i\kappa, \bar{\rho})$ (see (4.62)) for dark solitons propagating on the simple-wave hydrodynamic background $\bar{\rho}, \bar{u}(\bar{\rho}) = 2(\sqrt{\bar{\rho}} - 1)$. Using (4.69) we obtain

$$\tilde{\Omega}_0(\kappa, \bar{\rho}) = \kappa \left(2\sqrt{\bar{\rho}} - 2 + \sqrt{\bar{\rho} - \frac{\kappa^2}{4}} \right). \tag{4.77}$$

Substituting (4.77) into ODE (4.65) we reduce it to

$$\frac{d\tilde{\alpha}}{d\tilde{\rho}} = -\frac{\tilde{\alpha}^2 + 1}{2\bar{\rho}}, \qquad \tilde{\alpha}(1) = 1, \tag{4.78}$$

where $\tilde{\alpha} = \sqrt{1 - \frac{\kappa^2}{4\bar{\rho}}}$. Equation (4.78) can be readily integrated to give

$$\tilde{\alpha}(\bar{\rho}) = \frac{2}{\sqrt{\bar{\rho}}} - 1. \tag{4.79}$$

The velocity of the trailing soliton s^- is determined by equation (4.61), which becomes (using

$\rho^- = \rho_0$)

$$s^- = \frac{\tilde{\Omega}_0(\kappa^-, \rho_0)}{\kappa^-} = 2\sqrt{\rho_0} - 2 + \sqrt{\rho_0}\tilde{\alpha}(\rho_0) = \sqrt{\rho_0}\,. \tag{4.80}$$

which is consistent with formula (4.14) obtained from the global solution (4.13) of the NLS-Whitham equations.

The speed of the DSW trailing edge s^- is the speed of the trailing soliton c_s propagating on the background ρ_0, u_0. It is defined by formula (3.33) with $\sigma = -1$ (right-propagating soliton). The amplitude of the trailing soliton a_s is then obtained from as

$$a_s = (s^- - u_0)^2 - \rho_0 = 4(\sqrt{\rho_0} - 1), \tag{4.81}$$

which, again, matches with the previously obtained result (4.15).

(iii) **The 'entropy' conditions.**

It can be readily verified that inequalities (4.66) are satisfied for all values of $\rho_0 > 1$.

The DSW fitting method will be used in Chapter 7 to calculate parameters of the interaction of DSW and RW in photorefractive materials described by the defocusing NLS equation with saturable nonlinearity (2.63), whose modulation equations do not possess the Riemann invariant structure.

Chapter 5

Transcritical NLS flows past penetrable barriers

Fluid flow past an obstacle is of great importance in both normal fluids and superfluids (a quantum state of matter in which viscosity (or friction) of a fluid vanishes, e.g. superfluid helium, BEC). The problem of fluid flow past an obstacle for the dynamics of viscous compressible flows has a strong relationship with viscous shocks (see, e.g. [12, 75]). In the theoretical study of surface water waves it has lead to the detailed description of ship waves and corresponding drag forces (see e.g. [76]). In the dynamics of superfluids, one of the most interesting phenomenon is the existence of a critical velocity in the flow past an obstacle, where below this velocity the flow becomes frictionless (or a superfluid) and above this velocity the obstacle induces dissipation (drag) and superfluidity breaks down. Understanding this feature was most important in developing superfluid theory [7, 8, 77]. It was found by Feynman [8] that below this velocity for sufficiently large obstacles quantised vortices were generated.

It was a matter-of-course that this problem attracted much interest in the context of BEC dynamics, where DSWs and ship waves have been studied theoretically [2, 36, 38, 40, 78–80] and experimentally [2, 38, 78]. Hypersonic flow of a BEC with repulsive interactions past a

slender 'wing' was investigated in [24], vortex shedding from an obstacle potential moving in a BEC was investigate in [81] and quantum turbulence in the supersonic BEC flow around a corner was investigated in [43], in all these investigations existence of a single critical velocity v_c was found, where for velocities $v > v_c$ nonlinear waves were generated.

Experimental, numerical and analytical investigations in BECs have focused mainly on physically multi-dimensional problems. In some cases these could be asymptotically reduced to effectively 1D models for the purposes of mathematical convenience. There however, exist essentially 1D situations when the phenomena observed are specific to the 1D case only. One such problem appears in the description of the water flow over a bottom ridge [10, 82, 83]. In the context of BEC, an effectively 1D problem of this type arises when one considers a BEC flow induced by a penetrable barrier moving through an elongated BEC. This configuration has been recently experimentally investigated by Engels and Atherton [6]. The most characteristic phenomenon observed in the experiment, is that a chain of dark solitons is generated for a finite interval, $v_- < v < v_+$, of the barrier velocities v. The existence of a critical threshold velocity v_- matches with the main concepts of the superfluidity theory introduced by Landau [7] and also matches with the earlier observations of experiments [84] on the appearance of a critical velocity for an impenetrable obstacle moving through the condensate at different velocities. The formation of vortices is impossible in a quasi-1D setting, taking this into account one can deduce from the dispersion relation for linear Bogoliubov excitations in weakly non-ideal Bose gas that the velocity v_- coincides with the sound velocity, and this conclusion was confirmed in the experiments [84]. However, the nonlinear effects present modify the Landau criterion noticeably. For example, in the case of a wide smooth potential used in [6] one has to take into account nonlinear effects which makes possible the generation of nonlinear excitation, in particular dark solitons, and which reduce the critical velocity v_- to a subsonic value [9]. It was noticed in [9, 85] that the near-critical NLS flow through the delta-function potential showed that for some barrier velocity the flow looses stability through a saddle-node bifurcation resulting in the generation

of dark solitons for $v > v_-$. It is remarkable that this nonlinear mechanism is effective for a finite interval of the barrier velocities only. As was first noticed in [86], there exist such special forms of the barrier potential that no radiation is generated at supersonic velocities greater than a second velocity v_+. The result was confirmed numerically for the potentials of a more general form. It was noticed in [87], that while some linear radiation still exists for $v > v_+$, its amplitude decreases exponentially with the growth of the ratio of the obstacle size to the healing length, so that broad and smooth potentials can always be considered as radiationless outside the interval $[v_-, v_+]$. These results were also confirmed by the numerical simulations of waves generated by supersonic motion of a repulsive rectangular potential [88] and the oscillating supersonic motion of the Gaussian potential [89].

Thus, for smooth wide penetrable potentials the production of solitons is effective only in a finite range of barrier velocities. In this chapter, motivated by the experimental results of [6] and the theoretical setting of [9, 10, 83], we develop full asymptotic theory of the transcritical BEC flow for the case of a broad repulsive potential.

We note that, although the experiment [6] was performed with a dense BEC for which the radial motion of the gas is essential, we shall confine ourselves here to the case of a rarefied gas with a frozen radial motion when the full GP equation can be reduced to the 1D NLS equation (see, e.g. [90]). This limiting case qualitatively reproduces all the main characteristic features of the phenomenon. In addition, the present formulation in the framework of the 1D GP equation can be used for the quantitative description of nonlinear wave tunneling in optical crystals [5].

The results presented in this chapter were published in joint paper [20].

5.1 Mathematical model

Engels and Atherton [6] considered a wide penetrable barrier moving with constant speed through an elongated BEC confined to an elongated cigar-shaped trap. This setup is illus-

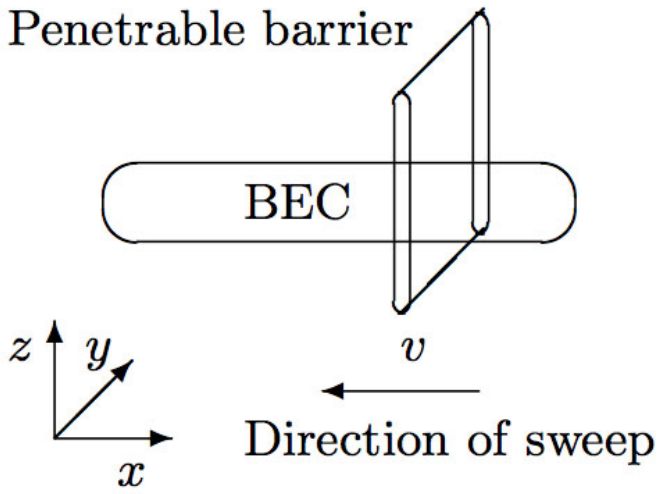

Figure 5.1: Sketch of experimental setup in Ref. [6]. The potential barrier created by the laser beam is moved through the BEC along the $-x$ direction. The trap tightly confines the BEC in the radial y, z directions.

trated schematically in Figure 5.1. In the experiment, the role of the barrier was played by a repulsive potential created by the laser beam which is swept through the BEC with the velocity v along the $-x$ direction. The dynamics of the BEC can be described by the GP equation with moving potential, which in standard non-dimensional units has the form

$$i\psi_t + \tfrac{1}{2}\psi_{xx} - |\psi|^2\psi = V(x+vt)\psi, \tag{5.1}$$

where $V(x+vt) > 0$ is the moving potential barrier. We have seen in Chapter 3, that it is convenient to transform this equation by means of the substitution

$$\psi(x,t) = \sqrt{\rho(x,t)}\exp\left(i\int^x u(x',t)dx'\right) \tag{5.2}$$

to a hydrodynamic-like form. Performing this transformation and passing to the reference frame moving with the velocity $-v$ by introducing $x' = x + vt$, $u' = u + v$ we obtain, on

omitting primes,

$$\begin{aligned} \rho_t + (\rho u)_x &= 0, \\ u_t + u u_x + \rho_x + \left(\frac{\rho_x^2}{8\rho^2} - \frac{\rho_{xx}}{4\rho} \right)_x + V_x(x) &= 0. \end{aligned} \tag{5.3}$$

Here ρ and u are the condensate density and velocity, respectively. It is supposed that in this reference frame and in our non-dimensional units the flow at infinity satisfies the conditions

$$\rho \to 1, \quad u \to v \quad \text{as} \quad |x| \to \infty, \tag{5.4}$$

that is the length of the elongated condensate is assumed to be much longer than the size of the wave structures generated in the flow. Thus, equations (5.3)-(5.4) represent an idealised mathematical model for the description of BEC dynamics in the configuration of our interest.

The study of the problem (5.3)-(5.4) was initiated in the paper by Hakim [9] where the time-independent flows induced by a slowly varying in space barrier moving with subcritical velocity were analysed. Unsteady supercritical flows were considered in [9] numerically and it was noticed there that the results are reminiscent of those for the flow of a stratified fluid over a broad localised topography [10, 91]. In [10, 11] the shallow water flow past topography problem was studied in the framework of the fKdV equation, and this approach provides a clue to solving our NLS equation problem (5.3)-(5.4). The first step in this direction is the study of the stationary solutions of Eqs. (5.3)-(5.4) in the case of a wide and smooth potential $V(x)$ so that the dispersion terms in (5.3) can be neglected and one can take advantage of the so-called 'hydraulic' or 'hydrostatic' approximation.

5.2 Slowly varying potentials: hydraulic solution

Let the potential $V(x)$ be localised in the interval $(-l, l)$, where $l \gg 1$ (i.e. the spatial range of the potential in dimensional units is supposed to be much greater that the healing length

(distance over which the condensate wave-function tends to its bulk value when subject to a localised perturbation) of the BEC. Then one can make use of the hydraulic approximation by assuming that the characteristic length at which all variables change has the order of magnitude of l. Thus one can neglect the terms with the higher derivatives in (5.3) and consider the stationary solutions described by the system

$$\begin{aligned} (\rho u)_x &= 0, \\ u u_x + \rho_x + V_x(x) &= 0. \end{aligned} \tag{5.5}$$

Actually, these are equations for the stationary hydraulic flow in the reference frame with the barrier at rest. Both equations (5.5) are readily integrated once to give

$$\begin{aligned} \rho u &= v, \\ \tfrac{1}{2}u^2 + \rho + V(x) &= \tfrac{1}{2}v^2 + 1\,, \end{aligned} \tag{5.6}$$

where the integration constants are found from the boundary conditions (5.4). Equations (5.6) thus define a stationary flow that connects smoothly to $\rho = 1$, $u = v$ at both infinities. Eliminating ρ we obtain an implicit equation for the flow velocity u as a function of x,

$$V(x) = F(u), \quad \text{where} \quad F(u) = \tfrac{1}{2}(v^2 - u^2) - \frac{v}{u} + 1. \tag{5.7}$$

It is clear that the maximum of $V(x)$ is attained when $F(u)$ attains its maximum (i.e when $\frac{dF}{du} = 0$). Thus

$$\frac{dF}{du} = -u + \frac{v}{u^2} = 0. \tag{5.8}$$

Thus, the maximum of $F(u)$ is attained when $u = u_m = v^{\frac{1}{3}}$, and so the maximum of $V(x)$ is given by

$$V_m = \tfrac{1}{2}v^2 - \tfrac{3}{2}v^{2/3} + 1, \tag{5.9}$$

where $V_m = \max V(x)$.

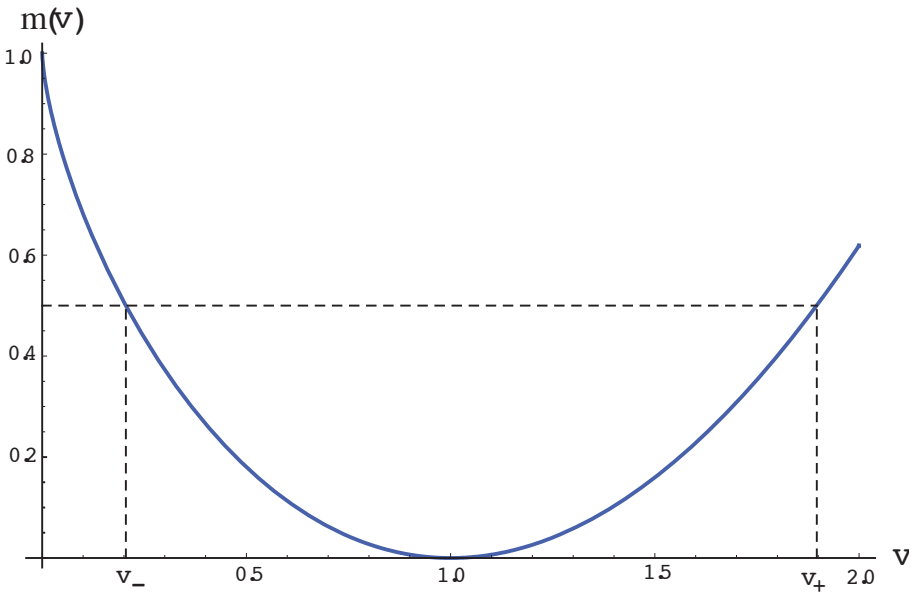

Figure 5.2: Plot of the function $\mu(v)$; for $V_m = 0.5$ the critical values are equal to $v_- \approx 0.2$, $v_+ \approx 1.9$.

For (5.5) to have a solution defined for all x we require that

$$V_m \leq \tfrac{1}{2}v^2 - \tfrac{3}{2}v^{2/3} + 1\,. \tag{5.10}$$

Indeed, the function $F(u)$ varies within the interval $-\infty < F(u) \leq \mu(v)$, where $\mu(v) = \max\{F(u)\} = \frac{1}{2}v^2 - \frac{3}{2}v^{2/3} + 1$. So for the equation (5.7) to have a real solution for all x the interval $[0, V_m]$ must lie within the range of the function $F(u)$ (the condition (5.10) in the present superfluid context was obtained in [9, 87] but can also be found in earlier studies on shallow water flows past topography — see, for instance [83]).

Inequality (5.10) defines the subcritical $v \leq v_-$ and supercritical $v \geq v_+$ regimes where $v_\pm$ are the roots of the equation (see Figure 5.2)

$$\mu(v) = \tfrac{1}{2}v^2 - \tfrac{3}{2}v^{2/3} + 1 = V_m \tag{5.11}$$

and we have $v_- = 0$ for $V_m \geq 1$.

If $V_m \ll 1$, then $v_\pm$ must be close to unity. So introducing the expansion of v with respect to small parameter $\epsilon \ll 1$

$$v = 1 + v_1\epsilon + v_2\epsilon^2 + \cdots, \tag{5.12}$$

and substituting it into (5.11), we have

$$\tfrac{1}{2}(1 + v_1\epsilon + v_2\epsilon^2 + \cdots)^2 - \tfrac{3}{2}(1 + v_1\epsilon + v_2\epsilon^2 + \cdots)^{2/3} + 1 = V_m. \tag{5.13}$$

It is clear the terms of the orders ϵ^0 and ϵ vanish. Gathering coefficients of order ϵ^2 and ϵ^3, we obtain

$$\begin{aligned} O(\epsilon^2): &\quad \tfrac{2}{3}v_1^2\epsilon^2 = V_m, \\ O(\epsilon^3): &\quad \tfrac{4}{3}v_1v_2 - \frac{2}{27}v_1^3 = 0. \end{aligned} \tag{5.14}$$

Thus,

$$\begin{aligned} v_1\epsilon &= \pm\sqrt{\tfrac{3}{2}V_m}, \\ v_2\epsilon^2 &= \frac{1}{12}V_m. \end{aligned} \tag{5.15}$$

Thus, the controlling small parameter $\epsilon \sim \sqrt{V_m}$. So, to the second order, the critical velocities are equal to

$$v_\pm \approx 1 \pm \sqrt{\frac{3V_m}{2}} + \frac{V_m}{12}. \tag{5.16}$$

In the transcritical regime, $v_- < v < v_+$, condition (5.10) does not hold so it is natural first to look closer at what happens with the hydraulic solution when v approaches its boundaries from outside. We now look at the dependence of the flow velocity $u(x)$ and the density $\rho(x)$ on the space coordinate x determined by equations (5.6), (5.7) which can be re-written as

$$\tfrac{1}{2}u^2 + \frac{v}{u} + V(x) = \tfrac{1}{2}v^2 + 1 \tag{5.17}$$

and

$$\frac{v^2}{2\rho^2} + \rho + V(x) = \tfrac{1}{2}v^2 + 1, \tag{5.18}$$

respectively. Formally, the solution to (5.17) (or (5.18)) has two branches only one of which satisfies the necessary boundary conditions (5.4) so just this branch should be considered as the physical one. These two branches of the solution for the flow velocity $u(x)$ are plotted in Figure 5.3 for the case of the potential

$$V(x) = \frac{V_m}{\cosh(x/\sigma)} \tag{5.19}$$

with $V_m = 0.5$, $\sigma = 2$, for which equation (5.11) yields $v_- \approx 0.2$, $v_+ \approx 1.9$. We see that the subcritical ($v \leq v_-$) and supercritical ($v \geq v_+$) hydraulic solutions have similar structure but are characterised by the "exchanged" relative positions of the physical and non-physical branches.

In Figure 5.4 we have plotted two series of hydraulic solutions for different subcritical and supercritical values of the velocity v. As one can see, the physical and non-physical families are separated by two separatrices. When one approaches $v = v_-$ from below (Figure 5.4a), the physical branch becomes more and more pointed up at the centre of the barrier ($x = 0$), and when $v = v_-$, it bifurcates into the separatrix line. This separatrix solution satisfies the necessary boundary condition $v = v_-$ as $x \to -\infty$ (effectively at $x = -l$) but it fails to satisfy the same equilibrium condition at $x \to +\infty$ so one can expect that this bifurcation will be accompanied by the generation of an unsteady flow downstream.

Indeed, the analysis of the near-critical NLS flow through the delta-functional potential $V(x)$ in [9, 85] shows that for some $v = v_{cr}(V_m)$ the flow loses its stability through the saddle-node bifurcation resulting in the generation of dark solitons for $v > v_{cr}$. The numerical simulations in [9] also suggest that one can expect a qualitatively similar scenario with the soliton train generation for slowly varying potentials moving with the supercritical velocity.

To describe this generation of solitons in the NLS flow past broad potential barrier quan-

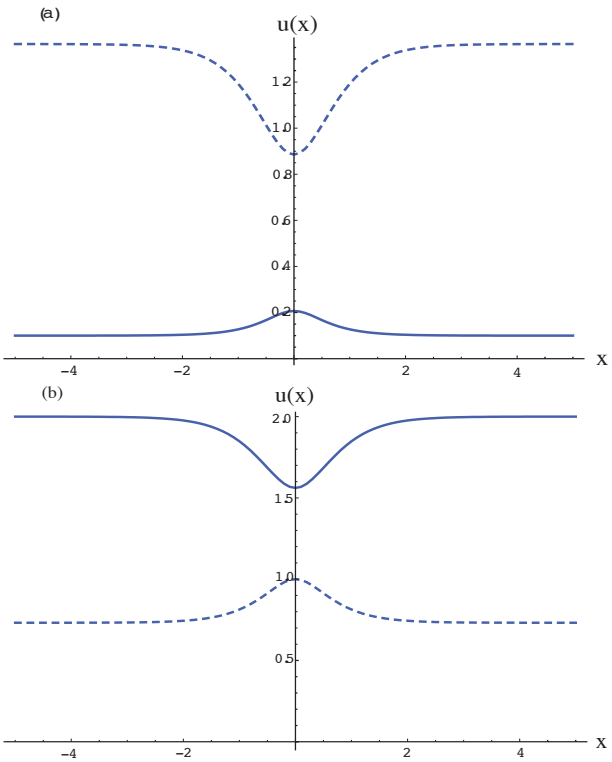

Figure 5.3: Plots of the fluid velocity $u(x)$ in the hydraulic solution (5.17) for the potential barrier (5.19) for which $v_- \approx 0.2$, $v_+ \approx 1.9$; (a) corresponds to subcritical velocity $v = 0.1$ and (b) to supercritical velocity $v = 2.0$. The physical branches are shown by solid lines and non-physical by dashed lines.

titatively, we shall take advantage of the analytical construction proposed in [10], where the transcritical shallow water flow past extended localised topography was considered in the framework of the fKdV equation. The key in this construction is the assumption (confirmed numerically *a posteriori*) of the existence, for certain interval of the flow velocities, of the local steady transcritical transition over the forcing region, which is described by the relevant hydraulic solution. This solution does not satisfy the equilibrium boundary conditions outside the spatial range $[-l, l]$ of the forcing, so one introduces discontinuities at $x = \pm l$, which are resolved into the equilibrium state with the aid of unsteady nonlinear wave trains – the DSWs. By applying a similar assumption here for $v = v_-$ we consider the described above separatrix hydraulic solution as a local one defined on the interval $[-l, l]$. Then we get a discontinuity at $x = l$, which should be further resolved into the undisturbed state

$u = v, \rho = 1$ as $x \to \infty$ via the DSW. Thus, when the BEC flow velocity is equal to $v = v_-$, the formation of DSW downstream of the potential barrier is expected.

In a similar way, when we get closer to $v = v_+$ from above (Figure 5.4b), the physical solution becomes pointed down, and at $v = v_+$ it bifurcates into the separatrix line which satisfies the boundary condition $u = v_+$ as $x \to +\infty$ (effectively at $x = l$) and a discontinuity $u = u_- \neq v_+$ occurs at the left edge $x = -l$. Hence, in this case $v = v_+$ we expect the formation of the upstream DSW. One should note that in the NLS dispersive hydrodynamics a general discontinuity resolves into a certain combination of two waves: dispersive shock(s) and/or rarefaction wave(s). The actual combination depends on the relation between the specific initial jump values for the density and velocity [18, 19] – see the decay of an initial discontinuity classification in Section 4.4. The closure conditions enabling one to single out the unique combination in our problem will be formulated in the next section.

Thus, one can suggest that in the two limiting cases $v = v_\pm$ the full solution can be built of two parts: the steady hydraulic transition solution defined within the spatial range of the potential barrier and the unsteady DSW/RW combination at one of the sides of the barrier. Since the DSW is generated essentially outside the spatial range of the potential, one can use the potential-free NLS equation for its description and take advantage of the theory developed in [18, 19] on the basis of the original Gurevich-Pitaevskii approach (outlined in Chapter 4) using the Whitham method of slow modulations [16, 17]. This modulation theory of the NLS DSWs was recently applied to the description of DSWs in freely expanding BECs in [2, 40].

Generally we are interested in the flow corresponding to the transcritical region

$$v_- \leq v \leq v_+ \tag{5.20}$$

so one can expect formation of both upstream and downstream discontinuities with their further dispersive resolution into the undisturbed states at $x \to \pm\infty$. To be precise, we expect a subcritical jump upstream, a supercritical jump downstream and the exact crit-

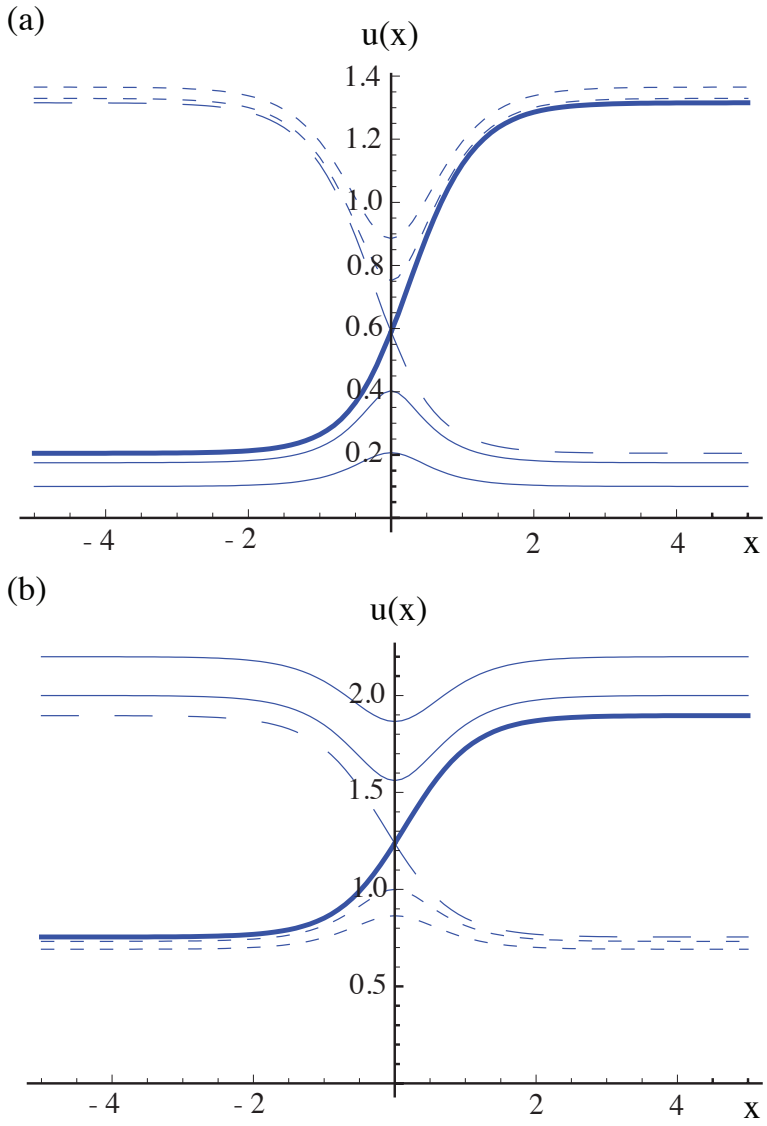

Figure 5.4: a) subcritical hydraulic solutions for u at different values of $v < v_-$ (thin solid lines) and a separatrix solution at $v = v_-$ (thick solid line); b) supercritical hydraulic solution at different values of $v > v_-$ (thin solid lines) and separatrix solution at $v = v_+$ (thick solid line). Short-dashed lines: non-physical branches. Long-dashed line: non-physical separatrix.

icality at the top of the potential. One should emphasise that the suggested description of the transcritical BEC flow as a combination of local hydraulic solution connected with the equilibrium state at infinities by unsteady DSW(s) is an *assumption* which should be validated by the comparison of the analytical solution with direct numerical simulations for a range of the oncoming flow/potential barrier parameters. As we shall see, this assumption works very well when the oncoming flow velocity is not too close to the transcritical region boundaries $v_{\pm}(V_m)$. The reason for that is clear: if the speed v is close to one of its critical values $v_{\pm}(V_m)$, the characteristic relaxation time is expected to be very large (see [85] for the bifurcation scaling analysis in the case of the delta-functional potential) so the local transcritical steady flow does not establish in finite time. Nevertheless, it is instructive to perform the analysis, based on the above assumption, for the whole range of velocities in the interval $[v_-, v_+]$ and then see how well this approximation works for different parameter values.

We denote the values of the density and velocity at the boundaries $x = \pm l$ of the hydraulic solution as

$$\rho(-l) \equiv \rho^u, \quad u(-l) \equiv u^u \quad \text{(upstream of the barrier)} \tag{5.21}$$

and

$$\rho(l) \equiv \rho^d, \quad u(l) \equiv u^d \quad \text{(downstream of the barrier)}\,. \tag{5.22}$$

We assume that the potential maximum is located at $x = 0$, i.e. $V_x(0) = 0$. The transcritical hydraulic solution of our interest is then distinguished by two sets of conditions:

$$\text{(i)} \quad u_x \neq 0 \ \text{ at } \ x = 0; \tag{5.23}$$

$$\text{(ii)} \quad u^u \leq u_m, \quad \rho^u \geq \rho_m \ \text{ and } \quad u^d \geq u_m, \quad \rho^d \leq \rho_m, \tag{5.24}$$

where u_m, ρ_m are the values of u and ρ at $x = 0$. As we shall see the condition (i) actually coincides with the requirement that u_m is equal to the local sound velocity at the top of

the potential (exact criticality) – this is why the problem can be viewed as the *resonant generation* of unsteady nonlinear wavetrains.

Now we take the solution of the hydraulic equations (5.5) in the general form

$$\rho u = c_1, \quad \tfrac{1}{2}u^2 + \rho + V(x) = c_2, \tag{5.25}$$

$c_{1,2}$ being arbitrary constants, so that instead of (5.7) we obtain

$$c_2 - \frac{u^2}{2} - \frac{c_1}{u} = V(x)\,. \tag{5.26}$$

Differentiating (5.26) we obtain

$$\left(u - \frac{c_1}{u^2}\right) u_x = V_x\,. \tag{5.27}$$

Applying condition (5.23) we get

$$c_1 = u_m^3\,. \tag{5.28}$$

Combining this relation with the first integral (5.25) applied to the point $x = 0$ yields

$$\rho_m = u_m^2\,, \tag{5.29}$$

which simply means that the local sound velocity at $x = 0$ is $\sqrt{\rho_m} = u_m$.

Substituting (5.28), (5.29) into the second integral (5.25) gives the value of c_2:

$$c_2 = \frac{3}{2}u_m^2 + V_m. \tag{5.30}$$

On the other hand, the integrals (5.25) applied to the upstream and downstream boundaries $x = \pm l$ where $V(x) \to 0$ yield the relations

$$\rho^{u,d}u^{u,d} = u_m^3, \quad \tfrac{1}{2}(u^{u,d})^2 + \rho^{u,d} = \tfrac{3}{2}u_m^2 + V_m. \tag{5.31}$$

Eliminating u_m we get three equations

$$\rho^u u^u = \rho^d u^d\,, \quad \tfrac{1}{2}(u^u)^2 + \rho^u = \tfrac{1}{2}(u^d)^2 + \rho^d\,, \quad \tfrac{1}{2}(u^u)^2 + \rho^u - \tfrac{3}{2}(\rho^u u^u)^{2/3} = V_m \tag{5.32}$$

for four quantities $\rho^{u,d}$, $u^{u,d}$. Obviously, the last equation can be replaced by

$$\tfrac{1}{2}(u^d)^2 + \rho^d - \tfrac{3}{2}(\rho^d u^d)^{2/3} = V_m, \tag{5.33}$$

that is u^u, ρ^u and u^d, ρ^d satisfy the same set of equations. One more equation is needed for closing the system, and this will be obtained in the next subsection.

Once $u^{u,d}$ and $\rho^{u,d}$ are found, the integration constants c_1 and c_2 in (5.25) are expressed as

$$c_1 = \rho^{u,d} u^{u,d}, \quad c_2 = \tfrac{1}{2}(u^{u,d})^2 + \rho^{u,d}. \tag{5.34}$$

Hence, the transcritical hydraulic solution (5.25) is given by

$$\tfrac{1}{2}u^2 + \frac{\rho^{u,d}u^{u,d}}{u} + V(x) = \tfrac{1}{2}(u^{u,d})^2 + \rho^{u,d}, \tag{5.35}$$

$$\tfrac{1}{2}\left(\frac{\rho^{u,d}u^{u,d}}{\rho}\right)^2 + \rho + V(x) = \tfrac{1}{2}(u^{u,d})^2 + \rho^{u,d}. \tag{5.36}$$

At the boundaries $v = v_\pm$ of the transcritical region, where either $\rho^u = 1$, $u^u = v_-$ or $\rho^d = 1$, $u^d = v_+$, equations (5.35), (5.36), reduce to (5.17), (5.18) respectively as it should be.

5.2.1 Closure conditions

To get the closure condition for (5.32) we shall take advantage of the transition condition across the DSW, which is most conveniently formulated in terms of the Riemann invariants of the dispersionless hydrodynamic system associated with the NLS equation (see equation

(3.6))

$$\begin{aligned} \rho_t + (\rho u)_x &= 0, \\ u_t + u u_x + \rho_x &= 0\,, \end{aligned} \tag{5.37}$$

and is equivalent to the classical SWEs (2.1). Introducing the Riemann invariants

$$\lambda_\pm = \tfrac{1}{2}u \pm \sqrt{\rho}, \tag{5.38}$$

we represent (5.37) in the diagonal form (see equation (2.7))

$$\frac{\partial \lambda_+}{\partial t} + \tfrac{1}{4}(3\lambda_+ + \lambda_-)\frac{\partial \lambda_+}{\partial x} = 0, \quad \frac{\partial \lambda_-}{\partial t} + \tfrac{1}{4}(\lambda_+ + 3\lambda_-)\frac{\partial \lambda_-}{\partial x} = 0\,. \tag{5.39}$$

In the problem of the decay of an initial discontinuity in the NLS hydrodynamics the transition across the DSW is characterised by the zero jump of one of the hydrodynamic Riemann invariants (5.38) (see [18, 19], and Chapter 4). It should be stressed that this condition is not a small-amplitude approximation of the classical shock jump condition but rather is a non-perturbative consequence of the data transfer along characteristics of the associated Whitham modulation system describing DSW region [53]. It will transpire later that in the present problem of the right-propagating BEC through a potential barrier at rest, the "conserving" invariant is λ_+ (this corresponds to the waves propagating to the left (see Chapter 4) which might seem somewhat counter-intuitive with regard to the downstream DSW).

The upstream DSW is adjacent to the oncoming flow $\rho = 1$, $u = v$ so the Riemann invariant condition yields the relationship

$$\tfrac{1}{2}u^u + \sqrt{\rho^u} = \tfrac{1}{2}v + 1\,, \tag{5.40}$$

which closes the system (5.32). We also recall that we are interested in the solution satisfying condition (5.24) which allows one to identify the roots of (5.32), (5.40) as upstream and

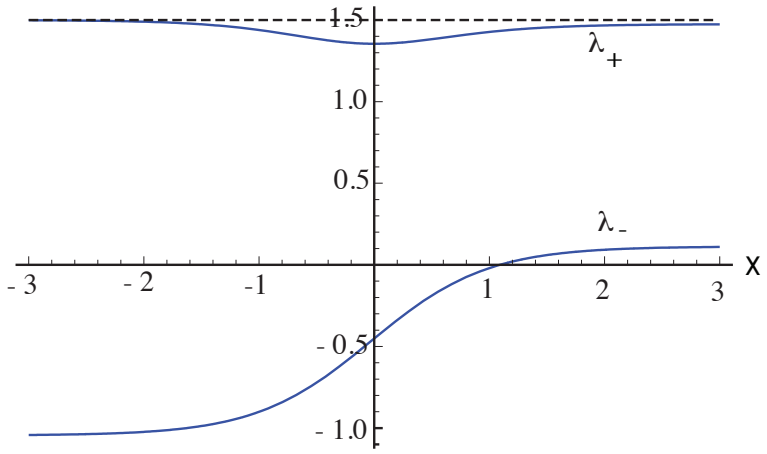

Figure 5.5: Riemann invariants $\lambda_\pm$ as functions of x in the hydraulic solution (5.35), (5.36) for the potential (5.19) with $V_m = 0.5$. Note: $\lambda_+^u \approx \lambda_+^d$.

downstream ones. Now all four values $\rho^{u,d}, u^{u,d}$ are fixed in terms of V_m, v, which, in particular, implies that the downstream discontinuity generally cannot be resolved by a single DSW but requires an additional right-propagating RWs to adjust to the undisturbed flow at $+\infty$. While the introduction of this RW does not present one with a serious technical problem, we shall see that in practical terms this additional complication is not actually necessary.

First we note that, since the matching of the (external) hydrodynamic solution and the (internal) modulation solution describing DSW is most naturally formulated in terms of Riemann invariants (see [18, 19] and Chapter 4 for details) it is instructive to plot the transcritical hydraulic solution (5.25), (5.28), (5.30) in terms of $\lambda_\pm$ (the physical branch of the solution is selected using inequalities (5.24)). The plot in Figure 5.5 suggests that for weak enough potentials one can neglect the change of λ_+ across the barrier, which would remove the necessity of introducing an additional RW. To justify this supposition we first eliminate $\rho^{u,d}$ from the second equation (5.31) to represent it in the form

$$\frac{(u^{u,d})^2}{2} + \frac{u_m^3}{u^{u,d}} - \frac{3}{2}u_m^2 = V_m. \tag{5.41}$$

Introducing the normalised quantities $\nu_\pm = u^{d,u}/u_m$ we represent (5.41) as

$$\nu_\pm^2 + \frac{2}{\nu_\pm} - 3 = \alpha, \tag{5.42}$$

where $\alpha = 2V_m/u_m^2$. Now let us suppose that $V_m \ll 1$, which implies $\nu_\pm \approx 1$, $u \approx u_m \approx 1$, $\alpha \ll 1$. Then from (5.42) we get the expansion

$$\nu_\pm = 1 \pm \left(\frac{\alpha}{3}\right)^{1/2} + \frac{\alpha}{9} + c_\pm \alpha^{3/2} + \dots , \tag{5.43}$$

i.e. the controlling small parameter is again $\epsilon \sim V_m^{1/2}$ (note that the coefficients $c_\pm$ in (5.43) will not contribute to the result so we do not present them explicitly). We now consider the boundary values of the Riemann invariant λ_+ (5.38)

$$\lambda_+^{u,d} = \frac{1}{2}u^{u,d} + \sqrt{\rho^{u,d}} = \frac{1}{2}u^{u,d} + \frac{u_m^{3/2}}{(u^{u,d})^{1/2}}\,. \tag{5.44}$$

Again, normalising, $\Lambda^{u,d} = \lambda_+^{u,d}/u_m$, and expanding for small V_m we obtain

$$\Lambda^{d,u} = \frac{1}{2}\nu_\pm + \frac{1}{\nu_\pm^{1/2}} = \frac{3}{2} + \frac{\alpha}{8} \mp \frac{1}{48\sqrt{3}}\alpha^{3/2}\dots \tag{5.45}$$

Now, taking into account that $u_m = 1$ to leading order, we get

$$\delta = \lambda_+^u - \lambda_+^d = \left(\frac{V_m}{6}\right)^{3/2} + \cdots \tag{5.46}$$

Thus, for weak potentials the jump of the Riemann invariant λ_+ across the potential has the third order in the controlling small parameter $(V_m)^{\frac{1}{2}}$. This result has certain analogy with the classical result from the shock wave theory which reads that the relevant Riemann invariant has just the third order jump across the weak shock [6, 10]. The coefficient $(1/6)^{3/2}$ before $V_m^{3/2}$ suggests that one can neglect the jump of λ_+ even for the potentials of moderate strength (of course, provided that the coefficients for the successive powers of the small

parameter $V_m^{1/2}$ in the expansion (5.46) are reasonably small). Indeed, for our potential (5.19) with $V_m = 0.5$ we have $\lambda_+^{u,d} \approx 1.5$ while according to (5.46) $\delta \approx 0.025$ i.e. just about 1.7%, which is confirmed by the numerical transcritical hydraulic solution shown in Figure 5.5. So, for weak to moderate potentials one can safely assume that the value of the Riemann invariant λ_+ is preserved across the potential, which allows one to use an additional closure condition

$$\tfrac{1}{2}u^u + \sqrt{\rho^u} = \tfrac{1}{2}u^d + \sqrt{\rho^d} = \tfrac{1}{2}v + 1\,. \tag{5.47}$$

Relation (5.47) is asymptotically consistent with exact conditions (5.32), (5.40) and will be especially useful in our further consideration of the dispersive resolution of the downstream discontinuity. We also note that an immediate implication of (5.47) is that both upstream and downstream DSWs are "based" on the same family of characteristics corresponding to left-propagating hydrodynamic simple-waves, which will be essential for the modulation solution in the subsequent sections.

5.2.2 Weak potentials: explicit formulae

Using asymptotic closure conditions (5.47) one can obtain simple approximate explicit expressions for $\rho^{u,d}$, $u^{u,d}$ in terms of v, V_m, which will be useful later. We use (5.47) to eliminate $\rho^{u,d}$ from (5.32) to obtain a single equation for $w = u^{u,d}$,

$$\frac{w^2}{2} + \left(\frac{v-w}{2} + 1\right)^2 - \frac{3}{2}\left[w\left(\frac{v-w}{2} + 1\right)^2\right]^{2/3} = V_m. \tag{5.48}$$

This equation has two roots, the larger one corresponds to u^d and the smaller one to u^u (see (5.24)).

Equation (5.48) can be solved approximately for $V_m \ll 1$. It is easy to see that for $V_m = 0$ this equation is satisfied if $w = 1 + (v - w)/2$ i.e. $w = (v + 2)/3$. In the next approximation

we obtain

$$u^u = 1 + \frac{1}{3}(v-1) - \sqrt{\frac{2V_m}{3}}, \quad u^d = 1 + \frac{1}{3}(v-1) + \sqrt{\frac{2V_m}{3}}, \tag{5.49}$$

where we have used that v takes its values in the transcritical region (see (5.16))

$$1 - \sqrt{\frac{3V_m}{2}} < v < 1 + \sqrt{\frac{3V_m}{2}}. \tag{5.50}$$

Respectively, with the same accuracy we get from (5.47)

$$\rho^u = 1 + \frac{2}{3}(v-1) + \sqrt{\frac{2V_m}{3}}, \quad \rho^d = 1 + \frac{2}{3}(v-1) - \sqrt{\frac{2V_m}{3}}. \tag{5.51}$$

Using (5.49), (5.51) we calculate the upstream and downstream values of the Riemann invariant $\lambda_- = \frac{1}{2}u - \sqrt{\rho}$, which undergoes discontinuities at both edges of the transcritical hydraulic solution (see Figure 5.5),

$$\lambda_-^u = \lambda_-(-l) = -\frac{1}{2} - \frac{1}{12}(v-1) - \sqrt{\frac{2V_m}{3}}\,, \qquad \lambda_-^d = \lambda_-(l) = -\frac{1}{2} - \frac{1}{12}(v-1) + \sqrt{\frac{2V_m}{3}} \tag{5.52}$$

Obviously, $\lambda_-^u < \lambda_-^\infty$, $\lambda_-^d > \lambda_-^\infty$, where $\lambda_-^\infty = v/2 - 1$ is the value of λ_- for the undisturbed flow at infinity.

5.3 Resolution of downstream and upstream discontinuities

Summarising the results of the previous section, we have the following values for the Riemann invariants $\lambda_\pm$ at the boundaries $x = \pm l$ of the hydraulic transition and at $x = \pm\infty$:

$$\lambda_+(-\infty) = \lambda_+^d = \lambda_+^u = \lambda_+(+\infty) = \tfrac{1}{2}v + 1\,, \tag{5.53}$$

$$\lambda_-(-\infty) = \lambda_-(+\infty) = \tfrac{1}{2}v - 1\,, \tag{5.54}$$

$$\lambda_-^d = \tfrac{1}{2}u^d - \sqrt{\rho^d}\,, \qquad \lambda_-^u = \tfrac{1}{2}u^u - \sqrt{\rho^u}. \tag{5.55}$$

From now on we consider the values $\lambda_-^{u,d}(v, V_m)$ as known. Thus, there are upstream and downstream discontinuities in λ_- and no discontinuities in λ_+.

As was mentioned above, the upstream and downstream discontinuities are resolved through the generation of DSWs which can be described using modulated periodic solutions of the defocusing NLS equation (5.1) without the barrier potential $V(x+vt)$. The potential term can be neglected because the shock resolution occurs essentially outside the potential range $-l < x < l$. The potential-free NLS equation is Galilean invariant and hence it preserves its form (up to inessential in our case phase factor in ψ-function) after the transformation to the reference frame with the barrier at rest which is used in our calculations.

The periodic solution of the NLS equation for $\rho(x,t), u(x,t)$ can be found in Chapters 3, see equation (3.52). The wavelength L is given by (3.41).

The parameters $\lambda_1 \le \lambda_2 \le \lambda_2 \le \lambda_4$ vary slowly through the DSW and their evolution is governed by the Whitham modulation equations (3.39) where the characteristic velocities are given by equations (3.44).

The waveform (3.52) within the DSW wave region gradually changes from the vanishing amplitude harmonic wave at one of the edges to a dark soliton at the opposite edge so that generally the modulus m runs over the whole range from 0 to 1. The Riemann invariants λ_j of the Whitham equations are matched with the "external" hydrodynamic invariants $\lambda_\pm$ at some free boundaries $x^\pm(t)$ defined by the conditions $m = 0$ (harmonic edge) or $m = 1$ (soliton edge). The specific matching conditions and relative position of the harmonic and soliton edges depend on whether one considers the left- or right-propagating DSW (see [19] and Chapter 4).

For the left-propagating case of our interest the matching conditions are given by (4.4),

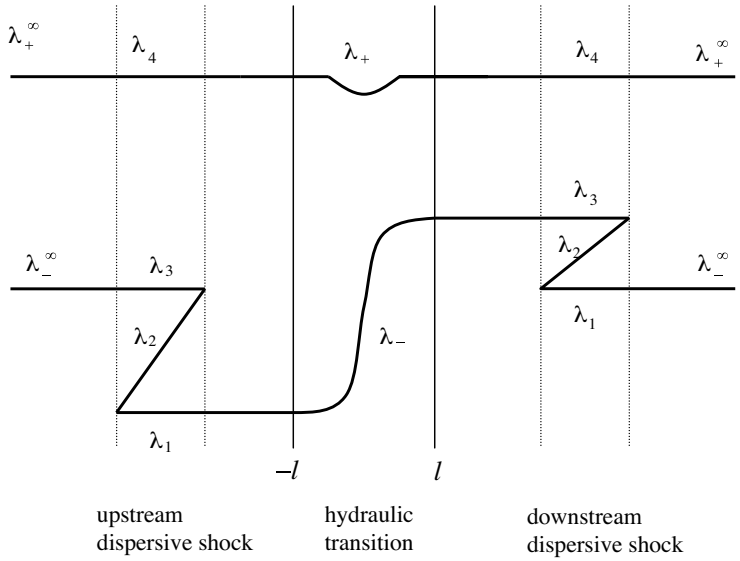

Figure 5.6: Qualitative behavior of the Riemann invariants λ_j as functions of x in the full hydraulic/modulation solution.

repeated they are

$$\begin{aligned} &\lambda_2 = \lambda_1\,, \quad \lambda_4 = \lambda_+, \quad \lambda_3 = \lambda_- \quad \text{at} \quad x = x^-(t); \\ &\lambda_2 = \lambda_3\,, \quad \lambda_4 = \lambda_+, \quad \lambda_1 = \lambda_- \quad \text{at} \quad x = x^+(t). \end{aligned} \tag{5.56}$$

Since DSWs expand with time, their widths at sufficiently large t are much greater than the range l of the barrier potential, so for $t \gg l$ one can assume the hydraulic solution to be asymptotically localised at $x = 0$ and use the similarity solutions of the Whitham equations (3.39) with only one variable changing through each DSW [18] (note that the formal condition of applicability of the Whitham method itself to the decay of a step problem is $t \gg 1$ — see [17, 53]). From the matching conditions (5.56) it is clear that the varying invariant should be λ_2. Thus, in each DSW the invariants λ_1, λ_3, λ_4 are constant and the invariant λ_2 varies according to the similarity solution (4.21). Repeated again this is,

$$V_2(\lambda_1, \lambda_2, \lambda_3, \lambda_4) = \frac{x}{t}, \tag{5.57}$$

where

$$V_2(\lambda_1,\lambda_2,\lambda_3,\lambda_4)=\tfrac{1}{2}\sum\lambda_i+\frac{(\lambda_3-\lambda_2)(\lambda_2-\lambda_1)K(m)}{(\lambda_3-\lambda_2)K(m)-(\lambda_3-\lambda_1)E(m)}\,. \tag{5.58}$$

The values of $\lambda_1,\lambda_3,\lambda_4$ in (5.58) are fixed and the Riemann invariant λ_4 must have the same constant value

$$\lambda_4=\tfrac{1}{2}v+1 \tag{5.59}$$

in both downstream and upstream DSW since the value of λ_+ is transferred through the hydraulic transition (see (5.53)). At the same time, the values of λ_1 and λ_3 are different upstream and downstream of the barrier so we shall consider the downstream and upstream DSWs separately. Before we proceed with the detailed analysis of the DSWs it is instructive to get a picture of qualitative behavior of the Riemann invariants in the entire flow. For that, we use the matching conditions (5.56) and the inequality $\partial\lambda_2/\partial x>0$ following from the similarity modulation solution (5.57) and the general property $\partial v_i/\partial\lambda_i>0$ of the characteristic velocities (3.44). As a result, one arrives at the qualitative scheme of the behaviour of the Riemann invariants sketched in Figure 5.6.

5.3.0.1 Downstream DSW/soliton train

In the downstream DSW we have (see the matching conditions (5.56) and Figure 5.6)

$$\lambda_1=\lambda_-^\infty=\frac{v}{2}-1,\quad \lambda_3=\lambda_-^d,\quad \lambda_4=\lambda_+^\infty=\frac{v}{2}+1, \tag{5.60}$$

and λ_2 as a function of the self-similar variable x/t is determined by the equation

$$V_2(v/2-1,\lambda_2,\lambda_-^d,v/2+1)=\frac{x}{t}. \tag{5.61}$$

In the linear limit $\lambda_2\to\lambda_1$ (i.e. $m\to 0$) we have

$$V_2(\lambda_1,\lambda_1,\lambda_3,\lambda_4)=\lambda_1+\tfrac{1}{2}(\lambda_3+\lambda_4)+\frac{2(\lambda_3-\lambda_1)(\lambda_4-\lambda_1)}{2\lambda_1-\lambda_3-\lambda_4}\,. \tag{5.62}$$

This velocity determines the speed s_-^d of the trailing edge of the downstream DSW and it is not difficult to check using formulae (5.49), (5.52) that for $V_m \ll 1$ it is negative, that is at least for weak potentials the trailing edge cannot be located in the downstream region. Hence, in the equation (5.61) the variable λ_2 is limited from below by some cut-off value λ_2^*, and, as a result, the downstream shock gets attached to the barrier at its boundary $x \approx l$. Then one can find λ_2^* in the approximation described above by taking $l/t \to 0$ in equation (5.61), which yields

$$V_2(v/2-1, \lambda_2^*, \lambda_-^d, v/2+1) = 0. \tag{5.63}$$

Since V_2 has the meaning of nonlinear group velocity, equation (5.63) can be interpreted as an asymptotic condition that the modulated wave "stops" at $x = 0$ and this is why it can be directly connected (on the level of the Riemann invariants, i.e. in the "averaged" sense) to the stationary hydraulic transition, which on the modulation length scale can be viewed as a discontinuity located at $x = 0$. In more precise terms, relation (5.63) means that for the solution under study the characteristic of the Whitham equations $dx/dt = V_2$ coincides with the characteristic $dx/dt = 0$ of the dispersionless equations (5.37) in the hydraulic approximation at $x = 0$ so the modulation solution can be "terminated" at $x = 0$ and the free-boundary matching conditions (5.56) at the (non-existent) trailing edge $x^- < 0$ can be replaced with the boundary conditions at $x = 0$:

$$\lambda_3 = \lambda_-^d, \quad \lambda_4 = \tfrac{1}{2}v + 1, \quad \lambda_1 = \tfrac{1}{2}v - 1 \quad \text{at} \quad x = 0. \tag{5.64}$$

The modulation solution is then considered in the upper right quarter of x, t-plane, $x > 0, t > 0$. One should mention that the similar situation occurs in the problem of the transcritical shallow water fluid flow past an obstacle described by the fKdV equation where the "partial undular bore" attached to the obstacle is generated in the upstream flow [10, 11] (see also [92]). Qualitative behavior of the Riemann invariants in the attached downstream DSW is

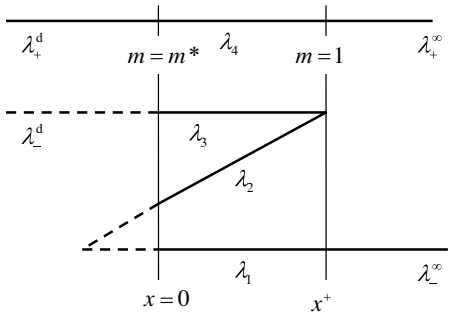

Figure 5.7: Qualitative behavior of the Riemann invariants in the partial (attached) downstream DSW.

shown in Figure 5.7. Equation (5.63) determines λ_2^*, and therefore, using the formula for c (3.38), the value of the modulus m^* at which the downstream DSW is generated at $x = 0$. This value is equal to

$$m^* = \frac{(\lambda_2^* - \frac{1}{2}v + 1)(\frac{1}{2}v + 1 - \lambda_-^d)}{(\frac{1}{2}v + 1 - \lambda_2^*)(\lambda_-^d - \frac{1}{2}v + 1)}. \tag{5.65}$$

Within the partial DSW the modulus changes in the interval $m^* \leq m \leq 1$. The dependence of the cut-off modulus m^* on the BEC flow velocity v is shown in Figure 5.8a for $V_m = 0.5$. One can see that for this case the cut-off modulus ranges in the interval $0 < m^* \lesssim 0.75$ and for the transcritical flow velocities v sufficiently close to the lower boundary v_- one can treat the downstream DSW as a dark soliton train slowly propagating to the right relative to the barrier. This is the dark soliton train that should remain within the finite elongated BEC for some time after the potential has been swept and, therefore, could be observed in the experiment. Therefore it is instructive to study its parameters in more detail.

First we calculate the downstream soliton emission rate. This can be done using the formula

$$f^* = c^*/L^*\,, \tag{5.66}$$

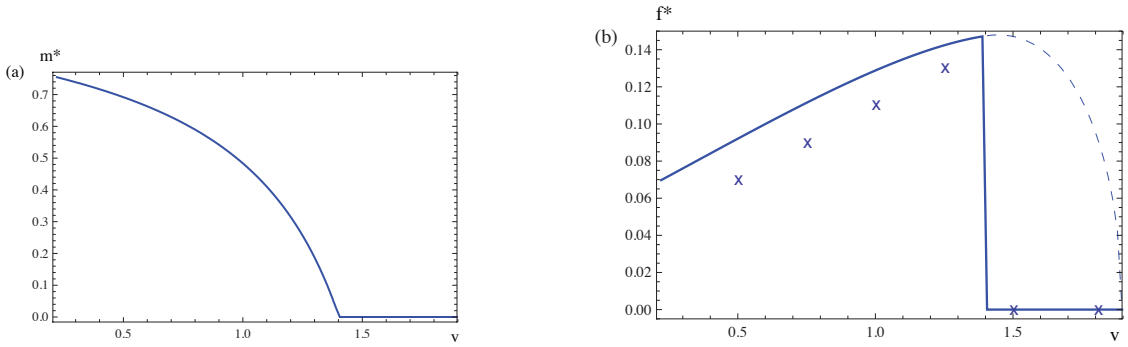

Figure 5.8: a) Cut-off modulus m^* in the downstream DSW (dark soliton train) and b) Downstream dark soliton emission rate f^* at the potential location vs oncoming BEC velocity v. Both figures correspond to $V_m = 0.5$. At $v \approx 1.4$ the downstream DSW detaches from the potential. Crosses in (b) correspond to the numerical simulations data. The dashed line in (b) corresponds to the frequency at the trailing edge of the detached downstream DSW.

where

$$c^* = \tfrac{1}{2}(\lambda_1 + \lambda_2^* + \lambda_3 + \lambda_4) = \tfrac{1}{2}(v + \lambda_-^d + \lambda_2^*)\,,$$
$$L^* = L(\lambda_1, \lambda_2^*, \lambda_3, \lambda_4) = \frac{2K(m^*)}{\sqrt{(\frac{1}{2}v + 1 - \lambda_2^*)(\lambda_d^- - \frac{1}{2}v + 1)}} \tag{5.67}$$

are the phase velocity (3.38) and the wavelength (3.41) respectively, calculated at the soliton train generation point $x = 0$.

Dependence $f^*(v)$ for $V_m = 0.5$ is shown in Figure 5.8b where it is also compared with the data from the direct numerical simulation using the potential (5.19) with $V_m = 0.5$, $\sigma = 2$. Some features seen on this plot deserve additional explanation. Firstly we notice that the analytically obtained value for the soliton emission frequency is finite for the flow velocities close to (but slightly greater than) the lower transcritical boundary $v_- \approx 0.2$. At the same time, the numerically obtained values of f^* suggest that the rate of soliton production tends to zero as one approaches the lower transcritical region boundary $v_- \approx 0.2$ (we did not observe any soliton generation at $v = 0.25$ for the time range up to $t = 50$). The disagreement between the analytical solution and actual behaviour of the soliton emission frequency is due to the failure, close to the transcritical region boundary $v = v_-$, of our

main assumption about the existence of the local transcritical hydraulic solution forming discontinuities with the equilibrium basic flow (see the discussion in Section 5.6). We note that the detailed analysis of the dynamical scaling law for the soliton emission frequency for near-critical NLS flows through short-range (delta-function) potentials was performed in [85], where the frequency was shown to vanish as $\delta^{1/2}$, δ being the deviation of the controlling parameter (for instance, potential strength) from its critical value.

The second "non-standard" feature in Figure 5.8b is an abrupt change, back to zero, of the emission frequency f^* for $v \approx 1.4$. This change does not constitute the cease of the soliton generation downstream but simply reflects the fact that the downstream DSW gets detached from the obstacle potential for velocities greater than some $v = v^*$, so there are no waves generated at the potential location at $x = 0$ (where the frequency f^* is defined). Indeed, as v increases within the transcritical region $[v_-, v_+]$, the speed s_-^d of the trailing edge (computed formally by (5.62)) can change the sign from minus to plus (see Figure 5.9), which implies that for some $v = v^*$ the downstream DSW must detach from the barrier. The detachment threshold velocity is determined from the condition

$$s_-^d(v^*) = 0, \tag{5.68}$$

where $s_-^d(v) = V_2(m = 0)$ is given by equation (5.62). For $V_m = 0.5$ this velocity is $v^* \approx 1.4$ (which can also be clearly seen in Figures 5.8a,b).

One of the physical consequences of the downstream DSW detachment from the obstacle is the zero frequency of oscillations for the drag force (see Section 5.5 below). At the same time, one should note that at the point of the detachment, the amplitude of the DSW vanishes, so the described discontinuity in the emission frequency at the obstacle has no practical significance. We stress that the solitons keep get generated downstream for $v^* < v < v_+$, but the generation point—the trailing edge of the downstream DSW – now moves away from the potential with constant velocity s_-^d. The corresponding wave frequency at the moving generation point is shown in Figure 5.8b by the dashed line.

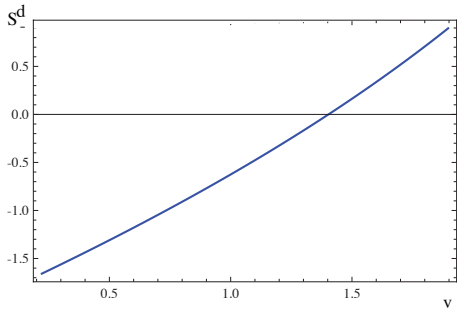

Figure 5.9: Dependence of the downstream DSW trailing edge speed s_-^d vs transcritical BEC velocity v calculated by formula (5.62). The detachment point $v = v^* \approx 1.4$ is found from the condition $s_-^d = 0$.

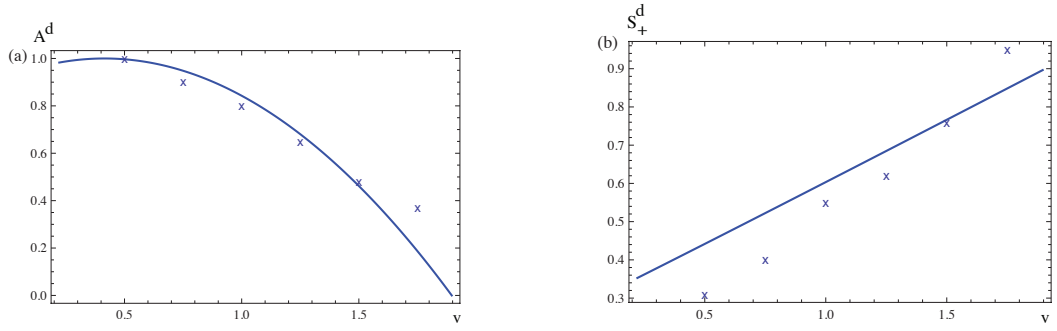

Figure 5.10: Leading soliton parameters: a) amplitude A^d and b) speed s_+^d — in the downstream DSW (dark soliton train) vs oncoming BEC velocity v for $V_m = 0.5$. Solid line: modulation solution; Crosses: direct numerical solution.

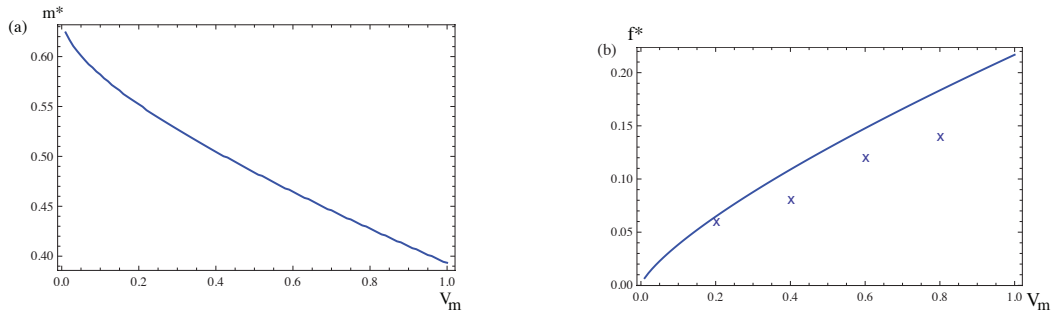

Figure 5.11: a) Cut-off modulus m^* in the downstream DSW and b) Downstream dark soliton emission rate f^* vs potential strength V_m. Both figures correspond to $v = 1.0$. Crosses in (b) correspond to the numerical simulations data.

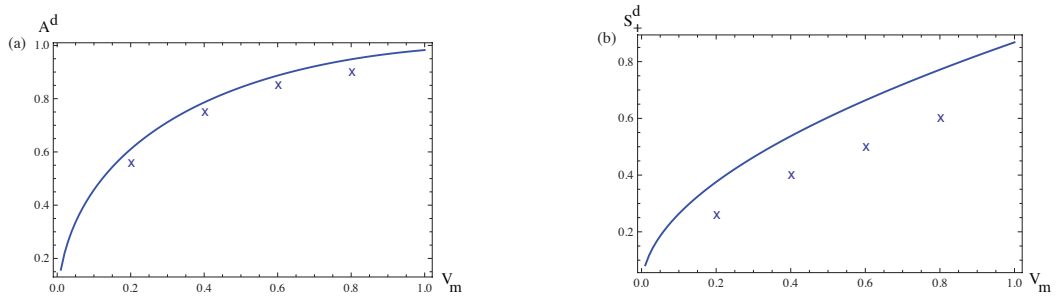

Figure 5.12: Leading soliton parameters: a) amplitude A^d and b) speed s_+^d — in the downstream DSW (dark soliton train) vs potential strength V_m. Both figures correspond to $v = 1.0$. Solid line: modulation solution; Crosses: direct numerical solution.

The limit $\lambda_2 \to \lambda_3$ ($m \to 1$) corresponds to the leading edge x^+ of the downstream DSW. The amplitude of the leading soliton is given by

$$A^d = (\lambda_4 - \lambda_3)(\lambda_3 - \lambda_1) = (2 + v - u^d)(u^d - v), \tag{5.69}$$

and it moves with the velocity

$$s_+^d = V_2(\lambda_-^\infty, \lambda_-^d, \lambda_-^d, \lambda_+^\infty) = u^d - 1. \tag{5.70}$$

The dependencies $A^d(v)$ and $s_+^d(v)$ for $V_m = 0.5$ are shown in Figure 5.10 along with the corresponding numerical simulations data. In Figures 5.11, 5.12 we plot the same set of quantities: A^d, s_+^d, m^* and f^*—as functions of the potential strength V_m for fixed $v = 1$. One can see that our solution predicts the main physical parameters of the downstream wave quite well provided the flow velocity is not too close to the critical values $v_\pm$ and the potential strength V_m is not too large.

Summarising, the downstream DSW occupies the region

$$s_-^* \cdot t < x < s_+^d \cdot t, \tag{5.71}$$

where $s_-^* = 0$ for $v_- < v < v^*$ and $s_-^* = s_-^d$ for $v^* < v < v_+$.

5.3.0.2 Upstream DSW

The calculations in this case are very similar to those for the downstream DSW. Now the constant Riemann invariants are equal to

$$\lambda_1 = \lambda_-^u, \quad \lambda_3 = \lambda_-^\infty = v/2 - 1, \quad \lambda_4 = \lambda_+^\infty = v/2 + 1, \tag{5.72}$$

and λ_2 as a function of x/t is determined by the equation

$$V_2(\lambda_-^u, \lambda_2, v/2 - 1, v/2 + 1) = x/t. \tag{5.73}$$

The zero-amplitude leading edge with $\lambda_2 \to \lambda_1$ propagates with the velocity

$$s_-^u = V_2(\lambda_-^u, \lambda_-^u, v/2 - 1, v/2 + 1) = 2\lambda_-^u - \frac{1}{\lambda_-^u - v/2} \tag{5.74}$$

which is always negative. The limit $\lambda_2 \to \lambda_3$ corresponds to the trailing (soliton) edge. The amplitude of the trailing soliton is equal to

$$A^u = 2(v - u^u), \tag{5.75}$$

and it moves with the velocity

$$s_+^u = V_2(\lambda_-^u, v/2 - 1, v/2 - 1, v/2 + 1) = \tfrac{1}{2}(u^u + v - 2). \tag{5.76}$$

In the case of of small $V_m \ll 1$ we get on using expansion (5.49) that

$$s_+^u \cong \tfrac{2}{3}(v - 1) - \sqrt{\frac{V_m}{6}}\,, \tag{5.77}$$

which implies that in the transcritical interval (5.50) s_+^u positive. Thus there exists the range of velocities v for which the upstream DSW is also attached to the barrier and realised only

partially. In contrast to the attached downstream DSW, in the partial upstream DSW the modulus m varies between 0 and some cut-off value $m^{**} < 1$, i.e. this wave can be viewed as a nonlinear oscillatory tail rather than solitary wave train.

The value $\lambda_2 = \lambda_2^{**}$, is found from the equation

$$V_2(\lambda_-^u, \lambda_2^{**}, v/2 - 1, v/2 + 1) = 0, \tag{5.78}$$

and determines the value of the cut-off modulus m^{**} via (3.38). The threshold velocity $v = v^{**}$ at which the upstream dispersive shock gets attached to the potential is found from the condition $s_+^u = 0$ and is determined implicitly by the equation

$$u^u(v) = 2 - v, \tag{5.79}$$

so that in the interval of velocities

$$v^{**} < v < v_+ \tag{5.80}$$

the upstream DSW is attached to the barrier. Thus, the upstream shock occupies the region

$$s_-^u \cdot t < x < s_+^{**} \cdot t, \tag{5.81}$$

where $s_+^{**} = 0$ for the velocities v in the interval (5.80) and $s^{**} = s_+^u$ for $v_- < v < v^{**}$.

5.4 Consolidated wave pattern

Putting together the analytical results of this Chapter, we obtain full asymptotic description of the wave pattern generated in the transcritical 1D flow of a BEC past a wide penetrable barrier. The pattern consists of two DSWs propagating upstream and downstream of the barrier and connected with each other by the transcritical hydraulic transition localised over the potential barrier spatial range. The behavior of the density and velocity within the

DSWs is obtained by the substitution of the slowly varying similarity modulation solutions (5.60), (5.61) and (5.72), (5.73) for λ_j into the rapidly oscillating travelling wave solution (3.38). One should note that the matching conditions (5.56) used in the construction of the modulation solution only guarantee the continuous matching of the average flow at the DSW boundaries. To get exact matching of the rapidly oscillating wave field within the DSWs with the constant (or slowly varying) flow outside, one should use the higher order analysis. The "weak limit" formulation of the DSW problem used above is now well established owing to the studies based on the Lax-Levermore-Venakides rigorous approach (see [68, 70] and references therein).

The obtained combined modulated/hydraulic solution is shown in Figure 5.13 at $t = 30$ for the potential with $V_m = 0.5$ and the oncoming flow velocity $v = 1$ (phase adjustments within the accuracy of the modulation theory are made to ensure continuity of the graph at the boundaries of the DSWs).

We have also performed direct numerical integration the GP equation (5.3) with boundary conditions (5.4). The simulations were performed using two different methods: the classical finite difference explicit scheme [93] and the quasi-spectral split step method [94]. Both methods gave the same results. In Figure 5.14 the numerical solution of the GP equation (5.3) is plotted for the potential (5.19) with $V_m = 0.5$ and $\sigma = 2$. One can see excellent agreement between the wave patterns in Figures 5.13 and 5.14

An additional small wave located about $x = 60$ in the numerical solution (Figure 5.14) is due to the generation of a small-amplitude right-propagating wave packet formed from the Bogoliubov linear waves created by a switching on the obstacle's potential (see [95]). The group velocity $v_g = d\omega/dk$ of the Bogoliubov waves obeying the dispersion relation $\omega(k) = k\sqrt{1 + k^2/4}$ is always greater than the sound speed $c_s = \sqrt{\rho} = 1$ and tends to this value in the long wavelength limit $k \to 0$. Taking into account that this wave packet is convected by the flow with velocity v, we find that the wave packet occupies the region $x > (c_s + v) \cdot t$ and its predicted position is about $x > 60$ for the chosen parameters with

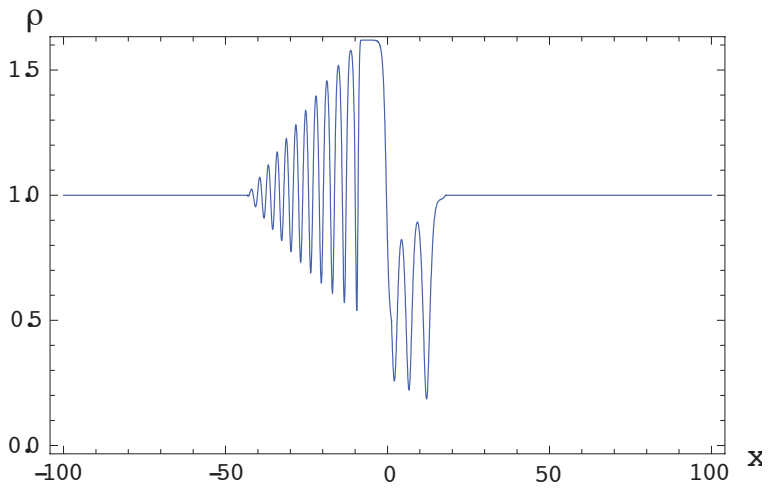

Figure 5.13: Plot of the combined analytical (hydraulic + modulated oscillatory) solution for the condensate density distribution in the wave pattern generated by a BEC flow with $v = 1$ through the potential barrier with $V_m = 0.5$ at $t = 30$.

$c_s = v = 1$ and $t = 30$ in agreement with the numerical results. Besides this wave packet, one can notice a tiny RW right before the wave packet. It is formed due to the small discrepancy between the upstream and downstream values of the Riemann invariant λ_+ (see Figure 5.5 and the related explanation of the closure conditions). It is not difficult to show using standard hydrodynamic reasoning that to leading order the density jump across this RW should be $\Delta\rho \approx \delta = (V_m/6)^{3/2}$ (see (5.46)) while the RW speed is calculated as $u + \sqrt{\rho} \approx v + 1$. For the parameters $V_m = 0.5$, $v = 1$ used in our numerical simulation this implies $\Delta\rho \approx 0.025$ and at $t = 30$ the predicted position of the RW is about $x = 60$. Both predictions completely agree with the numerical solution.

The agreement between the analytical and numerical solutions seen in Figures 5.13 and 5.14 is especially remarkable in view of the relatively small width of the potential, $\sigma = 2$, used in the numerical simulations. This width is comparable with the dispersion length in the system, which is of order of unity, so the formal requirement $l = \sigma/2 \gg 1$ of the applicability of the local hydraulic solution is clearly violated. The robustness of the hydraulic solution here looks quite surprising and deserves special attention. In this regard we note that our analytical construction implies that two potentially conflicting requirements should be

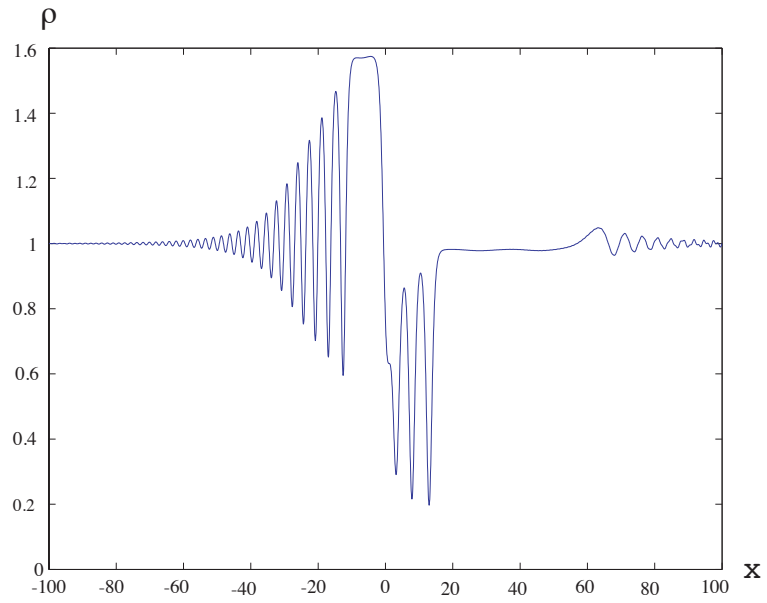

Figure 5.14: Numerical simulation of the condensate density distribution as a function of the space coordinate x in the wave pattern generated by a BEC flow with $v = 1$ through the potential barrier (5.19) with $V_m = 0.5$, $\sigma = 2$. The evolution time is equal to $t = 30$.

satisfied: the potential barrier should be (i) broad enough for the hydraulic approximation to be applicable but (ii) not too broad for the similarity modulation solution to be used for the description of the DSWs (i.e. the characteristic time of the establishing of the steady transcritical hydraulic solution should be much less than the characteristic time of the formation of the DSW). While it might look that these requirements are difficult to satisfy simultaneously, our numerical simulations show that the resulting analytical solution works quite well when $\sigma = O(1)$. We have also performed numerical simulations for $v = 1$ with potentials of different shapes with the conclusion that for potentials with $V_m \lesssim 1$ and $\sigma = O(1)$ the parameters of the oscillatory structure almost do not depend on the actual potential width and shape. This implies that for a reasonably broad range of the barrier potentials the whole wave pattern is characterised only by the potential strength V_m and the flow velocity v, which agrees with the parametrisation in our analytical solution. On the other hand, our simulations with very broad potentials $\sigma = O(10)$ show that the steady hydraulic transition with constant jumps outside the potential does not form within a finite

time interval so the developed quantitative description of the DSWs with the aid of the similarity modulation solutions does not apply.

As we see in Figures 5.13 and 5.14, the parameters $v = 1$, $V_m = 0.5$ correspond to the case when the downstream DSW is attached to the obstacle. It is natural to ask at which values of the parameters v, V_m the upstream DSW gets detached and whether there exists the region of the parameters when both shocks are detached from the obstacle. To answer these questions, we first notice that the downstream DSW detaches from the obstacle when the velocity of the trailing ($m = 0$) edge of the shock $V_2(v/2-1, v/2-1, \lambda_-^d, v/2+1)$ defined by equation (5.62) vanishes. This condition gives the equation

$$\tfrac{3}{4}v^2 - (9 + \lambda_-^d)v - (\lambda_-^d)^2 + 6\lambda_-^d + 11 = 0. \tag{5.82}$$

Taking into account equation (5.47) we find $\lambda_-^d = u^d/2 - \sqrt{\rho^d} = u^d - v/2 - 1$, and cast this equation to the form

$$v^2 - 12v - (u^d)^2 + 8u^d + 4 = 0, \tag{5.83}$$

which gives the value v^* of the "detachment" velocity

$$v^* = 6 - \sqrt{(u^d - 4)^2 + 16}, \tag{5.84}$$

where u^d is the greater root of the equation (5.48). In the weak potential limit $V_m \ll 1$ we obtain the series expansion

$$v^* = 1 + \frac{1}{2}\sqrt{\frac{3V_m}{2}} - \frac{V_m}{8} + \dots. \tag{5.85}$$

The upstream DSW detaches from the obstacle at velocity v^{**} which satisfies the equation (5.79) and again in the weak potential limit we obtain

$$v^{**} = 1 + \frac{1}{2}\sqrt{\frac{3V_m}{2}} - \frac{V_m}{24} + \dots. \tag{5.86}$$

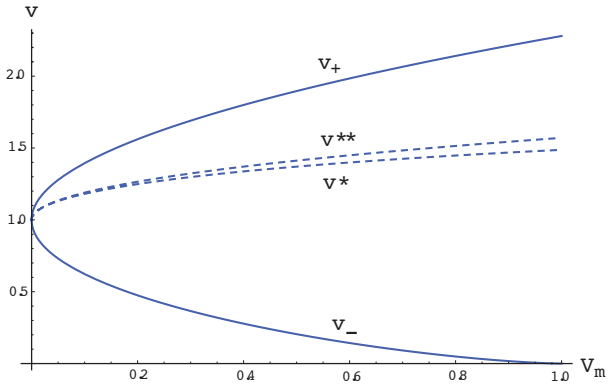

Figure 5.15: Dependence of the velocities v_- and v_+ at the boundaries of the transcritical region (solid lines) and of the velocities of v^* and v^{**} (dashed lines) on the maximum value V_m of potential.

It is easy to see that the region $v^* < v < v^{**}$ is located inside the transcritical region (5.50) and is relatively narrow; its position is illustrated in Figure 5.15.

We have verified the above predictions by constructing numerical solutions of the GP equation with $V_m = 0.5$ and $v = 1.4$ ($v^* < v < v^{**}$), $v = 1.8$ ($v > v^{**}$). The respective plots are presented in Figure 5.16.

In Figure 5.16a both DSWs are completely developed and actually they both are detached from the obstacle although because of the small difference between the soliton edge velocity of the upstream shock and the velocity of the small amplitude edge of the downstream shock, it takes very long time to reach a well developed hydraulic transition solution located near $x = 0$ solution. Nevertheless we see that both DSWs are not cut off at the edges close to the obstacle which means their detachment from the obstacle. In contrast, in Figure 5.16b the downstream DSW is detached from the obstacle whereas the upstream shock is attached and is cut off towards the soliton edge. However, one should notice that the parameters of the DSWs for the velocity v near the upper boundary v_+ of the transcritical region do not agree well enough with the analytical predictions. This disagreement has already been discussed in Section 5.2 and is due to the violation of our main supposition that the flow forms a steady hydraulic transition over the potential range interval with the jumps at the both its sides: here we cannot neglect the time of forming of the hydraulic

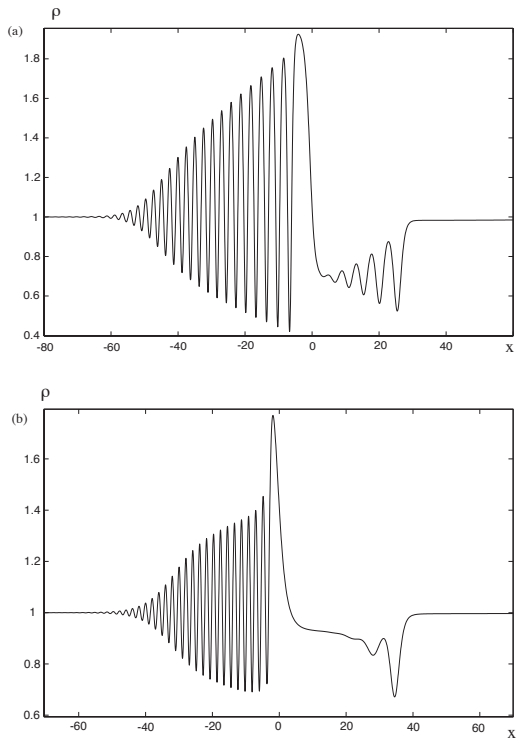

Figure 5.16: Numerical simulation of the condensate density distributions as functions of x in the wave pattern generated by the potential barrier (5.19) with $V_m = 0.5$ and (a) $v = 1.4$, (b) $v = 1.8$. Evolution time $t = 45$.

solution compared with the time of the development of the DSWs and therefore, the self-similar solutions used in the analytical theory are not accurate enough. In spite of this reservation, the developed theory qualitatively agrees with numerics even in this region: one can easily distinguish in the numerically obtained pattern all the characteristic ingredients of our analytical construction, namely, the smooth transition region over the potential range and downstream and the upstream DSWs.

5.5 Drag force

We now consider the drag force, i.e. the force exerted on the BEC due to its motion through the potential barrier. This force can be calculated as the spatial mean value of the operator

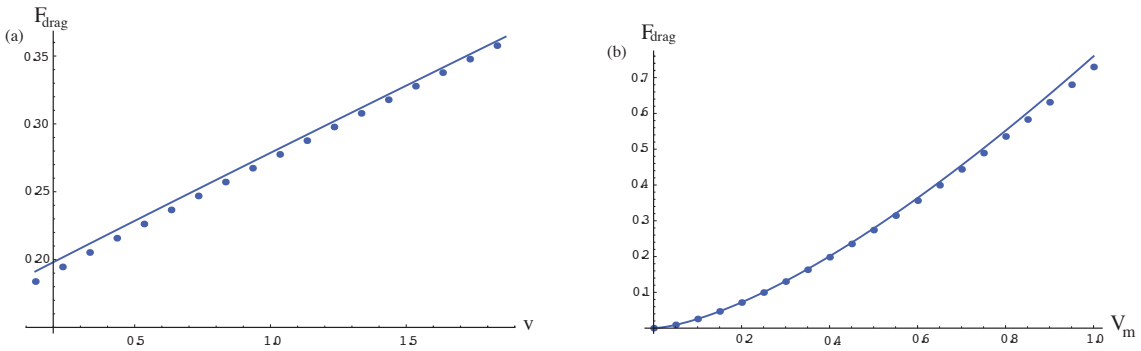

Figure 5.17: The drag force F_{drag} vs: a) BEC oncoming flow v in the transcritical region (v_-, v_+) and b) potential strength V_m for fixed $v = 1$. Solid lines are drawn according to the approximate equation (5.96) and dots correspond to the full numerical solution of equation (5.92).

$dV(x)/dx$ over the condensate wave function (see [88] for a detailed derivation),

$$F_{drag} = \int_{-\infty}^{\infty} \psi^* \frac{\partial V}{\partial x} \psi dx = \int_{-\infty}^{\infty} \rho \frac{\partial V}{\partial x} dx \,. \tag{5.87}$$

For subcritical and supercritical flows, $\rho = \rho(x)$ is given by the hydraulic solution (5.18) which connects smoothly to $\rho = 1$ as $|x| \to \infty$ and satisfies the system (5.5). Then integrating the associated Bernoulli equation

$$(\rho u^2 + \rho^2/2)_x + \rho V_x = 0 \tag{5.88}$$

from $-\infty$ to $+\infty$, and using that $\rho \to 1$, $u \to v$ as $|x| \to \infty$ we obtain $F_{drag} = 0$ which is the expression of BEC superfluidity at sub- and supercritical velocities. Strictly speaking, the superfluidity is exact for $v < v_- < c_s = 1$ where no excitations are generated. In the supersonic region $v > v_+ > c_s = 1$ the generation of excitations exists but it is exponentially small for a slowly varying obstacles's potential [87] and this generation is neglected in the hydraulic approximation used here.

For the transcritical regime, $v_- \leq v \leq v_+$, there is no global hydraulic solution and the

integral (5.87) can be split into three parts

$$F_{drag} = \int_{-\infty}^{-l} \rho_d(x,t)\frac{\partial V}{\partial x}dx + \int_{-l}^{l} \rho_{tr}(x)\frac{\partial V}{\partial x}dx + \int_{l}^{\infty} \rho_u(x,t)\frac{\partial V}{\partial x}dx. \tag{5.89}$$

Here $\rho_{u,d}(x,t)$ are the unsteady upstream and downstream solutions describing the density behavior in respective DSWs and $\rho_{tr}(x)$ is the local transcritical hydraulic solution (5.36) defined on the interval $(-l,l)$. Assuming that the potential $V(x)$ sufficiently rapidly decays for $|x| > l$ together with its first derivative V_x, one can neglect the contributions of the first and third integrals in (5.89). The remaining second integral can be evaluated again with the use of the Bernoulli equation (5.88) to obtain

$$F_{drag} = \rho^u(u^u)^2 + \tfrac{1}{2}(\rho^u)^2 - \rho^d(u^d)^2 - \tfrac{1}{2}(\rho^d)^2. \tag{5.90}$$

If the downstream or upstream shock is attached to the hydraulic solution, then the limiting values of the density and the flow velocity in the right-hand side of equation (5.90) oscillate with time according to the DSW solution (3.52) considered at $x = 0$ and the parameter m equal to m^* or m^{**} depending on whether the downstream or upstream DSW is attached. The frequency of the drag force oscillations for the downstream attachment case is given by formula (5.66) (a similar formula can be easily obtained for the upstream attachment case as well). Averaging of the expression (5.90) over time yields the mean value of the drag force. The situation simplifies greatly when both dispersive shocks are detached from the obstacle and $\rho^{u,d}$ and $u^{u,d}$ are given by the limiting values of the hydraulic solution. Although the corresponding region of the potential maximum V_m and velocity v values is rather narrow, the discussion of this case is quite instructive and enables one to estimate the accuracy of the drag force series expansion in powers of $V_m^{1/2}$ for small V_m.

As was shown above, $w = u^{u,d}$ are two roots of the equation (5.48) which can be rewritten

in a more convenient form after introduction of new variables

$$w = u_0(1-z), \quad \rho = u_0^2(1+z/2)^2, \quad u_0 = (v+2)/3, \quad \epsilon = V_m/u_0^2 = 9V_m/(v+2)^2, \quad (5.91)$$

so that equation (5.48) takes the form

$$\tfrac{1}{2}(1-z)^2 + (1+z/2)^2 - \tfrac{3}{2}(1-z)^{2/3}(1+z/2)^{4/3} = \epsilon. \quad (5.92)$$

One can easily derive series expansions of the roots of this equation in powers of $\epsilon^{1/2}$ to obtain

$$z^u = \sqrt{\frac{2\epsilon}{3}} - \frac{\epsilon}{18} + \dots, \quad z^d = -\sqrt{\frac{2\epsilon}{3}} - \frac{\epsilon}{18} + \dots, \quad (5.93)$$

where the first order terms reproduce actually Eqs. (5.49) after taking into account inequalities (5.50). With the use of equation (5.92) we represent equation (5.90) as

$$F_{drag} = u_0^4 \left[G(z^u) - G(z^d)\right] \quad (5.94)$$

where

$$G(z) = (1-z)^2(1+z/2)^2 + \tfrac{1}{2}(1+z/2)^4. \quad (5.95)$$

Then substitution of (5.93) into (5.94) yields with the accepted accuracy the expression

$$F_{drag} \cong u_0^4 \left(\sqrt{\frac{2}{3}}\epsilon^{3/2} - \frac{5}{6\sqrt{6}}\epsilon^{5/2}\right) \cong \left(\frac{V_m}{6}\right)^{3/2} \left[4(v+2) - \frac{5}{6}V_m\right], \quad (5.96)$$

where v varies in the transcritical region (5.50). In Figure 5.17 we compare the plots of dependence of F_{drag} on v and V_m according to equation (5.96) and calculated by means of the exact numerical solution of equation (5.92). As we see, the accuracy is very good even for $V_m = 1$.

5.6 Discussion

In the experiment [6] it was found that the solitons are generated by a moving potential barrier in the interval of velocities

$$0.3\text{mm/s} < v < 0.9\text{mm/s}. \tag{5.97}$$

This result agrees qualitatively with existence of the finite interval (5.20) for which the expanding DSWs are generated. However, we encounter a quantitative contradiction if we accept the value of the sound velocity calculated in [6] $c_s = 2.1$mm/s as correct, because in our non-dimensional units the sound velocity is equal to unity and hence it must be located inside the interval (5.20), (see Figure 5.2), or, in dimensional units, inside the interval (5.97). This disagreement can be explained by noticing that the above value of the sound velocity was calculated in [6] according to the expression

$$c_s^0 = \sqrt{\frac{\rho_0 g}{2m}}, \tag{5.98}$$

where ρ_0 is the condensate density at the center of the trap. Here

$$g = 4\pi\hbar^2 a_s/m \tag{5.99}$$

is the effective coupling constant in the BEC consisting of atoms with mass m and s-wave scattering length a_s. But this expression is correct only for a rarefied enough condensate confined to the cigar-shaped trap with "frozen" radial motion and this condition was not fulfilled in [6].

Dynamics of a dense BEC is described by the full 3D GP equation, which can be reduced to some effectively 1D systems much more complicated than the NLS equation (5.1). For example, the variational approach to the dynamics of the dense BEC was developed in [96] where it was shown that the sound velocity along the axial direction of the trap is given by

the expression (see Eqs. (67) and (70) in [96])

$$c_s = c_s^0 \cdot \frac{(1+3G/2)^{1/2}}{(1+2G)^{3/4}}, \tag{5.100}$$

where the parameter G is calculated by the formula

$$G = \frac{a_\perp^2}{8\xi^2}\left(\sqrt{1+\left(\frac{a_\perp^2}{8\xi^2}\right)^2}+\frac{a_\perp^2}{8\xi^2}\right). \tag{5.101}$$

Here $a_\perp = \sqrt{\hbar/m\omega_\perp}$ is the radial "oscillator length" and $\xi = \hbar/\sqrt{2m\rho_0 g}$ is the healing length. Equation (5.100) reduces to equation (5.98) in the limit $G \ll 1$ of a rarefied BEC. In the experiment [6] these parameters were equal to $a_\perp = 0.73 \cdot 10^{-4}$cm and $\xi = 0.17 \cdot 10^{-4}$cm, so that equation (5.101) gives $G = 11.4$, that is the experiment [6] corresponds to the opposite limit of dense BEC. The sound velocity calculated according to equation (5.100) is equal to $c_s = 0.8$mm/s, and this value agrees much better with the interval (5.97). Thus, for quantitative description of the experiment [6] the theory of dispersive shocks in a dense BEC should be developed what is beyond the scope of this thesis. Therefore we shall confine ourselves here to some qualitative remarks only.

The famous Landau criterion [7] for the loss of superfluidity was based on the consideration of linear excitations only and it contradicted to the experiments with liquid HeII. This discrepancy was explained by Feynman by taking into the consideration the formation of such nonlinear structures as vortices in the flow of a superfluid in capillaries or past obstacles. However, the notion of the threshold velocity below which the flow is superfluid has not been changed by this modification of the theory. Taking into account the generation of DSWs in 2D situation [36, 97] did not change this notion either, since the stationary spatial DSWs are generated by the supersonic flow of BEC only. Our results, as well as the results of the previous works [9, 86–89], show that the situation can be more subtle in the case of 1D flows. In this case, the flow past a broad barrier leads to the generation of DSWs

for a finite interval of the flow velocities bounded not only from below but *also from above*. Moreover, the lower boundary value of the velocity v_- can become equal to zero for strong enough barriers, that is even very slow motions could lead to the generation of solitons. This observation is in striking contrast with the standard reasonings based on the linear theory of excitations.

In conclusion we note that the obtained results can be used for the description of the nonlinear optical wave tunneling through penetrable barriers. Observation of the generation of DSWs in the plane wave tunneling through a refractive index defect in a photorefractive crystal was reported in the very recent paper by Wan, Muenzel and Fleischer [5]. The qualitative dynamics observed in [5] agree with the NLS theory presented in this Chapter. The quantitative theory can be constructed in the framework of the NLS equation with saturable nonlinearity (2.63) (see Section 2.4.3.2) using the DSW fitting method described in Chapter 4 (Section 4.7).

Chapter 6

DSW refraction in Kerr media

The problem of the interaction of viscous shock waves with RWs is a canonical problem in gas and fluid dynamics. It was first mathematically formulated by Courant and Friedrischs in 1943 [98] and has been later the subject of numerous studies (see some of the original research papers [99–102] as well as classical monographs [12, 74]). One can distinguish two types of such interactions: unidirectional (overtaking) and bidirectional (head-on). The problem of the the interaction of a shock wave with a simple RW is often referred to as the shock wave refraction problem since, after the interaction, the intensity and the speed of the shock wave change, which corresponds to the 'refraction' of the shock trajectory in the x, t-plane.

It is clear that the shock wave refraction problem can be considered for dispersive conservative media such as BECs or optical media. In such media, viscous shocks are replaced by DSWs while the RW description remains the same. Ablowitz, Baldwin and Hoefer [15] considered the problem of the overtaking interactions of DSWs and RWs associated with the KdV equation. Their analysis performed using the analytical inverse scattering transform (IST) solutions for the KdV equation and numerical solutions of the KdV-Whitham equations has revealed certain similarities as well as fundamental differences between classical and dispersive-hydrodynamic overtaking shock wave-RW interactions. In many physical

settings, however, one has to deal with *bi-directional* (head-on) wave collisions which cannot be captured by the KdV type models and should be studied in the framework of appropriate two-wave equations.

In this Chapter we consider head-on collisions of DSWs and RWs in the framework of the defocusing NLS equation with cubic (Kerr) nonlinearity, which is the main mathematical model used in the Thesis. This problem is fundamentally important as a dispersive counterpart of a classical gas dynamic problem and also can find applications in superfluid dynamics and nonlinear optics.

The results presented in this Chapter have been published in the joint paper [21].

6.1 Formulation of the problem

We consider the NLS equation (3.1) and rewrite it in its dispersive-hydrodynamic form (3.5)

$$\begin{aligned} \rho_t + (\rho u)_x = 0, \\ u_t + u u_x + \rho_x + \epsilon^2 (\frac{\rho_x^2}{8\rho^2} - \frac{\rho_{xx}}{4\rho})_x = 0 \end{aligned} \tag{6.1}$$

with the explicitly introduced dispersion parameter ϵ. We note that, since the results of the modulation theory do not depend on the value ϵ in (6.1), we shall be assuming $\epsilon = 1$ in the analytical representations of the periodic solutions (i.e. will make use of the results in Section 3.1.2, while in the numerical simulations we shall normally be using smaller values of ϵ to reduce the numerical time of the slowly modulated DSW structure establishment. This proved to be essential in the modelling of the DSW-RW interaction problem because the time required for the waves to settle down to their 'quasi-steady' profiles after the interaction can be very significant.

As we have seen in Section 3.1.1.2, the dispersionless ($\epsilon = 0$) limit of the hydrodynamic system (6.1) (the SWE (3.6)) can be written in diagonal form (2.7) by introducing the Riemann invariants $\lambda_\pm = \frac{1}{2}u \pm \sqrt{\rho}$, where the associated characteristic velocities $V_\pm$ are

given by (2.8).

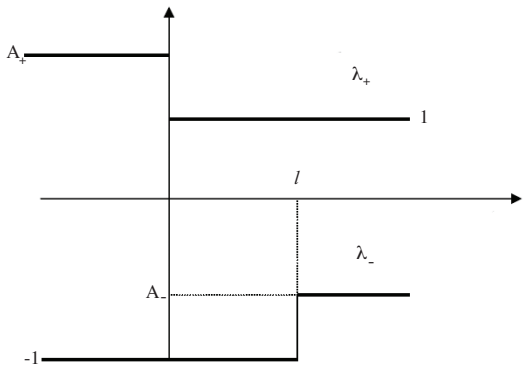

Figure 6.1: Initial conditions for the NLS equation (6.1) leading to the head-on DSW-RW interaction: profiles of hydrodynamic Riemann invariants $\lambda_\pm$ (6.2).

To model the interaction of a DSW and RW we consider the IVP for the NLS equation (6.1), formulated in terms of the shallow water Riemann invariants $\lambda_\pm$ rather than ρ and u separately as in Chapter 4. Namely, we consider two jumps for $\lambda_\pm$, which have different polarity and which are separated from one another by a distance l, see Figure 6.1:

$$\lambda_+ = \begin{cases} 1 & for \quad x > 0, \\ A_+ & for \quad x < 0, \end{cases} \qquad \lambda_- = \begin{cases} -1 & for \quad x > l, \\ A^- & for \quad x > l. \end{cases} \tag{6.2}$$

where $A^+ > 1$ and $-1 < A^- < 1$. In terms of the density ρ and velocity u initial conditions (6.2) assume the form (see Figure 6.2):

$$\rho(x,0) = \begin{cases} \frac{1}{4}(1+A^+)^2 > 1 & for \quad x < 0, \\ 1 & for \quad 0 < x < l, \\ \frac{1}{4}(1-A^-)^2 < 1 & for \quad x > l; \end{cases} \qquad u(x,0) = \begin{cases} A^+ - 1 > 0 & for \quad x < 0, \\ 0 & for \quad 0 < x < l, \\ 1 + A^- > 0 & for \quad x > l. \end{cases} \tag{6.3}$$

With these initial conditions, it is expected that the NLS dynamics will lead to the formation of a DSW and a RW (see Fig. 6.3) which, after a period of time, will begin to

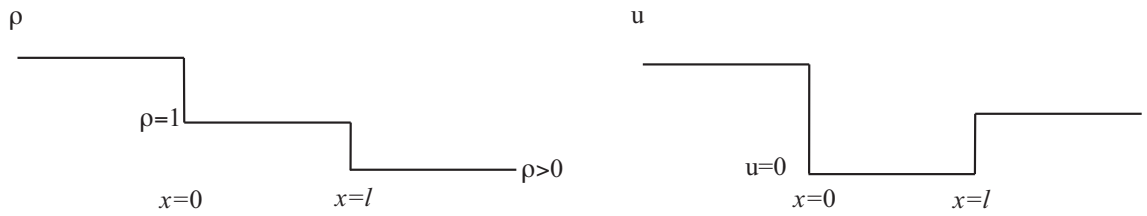

Figure 6.2: Piecewise constant initial conditions for density and velocity (6.3) corresponding to the Riemann invariant profiles (6.2).

interact and then will completely separate so that we get a refracted DSW and RW with new parameters. The crucial difference between the present problem (6.1), (6.3) and the canonical problem of the decay of an initial discontinuity described in Section 4.4, is that the two discontinuities for λ_+ and λ_- are now spaced a large distance l so the modulation problem is no longer self-similar and a more general, hodograph solution is required to describe the interaction of the two waves.

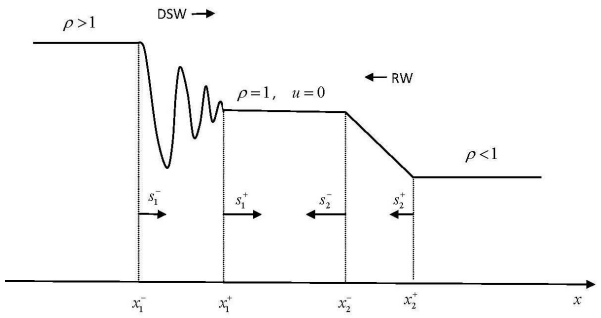

Figure 6.3: Sketch of the density profile in the NLS flow prior to head-on DSW-RW interaction

6.2 Refraction of shock waves in classical gas dynamics

Before we proceed with the analysis of the bidirectional dispersive refraction problem (3.1), (6.3) we outline some classical results on the head-on interaction of viscous shocks and RWs (see e.g. [98, 99]).

Consider a one-dimensional motion of a polytropic isentropic gas, i.e. a gas with the

equation of state $p = c\rho^\gamma$, where p and ρ are the gas pressure and density respectively, γ is the adiabatic exponent and c is a constant (the dispersionless shallow water dynamics (2.1) is equivalent to the dynamics of the polytropic gas with $\gamma = 2$). Let the gas motion at some moment of time, say $t = t_c \geq 0$ consist of three regions of constant flow separated by two waves: a right-propagating shock wave (SW) located at some $x = x_c$ and a left-propagating RW centred at $x = l$ and occupying a finite region of space, such a configuration can be created by piston motion inside a tube (see e.g. [99]). Let the density and velocity of the flow be (ρ_1, u_1) as $x \to -\infty$ and (ρ_2, u_2) as $x \to +\infty$. Then the gas motion at $t > t_c$ can be qualitatively described as follows:

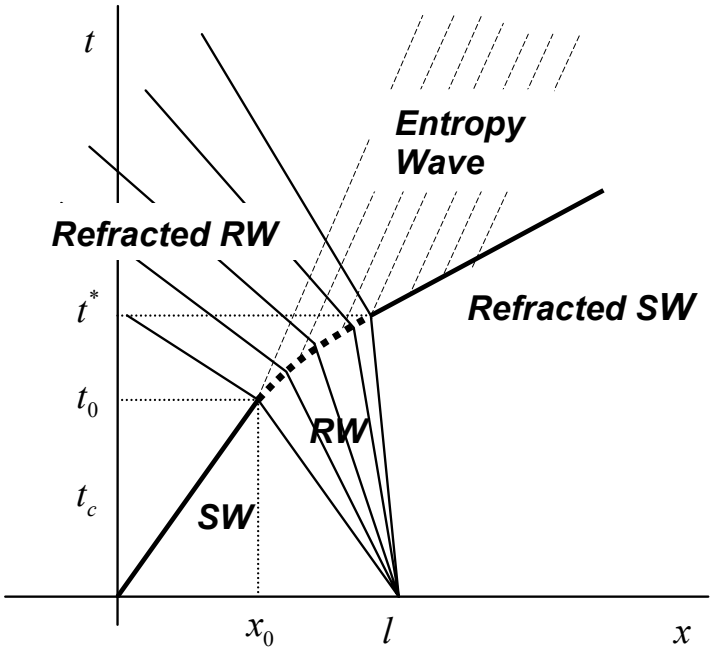

Figure 6.4: Head-on interaction of shock wave and RW in classical gas dynamics

- The shock wave and RW propagate independently until the moment $t = t_0$, when the shock enters the RW region at some $x = x_0$ say. Before that moment, i.e. for $0 < t < t_0$, the entropy undergoes a rapid constant change across the shock wave so the shock wave speed and strength (the pressure excess across it) are determined by the standard Rankine-Hugoniot conditions. The RW is described by the centred left-

propagating simple-wave solution of the inviscid hydrodynamic equations of motion. The parameters of the constant flow between the shock wave and RW are found at the intersection of the $\rho - u$ diagrams for the shock wave and RW (see e.g. [12]).

- During certain time interval $t_0 < t < t^*$ the shock wave and the RW interact. The interaction is accompanied by the variations of the shock strength and results in the formation of the varying entropy region (the so-called 'entropy wave') behind the shock wave. Therefore, the flow behind the refracted shock wave is not isentropic.

- At $t = t^*$ the shock wave exits the RW region and the two waves again propagate separately in opposite directions, each having an altered (as compared with the values before the interaction) set of parameters. An important general result is that the speeds of the refracted shock wave and RW and the density/velocity jumps across them are exactly as they would have been in the corresponding origin-centred Riemann problem (i.e. in the decay of an initial discontinuity problem with the gas parameters (ρ_1, u_1) at $x < 0$ and (ρ_2, u_2) at $x > 0$), however, the spatial locations of the refracted waves differ from those in the corresponding Riemann problem. The refracted shock wave always has greater speed and strength than the original one.

As already was mentioned, the presence of the 'entropy wave' behind the refracted shock wave radically complicates quantitative analysis of the motion and, as a result, the shock wave-RW head-on collision problem can generally be treated only numerically. In contrast to classical gas dynamics, dispersive hydrodynamic flows governed by completely integrable equations often admit full analytical description. In particular, such a description is available for the DSW refraction process. This description can also be generalised (to some extent) to certain types of non-integrable dispersive equations. The generalisation to the NLS equation with saturated nonlinearity will be described in Chapter 7.

6.3 DSW-RW interaction: numerical simulations

In Figures 6.5 and 6.6 the results of direct numerical simulations of the DSW-RW interaction are presented. Details of the numerical methods used can be found in the Appendix. In

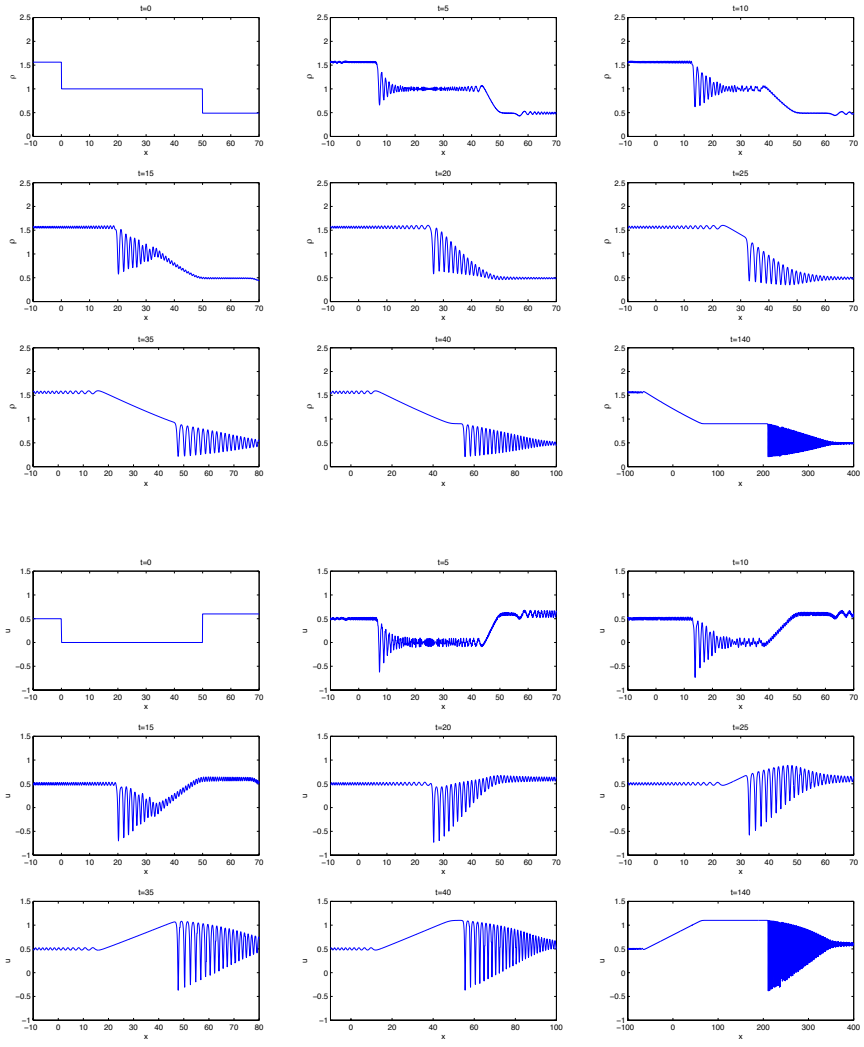

Figure 6.5: Numerical simulation of the bidirectional interaction of a DSW and RW: density (upper panel) and velocity (lower panel) profile; Initial data parameters: $A^+ = 1.5$, $A^- = -0.4$, $l = 50$. The value of the dispersion parameter ϵ used in the simulations is 0.4

Figure 6.5 the plots for the density and velocity profiles at different stages of the NLS evolution of the initial profile (6.2) are shown. In Figure 6.6 a density x, t plot is presented for the same evolution. One can clearly see the change of the DSW and RW parameters due

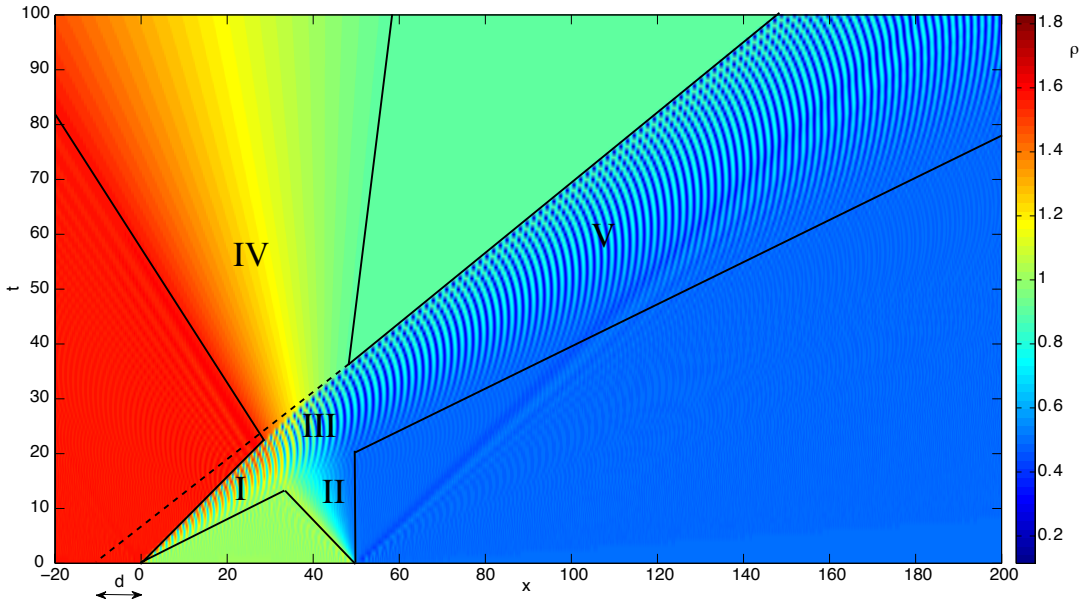

Figure 6.6: Density plot corresponding to the DSW-RW interaction shown in Figure 6.5. The regions are as follows: I – incident DSW; II – incident RW; III – DSW-RW interaction region; IV – Refracted RW; V – Refracted DSW.

to the interaction, and the DSW refraction phase shift d.

6.4 Modulation solution

In the problem we are considering, we have an initial discontinuity in the Riemann invariant λ_+ at $x = 0$ evolving into a right-propagating simple DSW and a discontinuity in the Riemann invariant λ_- at $x = l$ evolving into a left-propagating simple RW. These wave structures remain separated until some time t_0. They then interact during the time interval $t_0 < t < t^*$ and for $t > t^*$ the DSW and RW again separate but now each having a new set of parameters.

In this section we construct modulation solutions describing all stages of the evolution of the DSW and RW. We shall assume the general modulation description of DSWs and RWs presented in Chapters 3 and 4 and apply it to the specific IVP (6.1), (6.2). Along with the self-similar (x/t) modulation solutions found in Section 4.2. we shall need a more general, hodograph solution (4.5) from Section 4.5 to describe the DSW-RW interaction region and then determine the parameters of the refracted DSW and RW.

6.4.1 Before interaction, $0 < t < t_0$

6.4.1.1 Incident DSW

Translating the initial dicontinuity (6.2) at $x = 0$ into the Gurevich-Pitaevskii matching conditions (4.3) (see also the self-similar version (4.8)) we obtain

$$\begin{aligned} x = x^-(t): \quad & \lambda_3 = \lambda_2,\ \lambda_4 = A^+,\ \lambda_1 = -1, \\ x = x^+(t): \quad & \lambda_3 = \lambda_4,\ \lambda_2 = 1,\ \lambda_1 = -1. \end{aligned} \tag{6.4}$$

The similarity modulation solution satisfying matching conditions (6.4) has the form (see (4.12)

$$\begin{aligned} & \lambda_1 = -1, \quad \lambda_2 = 1, \quad \lambda_4 = A_+, \\ \frac{x}{t} = V_3(-1, 1, \lambda_3, A_+) = \frac{\lambda_3 + A_+}{2} - & \frac{(A_+ - \lambda_3)(\lambda_3 - 1)\mathrm{K}(m)}{(\lambda_3 - 1)\mathrm{K}(m) - (A_+ - 1)\mathrm{E}(m)}, \end{aligned} \tag{6.5}$$

where

$$m = \frac{2(A_+ - \lambda_3)}{(A_+ - 1)(\lambda_3 + 1)}. \tag{6.6}$$

The schamatic behaviour of the Riemann invariants in the obtained modulation solution is shown in Figure 6.7.

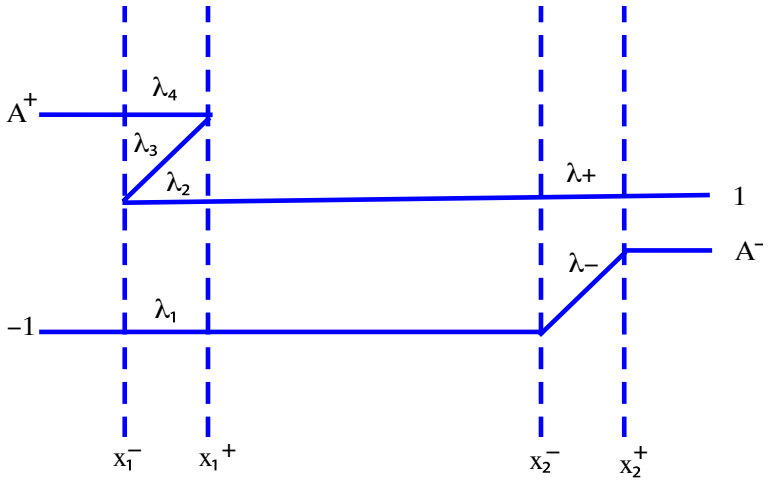

Figure 6.7: Schematic behaviour of the Riemann invariants before the interaction of the DSW and RW, $0 < t < t_0$.

The boundaries of the DSW are found from (6.5) by assuming $m = 0$ (i.e. $\lambda_3 = A^+$ – leading edge x_1^+) and $m = 1$ (i.e. $\lambda_3 = 1$ – trailing edge x_1^-):

$$x_1^- = \frac{1 + A_+}{2}t, \quad x_1^+ = \frac{2A_+^2 - 1}{A_+}t. \tag{6.7}$$

The dark soliton at the trailing edge x_1^- of the DSW has the amplitude a_s and propagates on the background ρ_s defined by

$$a_s = 2(A^+ - 1), \quad \rho_s = \tfrac{1}{4}(1 + A^+)^2\,. \tag{6.8}$$

The value $A^+ = 3$ corresponds to the formation of a vacuum point at the trailing edge of the DSW [19] so that the density at the dark soliton minimum is $\rho_s - a_s = 0$. For $A^+ > 3$

the vacuum point occurs inside the DSW at some point x_v where $x^- < x_v < x^+$ (see Section 4.2.3).

We define the DSW intensity I as the relative jump across it:

$$I = \frac{\rho_1}{\rho_2}, \tag{6.9}$$

where ρ_1 and ρ_2 are the values of the density upstream and downstream of the DSW respectively. For the incident DSW, i.e. before interaction, we have $\rho_1 = \rho_s$ and $\rho_2 = 1$ and therefore its intensity is

$$I_0 = \tfrac{1}{4}(1 + A^+)^2. \tag{6.10}$$

6.4.1.2 Incident RW

Now, the left-propagating RW is asymptotically described by the centred at $x = l$ similarity solution of the NLS dispersionless limit equations (3.6) – see Section 4.3. The relevant solution in Riemann invariants has the form

$$\lambda_+ = 1, \tag{6.11}$$

$$\frac{x-l}{t} = V_-(\lambda_-, 1) = \begin{cases} \lambda_- = -1, & x < x_2^-, \\ \dfrac{3\lambda_- + 1}{2}, & x_2^- \le x \le x_2^+, \\ \lambda_- = A_-, & x > x_2^+. \end{cases} \tag{6.12}$$

The behaviour of the Riemann invariants in the RW is shown in Figure 6.7. The boundaries $x_2^\pm$ are given by

$$x_2^- = l - t, \quad x_2^+ = l + \frac{3A_- + 1}{2}t. \tag{6.13}$$

Note, the modulation system (3.39) in the harmonic limit is consistent with the SWE

(2.7), (2.8) — see (3.50), the RW solution (6.11), (6.12) can also be found to be a solution of the full modulation system (3.39), (3.44), namely

$$\lambda_3 = \lambda_4 = A^+, \quad \lambda_2 = \lambda_+ = 1, \quad \lambda_1 = \lambda_-(x,t). \tag{6.14}$$

The DSW and RW evolve independently until they meet at the moment $t = t_0$, when the leading edge of the DSW overtakes the trailing edge of the RW. So at t_0 we have $x_0 = x_1^+(t_0) = x_2^-(t_0)$. Now using (6.7) and (6.13) we obtain

$$t_0 = \frac{A_+ l}{2A_+^2 + A_+ - 1}, \quad x_0 = \frac{2A_+^2 - 1}{2A_+^2 + A_+ - 1} l. \tag{6.15}$$

6.4.2 DSW-RW interaction, $t_0 < t < t^*$

At $t > t_0$ the DSW and RW begin to overlap so that a nonlinear interaction region $[x_2^-, x_1^+]$ forms (see Figure 6.8) and evolves in time up to a time $t = t^*$ when the DSW completely overtakes the RW and the waves separate from each other. At the point of separation we have $x_2^+(t^*) = x_1^-(t^*)$. Both waves at this point acquire new sets of parameters λ_j, different from their initial Riemann invariant distributions found in previous Section. Schematic behaviour of the Riemann invariants in the interaction zone is shown in Figure 6.8. One should stress that, for $t > t_0$ the functions $x_1^\pm(t)$ and $x_2^\pm(t)$ are no longer described by the formulae (6.7), (6.13) from the previous Section.

In the interaction region $[x_2^-, x_1^+]$ one still has $\lambda_2 = 1$ and $\lambda_4 = A^+$ but the remaining two Riemann invariants (λ_1 and λ_3) now vary so the modulation solution is no longer self-similar and a more general, hodograph solution (4.38), (4.39) for $k = 1$, $l = 3$ is needed. This is found via the additional transformation (4.41),

$$W_i = \left(1 - \frac{L}{\partial_i L}\partial_i\right) g\,, \quad i = 1, 3, \tag{6.16}$$

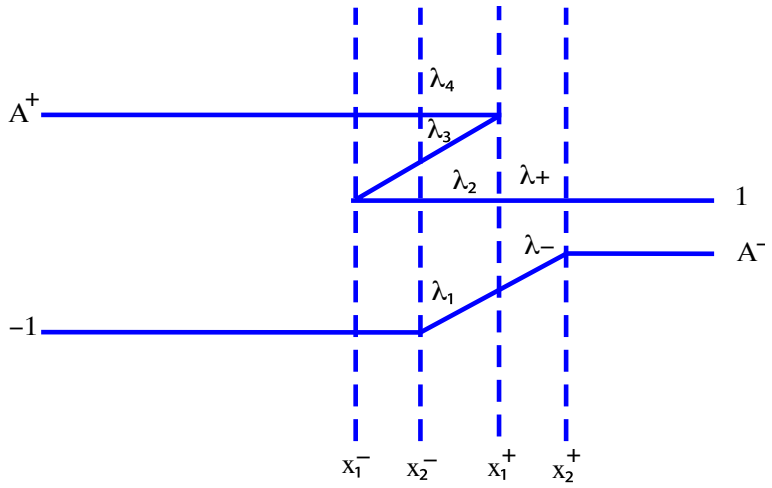

Figure 6.8: Schematic behaviour of the Riemann invariants during the interaction of the DSW and RW, $t_0 < t < t^*$.

reducing Tsarev's equations (4.39) for $W_{1,3}(\lambda_1, \lambda_3) \equiv W_{1,3}(\lambda_1, 1, \lambda_3, A^+)$ to a single EPD equation (4.43)

$$2(\lambda_3 - \lambda_1)\partial_{31}^2 g = \partial_3 g - \partial_1 g\,. \tag{6.17}$$

The general solution (4.44) of the EPD equation (6.17)

$$g(\lambda_1, \lambda_3) = \int_{a_1}^{\lambda_1} \frac{\phi_1(\lambda)d\lambda}{\sqrt{(\lambda - \lambda_1)(\lambda_3 - \lambda)}} + \int_{a_2}^{\lambda_3} \frac{\phi_2(\lambda)d\lambda}{\sqrt{(\lambda - \lambda_1)(\lambda_3 - \lambda)}}\,, \tag{6.18}$$

is parametrised by two arbitrary functions $\phi_{1,2}(\lambda)$ and two constants $a_{1,2}$, which should be found from appropriate boundary conditions. These conditions, in their turn, must follow from the continuity matching conditions for λ_1 and λ_3 at the unknown boundaries $x_2^-(t)$ and $x_1^+(t)$.

At the left boundary $x = x_2^-(t)$ of the interaction region (segment PQ in the interaction diagram in Figure 6.9, left), we have (see Figure 6.8)

$$\lambda_1 = -1, \quad \lambda_2 = 1, \quad \lambda_3 = \lambda_3^s(x_2^-(t), t), \quad \lambda_4 = A_+, \tag{6.19}$$

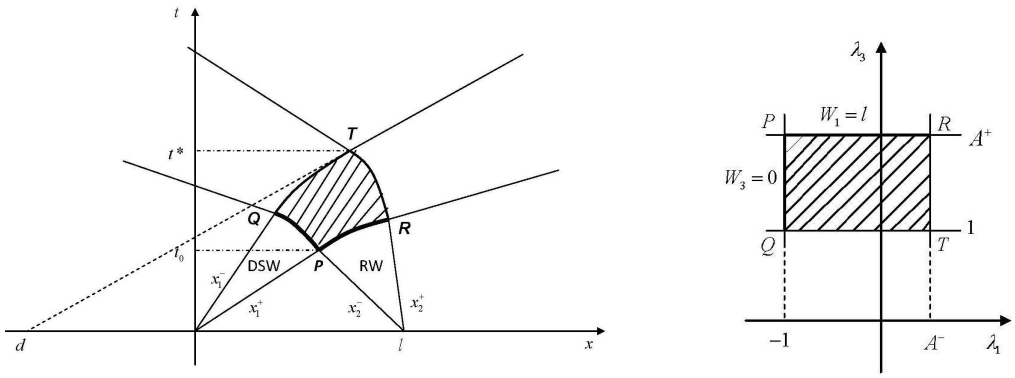

Figure 6.9: DSW-RW interaction diagram. Left: physical, (x,t) plane; Right: hodograph, $(\lambda_1\lambda_3)$ plane.

where $\lambda_3^s(x,t) = \lambda_3(x/t)$ is found from the similarity modulation solution (6.5).

At the right boundary $x = x_1^+(t)$ of the interaction zone (segment PR in the interaction diagram in Figure 6.9, left), we have (see Figure 6.8)

$$\lambda_1 = \lambda_-^r(x_1^+(t),t), \quad \lambda_2 = 1, \quad \lambda_3 = \lambda_4 = A_+, \tag{6.20}$$

where $\lambda_-^r(x,t) = \lambda_-((x-l)/t)$ is found from the rarefaction solution (6.11) and (6.12).

The boundary conditions (6.19) and (6.20) have to be translated into the boundary conditions for the function $g(\lambda_1,\lambda_3)$ satisfying the EPD equation (6.17). This can be done in two steps. In the first step, we derive the boundary conditions for the functions $W_1(\lambda_1,\lambda_3)$ and $W_3(\lambda_1,\lambda_3)$ satisfying the system of linear PDEs (4.39)

$$\frac{\partial_k W_l}{W_k - W_l} = \frac{\partial_k V_l}{V_k - V_l}\ ; \quad k,l = 1,3, \quad k \neq l, \tag{6.21}$$

and defining the hodograph solution (4.38)

$$x - V_1 t = W_1, \qquad x - V_3 t = W_3\,. \tag{6.22}$$

Using the boundary condition (6.20) at $x = x_1^+$ and the expression (3.50)for the characteristic

velocity V_1 for the degenerate case when $\lambda_3 = \lambda_4$, the first equation in (6.22) becomes

$$x - \frac{3\lambda_1 + 1}{2} t = W_1(\lambda_1, A_+). \tag{6.23}$$

Due to the matching condition (6.20) we have $\lambda_1 = \lambda_-$ at $x = x_1^+$, then we get by comparing (6.23) with the RW solution (6.11) and (6.12) that

$$W_1(\lambda_1, A_+) = l. \tag{6.24}$$

Next we turn to the boundary condition (6.19) and deduce from the comparison of second equation (6.22) with similarity solution (6.5) that

$$W_3(-1, \lambda_3) = 0\,. \tag{6.25}$$

Thus, the unknown at the onset curvilinear interaction zone $PQTR$ in the (x,t)-plane (Figure 6.9, left) maps to the prescribed rectangle $PQTR$ in the hodograph $(\lambda_1\lambda_3)$ plane (Figure 6.9, right). We also note that, in contrast to the original free-boundary matching conditions (6.19), (6.20) for the Riemann invariants $\lambda_j(x,t)$, the boundary conditions (6.24) and (6.25) for the functions $W_{1,3}(\lambda_1, \lambda_3)$ are *linear* (i.e. they do not depend on the particular solution).

To deduce boundary conditions for the EPD equation (6.17) from conditions (6.24), (6.25) for the Tsarev equations (6.21) we use the relations (6.16) between $W_{1,3}(\lambda_1, \lambda_3)$ and the scalar function $g(\lambda_1, \lambda_3)$. From (6.24) and (6.16) considered for $\lambda_2 = 1$ we obtain a simple ODE

$$g(\lambda_1, A_+) - \frac{L(\lambda_1, 1, A_+, A_+)}{\partial_1 L(\lambda_1, 1, A_+, A_+)} \partial_1 g(\lambda_1, A_+) = l, \tag{6.26}$$

which can be easily integrated, giving boundary value of the function $g(\lambda_1, A_+)$ at $\lambda_3 = A_+$,

$$g(\lambda_1, A_+) = C_1 L(\lambda_1, 1, A_+, A_+) + l = \frac{C_1}{\sqrt{A_+ - \lambda_1}} + l, \tag{6.27}$$

where C_1 is an arbitrary constant of integration.

From (6.25) we find, using relation (6.16)

$$g(-1, 1, \lambda_3, A_+) - \frac{L(-1, 1, \lambda_3, A_+)}{\partial_3 L(-1, 1, \lambda_3, A_+)} \partial_3 g(-1, 1, \lambda_3, A_+) = 0. \tag{6.28}$$

So the solution is found to be

$$g(-1, \lambda_3) = C_2 L(-1, 1, \lambda_3, A_+), \tag{6.29}$$

where C_2 is a second constant of integration.

Important note, we aim to satisfy the boundary conditions (6.24) and (6.25) for $W_{1,3}$. For that, we have two arbitrary functions $\phi_{1,2}(\lambda)$ and two arbitrary constants $C_{1,2}$. We first observe that, according to Section 4.6, the function $g(-1, \lambda_3)$ has the meaning of the modulation phase shift in the incident DSW. Since this DSW is described by a centred simple wave modulation solution, this phase shift must be equal to zero (see the end of Section 4.6). Thus we set $C_2 = 0$ so that condition (6.29) assumes the form

$$g(-1, \lambda_3) = 0. \tag{6.30}$$

Then setting $\phi_2(\lambda) \equiv 0$ and $a_1 = -1$ in the general solution (6.18) of the EDP equation (6.17) we have

$$g = \int_{-1}^{\lambda_1} \frac{\phi_1(\lambda) d\lambda}{\sqrt{(\lambda_3 - \lambda)(\lambda_1 - \lambda)}}. \tag{6.31}$$

Now we substitute conditions (6.27) and (6.30) in an aim to find $\phi_1(\lambda)$ and C_1. Doing so we obtain

$$\int_{-1}^{\lambda_1} \frac{\phi_1(\lambda)d\lambda}{\sqrt{(\lambda_3-\lambda)(\lambda_1-\lambda)}} = \frac{C_1}{\sqrt{A_+-\lambda_1}} + l, \tag{6.32}$$

which is an Abel integral equation for $\phi_1(\lambda)$ (see e.g. [65]). Recall,

$$if \quad \int_a^x \frac{\phi(\zeta)}{\sqrt{x-\zeta}}d\zeta = f(x), \quad then \quad \phi(x) = \frac{1}{\pi}\frac{d}{dx}\int_a^x \frac{f(\zeta)}{\sqrt{x-\zeta}}d\zeta. \tag{6.33}$$

The solution to (6.32) can then be obtained

$$\phi_1(\lambda) = \frac{1}{\pi\sqrt{\lambda+1}}\big(C_1\sqrt{\frac{A_++1}{A_+-\lambda}} + l\sqrt{A_+-\lambda}\big). \tag{6.34}$$

Equation (6.30) is now satisfied by (6.31) and (6.34) only if $\phi_1(-1) = 0$ which implies that $c_1 = -l\sqrt{A_++1}$, so

$$\begin{aligned} g(\lambda_1,\lambda_3) &= -\frac{l}{\pi}\int_{-1}^{\lambda_1} \frac{\sqrt{\lambda+1}\,d\lambda}{\sqrt{(A_+-\lambda)(\lambda_3-\lambda)(\lambda_1-\lambda)}} \\ &= -\frac{2l(A_++1)}{\sqrt{(A_+-\lambda_1)(\lambda_3+1)}}(K(z)-\Pi_1(s,z)), \end{aligned} \tag{6.35}$$

where

$$z = \frac{(A_+-\lambda_3)(\lambda_1+1)}{(A_+-\lambda_1)(\lambda_3+1)}, \quad s = -\frac{\lambda_1+1}{A_+-\lambda_1}. \tag{6.36}$$

Then the exact modulation solution describing the interaction of counter-propagating DSW and RW is given by the formulae

$$\lambda_2 = 1, \quad \lambda_4 = A_+, \quad x - V_{1,3}(\lambda_1,1,\lambda_3,A_+)t = \big(1-\frac{L}{\partial_{1,3}L}\partial_{1,3}\big)g(\lambda_1,\lambda_3), \tag{6.37}$$

where $g(\lambda_1, \lambda_3)$ is given by (6.35).

The interaction takes place until time $t = t^*$ given by

$$t^* = \frac{2\sqrt{2}l\mathrm{E}(r)}{\pi(1-A_-)\sqrt{A_+ - A_-}}, \tag{6.38}$$

where

$$r = \frac{(A_+ - 1)(A_- + 1)}{2(A_+ - A_-)}. \tag{6.39}$$

x_* is given by, $x_* = P(1)$ (see (6.46) below).

6.4.3 After interaction, $t > t^*$

At $t = t^*$ the DSW exits the RW region and the two waves separate.

6.4.3.1 Refracted DSW

The modulation solution describing the DSW after the separation is given by three constant invariants, see Figure 6.10

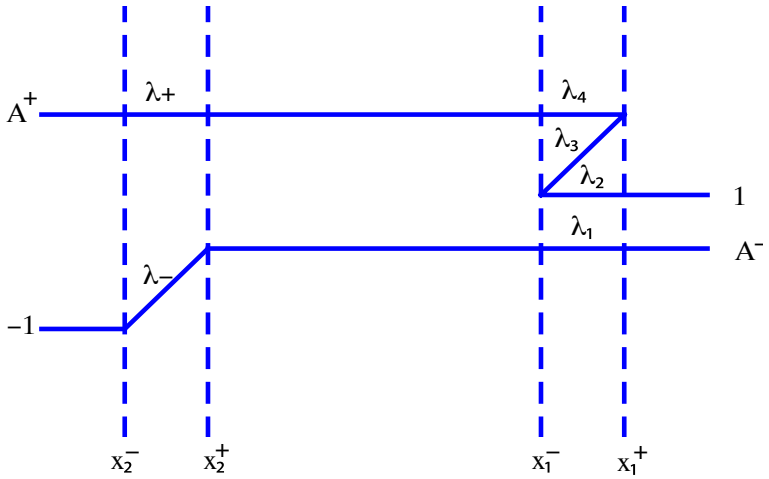

Figure 6.10: Schematic behaviour of the Riemann invariants after the interaction of the DSW and RW, $t > t^*$.

$$\lambda_1 = A^-, \quad \lambda_2 = 1, \quad \lambda_4 = A^+, \tag{6.40}$$

while for the remaining one, λ_3, we have from (6.37) a simple-wave modulation solution (cf. (6.5))

$$\begin{aligned} x &= V_3(A^-, 1, \lambda_3, A^+)t + P(\lambda_3) \\ &= (\tfrac{1}{2}(1 + A^- + A^+ + \lambda_3) + \frac{(A^+ - \lambda_3)(\lambda_3 - 1)(\lambda_3 - 1)}{(\lambda_3 - A^-)\mu(m)})t + P(\lambda_3), \end{aligned} \tag{6.41}$$

where

$$m = \frac{(1 - A^-)(A^+ - \lambda_3)}{(A^+ - 1)(\lambda_3 - A^-)}, \quad \mu(m) = \mathrm{E}(m)/\mathrm{K}(m) \tag{6.42}$$

and the function $P(\zeta)$ is found as

$$\begin{aligned} P(\zeta) = W_3(A^-, \zeta) &= (1 - \frac{L(A^-, 1, \zeta, A^+)}{\partial_3 L(A^-, 1, \zeta, A^+)}\partial_3) g(A^-, \zeta) \\ &= \frac{2l}{\pi\sqrt{(A^+ - A^-)(\zeta + 1)}}((A^+ + 1)\Pi_1(p, z) + \\ &\frac{[(A^+)^2 - 1](\zeta - A^-)\mathrm{K}(z)\mu(y) - [\zeta^2 - 1][A^+ - A^-]\mathrm{E}(z)}{(\zeta - A^-)[(\zeta - 1) - (A^+ - 1)\mu(y)]}), \end{aligned} \tag{6.43}$$

where

$$p = -\frac{A^- + 1}{A^+ - A^-}, \quad z = \frac{A^- + 1}{A^+ - A^-}\frac{A^+ - \zeta}{\zeta + 1}, \quad y = \frac{(1 - A^-)(A^+ - \zeta)}{(A^+ - 1)(\zeta - A^-)}, \tag{6.44}$$

Expressions (6.44) are obtained from formulae (6.36), where one sets $\lambda_1 = A^-, \lambda_3 = \zeta$, and the modulus m in (6.43) is specified by (6.42) where λ_3 is replaced by ζ. Thus, as a result of the interaction, the DSW is no longer described by the similarity modulation solution in the form of an expanding centred fan but rather becomes a general simple wave solution of the modulation system corresponding to the following IVP for the NLS equation (6.1):

$$\lambda_-(x, 0) = A^-, \quad \lambda_+(x, 0) = P^{-1}(x), \tag{6.45}$$

$P^{-1}(x)$ being inverse of the function $x = P(\lambda_+)$. The function $P(\lambda_+)$ in (6.41) represents the DSW de-centring distribution acquired as a result of the interaction with the RW. It is related to the modulation phase shift $\theta_0(x,t)$ via (4.52), (4.53), so we shall call it the refraction shift function.

It is not difficult to verify that $P(\zeta) \equiv 0$ for $A^- = -1$. This is exactly what one should expect since when $A^- = -1$, there is no RW generated and therefore no refraction of the DSW.

The boundaries x_1^- and x_1^+ of the refracted DSW are found by setting in (6.41) $\lambda_3 = 1$ (i.e. $m = 1$) and $\lambda_3 = A^+$ (i.e. $m = 0$) respectively

$$x_1^- = (1 + \frac{A^- + A^+}{2})t + P(1), \quad x_1^+ = (2A^+ - \frac{(1-A^-)^2}{2(2A^+ - 1 - A^-)})t + P(A^+). \tag{6.46}$$

The density background and the amplitude of the trailing dark soliton in the refracted DSW are

$$\rho_{sr} = \tfrac{1}{4}(A^+ - A^-)^2, \quad a_{sr} = (A^+ - 1)(1 - A^-). \tag{6.47}$$

The intensity I_r of the refracted DSW is determined using

$$I_r = \frac{\rho_1}{\rho_2} \tag{6.48}$$

where $\rho_1 = \rho_{sr}$ and $\rho_2 = \frac{1}{4}(1 - A^-)^2$, thus

$$I_r = (\frac{A^+ - A^-}{1 - A^-})^2. \tag{6.49}$$

6.4.3.2 Refracted RW

The solution for the refracted RW, is found from the hodograph modulation solution (6.37) by setting in it $\lambda_4 = \lambda_+ = A^+, \lambda_3 = \lambda_2 = 1, \lambda_1 = \lambda_-$ (see (6.11)) and using that

$V_1(\lambda_1, \lambda_3, \lambda_3, \lambda_4) = V_-(\lambda_1, \lambda_4)$ (see 6.28). As a result we get

$$\lambda_+ = A^+, \quad x = V_-(\lambda_-, A^+)t + G(\lambda_-) = \frac{3\lambda_- + \lambda^+}{2}t + G(\lambda_-), \tag{6.50}$$

where the function $G(\zeta)$ has the form

$$\begin{aligned} G(\zeta) = W_1(\zeta, A^+) &= (1 - \frac{L(\zeta, 1, 1, A^+)}{\partial_1 L(\zeta, 1, 1, A^+)}\partial_1) g(\zeta, A^+) \\ &= \frac{l\sqrt{2}}{\pi\sqrt{A^+ - \zeta}}[(A^+ + 1)(\Pi_1(n, r) - \mathrm{K}(r)) + 2\mathrm{E}(r)], \end{aligned} \tag{6.51}$$

where

$$r = \frac{(A^+ - 1)(\zeta + 1)}{2(A^+ - \zeta)}, \quad \rho = -\frac{\zeta + 1}{A^+ - \zeta}. \tag{6.52}$$

Similar to the refracted DSW, the refracted RW is no longer described by a centred fan solution but rather a general simple-wave solution of the shallow water system (3.3), (3.4) with the effective initial conditions $\lambda_+ = 1$ and $\lambda_-(x, 0)$ given by the function inverse to the refraction shift function $G(\lambda_-)$.

The boundaries of the refracted RW are given by the expressions

$$x_2^- = \frac{A^+ - 3}{2}t + G(-1), \quad x_2^+ = \frac{3A^- + A^+}{2}t + G(A^-). \tag{6.53}$$

6.4.4 Vacuum points

As was described in Section 4.2.3, an important feature of the DSWs in the defocusing NLS flows is the possibility of the vacuum ($\rho = 0$) point(s) occurrence in the solutions for the problems not containing vacuum states in the initial data [19]. This effect has no analogue in both viscous shock dynamics and in the DSW dynamics in media with negative dispersion supporting bright solitons. Across the vacuum point, the flow speed changes its sign, which implies the generation of a counterflow. The DSW counterflow due to the vacuum point occurrence has been recently observed in the experiments on nonlinear plane wave

tunneling through a broad penetrable repulsive potential barrier (refractive index defect) in photorefractive crystals [5].

If we fix the state $\rho_1 = 1$, $u_1 = 0$ in front of the DSW (as we do for the incident wave), then, by increasing the density jump ρ_2 across the DSW we will be able to increase the DSW relative intensity only up to the value $I = 4$ at which the vacuum point occurs at the DSW trailing edge [18] (recall, we denoted by ρ_1 and ρ_2 the values of the density upstream and downstream DSW respectively – see Section 6.3.1). If ρ_2 increases further, beyond the vacuum point threshold, the relative intensity of the compression part of the DSW decreases and, asymptotically as $\rho_2/\rho_1 \to \infty$, vanishes so that the DSW completely transforms into the classical (smooth) left-propagating RW [19]. This limit can alternatively be achieved by keeping the upstream state ρ_2 fixed and letting $\rho_1 \to 0$: then we arrive at the well-known solution of the classical shallow water dam-break problem (see e.g. [16]).

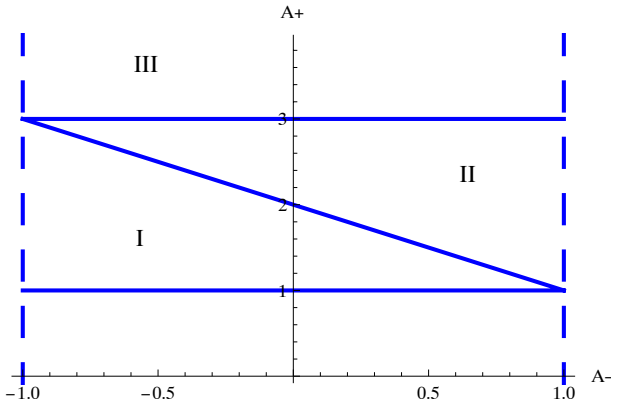

Figure 6.11: Regions in the plane of initial parameters (A^-, A^+) — the classification with respect to the vacuum point occurrence. (I): No vacuum points; (II): No vacuum points in the incident DSW, a vacuum point in the refracted DSW; (III): Vacuum points in both incident and refracted DSWs.

If $a_{sr} = \rho_{sr}$, which by (6.47), yields the relation $A^+ = 2 - A^-$, then the condition for the vacuum point appearance in the refracted DSW assumes the form

$$A^+ \geq 2 - A^- \,. \tag{6.54}$$

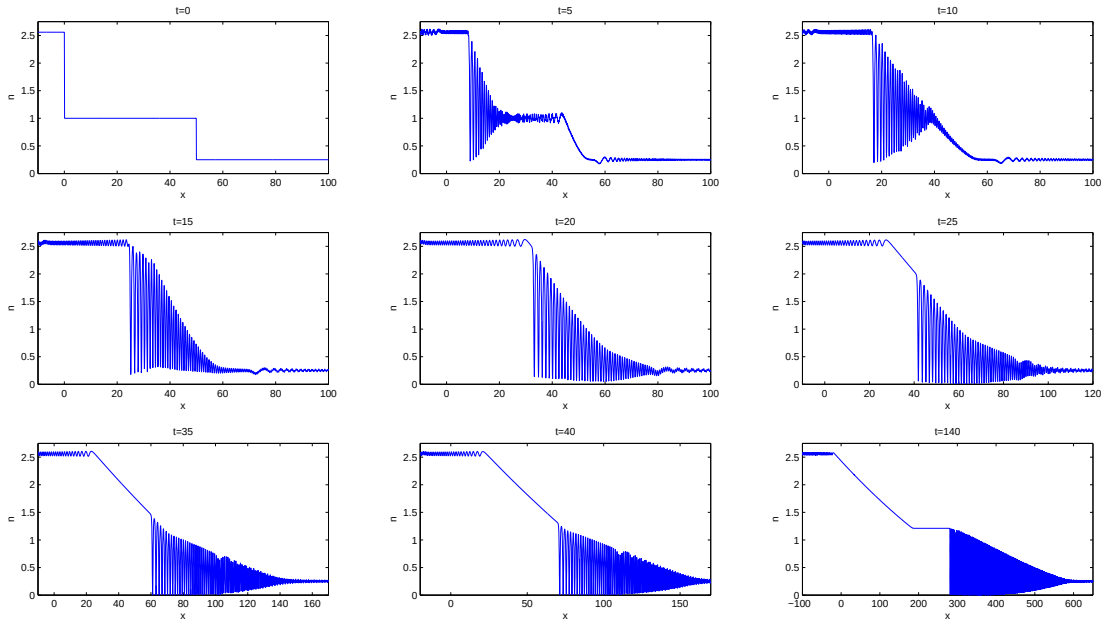

Figure 6.12: Numerical simulation: evolution of the profile (2.11) with $A^- = 0$, $A^+ = 2.2$, $l = 50$ (Region II in Fig. 6.11) leading to the occurrence of a vacuum point in the refracted DSW.

Setting $A^- = -1$ we recover the already mentioned criterion $A^+ \geq 3$ for the vacuum point occurrence in the incident DSW. The regions of the A^-, A^+ plane corresponding to different (with respect to the vacuum point appearance) flow configurations arising in the IVP (6.1), (6.2) are presented in a diagram shown in Fig. 6.11. An example of the particular flow evolution corresponding to Region II is shown in Fig. 6.12. One can see that the vacuum point occurs in the refracted DSW as predicted by our theory.

We stress that, although the vacuum point appearance modifies the oscillatory DSW profile (the lower DSW density envelope becomes non-monotonous and the velocity profile acquires a singularity at the vacuum point — see Figure 4.3), all the dependencies of the DSW edge speeds, density jumps and trailing soliton amplitudes on the initial data A^+, A^- remain unchanged.

6.5 DSW refraction parameters: comparison with numerical simulations

It is convenient to characterise the DSW refraction by three key parameters:

a. The amplification coefficient ν defined as the ratio of intensities (6.48) of the refracted and the incident DSWs.

b. The acceleration coefficient σ which we define as the difference between the values of the DSW trailing dark soliton speed s^- after and before the interaction.

c. The refraction shift d which we define as the phase shift of the DSW trailing soliton due to the DSW interaction with the RW.

For ν we have from (6.10) and (6.49)

$$\nu = \frac{I_r}{I_0} = (\frac{2(A^+ - A^-)}{(1 - A^-)(1 + A^+)})^2. \tag{6.55}$$

For σ we have from (6.7) and (6.53)

$$\sigma = s_r^- - s_0^- = \frac{dx_1^-}{dt}|_{t>t*} - \frac{dx_1^-}{dt}|_{t<t_0} = \frac{1 + A^-}{2} > 0. \tag{6.56}$$

Here we have used the subscript 'r' to denote the refracted wave and the subscripted '0' to denote the incident wave. The acceleration coefficient σ does not depend on the DSW intensity before refraction (i.e. on A^+). It is completely determined by the initial jump A^-, of the Riemann invariant λ_- across the RW. Since $A^- > -1$, one has $\sigma > 0$, therefore the DSW is always accelerated as a result of a head-on collision with a RW. This matches with the classical gas dynamics result that the shock wave is always accelerated after a head-on collision with a RW because the shock waves meet the gas of decreasing density [99].

Unlike the acceleration coefficient σ, the amplification coefficient ν can have both signs depending on the specific values of A^+ and A^- chosen, the boundary between the regions

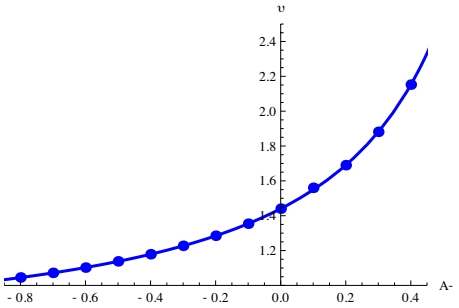

Figure 6.13: DSW amplification coefficient ν. Solid lines: analytic curve (6.55), $\nu(A^-)$ for $A^+ = 1.5$, circles: numerical simulations data.

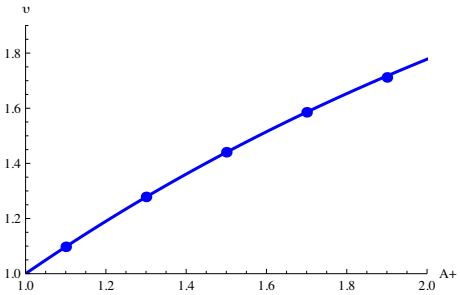

Figure 6.14: DSW amplification coefficient ν. Solid lines: analytic curve (6.55), $\nu(A^+)$ for $A^- = 0$, circles: numerical simulations data.

of the DSW (relative) strengthening and attenuation being given by equation $A^+ = (1 - A^-)/(1 + A^-)$. We also note that, while the amplification coefficient ν is formally defined for the full range of values of A^+ and A^-, its original significance is retained only for the DSWs not containing vacuum points.

The function (see (6.43), (6.53))

$$d(A^+, A^-) = P(1) = \frac{\sqrt{2}l}{\pi} \frac{A^+ - 1}{\sqrt{A^+ - A^-}} (\Pi_1(p, z^*) - \mathrm{K}(z^*)), \tag{6.57}$$

where

$$z^* = \frac{A^- + 1}{A^+ - A^-} \frac{A^+ - 1}{2}, \quad p = -\frac{A^- + 1}{A^+ - A^-}, \tag{6.58}$$

describes the *refraction shift* of the trailing dark soliton in the DSW as a function of the initial parameters A^+, A^-. This phase shift d can be clearly seen in Figure 6.6.

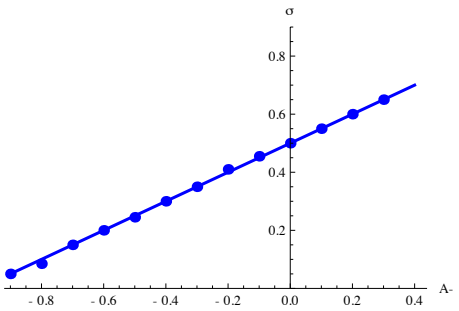

Figure 6.15: DSW acceleration coefficient σ. Solid lines: analytic curve (6.56), $\sigma(A^-)$ for $A^+ = 1.2$, circles: numerical simulations data.

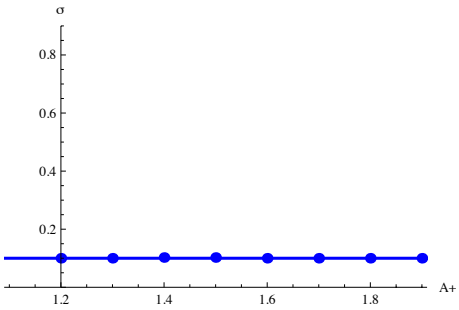

Figure 6.16: DSW acceleration coefficient σ. Solid lines: analytic curve (6.56), $\sigma(A^+)$ for $A^- = -0.8$, circles: numerical simulations data.

One can observe by comparing (6.57) with the solution $g(\lambda_1, \lambda_3)$ (6.35), (6.36) of the EPD equation for the DSW-RW interaction region, that

$$d(A^+, A^-) = g(A^-, 1), \tag{6.59}$$

which corresponds to the value of g at the moment $t = t^*$ (see (6.38)), when the DSW exits the interaction region. This is of course expected from the general modulation phase shift consideration described in Section 4.6.

Comparisons for the modulation parameters (6.55), (6.56) and (6.57) with the direct numerical simulations data for the IVP (6.1), (6.2) are presented in Figures 6.13 — 6.18. One can see an excellent agreement. One can also observe that the dependencies of the acceleration coefficient σ and the refraction shift d on the intensity of the RW (roughly proportional to A^-) are much stronger than on the intensity of the incident DSW (proportional to A^+).

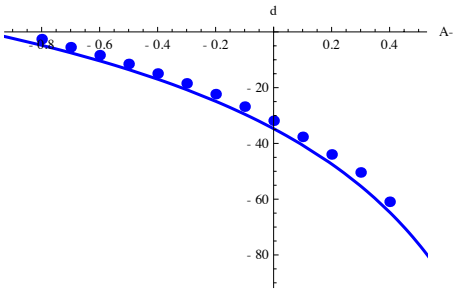

Figure 6.17: DSW refraction phase shift d. Solid line: formula (6.57), $d(A^-)$ for fixed $A^+ = 1.5$, circles: direct numerical simulations data.

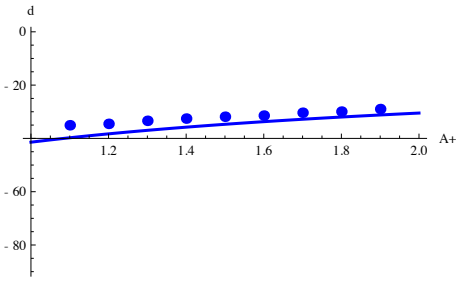

Figure 6.18: DSW refraction phase shift d. Solid line: formula (6.57), circles: direct numerical simulations data. Dependence $d(A^+)$ for fixed $A^- = 0$.

6.6 Discussion

In this Chapter, we have considered a dispersive counterpart of the classical gas dynamics problem of the interaction of a shock wave with a counter-propagating simple RW often referred to as the shock wave refraction problem. Apart from the obvious contrast between both local and global structures of viscous shock waves and DSWs, there is a fundamental difference between the classical dissipative, and the present, dispersive conservative settings. While the parameters defining the flow containing shock waves in classical gas dynamics are determined by appropriate systems of shock conditions, which take into account the changes of the thermodynamic properties of the medium through which the shock waves propagate, in dispersive dynamics the change of the hydrodynamic flow across the DSW is completely determined by the transfer of the Riemann invariants along the characteristics of the governing hyperbolic (Whitham) system, which makes possible a complete asymptotic description of the flow.

One can trace certain analogy between the considered DSW-RW interaction and the two-soliton collisions in integrable systems: both interactions are elastic in the sense that they both can be interpreted in terms of the "exchange" of spectral parameters by the interacting waves so that the global spectrum in the associated linear scattering problem remains unchanged. In the DSW-RW interaction the role of isospectrality is played by the transfer of the constant values of appropriate Riemann invariants of the modulation system through the varying DSW and RW regions so that one can predict the jumps of density and velocity across the refracted DSW and RW without constructing the full modulation solution. At the same time, the DSW and RW do not simply pass through each other and "exchange" the constant Riemann invariants: there are additional phase shifts for both interacting waves, similar to the classical soliton phase-shifts.

We conclude with the remark that the approach used in this Chapter can also be applied to obtain analytical solution to the problem of the *overtaking* DSW-RW interaction in the NLS flows. While this problem was studied in the KdV equation framework in [15], we believe that it deserves special attention in the context of the defocusing NLS flows since, due to a different dispersion sign and the possibility of the vacuum point occurrence within the DSW one can expect a number of qualitative and quantitative differences compared to the KdV flows. Also, the developed theory can be readily extended to the problem of the generation of DSWs by the interference of two simple RWs studied numerically in [14].

Chapter 7

DSW refraction in optical media with saturable nonlinearity

In this Chapter we perform analysis of the DSW refraction in the framework of the NLS equation with saturable nonlinearity (sNLS equation (2.63) describing, in a certain approximation, the one-dimensional propagation of a plane stationary light beam through a photorefractive crystal (see e.g. [103, 104]). This particular choice of the mathematical model has a clear physical motivation: there have been recently a number of major experiments involving DSWs in photorefractive materials (see e.g. [3, 5]). Also, photorefractive crystals are widely used for an all-optical modelling of the hydrodynamic effects of BECs so it is important to be able to quantify the contribution of the optical saturation to the purely 'superfluid' DSW evolution. As we already mentioned, the sNLS equation is not integrable by the IST method, thus the associated system of averaged conservation laws (the Whitham modulation system) does not possess Riemann invariants. That means that the modulation analysis of Chapter 6 based on the Riemann invariant representation of the Whitham equations is not applicable. Instead, we shall use the DSW fitting method of [53] outlined in Section 4.7 of Chapter 4.

7.1 sNLS equation: some basic properties

The Madelung transformation (5.2) maps equation (2.63) to the dispersive hydrodynamics system (cf. (3.1)),

$$\begin{aligned} \rho_t + (\rho u)_x &= 0, \\ u_t + u u_x + \left(\frac{\rho}{1+\gamma\rho} \right)_x + \left(\frac{\rho_x^2}{8\rho^2} - \frac{\rho_{xx}}{4\rho} \right)_x &= 0\,. \end{aligned} \tag{7.1}$$

Here ρ has the meaning of the light beam intensity and u is the local value of the wave vector component transversal to the beam propagation direction; $\gamma > 0$ is the saturation parameter. We repeat that in the nonlinear optics context the role of the time variable t is played by the spatial coordinate z along the beam propagation direction while x is the transversal coordinate. If the saturation effects are negligibly small, $\gamma\rho \ll 1$, then the sNLS equation (7.1) reduces to the cubic NLS equation (3.1). A detailed study of the periodic solutions to (7.1) can be found in [57]. Here we present some of the properties of the sNLS traveling waves necessary for the subsequent DSW fitting analysis.

Linear dispersion relation

The sNLS linear dispersion relation for the waves of infinitesimally small amplitude propagating against the constant background flow with $u = u_0$, $\rho = \rho_0$ has the form

$$\omega = \omega_0(k, \rho_0, u_0) = k u_0 \pm k \sqrt{\frac{\rho_0}{(1+\gamma\rho_0)^2} + \frac{k^2}{4}}\,, \tag{7.2}$$

where ω is the wave frequency and k is the wavenumber.

Dispersionless limit

In the dispersionless limit, system (7.1) can be cast in the diagonal form (2.7) with the Riemann invariants $\lambda_\pm$ and characteristic velocities $V_\pm$ expressed in terms of the hydrody-

namic variables ρ and u as

$$\lambda_\pm = \frac{u}{2} \pm \frac{1}{\sqrt{\gamma}} \arctan\sqrt{\gamma\rho}, \quad V_\pm = u \pm \frac{\sqrt{\rho}}{1+\gamma\rho}\,. \tag{7.3}$$

When $\gamma \to 0$ expressions (7.3) go over to the shallow water relationships (2.6), (2.9).

Soliton speed-amplitude relationship

The sNLS equation supports dark solitons propagating on non-zero density background. Although explicit analytic expression for the photorefractive dark soliton profile is not available, one can derive the relationship connecting the soliton speed c, the background flow parameters ρ_0, u_0 and the soliton amplitude a [57]:

$$(c-u_0)^2 = \frac{2(\rho_0-a)}{\gamma a}\left[\frac{1}{\gamma a}\ln\frac{1+\gamma\rho_0}{1+\gamma(\rho_0-a)} - \frac{1}{1+\gamma\rho_0}\right]. \tag{7.4}$$

7.2 Problem formulation

Similar to (6.2), we specify initial conditions for (7.1) in terms of two spaced steps for the hydrodynamic Riemann invariants $\lambda_\pm$

$$\lambda_+(x,0) = \begin{cases} A^+ & \text{for} \quad x<0, \\ \frac{1}{\sqrt{\gamma}}\arctan\sqrt{\gamma} & \text{for} \quad x>0; \end{cases} \qquad \lambda_-(x,0) = \begin{cases} -\frac{1}{\sqrt{\gamma}}\arctan\sqrt{\gamma} & \text{for} \quad x<l, \\ A^- & \text{for} \quad x>l, \end{cases} \tag{7.5}$$

where $A^+ > \frac{1}{\sqrt{\gamma}}\arctan\sqrt{\gamma}$, and $-\frac{1}{\sqrt{\gamma}}\arctan\sqrt{\gamma} < A^- < \frac{1}{\sqrt{\gamma}}\arctan\sqrt{\gamma}$. The special values of λ_+ for $x>0$ and λ_- for $x<l$ are chosen such that initially the DSW and RW will propagate into an undisturbed "gas" (indeed one can readily see, using (7.3) that $\rho=1$, $u=0$ in the middle region $0<x<l$ (cf. (6.3)).

Our numerical simulations show that evolution (7.1), (7.5) for a broad range of initial data parameters $A^\pm$ leads to the same qualitative DSW refraction scenario as in the cubic NLS case described in Chapter 6 (see Figures 6.5, 6.6). The *quantitative* characteristics of

the DSW refraction, however, now depend not only on the initial data parameters $A^{\pm}$ but also on the saturation parameter γ entering the sNLS equation. The results of [57] suggest that this dependence could be quite strong. Thus the DSW-RW interaction problem in the framework of the sNLS equation deserves a separate study. As we already mentioned, the knowledge of the effects of photorefractive saturation on the parameters of a DSW is especially important in the context of an all-optical modelling of BEC dynamics (see [3]).

7.2.1 DSW transition conditions

We now use the DSW fitting method of [53] (see also Section 4.7 for the method description in application to the cubic NLS equation) to formulate the of the DSW transition relations for the sNLS equation (7.1).

Let the *right-propagating* simple DSW of the sNLS equation be confined to a finite region of space $x^- < x < x^+$ and connect two constant hydrodynamic states (ρ_1, u_1) at $x < x^-$ and (ρ_2, u_2) at $x > x^+$; $\rho_1 > \rho_2$. At the trailing edge x^- the DSW assumes the form of a dark soliton moving with constant velocity s^- and at the leading edge x^+ it degenerates into a vanishing amplitude linear wavepacket moving with constant group velocity s^+, $s^+ > s^-$. The lines $x^{\pm} = s^{\pm}t$ represent free boundaries where the continuous matching of the mean flow $(\bar{\rho}, \bar{u})$ in the DSW region with the external constant states (ρ_1, u_1) and (ρ_2, u_2) occurs (see Section 4.1).

Then the simple DSW transition between the hydrodynamic states (ρ_1, u_1) and (ρ_2, u_2) is described by the following relationships:

- The conservation of the value of the Riemann invariant λ_- across the DSW,

$$\frac{u_1}{2} - \frac{1}{\sqrt{\gamma}} \arctan \sqrt{\gamma \rho_1} = \frac{u_2}{2} - \frac{1}{\sqrt{\gamma}} \arctan \sqrt{\gamma \rho_2} \equiv \lambda_-^0 \,. \tag{7.6}$$

- The DSW edge speeds $s^{\pm}$ are defined by the kinematic conditions (cf. conditions (4.61)

for the cubic NLS case)

$$s^+ = \left.\frac{\partial\Omega_0}{\partial k}\right|_{\bar\rho=\rho_2,\ k=k^+}; \qquad s^- = \left.\frac{\widetilde\Omega_0}{\kappa}\right|_{\bar\rho=\rho_1,\ \kappa=\kappa^-}. \tag{7.7}$$

The quantities k^+ (the leading edge wavenumber) and κ^- (the trailing edge "soliton wavenumber" – the trailing soliton inverse half-width) in (7.7) represent the boundary values, $k^+ = k(\rho_2)$ and $\kappa^- = \kappa(\rho_1)$, of two functions $k(\bar\rho)$ and $\kappa(\bar\rho)$ satisfying the following ODEs:

$$\frac{dk}{d\bar\rho} = \frac{\partial\Omega_0/\partial\bar\rho}{v_+(\bar\rho) - \partial\Omega_0/\partial k}, \qquad k(\rho_1) = 0\,; \tag{7.8}$$

$$\frac{d\kappa}{d\bar\rho} = \frac{\partial\widetilde\Omega_0/\partial\bar\rho}{v_+(\bar\rho) - \partial\widetilde\Omega_0/\partial\kappa}\,, \qquad \kappa(\rho_2) = 0\,. \tag{7.9}$$

Here

$$v_+(\bar\rho) = V_+(\bar\rho, \bar u(\bar\rho)) = \bar u(\bar\rho) + \frac{\sqrt{\bar\rho}}{1+\gamma\bar\rho}\,, \tag{7.10}$$

$$\Omega_0(\bar\rho, k) = \omega_0(k, \bar u(\bar\rho), \bar\rho) = k\left[\bar u(\bar\rho) + \sqrt{\frac{\bar\rho}{(1+\gamma\bar\rho)^2} + \frac{k^2}{4}}\right], \qquad \widetilde\Omega_0(\bar\rho,\kappa) = -i\Omega_0(\bar\rho, i\kappa); \tag{7.11}$$

and

$$\bar u(\bar\rho) = 2\left(\lambda_-^0 + \frac{1}{\sqrt\gamma}\arctan\sqrt{\gamma\bar\rho}\right). \tag{7.12}$$

- The 'entropy' inequalities must hold ensuring that the hydrodynamic characteristics transfer data *into* the DSW region:

$$V_-^1 < s^- < V_+^1, \quad V_+^2 < s^+, \quad s^+ > s^-. \tag{7.13}$$

Here $V_\pm^1 \equiv V_\pm(\rho_1, u_1)$, $V_+^2 \equiv V_+(\rho_2, u_2)$ – see (7.3) for the definitions of $V_\pm(\rho, u)$.

Relationships (7.6) – (7.13) enable one to 'fit' the DSW into the solution of the dispersionless limit equations without the knowledge of the detailed solution of the full dispersive system within the DSW region (much as in classical gas dynamics shock wave is fitted into the

solution of the inviscid equations by means of the Rankine-Hugoniot conditions subject to Lax's entropy condition).

Using the speed-amplitude relationship (7.14) for the photorefractive dark solitons one can find the amplitude a_s of the DSW trailing soliton. Setting the value s^- (7.7) of the DSW trailing edge for the soliton velocity c and ρ_1, u_1 for the background flow ρ_0, u_0 in (7.14) we obtain:

$$(s^- - u_1)^2 = \frac{2(\rho_1 - a_s)}{\gamma a_s}\left[\frac{1}{\gamma a_s}\ln\frac{1+\gamma\rho_1}{1+\gamma(\rho_1 - a_s)} - \frac{1}{1+\gamma\rho_1}\right] \tag{7.14}$$

(note: $u_1(\rho_1)$ is given by the simple DSW transition condition (7.6)).

7.2.2 DSW refraction

Our concern here will be with the calculations of two DSW refraction parameters: the DSW amplification and acceleration coefficients, defined earlier in (6.56) and (6.55) as

$$\nu = \frac{I_r}{I_0} \qquad and \qquad \sigma = s_r^- - s_0^- \tag{7.15}$$

respectively. We note that analytical determination of the refraction phase shift d is, unfortunately, not feasible now as it requires knowledge of the full modulation solution, which is not available for the sNLS equation due to its non-integrability so we shall present only numerical results for d.

7.2.2.1 Before interaction, $t < t_0$

The previous analysis of [57] and our numerical simulations for the sNLD equation suggest that the decay of two spaced initial discontinuities (7.5) for the hydrodynamic Riemann invariants $\lambda_\pm$ would result, similar to the cubic NLS case, in a combination of a right-propagating simple DSW centred at $x = 0$ and a left-propagating simple RW centred at $x = l$. Indeed, the simple DSW transition condition (7.6) is satisfied by the initial step at $x = 0$, which implies a single DSW resolution of this step (provided the "entropy conditions"

(7.13) are satisfied – see [57] for the justification); similarly, the jump at $x = l$ with constant Riemann invariant λ_+ across it asymptotically produces a single left-propagating RW (see Figure 7.1). Indeed, our numerical simulations of the sNLS equation (7.1) for a range of the saturation parameter γ values confirm this scenario producing the plots qualitatively equivalent to that presented in Figure 6.6.

Now, following [57], we derive the key parameters of the simple photorefractive DSW in the form convenient for the further application to the refraction problem.

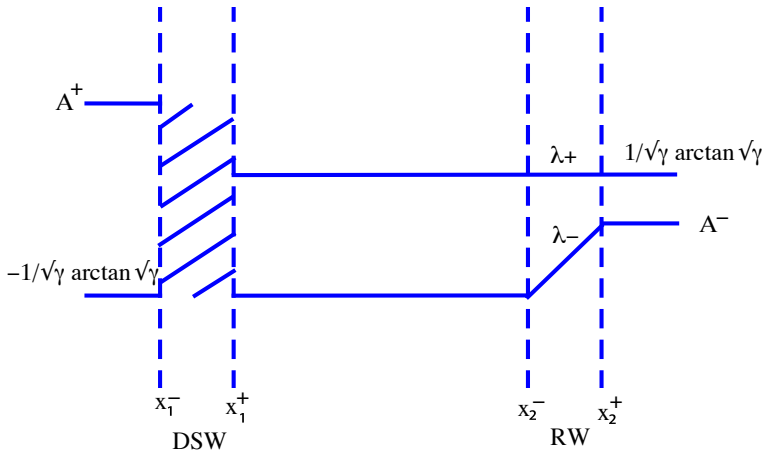

Figure 7.1: Distribution of the classical (dispersionless limit) Riemann invariants before the DSW-RW interaction

To take advantage of formulae (7.7) – (7.12) for the speeds of the DSW edges we first need to find the constant states (ρ_1, u_1) at $x < x^-$ and (ρ_2, u_2) at $x > x^+$ defining the hydrodynamic jumps across the DSW. These are readily found from the initial conditions (7.5) and the relationship (7.6) for the transfer of the Riemann invariant λ_- across the simple DSW. According to the initial conditions (7.5) the simple DSW must connect two hydrodynamic states with the same $\lambda_- = -\frac{1}{\sqrt{\gamma}} \arctan \sqrt{\gamma}$ while $\lambda_+ = A^+$ for $x < x^-$ and $\lambda_+ = \frac{1}{\sqrt{\gamma}} \arctan \sqrt{\gamma}$ for $x > x^+$ (see Figure 7.1). Then, using (7.6) and expressions (7.3)

relating the Riemann invariants and the hydrodynamic variables ρ, u we find

$$\rho_2 = 1, \quad u_2 = 0\,, \quad \rho_1 = \frac{1}{\gamma}\tan^2\left(\frac{A^+\sqrt{\gamma} + \arctan\sqrt{\gamma}}{2}\right), \quad u_1 = A^+ - \frac{1}{\sqrt{\gamma}}\arctan\sqrt{\gamma}\,. \tag{7.16}$$

Thus, the I_0 of the incident DSW defined by (6.9) is simply

$$I_0 = \frac{1}{\gamma}\tan^2\left(\frac{A^+\sqrt{\gamma} + \arctan\sqrt{\gamma}}{2}\right). \tag{7.17}$$

Next, from (7.6) we have $\lambda_-^0 = -\frac{1}{\sqrt{\gamma}}\arctan\sqrt{\gamma}$, which by (7.12) yields $\bar{u}(\bar{\rho}) = \frac{2}{\sqrt{\gamma}}(\arctan\sqrt{\gamma\bar{\rho}} - \arctan\sqrt{\gamma})$ and so completely defines, via (7.10), (7.11), ODEs (7.8), (7.9).

As was shown in [57], it is convenient to introduce a new variable $\widetilde{\alpha}$ instead of κ using the substitution

$$\widetilde{\alpha} = \sqrt{1 - \frac{\kappa^2(1+\gamma\bar{\rho})^2}{4\bar{\rho}}}\,, \tag{7.18}$$

which reduces ODE (7.9) to the form

$$\frac{d\widetilde{\alpha}}{d\bar{\rho}} = -\frac{(1+\widetilde{\alpha})[1+3\gamma\bar{\rho}+2\widetilde{\alpha}(1-\gamma\bar{\rho})]}{2\bar{\rho}(1+\gamma\bar{\rho})(1+2\widetilde{\alpha})}\,, \qquad \widetilde{\alpha}(1) = 1. \tag{7.19}$$

The form (7.19) has an advantage of being a separable ODE when $\gamma = 0$, which makes it especially useful for the asymptotic analysis for small γ . Once the function $\widetilde{\alpha}(\bar{\rho})$ is found, the velocity of the trailing soliton is determined by Eqs. (7.7), (7.11) as

$$s_0^- = \frac{2}{\sqrt{\gamma}}(\arctan\sqrt{\gamma\rho_1} - \arctan\sqrt{\gamma}) + \frac{\sqrt{\rho_1}}{1+\gamma\rho_1}\widetilde{\alpha}(\rho_1)\,, \tag{7.20}$$

where ρ_1 is given by Eq. (7.16).

The amplitude of the trailing soliton is given by speed-amplitude relationship (7.14). Using (7.14), (7.20) and the relationship $u_1 = \frac{2}{\sqrt{\gamma}}(\arctan\sqrt{\gamma\rho_1} - \arctan\sqrt{\gamma})$ following from (7.6) one can derive the condition of the vacuum point occurrence at the DSW trailing edge

(see [57]):

$$\widetilde{\alpha}(\rho_1) = 0. \tag{7.21}$$

Condition (7.21) yields, for a given value of the saturation parameter γ, the value of the initial density jump ρ_1 (and, therefore, of the parameter A^+ — see (7.16)) corresponding to the vacuum point appearance at the DSW trailing edge. Say, for $\gamma = 0.2$ this value of A^+ is about 2.18 (cf. the critical value $A^+ = 3$ for $\gamma = 0$)

In conclusion of this Section we present an asymptotic expansion of s_0^- for small γ. First, to leading order we have from (7.19) a separable ODE

$$\gamma = 0: \qquad \frac{d\widetilde{\alpha}}{d\bar{\rho}} = -\frac{1+\widetilde{\alpha}}{2\bar{\rho}}, \quad \widetilde{\alpha}(1) = 1, \tag{7.22}$$

which is readily integrated to give

$$\widetilde{\alpha}(\bar{\rho}) = \frac{2}{\sqrt{\bar{\rho}}} - 1 \equiv \widetilde{\alpha}_0(\bar{\rho}). \tag{7.23}$$

We now introduce

$$\widetilde{\alpha} = \widetilde{\alpha}_0 + \widetilde{\alpha}_1. \tag{7.24}$$

Substituting (7.24) into (7.19) and assuming $\widetilde{\alpha}_1 \sim \gamma$ for $\gamma \ll 1$ we obtain to first order

$$\frac{d\widetilde{\alpha}_1}{d\bar{\rho}} = -\frac{\widetilde{\alpha}_1}{2\bar{\rho}} + \frac{4-3\sqrt{\bar{\rho}}}{4-\sqrt{\bar{\rho}}}\frac{2\gamma}{\sqrt{\bar{\rho}}}. \qquad \widetilde{\alpha}_1(1) = 0, \tag{7.25}$$

Eq. (7.25) is readily integrated to give

$$\widetilde{\alpha}_1(\bar{\rho}) = \frac{2\gamma}{\sqrt{\bar{\rho}}}\left(3(\bar{\rho}-1) + 16(\sqrt{\bar{\rho}}-1) + 64\left[\ln\frac{4-\sqrt{\bar{\rho}}}{3}\right]\right). \tag{7.26}$$

Now, substituting (7.24), (7.26) into (7.20) and using expansion of ρ_1 (7.16) for small γ we

obtain to first order

$$s_0^- = \frac{A^+ + 1}{2} + \gamma \left(\frac{1}{12}[(A^+)^3 + 15(A^+)^2 + 219A^+ - 245] + 128 \ln \frac{7 - A^+}{6} \right) + O(\gamma^2)\,. \quad (7.27)$$

As one can see, expression (7.27) agrees to leading order with the cubic NLS result (6.7) for the trailing edge speed. We also notice that our perturbation approach formally breaks down for $A^+ \geq 7$ because of the logarithmic divergence in Eq. (7.27) as $A^+ \uparrow 7$ (we note that such values of A^+ correspond to very large density jumps ($\rho_1/\rho_2 > 10$) across the DSW — see [57]).

Formulae (7.16), (7.20) define all the key parameters of the incident simple photorefractive DSW. We have also checked that the 'entropy' inequalities (7.13) are satisfied for a broad range of parameters involved providing the consistency of the whole construction (see also [57]).

7.2.2.2 After interaction, $t > t^*$

Relations (7.6) – (7.13) describe a simple DSW transition between two *constant* states so they are not applicable to the varying transition in DSW-RW interaction zone. However, one should still be able to use these relations for the determination of the key parameters of the refracted DSW when the interaction is over, provided no new waves sre generated and the output pattern consists only of the pair of the refracted DSW and RW separated by a constant flow as it takes place in the Kerr nonlinearity case. In other words, relations (7.6) – (7.13) can be applied if the DSW-RW interaction is "clean" (elastic) *on the level of the averaged Whitham description* (which does not exclude the possibility of some constant-mean radiation due to non-integrability of the sNLS equation). If we accept this supposition (to be confirmed *a-posteriori*), then we can apply the transition relation (7.6) to the refracted DSW and determine the values of ρ_1 and u_1 in the 'plateau' region between the refracted DSW and RW. Since the refracted DSW propagates to the right into the region with $\lambda_- = A^-$ (see the initial conditions (7.5) at $x \to +\infty$) one must have, by (7.6), the same $\lambda_- = A^-$

across it, in the constant 'plateau' region.

Next, the refracted RW propagates to the left, into the region with $\lambda_+ = A^+$ (again, see initial conditions (7.5) at $x \to -\infty$) and, therefore $\lambda_+ = A^+$ everywhere through this wave and in the 'plateau' region. From the initial condition (7.6), the value of λ_- to the left of the RW is $\lambda_- = -\frac{1}{\sqrt{\gamma}} \arctan \sqrt{\gamma}$ and the value of λ_+ to the right of the DSW is $\lambda_+ = \frac{1}{\sqrt{\gamma}} \arctan \sqrt{\gamma}$. Thus, we arrive at the Riemann invariant diagram schematically shown in Figure 7.2 (cf. diagram in Figure 6.10 for the cubic NLS case).

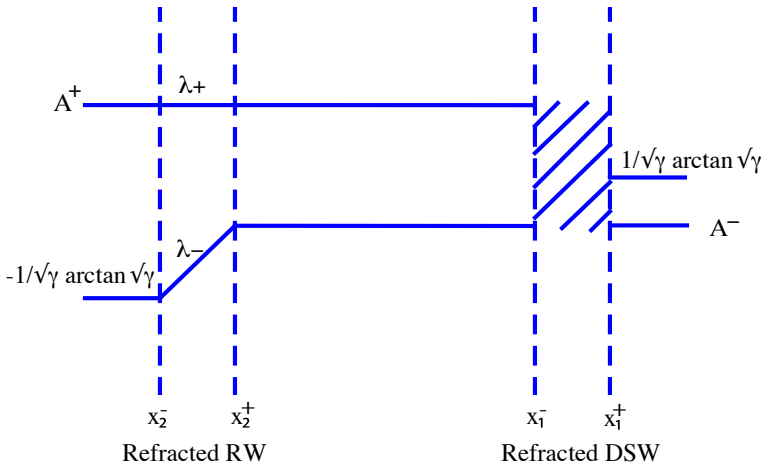

Figure 7.2: Distribution of the dispersionless limit Riemann invariants after the DSW-RW interaction.

Thus, using relationships (7.3) between the Riemann invariants $\lambda_\pm$ and the hydrodynamic variables ρ, u, one arrives at the set of equations determining the hydrodynamic states (ρ_1, u_1) and (ρ_2, u_2) at the trailing and leading DSW edges respectively:

$$\frac{u_1}{2} + \frac{1}{\sqrt{\gamma}} \arctan \sqrt{\gamma\rho_1} = A^+; \quad \frac{u_1}{2} - \frac{1}{\sqrt{\gamma}} \arctan \sqrt{\gamma\rho_1} = \frac{u_2}{2} - \frac{1}{\sqrt{\gamma}} \arctan \sqrt{\gamma\rho_2} = A^-;$$
$$\frac{u_2}{2} + \frac{1}{\sqrt{\gamma}} \arctan \sqrt{\gamma\rho_2} = \frac{1}{\sqrt{\gamma}} \arctan \sqrt{\gamma}\,. \tag{7.28}$$

So

$$\rho_1 = \frac{1}{\gamma}\tan^2\left(\sqrt{\gamma}\frac{A^+ - A^-}{2}\right), \quad u_1 = A^+ + A^-,$$
$$\rho_2 = \frac{1}{\gamma}\tan^2\left(\frac{1}{2}\arctan\sqrt{\gamma} - \frac{A^-}{2}\sqrt{\gamma}\right), \quad u_2 = A^- + \frac{1}{\sqrt{\gamma}}\arctan\sqrt{\gamma}\,. \tag{7.29}$$

To verify our key assumption about the 'semi-classically clean' DSW-RW interaction in the sNLS equation case we have compared the values of the density and velocity in the region between the refracted DSW and RW obtained from direct numerical simulations of the sNLS equation with the predictions for ρ_1 and u_1 of formulae (7.29) based on this assumption. As one can see from Figure 7.3 the comparisons show an excellent agreement confirming our hypothesis for a range of values of γ, A^+ and A^-. At the same, one can notice a small discrepancy visible at larger values of A^+ ($A^+ \gtrsim 1.7$) in the plots for $\nu(A^+)$. This is connected with the occurrence of the vacuum point in the refracted DSW for sufficiently large density jumps across it. As was observed in [57], for large-amplitude photorefractive DSWs the Riemann invariant transition condition (7.6) is replaced by the classical Rankine-Hugoniot shock jump conditions so relation (7.29) holds only approximately for large A^+.

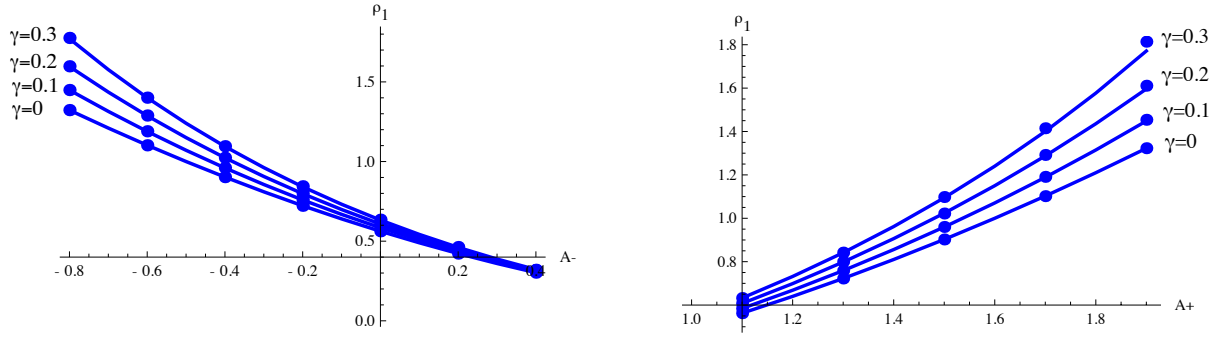

Figure 7.3: Density ρ_1 in the constant flow region between the refracted DSW and RW. Left: $\rho_1(A^-)$ for fixed $A^+ = 1.5$; Right: $\rho_1(A^+)$ for fixed $A^- = 0$. Solid lines: analytic (modulation theory) curves; dots: direct numerical simulations data.

Now, we shall use general relationships (7.7) — (7.14) to derive the trailing soliton parameters in the refracted DSW.

Comparing (7.6) and (7.28) we find $\lambda_-^0 = A^-$ so expression (7.12) for $\bar{u}(\bar{\rho})$ assumes the

form

$$\bar{u}(\bar{\rho}) = 2\left(A^- + \frac{1}{\sqrt{\gamma}}\arctan\sqrt{\gamma\bar{\rho}}\right). \tag{7.30}$$

Substituting (7.30) into (7.10) and (7.11) and using the same change of variable (7.18) in ODE (7.9) we arrive at the same ODE (7.19) for the function $\widetilde{\alpha}(\bar{\rho})$ but now with a general boundary condition $\widetilde{\alpha}(\rho_2) = 1$ since $\rho_2 \neq 1$ for the refracted wave (see (7.29)). As before, this condition follows from the boundary condition for κ in (7.9) and the relationship (7.18) between $\widetilde{\alpha}$ and κ. The velocity of the trailing soliton in the refracted DSW is determined by Eqs. (7.7), (7.11) as

$$s_r^- = 2\left(A^- + \frac{1}{\sqrt{\gamma}}\arctan\sqrt{\gamma\rho_1}\right) + \frac{\sqrt{\rho_1}}{1+\gamma\rho_1}\widetilde{\alpha}(\rho_1)\,, \tag{7.31}$$

where ρ_1 is now given by Eq. (7.29). Comparison for the dependence $s_r^-(A^+)$ for a fixed value of $A^- = -0.8$ is presented in Figure 7.5. One can see that the value of s_r^- quite strongly depends on the saturation parameter γ. Expanding s_r^- for small γ we get (cf. (7.27))

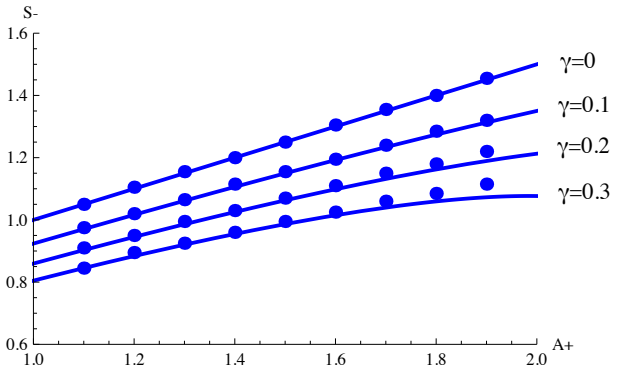

Figure 7.4: The refracted DSW trailing edge speed s_r^- as a function of an input parameter A^+ for fixed $A^- = -0.8$. Solid lines: modulation solution (7.31); dots: numerical simulations data.

$$s_r^- = 1 + \frac{A^- + A^+}{2} + \gamma\left[\frac{2}{3}\Delta^3 + 4\Delta^2\delta + 32\Delta\delta^2 - \frac{112}{3}\delta^3 + 128\delta^3\ln\frac{4-\Delta/\delta}{3} - \frac{1}{3}\right] + O(\gamma^2) \tag{7.32}$$

Here $\Delta = \frac{A^+ - A^-}{2}$, $\delta = \frac{1-A^-}{2}$. Again, one can see that the leading order of expansion (7.32)

agrees with the cubic NLS result (6.7) as expected.

Given the value of s_r^-, the trailing dark soliton amplitude a_s in the refracted DSW is found from formula (7.14). Comparisons of the analytically found values of a_s for $\gamma = 0.2$ with direct sNLS numerical simulation data are presented in Figure 7.5. and show excellent agreement. Also, the dashed lines show the dependencies $a_s(A^-)$ and $a_s(A^+)$ for $\gamma = 0$. As one can see, the nonlinearity saturation has strong effect on the refracted DSW soliton amplitude.

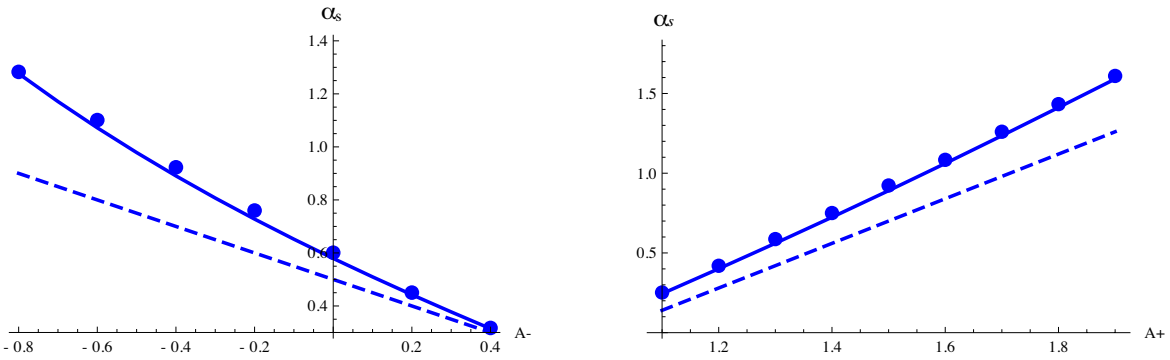

Figure 7.5: Trailing soliton amplitude a_s. Left: $a_s(A^-)$ for $A^+ = 1.5$; Right: $a_s(A^+)$ for $A^- = -0.4$. Solid line: analytic curve for $\gamma = 0.2$; Dots: direct numerical simulations data for $\gamma = 0.2$. Dashed line: the curve for $\gamma = 0$.

The condition $a_s = \rho_1$ defining the vacuum point occurrence at the trailing edge of the refracted DSW, leads to the same equation (7.21), which was obtained earlier for the incident DSW, with the only (essential) difference that ρ_1 is now given by (7.29). The vacuum point regions diagram for $\gamma = 0.2$ is presented in Figure 7.6.

Comparison with the analogous diagram for the Kerr nonlinearity case $\gamma = 0$ (Figure 11) shows that variations of the saturation parameter γ have rather significant effect on the vacuum point appearance. Our numerical simulations confirm this conclusion. As already was mentioned, in the developed modulation theory we assume a semiclassically "clean" DSW-RW interaction, which, strictly speaking, applies only to the region I in Figure 7.6. However, our comparisons show that, if the initial parameter A^+ is not too large, the DSW fitting approach [53] based on the Riemann invariant transition condition (7.6) gives reason-

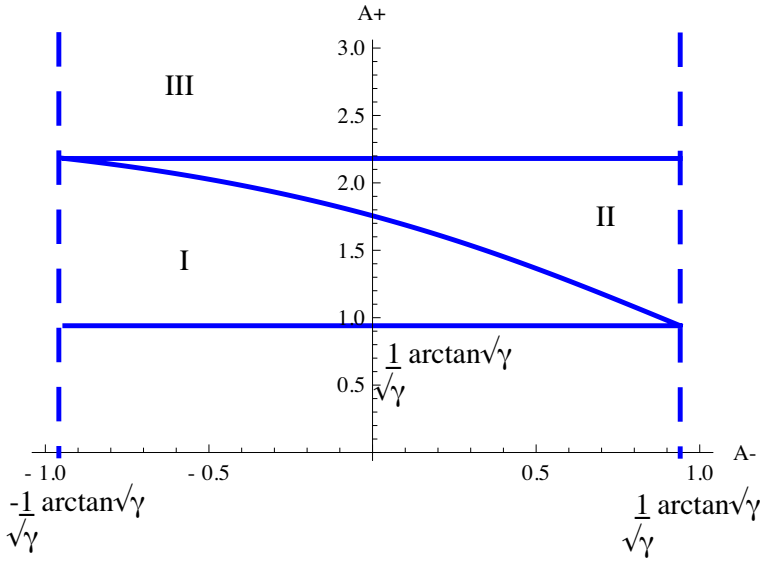

Figure 7.6: Regions of the plane of initial parameters A^-, A^+ for $\gamma = 0.2$: (I) No vacuum points; (II) No vacuum points in the incident DSW, a vacuum point in the refracted DSW; (III) Vacuum points in both incident and refracted DSWs.

ably good quantitative predictions for the refracted DSW parameters in regions II and III as well.

7.2.3 DSW refraction parameters

The DSW amplification coefficient is defined as $\nu = I_r/I_0$, where the incident DSW relative intensity I_0 is given by (7.17). Using (7.29) the relative intensity of the refracted DSW is readily found in terms of the input parameters A^+ and A^- as (see (6.9))

$$I_r = \frac{\rho_1}{\rho_2} = \frac{\tan^2\left(\sqrt{\gamma}\frac{A^+ - A^-}{2}\right)}{\tan^2\left(\frac{1}{2}\arctan\sqrt{\gamma} - \frac{A^-}{2}\sqrt{\gamma}\right)}\,. \tag{7.33}$$

In Figure 7.7 we present the dependencies $\nu(A^-)$ and $\nu(A^+)$. One can see that the amplification coefficient (unlike individual parameters of the incident and refracted DSWs — see e.g. Figure 7.3 above and Figs. 7.5, 7.6) shows a very weak dependence on the saturation parameter γ for rather broad intervals of A^+ and A^- so that one can safely use simple expression (6.55) obtained for $\gamma = 0$. The direct numerical simulations fully confirm this conclusion

(we do not present numerical points on Figure 7.7 to avoid cluttering the plot).

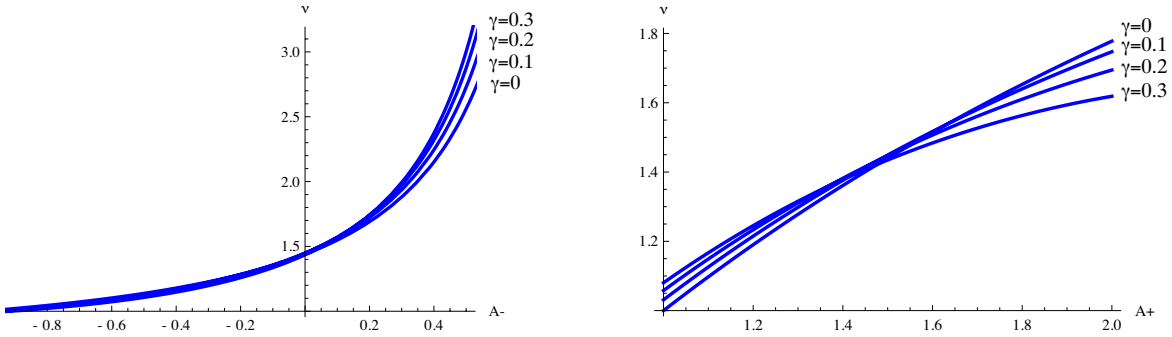

Figure 7.7: DSW amplification coefficient ν. Left: $\nu(A^-)$ at $A^+ = 1.5$, $A^+ = 1.5$. Right: $\nu(A^+)$ at $A^- = 0$;

Now we look at the behaviour of the acceleration coefficient $\sigma = s_r^- - s_0^-$, which is found analytically with the aid of formulae (7.31) and (7.20). The dependence $\sigma(\gamma)$ for $A^+ = 1.2$, $A^- = -0.7$ (Region I in Figure 7.7) is shown in Figure 7.8. One can see that, similar to the

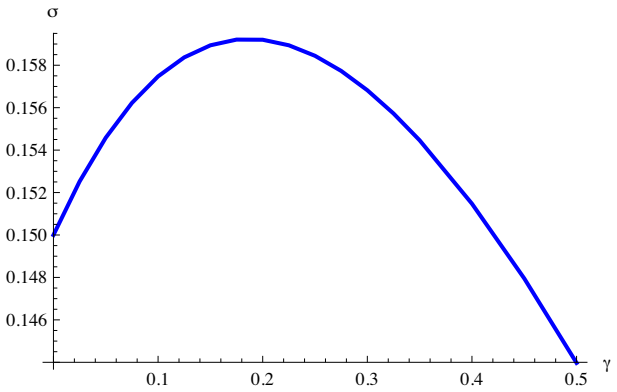

Figure 7.8: Analytical curve for the DSW acceleration coefficient σ as a function of the saturation parameter γ for $A^+ = 1.2$, $A^- = -0.7$.

amplification coefficient ν, the dependence of σ on γ and A^+ (i.e. on the intensity of the incident DSW) is quite weak. Indeed, the relative change of σ does not exceed 10% over the broad interval of γ from 0 to 0.5). Thus, at least in region I, one can safely assume the simple expression (6.56) $\sigma = (1 + A^-)/2$ obtained for the cubic nonlinearity case. The comparisons with numerics presented in Figure 7.9 confirm this observation. To analytically quantify the deviations of the quite complicated general "photorefractive" dependence $\sigma(A^+, A^-, \gamma)$ from

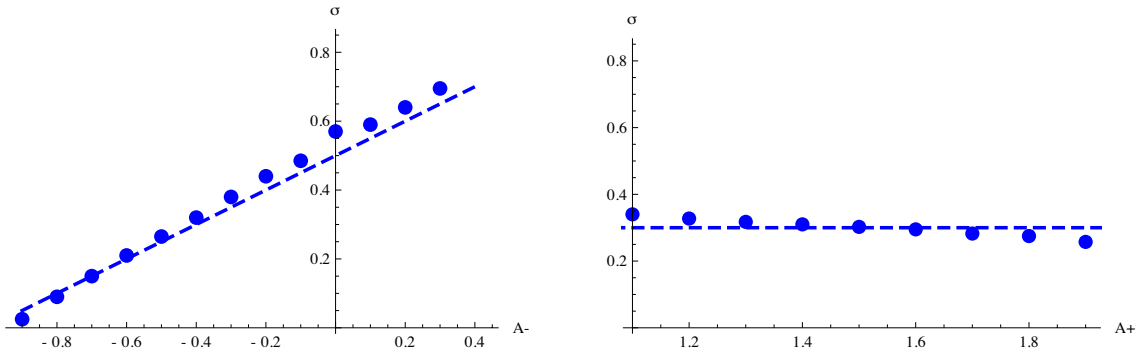

Figure 7.9: The DSW acceleration coefficient σ as a function of input parameters A^- and A^+. Dashed lines: analytic curves for $\gamma = 0$; Circles: numerical data for $\gamma = 0.2$. Left: $\sigma(A^-)$ at fixed $A^+ = 1.2$; Right: $\sigma(A^+)$ for fixed $A^- = -0.4$

the simple dependence $\sigma = (1 + A^-)/2$ in the cubic nonlinearity case given by (6.56), we derive an asymptotic expansion for σ for the case when both interacting waves have small intensity. Introducing ε_+ and ε_- by

$$A^- = -\frac{1}{\sqrt{\gamma}} \arctan\sqrt{\gamma} + \varepsilon_- , \qquad A^+ = \frac{1}{\sqrt{\gamma}} \arctan\sqrt{\gamma} + \varepsilon_+ \tag{7.34}$$

and assuming $\varepsilon_- \ll 1$, $\varepsilon_+ \ll 1$ we obtain from (7.27) and (7.32) on retaining second order terms,

$$\sigma = s_r^- - s_0^- = \frac{\varepsilon_-}{2} + \varepsilon_-\gamma + O(\varepsilon_-\gamma^2; \varepsilon_-^2\gamma; \varepsilon_-\varepsilon_+\gamma). \tag{7.35}$$

One can see that expansion (7.35) does not contain terms proportional to $\varepsilon_+\gamma$, which implies that, for the interactions involving weak photorefractive DSW and RW, the acceleration σ of the DSW up to second order does not depend on its initial intensity.

Finally, in Figure 7.10 we present numerical values for the DSW refraction shift d (see Figure 6.6) taken for the particular value of $\gamma = 0.3$. The numerics (circles) are put against the analytical curves $d(A^-, A^+)$ defined by formula (6.57) for the cubic nonlinearity case, $\gamma = 0$. One can see that, similar to other definitive DSW refraction parameters ν and σ, there is almost no dependence on A^+ and γ at a fixed value of A^- (roughly, the RW intensity), however, the departure of the dependence d on A^- from the Kerr case $\gamma = 0$ becomes more

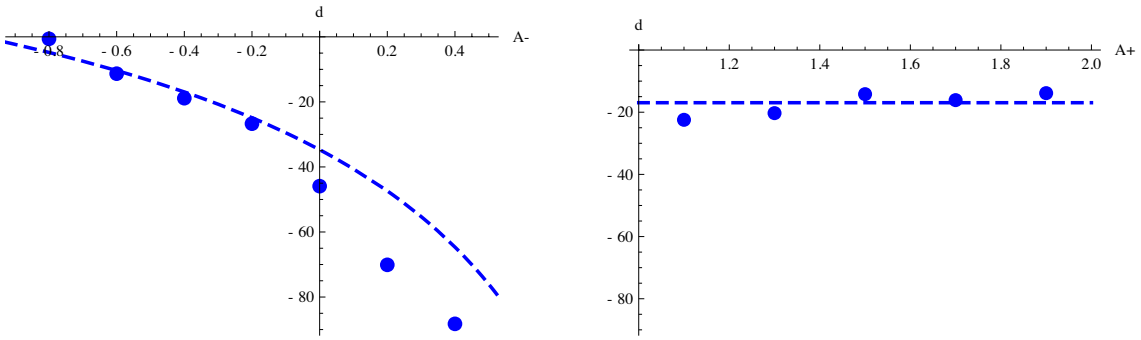

Figure 7.10: DSW refraction phase shift d. Left: dependence d on A^- for fixed $A^+ = 1.5$; Right: dependence d on A^+ for fixed $A^- = 0$. Dashed lines correspond to $\gamma = 0$, circles — to $\gamma = 0.3$.

pronounced with growth of A^-.

7.2.4 Discussion

Our consideration of 'non-integrable' DSW refraction in the framework of the NLS equation with saturable nonlinearity (7.1) is based on the assumption (confirmed by direct numerical simulations) that the head-on DSW-RW interaction is 'semiclassically elastic', i.e. is not accompanied by the generation of new DSWs or/and RWs. The comparisons of the key parameters of the photorefractive DSW refraction: the amplification coefficient ν and the acceleration coefficient σ defined by formulae (7.15 a) and (7.15 b) respectively, with their Kerr ($\gamma = 0$) counterparts have revealed a rather weak dependence of these particular parameters on the saturation coefficient γ, which could prove useful for the experimental all-optical modelling of the BEC DSW refraction using photorefractive materials.

A very good agreement of the predictions of our asymptotic analytical results with the direct numerical simulations in the DSW refraction problem provides further striking confirmation of the robustness of the modulation theory in non-integrable dispersive wave problems, now in the more complicated setting involving DSW-RW interactions.

Chapter 8

Conclusion

In the Thesis, two important theoretical problems arising in the theory of one-dimensional defocusing NLS flows have been investigated analytically and numerically: (i) the resonant (transcritical) generation of DSWs in one-dimensional NLS flow past a broad repulsive penetrable barrier; and (ii) the interaction of NLS counter-propagating DSW and a simple RW, which is referred to as the refraction of a DSW.

One-dimensional NLS flows have been considered not only because they arise naturally in BEC and nonlinear optics, but because these configurations are also of significant theoretical interest for two mutually complementary reasons: (a) 1D dynamics admit a full analytical description and provide important insights to the dynamics in the more complicated configurations; (b) some non-trivial features of 1D BEC dynamics are absent in higher dimensions.

The first problem (i) is motivated by the recent experimental observations of dark soliton radiation in BECs by moving a localised repulsive potential through a quasi-1D BEC (Engels and Atherton 2008 [6]) and is related to the fundamental issue of the onset of dissipation in superfluid flows; the second problem (ii) represents a dispersive-hydrodynamic counterpart of the classical gas-dynamics problem of the shock wave refraction on a RW (Courant & Friedrischs 1948 [12]), and, apart from its theoretical significance could also find applications

in superfluid dynamics.

As mentioned, both problems also naturally arise in nonlinear optics, where the NLS equation is a standard mathematical model and the 'superfluid dynamics of light' can be used for an all-optical modelling of BEC flows.

(i) In the problem of the BEC flow through a wide repulsive penetrable barrier it is found that in the plane of parameters (v, V_m), where v is the incident flow speed and V_m is the potential strength (amplitude), there is a finite region within which the generation of nonlinear waves occurs both upstream and downstream the potential. The global unsteady wave pattern is studied analytically using the combination of the local "hydraulic" solution of the 1D Gross-Pitaevskii equation and the solutions of the Whitham modulation equations describing the resolution of the upstream and downstream discontinuities through the generation of DSWs. It is shown that within the physically reasonable range of parameters, the downstream dispersive shock is attached to the potential barrier and effectively represents the train of very slow dark solitons, which can be observed in experiments. The rate of the soliton emission, the amplitudes of the solitons in the train and the drag force exerted on the potential are determined in terms of just two input parameters v and V_m. Remarkably, the key parameters of the generated wave pattern are shown to almost not depend on the potential barrier shape. A good agreement with direct numerical solutions is demonstrated.

In the experiment [6] it was found that the solitons are generated by a moving potential barrier in the interval of velocities $0.3\text{mm/s} < v < 0.9\text{mm/s}$. This result agrees qualitatively with existence of the finite interval $v_- < v < v_+$ for which the expanding DSWs are generated. However, we encounter a quantitative contradiction due to the experiment construction in a dense BEC, where the systems governing the 1D dynamics are much more complicated than the standard cubic NLS equation (5.1). Thus, the quantitative description of the experiment [6] is beyond the scope of this thesis. The theory of dispersive shocks in a dense BEC could be developed and would make for interesting further research.

The famous Landau criterion [7] for the loss of superfluidity was based on the consideration of linear excitations only and it contradicted to the experiments with liquid HeII. This discrepancy was explained by Feynman by taking into the consideration the formation of such nonlinear structures as vortices in the flow of a superfluid in capillaries or past obstacles. However, the notion of the threshold velocity below which the flow is superfluid has not been changed by this modification of the theory. Taking into account the generation of DSWs in 2D situation [36, 97] did not change this notion either, since the stationary spatial DSWs are generated by the supersonic flow of BEC only. Our results, as well as the results of the previous works [9, 86–89], show that the situation can be more subtle in the case of 1D flows. In this case, the flow past a broad barrier leads to the generation of DSWs for a finite interval of the flow velocities bounded not only from below but *also from above*. Moreover, the lower boundary value of the velocity v_- can become equal to zero for strong enough barriers, that is even very slow motions could lead to the generation of solitons. This observation is in striking contrast with the standard reasonings based on the linear theory of excitations.

The constructed analytical theory of the transcritical (resonant) NLS flows through wide penetrable repulsive potential barriers is supported by direct numerical simulations.

The theory can extended to the framework of the NLS equation with saturable nonlinearity (2.63) (see Section 2.4.3.2) using the DSW fitting method described in Chapter 4 (Section 4.7).

(ii) The refraction of a DSW due to its head-on collision with the centred RW has been considered in the framework of the one-dimensional defocusing cubic NLS equation. This is the dispersive counterpart of the classical gas dynamics problem of the interaction of a shock wave with a counter-propagating simple RW often referred to as the shock wave refraction problem. Apart from the obvious contrast between both local and global structures of viscous shock waves and DSWs, there is a fundamental difference between the classical dissipative, and the present, dispersive conservative settings. While the parameters defining the flow

containing shock waves in classical gas dynamics are determined by appropriate systems of shock conditions, which take into account the changes of the thermodynamic properties of the medium through which the shock waves propagate, in dispersive dynamics the change of the hydrodynamic flow across the DSW is completely determined by the transfer of the Riemann invariants along the characteristics of the governing hyperbolic (Whitham) system, which makes possible a complete asymptotic description of the flow.

In the Thesis, a full asymptotic description of the DSW refraction in the 1D defocusing NLS flows has been obtained by constructing appropriate exact solutions of the Whitham modulation equations.

One can trace certain analogy between the considered DSW-RW interaction and the two-soliton collisions in integrable systems: both interactions are elastic in the sense that they both can be interpreted in terms of the "exchange" of spectral parameters by the interacting waves so that the global spectrum in the associated linear scattering problem remains unchanged. In the DSW-RW interaction the role of isospectrality is played by the transfer of the constant values of appropriate Riemann invariants of the modulation system through the varying DSW and RW regions so that one can predict the jumps of density and velocity across the refracted DSW and RW without constructing the full modulation solution. At the same time, the DSW and RW do not simply pass through each other and "exchange" the constant Riemann invariants: there are additional phase shifts for both interacting waves, similar to the classical soliton phase-shifts.

The refraction of a DSW due to its head-on collision with the centred RW is also considered in the framework of the one-dimensional defocusing NLS equation with saturable nonlinearity (the sNLS equation) (7.1). Our consideration of 'non-integrable' DSW refraction in the framework of the sNLS equation is based on the assumption (confirmed by direct numerical simulations) that the head-on DSW-RW interaction is 'semiclassically elastic', i.e. is not accompanied by the generation of new DSWs or/and RWs.

Since the modulation system for the sNLS equation does not possess Riemann invari-

ants, we take advantage of the recently developed DSW fitting method, applicable to non-integrable dispersive systems, to obtain key parameters of the DSW refraction. Our modulation theory analytical results are supported by direct numerical simulations of the corresponding full dispersive IVPs.

The comparisons of the key parameters of the photorefractive DSW refraction: the amplification coefficient ν and the acceleration coefficient σ defined by formulae (7.15 a) and (7.15 b) respectively, with their Kerr ($\gamma = 0$) counterparts have revealed a rather weak dependence of these particular parameters on the saturation coefficient γ, which could prove useful for the experimental all-optical modelling of the BEC DSW refraction using photorefractive materials.

A very good agreement of the predictions of our asymptotic analytical results with the direct numerical simulations in the DSW refraction problem provides further striking confirmation of the robustness of the modulation theory in non-integrable dispersive wave problems, now in the more complicated setting involving DSW-RW interactions.

The approaches used in the latter problem (ii) can also be applied to obtain analytical solution to the problem of the *overtaking* DSW-RW interaction in the NLS flows. While this problem was studied in the KdV equation framework in [15], we believe that it deserves special attention in the context of the defocusing NLS flows since, due to a different dispersion sign and the possibility of the vacuum point occurrence within the DSW one can expect a number of qualitative and quantitative differences compared to the KdV flows. Also, the developed theory can be readily extended to the problem of the generation of DSWs by the interference of two simple RWs studied numerically in [14].

Appendix A

Numerical methods

With the advent of modern computers, numerical methods have exploded in popularity. It is now common to support analytical results with full numerical solutions.

Numerical methods are very useful, as we can quickly produce images of what happens in complicated nonlinear dispersive systems. These systems are often non-integrable and so obtaining analytical results can be impossible. Therefore, using numerical methods can sometimes be the only way to produce and visualise the solution without completing the experiment itself.

A.1 Spectral methods

Spectral methods are the group of numerical methods that discretise the continuous system and solve, often involving the use of the fast Fourier transform (FFT).

Spectral methods are very similar to finite difference and finite elements methods. However, spectral methods differ from these methods by rather than locally approximating the functions, spectral methods approximate functions globally. As such, spectral methods have excellent convergence and excellent error properties.

In finite difference methods, the derivative of a function depends on the neighbouring points. It can be approximately calculated by taking the value to the left and to the right

and dividing by the distance between those points. Contrastingly, in spectral methods functions are represented as finite sums of orthogonal functions, with the span being the entire domain. Derivatives can usually be taken analytically since the basis functions are known. The derivative at a point thus depends on the entire domain.

We shall be utilising spectral methods to produce direct numerical solutions to problems solved analytically in Chapters 5, 6 and 7. This is necessary to justify a number of assumptions used in the analytic asymptotic constructions of Chapters 5 –7. Such assumptions (like hyperbolicity of the averaged system associated with the sNLS equation) are often very difficult (or impossible) to verify analytically.

A.1.1 Discrete Fourier transform

The most well known example of spectral methods are operations involving Fourier series. We represent a periodic function $f(x)$ in one dimension, as

$$f(x) = \sum_{k=-\infty}^{\infty} a_k \exp^{ikx}, \tag{A.1}$$

over the interval $0 < x < 2\pi$.

If the function $f(x)$ is known and the coefficients are unknown, we can find the coefficients easily by taking advantage of the fact that $\exp^{ikx}$ is orthogonal. Taking k and m to be integers,

$$\int_0^{2\pi} \exp^{imx} \exp^{ikx}\, dx = 0; \quad k \neq -m. \tag{A.2}$$

When $k = -m$, the above integral is equal to 2π. Using this property, we can multiply both sides of equation (A.1) by $\exp^{imx}$ and integrate over the domain.

$$\int_0^{2\pi} \big(f(x) \exp^{imx} = \sum_{k=-\infty}^{\infty} a_k \exp^{ikx} \exp^{imx}\big) dx. \tag{A.3}$$

Using the orthogonality property, the above simplifies

$$a_k = \frac{1}{2\pi}\int_0^{2\pi} \big(f(x)\exp^{-imx}\big)dx. \tag{A.4}$$

This allows us to calculate the coefficient a_k in the Fourier series.

We are interested in the discrete version of this process. Let us assume we only know the function value along discrete points along $0 < x < 2\pi$. Then we can evaluate the integral numerically using he trapezium rule.

This simply breaks the function in the several trapezoids. The integral then become the sum of the areas of trapeziums, i.e.

$$\int_0^{2\pi} f(x)dx = \Delta x\big[\tfrac{1}{2}f(x_1) + \tfrac{1}{2}f(x_{N-1}) + \sum_{j=2}^{N-1} f(x_j)\big]. \tag{A.5}$$

Since, $f(0) = f(2\pi)$, we have

$$\int_0^{2\pi} f(x)dx = \Delta x \sum_{j=1}^{N-1} f(x_j). \tag{A.6}$$

Using this definition, we discretise the domain as $x_j = \frac{2\pi}{N}(0, 1\cdots, N-1)$ and the sum then runs over all points in the domain,

$$\int_0^{2\pi} f(x)dx = \frac{2\pi}{N} \sum_{j=1}^{N} f(x_j). \tag{A.7}$$

Thus, we compute the Fourier coefficient,

$$a_k = \frac{1}{N}\sum_{j=1}^{N} \exp^{-ikx_j} f(x_j). \tag{A.8}$$

Equation (A.8) defines the discrete Fourier transform (DFT).

A.1.2 Fast-Fourier Transform

The Fast-Fourier Transform (FFT) was developed in 1965 by Cooley and Tukey. The FFT enables one to compute the DFT and thus calculate spectral derivatives. It is essentially a more efficient algorithm for completing the DFT.

We take a discrete bounded subspace $[-L, L]$ of the infinite continuous physical space, and discretise in time. So we have the Figure A.1. Here N is even and is the number of discrete points. The points are uniformly spaced with the spacing being $h = 2L/N$.

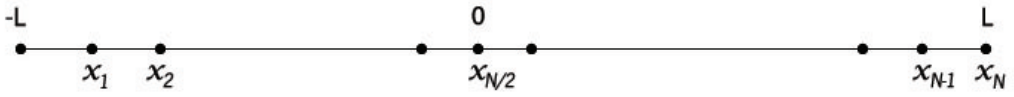

Figure A.1: Physical space transformed into discrete space.

Now considering the FT of these discrete points, we move into the Fourier space.

$$\begin{aligned} Physical\ space: &\qquad x \in \{-L+h, -L+2h, \cdots 0, \cdots L-h, L\} \\ Fourier\ space: &\quad k \in \{-\tfrac{1}{2}N+1, -\tfrac{1}{2}N+2, \cdots 0, \cdots, \tfrac{1}{2}N-1, \tfrac{1}{2}N\} \end{aligned}, \tag{A.9}$$

We have the map of the FFT shown in Figure A.2.

So completing a FFT of a function $u(x)$, we cross over from the physical space to the Fourier space. Then, multiplying by ik and returning to the physical space, via the inverse FFT (IFFT), we essentially complete a differentiation on the function $u(x)$, i.e. we have

$$u'(x) = IFFT[ik(FFT[u(x)])]. \tag{A.10}$$

A similar process may be complete for the second differential $u''(x)$,

$$u''(x) = IFFT[-k^2(FFT[u(x)])]. \tag{A.11}$$

In solving the NLS equation, we have utilised the FFT in the split-step method that we

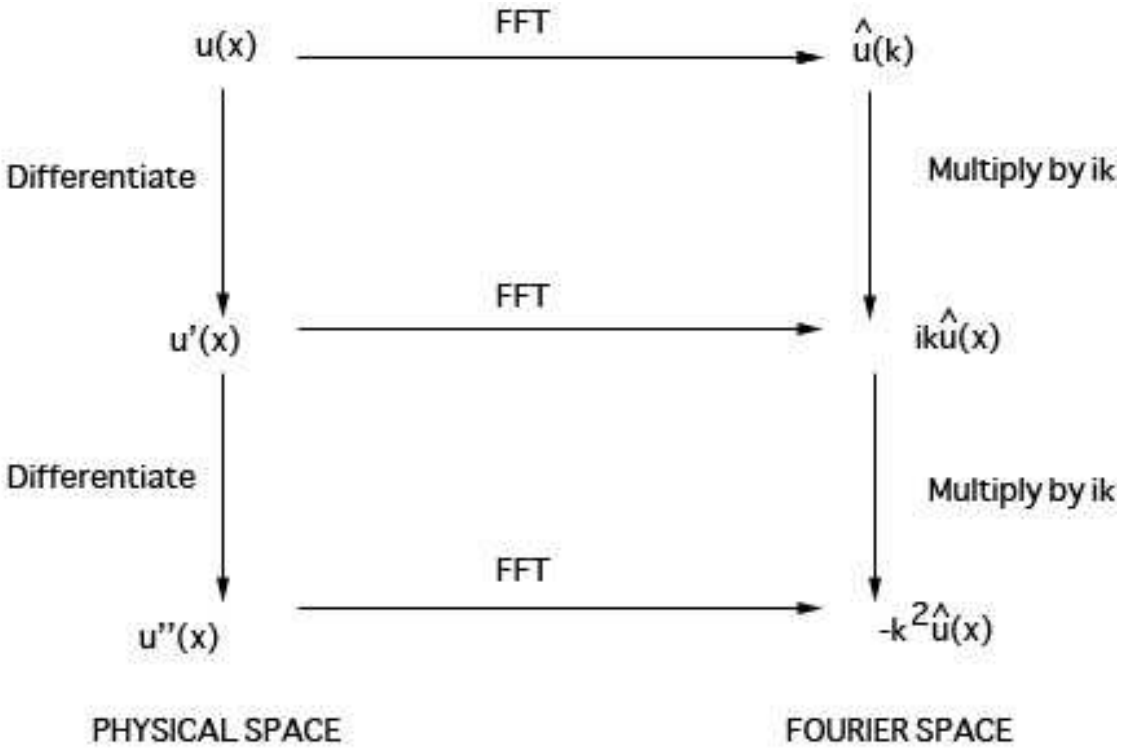

Figure A.2: FFT map.

shall now describe.

A.2 Split-step Method

This method was first suggested by Hardin and Tappert (1973). This method solves the NLS

$$i\psi_t + \frac{1}{2}\psi_{xx} - |\psi|^2\psi = 0, \tag{A.12}$$

subject to the initial conditions $\psi = \psi_0$.

The split-step method consists of two main steps. We write the NLS equation in the form

$$\psi_t = iL\psi + iN\psi, \tag{A.13}$$

where L, N are the linear and nonlinear parts respectively, so

$$L\psi = \tfrac{1}{2}\psi_{xx}, \quad and \quad N = -|\psi|^2\psi. \tag{A.14}$$

The solution can be obtained by solving the nonlinear part N exactly and linear part L separately using FFT.

The solution at $(x, t_0 + \Delta t)$ can be written in the form

$$\psi(x, t_0 + \Delta t) = S(\Delta t)\psi(x, t_0), \quad S(\Delta t) = \exp(i(L + N)\Delta t), \tag{A.15}$$

where $S(\Delta t)$ is the solution operator to time Δt.

Taking a series expansion of $S(\Delta t)$

$$S(\Delta t) = \exp(i(L+N)\Delta t) = 1 + i\Delta t(L+N) - \frac{\Delta t^2}{2}(L^2 + N^2 + LN + NL) + O(i\Delta t^3). \tag{A.16}$$

We can approximate the solution operator $S(\Delta t)$ by

$$\begin{aligned} \exp(iL\Delta t)\exp(iN\Delta t) &\approx \tilde{S}(\Delta t), \\ = 1 + i\Delta t L + i\Delta t N - \tfrac{1}{2}\Delta t^2(L^2 + N^2 + 2LN) &+ O(\Delta t^3). \end{aligned} \tag{A.17}$$

This expression matches exactly in (A.16) whenever L, N commute. Otherwise this approximation is first order accurate.

We see that the exact and approximate solution operators have the same expansion up to order Δt^2. We thus use the approximate operator to step forward in time. For a single time step of Δt this causes an error of Δt^3. The solution can thus be approximated at $(x, t_0 + T)$ by applying $\tilde{S}(\Delta t)$ until $T = N_T \Delta t$, where N_T is the number of iterations to get to T, i.e.

$$\psi(x, t_0 + T) = \tilde{S}(\Delta t)^{N_T}\psi(x, t_0). \tag{A.18}$$

If $N_T = O(1/\Delta t)$, the global error becomes $error = \Delta t^3 1/\Delta t = \Delta t^2$.

The problem can now be calculated in terms of the operator $\tilde{S}(\Delta t)$, in two steps (as mentioned before) using FFT.

Firstly, one advances the solution using the nonlinear part

$$i\psi_t = |\psi|^2\psi. \tag{A.19}$$

This is solved exactly by

$$\psi(x, t_0 + \Delta t) = \exp[-i|\psi(x, t_0)|^2\Delta t]\psi(x, t_0), \tag{A.20}$$

where Δt is the time step, and t_0 is the initial time.

$$\begin{aligned}\psi_t(x, t_0 + \Delta t) &= -i|\psi(x, t_0)|^2 \exp[-i|\psi(x, t_0)|^2\Delta t]\psi(x, t_0), \\ &= -i|\psi(x, t_0)|^2\psi(x, t_0 + \Delta t),\end{aligned} \tag{A.21}$$

where k is the Fourier wavenumber

Secondly, one then solves the linear part

$$i\psi_t = -\frac{1}{2}\psi_{xx}, \tag{A.22}$$

by means of the FFT

$$\begin{aligned}FFT[\psi]_t &= -\frac{1}{2}ik^2 FFT[\psi], \\ FFT[\psi(x, t_0 + \Delta t)] &= \exp(-\tfrac{1}{2}ik^2\Delta t)FFT[\psi(x, t_0)], \\ \psi(x, t_0 + \Delta t) &= IFFT[\exp(-\tfrac{1}{2}ik^2\Delta t)FFT[\psi(x, t_0)]].\end{aligned} \tag{A.23}$$

where FFT denotes the FFT, $IFFT$ denotes the inverse FFT and $k^2 = -\frac{4n\pi^2}{L^2}$ is the square wavenumber.

A.3 Sample cases: decay of an initial step

To demonstrate the FFT method, we shall numerically solve the decay of an initial discontinuity problem considered in Chapter 4. We shall consider the initial step values for $\rho = |\psi|^2$, $u = (\arg \psi)_x$ corresponding to different regions in diagram (4.5) to illustrate the classification presented in Section 4.4 and test our MATLAB code (see Appendix B) by comparing the numerical results with the exact (modulation) analytical solutions. The developed MATLAB code will be then appropriately modified (also presented in Appendix B) to be applied to the problems of transcritical NLS flow past broad penetrable barrier (Chapter 5) and DSW refraction on a simple RW (Chapters 6 and 7).

The test examples we are considering are the following:

1. one DSW and one RW (one left and one right propagating, separated by the region of constant flow),

2. two DSWs (one left and one right propagating, separated by the region of constant flow; no vacuum points),

3. two DSWs (one left and one right propagating, with one of the DSWs having a vacuum point),

4. two RWs (one left and one right propagating) separated by the region of constant flow.

In the following subsections, these cases will be characterised by two constant parameters ρ_0 and u_0 in the corresponding initial step data (4.32).

The number of Fourier modes used in the numerics is $N = 10,000$; the time step $\Delta t = 0.05$ and the half space period $L = 1000$.

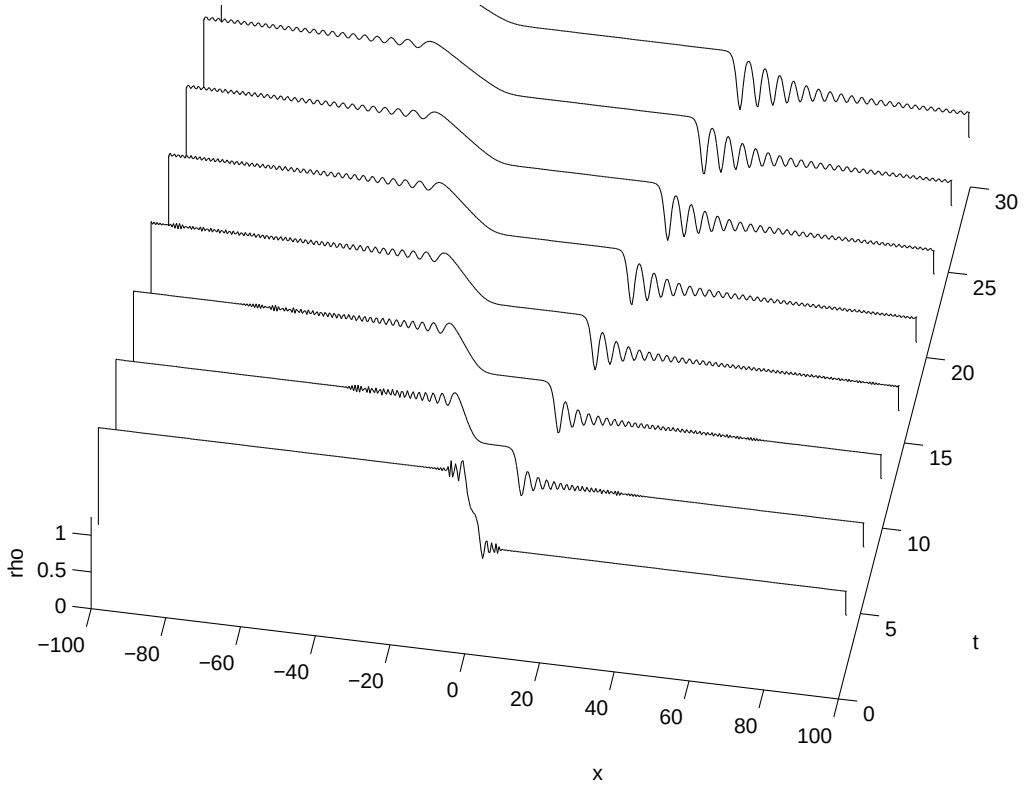

Figure A.3: The density profile in the decay pattern corresponding to the initial step parameters (A.24): right propagating DSW and left propagating RW separated by the constant flow region.

A.3.1 One DSW and one RW

We consider an initial step (4.32) with the following parameters (Region 1 in the parametric solution diagram Figure 4.5):

$$\rho_0 = 2, \quad u_0 = 0. \tag{A.24}$$

Running the numerical code we produce the plot in Figure A.3. As predicted by the analytical solution in Chapter 3, a right propagating DSW and a left propagating RW separated by the constant flow region are formed. The considered configuration corresponds to the Riemann invariant setup shown in Figure 4.6a. We have checked that the parameters of the DSW (the leading and trailing edge speeds, the trailing dark soliton amplitude, the hydrodynamic jumps of ρ and u across the DSW) in our numerical solution are in complete agreement with

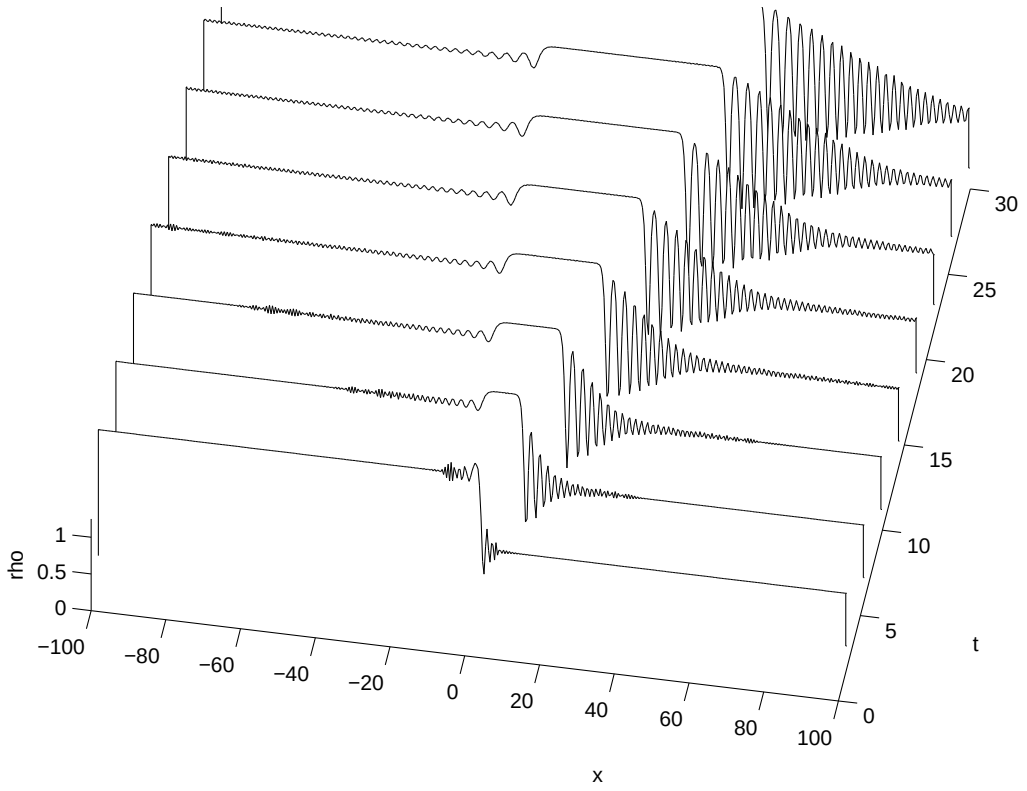

Figure A.4: The density profile in the decay pattern corresponding to the initial step parameters (A.25): two counter-propagating DSWs.

the exact modulation solutions from Section 4.2.1.

A.3.2 Two DSWs, no vacuum points

We consider an initial step characterised by the parameters

$$\rho_0 = 2, \quad u_0 = 2.8. \tag{A.25}$$

This step corresponds to the Region 2 (left part with respect to the vertical dashed line) in the parametric solution diagram Figure 4.5. Running the numerical code we obtain numerical solution, and obtain the plot in Figure A.4. One can see that the chosen initial step produces two counter-propagating DSWs without vacuum points, exactly as it is predicted by the

modulation theory. As in the previous case, the parameters of the DSWs have been checked to agree with the modulation solution.

A.3.3 Two DSWs, with one DSW having vacuum point

Typical parameters of the initial step producing two DSWs, with one DSW having a vacuum point, are:

$$\rho_0 = 2, \quad u_0 = 4. \tag{A.26}$$

This step corresponds to the Region 2 (right part with respect to the vertical dashed line) in the parametric solution diagram Figure 4.5. Running the numerical code we obtain the plot in Figure A.5 One can clearly see a vacuum point in the right-propagating DSW. All the DSW parameters agree with the modulation solutions.

A.3.4 Two RWs

Example of the parameters on the initial step producing two rarefaction waves (Region 4 in the parametric solution diagram Figure 4.5);

$$\rho_0 = 2, \quad u_0 = -2.8. \tag{A.27}$$

Running the numerical code we obtain the plot in Figure A.6 One can see small-amplitude wavetrains propagating from the points where the RWs match with the constant flow. The generation of these linear wavetrains is due to the dispersive resolution of the weak discontinuities (see Section 4.3). The amplitude of these wavetrains decays with time so asymptotically the numerical NLS solution for the chosen step (4.32), (A.27) becomes the classical solution of the dispersionless SWE in accordance with the theoretical predictions.

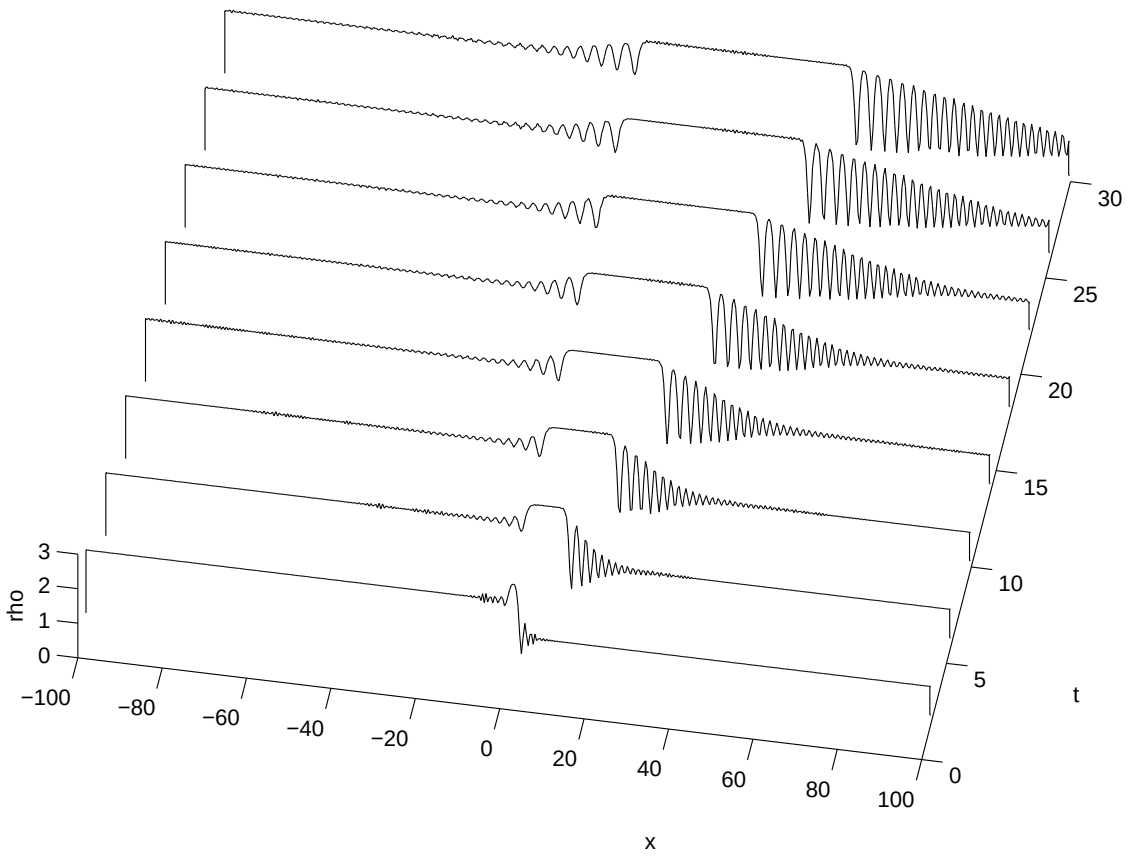

Figure A.5: The density profile in the decay pattern corresponding to the initial step parameters (A.26), two counter-propagating DSWs, vacuum point in the right-propagating DSW.

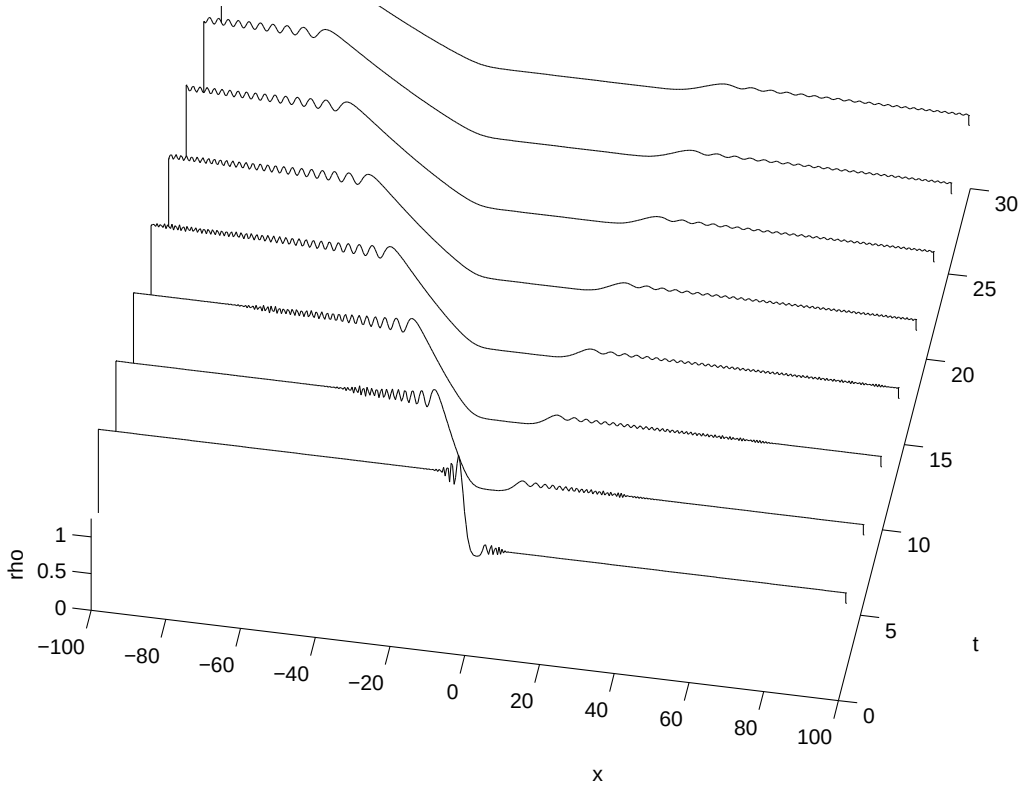

Figure A.6: The density profile in the decay pattern corresponding to the initial step parameters (A.27): two counter-propagating RWs.

A.4 Numerical solution of the GP equation

Clearly, to include a potential we must adjust the nonlinear part of the numerical solution.

So instead of (A.21) we have

$$\psi_t(x, t_0 + \Delta t) = -i(|\psi(x, t_0)|^2 + V_0(x, t))\psi(x, t_0 + \Delta t), \tag{A.28}$$

where $V_0(x, t)$ is the external potential of the system.

We can then proceed to solve the linear part of the GP equation (A.22) using the FFT in the same way as before.

Appendix B

MatLab numerical scheme

B.1 Potential barrier sweeping

```
% Antin Leszczyszyn March 2009
% Solves the nonlinear Schrodinger equation with the first order split-step Fourier method↩
    (Hardin and Tappert)

N = 10000;        % Number of Fourier modes
q = -1;           % Coefficient of nonlinear term
dt = 0.01;        % Time step
vm=0.5;           % Max of potential

T=30;                                %total time

M = T/dt;                            % Total number of time steps

J =10;                               % Steps between output, Total time


L = 2*1000;                          % Space period 1/2

h1 = 2*L/N;                          % Space step
n = [-N/2:1:N/2-1]';                 % Indices
x = n*h1;
```

```
%v=1;
r(1:N/2)=1;                          % Initial density x<0
r(N/2+1:N)=1;                        % Initial density x>0
v(1:N/2)=1;                          % Initial velocity x<0
v(N/2+1:N)=1;                        % Initial velocity x>0
u0 = sqrt(r').*exp(1i*v'*h1.*x);%

u=u0;
U = (abs(u));                       % Compute initial condition; save it in U
e = -4*n.*n*pi*pi/(4*L*L);          % Squares of wavenumbers.  *4 on the denomintor closes ↩
    up the spread

tdata=0;

h = waitbar(0,'Please wait while calculating...');
for m = 1:1:M


waitbar(m/M)


    % Start time evolution

u = exp(dt*1i*q*(abs(u).*abs(u))-1i*dt*vm*(sech(x+v'*m*dt)).^2).*u;% Solve nonlinear part ↩
    of NLS
c = fftshift(fft(u));                % Take Fourier transform
c = exp((1/2)*dt*1i*e).*c;           % Advance in Fourier space
u = ifft(fftshift(c));               % Return to physical space

if rem(m*dt,1) == 0
    tdata = [tdata; dt*m];           % Save output every J steps.
    m*dt;
U = [U (abs(u).^2)];                 % Solution of rho is stored in U.

end


end

 save('U.mat','U')            % Saves rho
```

```
 save('x.mat','x')            % Saves x
 save('tdata.mat','tdata')    % Saves t



z=U';

x=x(1:end-(4*N/10),:);  % Cuts the x range shorter
x=x(4*N/10:end,:);

Y=rand(2001,1)';

for j = 1:1:T                        % Cuts the rho range shorter and moves to the moving ↩
    referene frame
y=z(j,1:end-round((v*j)/(h1)));
y=y(1:end-(4*N/10));
y=y(4*N/10-round((v*j)/(h1)):end);
Y=[Y;y];
end




 % Calculate downstream lead soliton amplitude and speed

 Ad=0;

 for o = 1001:1:2001
if 1-Y(31,o)>Ad
    Ad=1-Y(31,o);        % Calculate amplitude downdtream
    Sd=x(o)/30;          % Calculate speed downstream
end
 end

 for o = 1001:1:1401
if Y(31,o)<0.95
   Sd=x(o)/30;           %  Calculate speed downstream
end
 end
```

```
Ad    % Amplitude downdtream
Sd    % Speed downstream



close(h)
```

B.2 Interaction of DSW and RW

```
% Antin Leszczyszyn July 2009
% Interaction of DSW and rarefaction wave in defocusing NLS



 clear

 for r=1:1:9    % Loop in Aplus



epsilon=0.4;    %0.4
L = 10000;      % Space period 1/2
N = 17*L;       % Number of Fourier modes
q = -1;         % Coefficient of nonlinear term
dt = 0.005;     % Time step
T=400;          %total time
M = T/dt;       % Total number of time steps
J =10;          % Steps between output, Total time
h1 = 2*L/N;                         % Space step
n = [-N/2:1:N/2-1]';                % Indices
x = n*h1;
l=100;          %gap between RW and DSW

Aplus=1.+0.1*r;
Aminus=-0.4;
lm=-1;
lp=1;

  A=[0.5  0.5;
       1  -1];      %in gennady's notation la+ and la-
```

```
    %%%%%%% region 1 downstream x<0

    B=[Aplus lm];        %in gennady's notation A+ and A-
    u1=(B/A)';
    u2=u1(1);  %u
    u3=u1(2);  %sqrt(rho)

    %%%%%%% region 2 0<x<l

    B=[lp lm];        %in gennady's notation 1 and A-
    u4=(B/A)';
    u5=u4(1);  %u
    u6=u4(2);  %sqrt(rho)

    %%%%%%% region 3 x>l

    B=[lp Aminus];        %in gennady's notation 1 and -1
    u7=(B/A)';
    u8=u7(1);  %u
    u9=u7(2);  %sqrt(rho)

%%%%%%%%%%%%%%%

        u0 = (u3.*(exp(1i*u2*x/epsilon))).*(x<=0);
        u0 = u0+(u6.*(exp(1i*u5*x/epsilon))).*(x>0 & x<l);
        u0 = u0+(u9.*(exp(1i*u8*x/epsilon))).*(x>=l);



u = u0;
U = (abs(u)).^2;                    % Compute initial condition; save rho in U
UU=(gradient(angle(u0),x/epsilon));% Compute initial condition; save u in UU
e = -4*n.*n*pi*pi/(4*L*L);          % Squares of wavenumbers.

tdata=0;

h = waitbar(0,'Please wait while calculating...');

for m = 1:1:M

waitbar(m/M)
```

```
% Check for Cancel button press
    if getappdata(h,'canceling')
        break
    end

% Start time evolution

u = exp(1/epsilon*dt*1i*q*(abs(u).*abs(u))).*u;% Solve nonlinear part of NLS
mu = fftshift(fft(u));                          % Take Fourier transform
mu = exp(0.5*epsilon*dt*1i*e).*mu;              % Advance in Fourier space
u = ifft(fftshift(mu));                         % Return to physical space




    if rem(m*dt,1) == 0
      tdata = [tdata; dt*m]; % Save output every J steps.
      %m*dt;                 % Counter, delete ; it view.
      U = [U (abs(u)).^2];                     %saves rho
      UU = [UU gradient(angle(u),x/epsilon)]; %saves u

                        % rho solution is stored in U
                        % u solution is stored in UU


       z=U';

 close(h)

      for ii=3:N-3       % Removes the excesive oscilation in the phase
        if UU(ii,141)>UU(ii+1,141)+pi/2 & UU(ii+3,141)>UU(ii+2,141)+pi/2
          UU(ii+1,141)=UU(ii,141);
           UU(ii+2,141)=UU(ii,141);
        elseif UU(ii,141)>UU(ii+1,141)+0.5 & UU(ii+3,141)>UU(ii+2,141)+0.75
            UU(ii+1,141)=UU(ii,141);
            UU(ii+2,141)=UU(ii+3,141);
        elseif UU(ii,141)<-1
            UU(ii+1,141)=UU(ii,141);
        elseif UU(ii,141)<UU(ii+1,141)-2 & UU(ii+3,141)<UU(ii+2,141)-2
```

```
            UU(ii+1,141)=UU(ii,141);
            UU(ii+2,141)=UU(ii+3,141);
        elseif UU(ii,141)>1.5
           UU(ii,141)=UU(ii+2,141);
           UU(ii+1,141)=UU(ii+2,141);
        end

      end
    end

end

 close(h)

 save(strcat(int2str(r),U.mat'),'U')  % Saves rho
 save(strcat(int2str(r),UU.mat'),'UU')% Saves u

 clear A Aminus Aplus B J L M N T U ans c dt e epsilon gamma h h1 l lm lp q tdata u u0 u1 ↩
     u2 u3 u4 u5 u6 u7 u8 u9
 %clear to make loop run faster

 end
```

B.3 Plotting

B.3.1 Multiple plots

```
 load x.mat
 load tdata.mat
 load U.mat

%Plot 1
 subplot(3,3,1)
 plot(x,U(:,321))
 title('t=0')
 axis([-20 75 0 1.75])
 ylabel n, xlabel x,
```

```
%Plot 2
 subplot(3,3,2)
 plot(x,U(:,331))
 title('t=5')
 axis([-20 75 0 1.75])
 ylabel n, xlabel x,
%Plot 3
 subplot(3,3,3)
 plot(x,U(:,341))
 title('t=10')
 axis([-20 75 0 1.75])
 ylabel n, xlabel x,
%Plot 4
 subplot(3,3,4)
 plot(x,U(:,351))
 title('t=15')
 axis([-20 75 0 1.75])
 ylabel n, xlabel x,
%Plot 5
 subplot(3,3,5)
 plot(x,U(:,361))
 title('t=20')
 axis([-20 75 0 1.75])
 ylabel n, xlabel x,
%Plot 6
 subplot(3,3,6)
 plot(x,U(:,371))
 title('t=35')
 axis([-20 150 0 1.75])
 ylabel n, xlabel x,
%%Plot 7
 subplot(3,3,7)
 plot(x,U(:,381))
 title('t=70')
 axis([-100 300 0 1.75])
 ylabel n, xlabel x,
%%plot 8
 subplot(1,2,1)
 plot(x,U(:,101))
 title('t=100')
 axis([-100 600 0 1.75])
```

```
 ylabel n, xlabel x,
%Plot 9
 subplot(1,2,2)
 plot(x,U(:,141))
 title('t=140')
 axis([-100 300 0 1.75])
 ylabel n, xlabel x,
```

B.3.2 Waterfall plot

```
 load x.mat
 load tdata.mat
 load Y.mat

waterfall(x,[2;6;10;14;18;22;26;30],[Y(3,:);Y(7,:);Y(11,:);Y(15,:);Y(19,:);Y(23,:);Y(27,:)↩
    ;Y(31,:)]);
axis([-5 5 0 T 0 1]), view(10,80), grid off %←L/5 L/5 0 T -1 2
colormap(1e-6*[1 1 1]); ylabel t, zlabel rho, xlabel x,
```

B.3.3 2-d colour plot

```
 load x.mat
 load tdata.mat
 load U.mat

imagesc(x,tdata,U');figure(gcf);axis([-20 300 0 140])
ylabel t, xlabel x,
```

References

[1] E.A. Cornell, Talk at the "Conference on Nonlinear Waves, Integrable Systems and their Applications", (Colorado Springs, June 2005); http://jilawww.colorado.edu/bec/papers.html.

[2] M.A. Hoefer, M.J. Ablowitz, I. Coddington, E.A. Cornell, P. Engels and V. Schweikhard, *Dispersive and classical shock waves in Bose-Einstein condensates and gas dynamics*, Physical Review A, **74**, 023623, 2006.

[3] W. Wan, S. Jia and J.W. Fleischer, *Dispersive superfluid-like shock waves in nonlinear optics*, Nature Physics, **3**, 46-51, 2007.

[4] C. Barsi, W. Wan, C. Sun, and J.W. Fleischer, *Dispersive shock waves with nonlocal nonlinearity*, Optics Letters, **32**, 2930-2932, 2007.

[5] W. Wan, S. Muenzel and J.W. Fleischer, *Wave tunneling and hysteresis in nonlinear junctions*, Physical Review Letters, **104**, 073903, 2010.

[6] P. Engels and C. Atherton, *Stationary and non-stationary fluid flow of a Bose-Einstein condensate through a penetrable barrier*, Physical Review Letters, **99**, 160405, 2007.

[7] L.D. Landau, Journal of Physics-USSR, **5,** 71, 1940; Journal of Physics-USSR, **11,** 91, 1947.

[8] R.P. Feynman, in *Progress in Low Temperature Physics,* Vol. I (ed. C.J. Gorter) p. 17, Amsterdam, North-Holland, 1955.

[9] V. Hakim, *Nonlinear Schrödinger flow past an obstacle in one dimension*, Physical Review E, **55**, 2835-2845, 1997.

[10] R. Grimshaw and N. Smyth, *Resonant flow of a stratified fluid over topography*, Journal of Fluid Mechanics, **169**, 429-264, 1986.

[11] N. Smyth, Modulation Theory solution for resonant flow over topography, Proceedings Royal Society, **409**, 79-97, 1987.

[12] R. Courant and K.O. Friedrichs, *Supersonic flow and shock waves*, Interscience, New York, 1948.

[13] M.A. Hoefer, M.J. Ablowitz, *Interaction of dispersive shock waves*, Physica D, 2007.

[14] J. J. Chang, P. Engels, and M. A. Hoefer, *Formation of Dispersive Shock Waves by Merging and Splitting Bose-Einstein Condensates*, Physical Review Letters, **101**, 170404, 2008.

[15] M. J. Ablowitz, D. E. Baldwin, and M. A. Hoefer, *Soliton Generation and Multiple Phases in Dispersive Shock and Rarefaction Wave Interaction*, Physical Review E, **80**, 016603, 2009.

[16] G.B. Whitham, *Linear and nonlinear waves*, Wiley-Interscience, New York, 1974.

[17] A.V. Gurevich and L.P. Pitaevskii, *Nonstationary structure of a collisionless shock wave*, Soviet Physics - JETP, **38** 291-297, 1974.

[18] A. Gurevich and A. Krylov, *Nondissipative shock waves in media with positive dispersion*, Zhurnal Eksperimental'noi i Teoreticheskoi Fiziki, **92**, 1684-1699, 1987.

[19] G. El, V. Geogjaev, A. Gurevich, A. Krylov, *Decay of an initial discontinuity in the defocusing NLS hydrodynamics*, Physica D, **87**, 186-192, 1995.

[20] A.M. Leszczyszyn, G.A. El, Yu.G. Gladush and A.M. Kamchatnov, *Transcritical flow of a Bose-Einstein condensate through a penetrable barrier*, Physical Review A, **79**, 063608, 2009.

[21] G.A. El, V.V. Khodorovskii and A.M. Leszczyszyn, *Refraction of dispersive shock waves*, http://arxiv.org/abs/1105.1920, 2011, submitted to Physica D.

[22] M.G. Forest and J.E. Lee, *Geometry and modulation theory for periodic nonlinear Schrödinger equation, in Oscillation Theory, Computation, and Methods of Compensated Compactness,* Eds. C. Dafermos et al, IMA Volumes on Mathematics and its Applications, **2,** Springer, New York, 1987.

[23] M. Pavlov, *Nonlinear Schödinger equation and the Bogolyubov-Whitham method of averaging*, Theoretical and Mathematical Physics, **71**, 584-588, 1987.

[24] G.A. El, A.M. Kamchatnov, V.V. Khodorovskii, E.S. Annibale and A. Gammal, *Two-dimensional supersonic nonlinear Schrödinger flow past an extended obstacle*, Physical Review E, **80**, 046317, 2009.

[25] A.M. Kamchatnov, *Nonlinear Periodic Waves and Their Modulations*, Singapore: World Scientific, 2000.

[26] G.A. El, chapter *Korteweg-de Vries equation: solitons and undular bores* in *Solitons in Fluids*, R.H.J. Grimshaw (ed), 19-53, ISBN: 1-84564-157-4, WIT Press, 2007. Available at http://www-staff.lboro.ac.uk/%7emage2/.

[27] F. Tricomi, F. *Differential equations*, Blackie and Sons, Boston, 1961.

[28] G. F. Carrier and H. P. Greenspan, *Water waves of finite amplitude on a sloping beach*, Journal of Fluid Mechanics, **4**, 97-109, 1958.

[29] G.B. Whitham, *Non-linear dispersive waves*, Proc. Roy. Soc. **A283** 238-291, 1965.

[30] M. Hoefer and M. Ablowitz, *Dispersive shock waves*, Scholarpedia, 4(11):5562, 2009.

[31] P.D. Lax and C.D. Levermore, *The small dispersion limit of the Korteweg – de Vries equation I, II, III*, Communications on Pure and Applied Mathematics, **36**, 253-290, 571-593, 809-829, 1983.

[32] S. Venakides, *The generation of modulated wavetrains in the solution of the Korteweg de vries equation*, Communications on Pure and Applied Mathematics, **38**, 883-909, 1985.

[33] E. A. Cornell, J. R. Ensher and C. E. Wieman, Experiments in dilute atomic Bose-Einstein condensation, 1995.

[34] K.B. Davis, M.O. Mewes, M.R. Andrews, N.J. van Druten, D.S. Durfee, D.M. Kurn, and W. Ketterle, *Bose-Einstein Condensation in a Gas of Sodium Atoms*, Physical Review Letters, **75**, 22: 39693973, 1995.

[35] P. Leboeuf and N. Pavloff, *Bose-Einstein beams: Coherent propagation through a guide*, Physical Review A, **64**, 033602, 2001.

[36] G.A. El and A.M. Kamchatnov, *Spatial dispersive shock waves generated in supersonic flow of Bose-Einstein condensate past slender body*, Physical Review A, **350,** 192-196, 2006; erratum: Phys. Lett. A **352,** 554, 2006.

[37] I. Carusotto, S.X. Hu, L.A. Collins, and A. Smerzi, *Bogoliubov-Cerenkov radiation in a Bose-Einstein condensate flowing against an obstacle*, Physical Review Letters, **97**, 260403, 2006.

[38] Y.G Gladush, G.A El, A. Gammal and A.M Kamchatnov, *Radiation of linear waves in the stationary flow of a Bose-Einstein condensate past an obstacle*, Physical Review A, **75**, 2007.

[39] L.P. Pitaevskii and S. Stringari, *Bose-Einstein Condensation*, Clarendon Press, Oxford, 2003.

[40] A.M. Kamchatnov, A. Gammal, and R.A. Kraenkel, *Dissipationless shock waves in Bose-Einstein condensates with repulsive interaction between atoms*, Physical Review A, **69,** 063605, 2004.

[41] V.M. Pérez-García, V.V. Konotop, V.A. Brazhnyi, *Feshbach Resonance Induced Shock Waves in Bose-Einstein Condensates*, Physical Review Letters, **92**, 220403, 2004.

[42] M. Hoefer, M. Ablowitz and P. Engels, *The piston dispersive shock wave problem*, Physical Review Letters, **100**, 084504, 2008.

[43] M. A. Hoefer and B. Ilan, *Theory of Two-Dimensional Oblique Dispersive Shock Waves in Supersonic Flow of a Superfluid*, Physical Review A, **80**, 06160, 2009.

[44] Y. Kodama, *The Whitham Equations for Optical Communications: Mathematical Theory of NRZ*, SIAM Journal on Applied Mathematics, **59**, 2162-2192, 1999.

[45] Yu.S. Kivshar and G.P. Agrawal, *Optical solitons. From Fibers to Photonic Crystals,* Academic Press, Amsterdam, 2003.

[46] W. Królikowski and B. Luther-Davies, IEEE Journal of Quantum Electronics, **39,** 3, 2003.

[47] P. Günter, J-P. Huignard, *Photorefractive materials and their applications 3: applications*, Springer Science, 2007.

[48] P. Yeh, *Introduction to photorefractive nonlinear optics*, Wiley (New York), 1993.

[49] H. Flaschka, G. Forest, & D.W. McLaughlin, D.W. *Multiphase averaging and the inverse spectral solutions of the Korteweg – de Vries equation*, Communications on Pure and Applied Mathematics, **33** 739-784, 1980.

[50] J. Frejlich, *Photorefractive Materials: Fundamental Concepts, Holographic Recording, and Materials Characterization*, Wiley-Blackwell, 2007.

[51] G. Duree, M. Morin. G. Salamo, M. Segev, B. Crosignani, P.D. Porto, E. Sharp and A. Yariv, *Dark Photorefractive Spatial Solitons and Photorefractive Vortex Solitons*, Physical Review Letters, **74**,1978-1981, 1995.

[52] G. Couton, H. Maillotte and M. Chauvet, *Self-formation of multiple spatial photovoltaic solitons*, Journal of Optics B: Quantum and Semiclassical Optics, **6**, 2004.

[53] G.A. El, *Resolution of a shock in hyperbolic systems modified by weak dispersion*, Chaos, **15**, 037103, 2005.

[54] A.V. Tyurina and G.A. El, *Hydrodynamics of modulated finite-amplitude waves in dispersive media*, Journal of Experimental and Theoretical Physics, **88**, 1999.

[55] G.A. El, V.V. Khodorovskii and A.V. Tyurina, *Undular bore transition in bi-directional conservative wave dynamics*, Physica D, **206**, 232-251, 2005.

[56] J.G. Esler and J.D. Pearce, *Dispersive dam-break and lock-exchange flows in a two-layer fluid*, Journal of Fluid Mechanics, **667**, 555-585, 2011.

[57] G.A. El, A. Gammal, E.G. Khamis, R.A. Kraenkel, and A.M. Kamchatnov, *Theory of optical dispersive shock waves in photorefractive media*, Physical Review A **76,** 053813, 2007.

[58] J.E. Rothenberg, D. Grischkowsky, *Observation of the Formation of an Optical Intensity Shock and Wave Breaking in the Nonlinear Propagation of Pulses in Optical Fibers*, Physical Review Letters, **62**, 1989.

[59] N. Ghofraniha, C. Conti, G. Ruocco, and S. Trillo, ıShocks in nonlocal media, Physical Review Letters, **99**, 043903, 2007.

[60] R. S. Johnson *A non-linear equation incorporating damping and dispersion* Journal of Fluid Mechanics **42**, 4960, 1970.

[61] S. P. Tsarev, *Poisson brackets and one-dimensional Hamiltonian-systems of the hydrodynamic type*, Doklady Akademii Nauk SSSR, **282**, 534-537, 1985.

[62] J.C. Luke, *A perturbation method for nonlinear dispersive wave problems*, Proc. Roy. Soc. **A292**, 403-412, 1966.

[63] E. Madelung, *Quantentheorie in hydrodynamischer Form*, Zeitschrift Für Physik A Hadrons and Nuclei, **40**, 1927.

[64] S.P. Novikov, S.V. Manakov, L.P. Pitaevskii and V.E. Zakharov, *The Theory of Solitons: The Inverse Scattering Method*, Consultants, New York, 1984.

[65] M. Abramowitz and I.A. Stegun, *Handbook of Mathematical Functions with Formulas, Graphs and Mathematical Tables*, New York, Dover Publications, 1972.

[66] A.V. Gurevich, A.L. Krylov and G.A. El, *Evolution of a Riemann wave in dispersive hydrodynamics*, Soviet Physics - JETP, **74,** 957, 1992.

[67] P.D. Lax, *Hyperbolic systems of conservation laws II*, Communications on Pure and Applied Mathematics, **10**, 537-566, 1957.

[68] S. Jin, C.D. Levermore, D.W. McLaughlin, Communications on Pure and Applied Mathematics, **52,** 613, 1999.

[69] G. Biondini, Y. Kodama, *On the Whitham Equations for the Defocusing Nonlinear Schrödinger Equation with Step Initial Data*, Journal of Nonlinear Science, **16**, 435-481, 2006.

[70] P.D. Lax, C.D. Levermore and S. Venakides, The generation and propagation of oscillations in dispersive initial value problems and their limiting behavior, in *Important Developments in Soliton Theory*, p. 205, eds. A.S. Focas and V.E. Zakharov, Springer-Verlag, New York, 1994.

[71] G. El and A.Krylov, *Solution of the Cauchy problem for the defocusing NLS equation in the Whitham limit*, Physics Letters A, **203**, 77-82, 1995.

[72] V. R. Kudashev, S. E. Sharapov, *Inheritance of KdV symmetries under Whitham averaging and hydrodynamic symmetries of the Whitham equations,* Theoretical and Mathematical Physics, **87**, 358363, 1991.

[73] Y. Kodama, V.U. Pierce, F.-R. Tian, *On the Whitham equations for the defocusing complex modified KdV equation,* SIAM Journal on Mathematical Analysis, **41**, 26-58, 2008.

[74] B.L. Rozhdestvenskii and N.N. Janenko, *Systems of quasilinear equations and their applications to gas dynamics*, Providence, RI: American Mathematical Society, 1983.

[75] L.D Landau and E.M. Lifshitz, *Fluid Mechanics*, Pergamon, Oxford, 1987.

[76] H. Lamb, *Hydrodynamics*, Cambridge University Press, Cambridge, 1932.

[77] L. Onsager, Nuovo Cimento, **6,** Suppl. 2, 249 and 281, 1949.

[78] T.P. Simula, P. Engels, I. Coddington, V. Schweikhard, E.A. Cornell, and R.J. Ballagh, *Observations on Sound Propagation in Rapidly Rotating Bose-Einstein Condensates*, Physical Review Letters, **94,** 080404, 2005.

[79] Yu.G. Gladush, L.A. Smirnov and A.M. Kamchatnov, *Generation of Cherenkov waves in the flow of a Bose-Einstein condensate past an obstacle*, Journal of Physics B, **41,** 160301, 2008.

[80] A.M. Kamchatnov and L.P. Pitaevskii, *Stabilization of Solitons Generated by a Supersonic Flow of Bose-Einstein Condensate Past an Obstacle*, Physics Review Letters, **100,** 160402, 2008.

[81] K. Sasaki, N. Suzuki and H. Saito, *Bénard-von Kármán Vortex Street in a Bose-Einstein Condensate*, Physical Review Letters, **104**, 150404, 2010.

[82] T. Akylas, *On the excitation of long nonlinear water waves by a moving pressure distribution*, Journal of Fluid Mechanics, **141**, 455-466, 1984.

[83] P. G. Baines, *A unified description of two-layer flow over topography*, Journal of Fluid Mechanics, **146,** 127-167, 1984.

[84] C. Raman, M. Köhl, R. Onofrio, D.S. Durfee, C.E. Kuklewicz, Z. Hadzibabic, and W. Ketterle, Phys. Rev. Lett. **83,** 2502, 1999.

[85] C.-T. Pham and M. Brachet, *Dynamical scaling laws in two types of extended Hamiltonian systems at dissipation onset*, Physica D, **183** 127, 2002.

[86] C.K. Law, C.M. Chan, P.T. Leung, and M.-C. Chu, *Motional Dressed States in a Bose-Einstein Condensate: Superfluidity at Supersonic Speed*, Physics Review Letters, **85,** 1598, 2000.

[87] M. Haddad and V. Hakim, *Superfluidity at Supersonic Speed?*, Physical Review Letters, **87**, 218901, 2001.

[88] N. Pavloff, *Breakdown of superfluidity of an atom laser past an obstacle*, Physical Review A, **66,** 013610, 2002.

[89] A. Radouani, *Soliton and photon production by an oscillating obstacle in a quasi-one-dimensional trapped repulsive Bose-Einstein condenstate*, Physical Review A, **70**, 013602, 2004.

[90] V.M. Pérez-García, H. Michinel, and H. Herrero, *Bose-Einstein solitons in highly asymmetric traps*, Physics Letters A, **57,** 3837, 1998.

[91] T.R. Akylas, *On the excitation of long nonlinear water waves by a moving pressure distribution*, Journal of Fluid Mechanics, **141,** 455, 1984.

[92] T.R. Marchant and N.F. Smyth, *The initial boundary problem for the Korteweg-de Vries equation*, IMA Journal of Applied Mathematics, **47,** 247, 1991; Proceedings Royal Society A, **458,** 857, 2002.

[93] Th.R. Taha and M.J. Ablowitz, *Numerical Simulations of Certain Nonlinear Evolution Equations of Physical Interest*, Journal of Computational Physics, **55,** 203, 1984.

[94] J. Javanainen and J. Ruostekoski, Journal of Physics A: Mathematical and General, **39,** L179, 2006.

[95] B.B. Baizakov, A.M. Kamchatnov, and M. Salerno, *Matter sound waves in two-component Bose-Einstein condensates*, Journal of Physics B, **41,** 215302, 2008.

[96] A.M. Kamchatnov and V.S. Shchesnovich, *Dynamics of Bose-Einstein condensates in cigar-shaped traps*, Physical Review A, **70**, 023604, 2004.

[97] G.A. El, A. Gammal, and A.M. Kamchatnov, *Oblique dark solitons in supersonic flow of a Bose - Einstein condensate*, Physics Review Letters, **97,** 180405, 2006.

[98] R. Courant and K. O. Friedrichs, *Interaction of shock and rarefaction waves in one-dimensional media*, National Defense Research Committee, Applied Mathematics Panel Report 38.1R, PB32196, AMG-1, 1943.

[99] H.E. Moses, *The head-on collision of a shock wave and a rarefaction wave in one dimension*, Journal of Applied Physics, **19**, 383, 1948.

[100] V. Ya. Arsenin, and N.N. Yanenko, On the interactions of progressive waves with shock waves in an isothermal gas, Dokl. Akad. Nauk SSSR, **109,** (1956), 713716

[101] Z. Hasimoto, Interaction of a simple expansion wave with a shock wave in two-dimensional flows of a gas, Physical Society of Japan, **19**, 1074-1078, 1964.

[102] J. Rosciszewski, Calculations of the motion of non-uniform shock waves, Journal of Fluid Mechanics, **8**, 337, 1960.

[103] S. Gatz and J. Herrmann, *Soliton propagation in materials with saturable nonlinearity*, Journal of the Optical Society of America B, **8**, 2296, 1991.

[104] D.N. Christodoulides and M.I. Carvalho, *Bright, dark, and gray spatial soliton states in photorefractive media*, Journal of the Optical Society of America B, **12**, 1628, 1995.